Brain oscillations : the neural mechanism underlying perceptual rhythms

Camille Fakche

Université Paris Cité

Ecole doctorale Cerveau, Cognition, et Comportement – n°158

Integrative Neuroscience and Cognition Center – UMR 8002

Brain oscillations: the neural mechanism underlying perceptual rhythms

Par **Camille FAKCHE**

Thèse de doctorat de Sciences Cognitives

Dirigée par **Laura DUGUÉ** et par **Thérèse COLLINS**

Présentée et soutenue publiquement le **09 Septembre 2022**

Devant un jury composé de :

Gregor THUT, Professor, Institute of Neuroscience and Psychology, University of Glasgow, **Rapporteur**

Frédéric CHAVANE, DR, Institut de Neurosciences de la Timone, Université Aix-Marseille, **Rapporteur**

Andrea ALAMIA, CR, Centre de Recherche Cerveau et Cognition, Université de Toulouse, **Examinateur**

Mathilde BONNEFOND, CR, Centre de Recherche en Neurosciences de Lyon, Université Claude Bernard Lyon 1, **Examinatrice**

Jean LORENCEAU, DR Emérite, Integrative Neuroscience and Cognition Center, Université Paris Cité, **Examinateur**

Laura DUGUÉ, MCU-HDR, Integrative Neuroscience and Cognition Center, Université Paris Cité, **Directrice de thèse**

Thérèse COLLINS, PU, Integrative Neuroscience and Cognition Center, Université Paris Cité, **Co-Directrice de thèse**

Abstract

Brain oscillations: the neural mechanism underlying perceptual rhythms

Brain oscillations are a ubiquitous phenomenon. They have been recorded in a wide range of species, at multiples brain scales, i.e., in cells, in local neuronal networks, and between cortical areas. The temporal features of brain oscillations, i.e., the phase and the amplitude, independently predict visual perception and cortical excitability. In perceptual rhythms, the phase accounts for less than 20% of the trial-by-trial variability in perceptual performance. In this PhD, we hypothesized that if brain oscillations are the substrates of perception, they should explain a larger portion of the variance observed in the empirical data. We aimed to better characterize the functional role of brain oscillations on visual perception, by considering the interaction between their temporal features and their spatial organization. To this aim, we used a multimodal approach comprising psychophysics, neuroimaging (EEG, MRI, oculometry) and TMS. First, we established a causal link between the phase and the amplitude of alpha oscillations, cortical excitability, and visual perception (Fakche et al., 2022). Second, we proposed that brain oscillations are the neural substrates of a complex visual perception phenomenon, serial dependance. Third, we showed that visual perception was modulated periodically across space and time by the phase of an oscillatory inducer, suggesting that alpha brain oscillations propagate across the retinotopic space (Fakche and Dugué, 2022, bioRxiv; Galas, Fakche, Baudouin, and Dugué, in preparation). Fourth, we tested whether the direction of alpha macroscopic traveling waves changed as a function of cognition. Finally, we investigated whether single pulses of TMS applied over V1 causally triggered a feedforward traveling wave at its natural frequency. Together, these studies provide strong evidence in favor of a functional role of the spatiotemporal organization of brain oscillations on human visual perception.

Keywords: *Brain oscillations; Traveling waves; Phase; Amplitude; Alpha; Psychophysics; EEG; TMS; Vision; Perceptual Rhythms*.

Les oscillations cérébrales : le support neuronal des rythmes perceptifs

Les oscillations cérébrales sont un phénomène ubiquitaire. Elles ont été enregistrées chez de nombreuses espèces, et à de multiples échelles cérébrales, i.e., dans les cellules, les réseaux neuronaux locaux, et entre les aires corticales. Les caractéristiques temporelles des oscillations cérébrales, i.e., la phase et l'amplitude, prédisent de manière indépendante la perception visuelle et l'état d'excitabilité cortical. Dans les rythmes perceptifs, la phase explique moins de 20% de la variabilité inter-essais dans les performances. Dans cette thèse, nous faisons l'hypothèse que si les oscillations cérébrales sont le support de la perception, alors elles devraient expliquer plus de variance dans les données empiriques. Notre but était de mieux caractériser le rôle fonctionnel des oscillations dans la perception visuelle, en considérant les interactions entre les caractéristiques temporelles, et l'organisation spatiale des oscillations

cérébrales. Dans ce but, nous avons utilisé une approche multimodale comprenant de la psychophysique, de la neuroimagerie (EEG, IRM, oculométrie) et de la TMS. Premièrement, nous avons montré l'existence d'un lien causal entre la phase et l'amplitude des oscillations alpha, l'excitabilité corticale, et la perception visuelle (Fakche et al., 2022). Deuxièmement, nous avons proposé que les oscillations cérébrales étaient le support neuronal d'une perception visuelle complexe, l'effet sériel. Troisièmement, nous avons montré que la perception visuelle était modulée périodiquement à travers le temps et l'espace par la phase d'une stimulation oscillante, suggérant que les oscillations cérébrales alpha se propagent à travers l'espace rétinotopique (Fakche and Dugué, 2022, bioRxiv ; Galas, Fakche, Baudouin, and Dugué, en préparation). Quatrièmement, nous avons étudié si la direction de propagation des oscillations alpha à l'échelle macroscopique était modulée par les fonctions cognitives. Enfin, nous avons testé si un pulse de TMS appliqué sur V1 déclenchait de manière causale une oscillation se propageant des aires occipitales aux aires frontales à la fréquence naturelle de V1. Ensemble, ces études montrent que l'organisation spatio-temporelle des oscillations cérébrales joue un rôle fonctionnel sur la perception visuelle chez l'humain.

Mots-clés : *Oscillations cérébrales ; Propagation de l'activité ; Phase ; Amplitude ; Alpha ; Psychophysique ; EEG ; TMS ; Vision ; Rythmes perceptifs.*

Acknowledgements

First of all, I wish to convey my huge gratitude to ***Laura Dugué***. Doing a PhD under your supervision was an incredible experience, both at the scientific and at the human level. You allowed me to achieve one of my life projects, doing a PhD in cognitive neuroscience, in the best possible way. I had the feeling that we shared the same scientific interests, the same way of working, and the same enthusiasm and motivation on my PhD projects that truly passionate me. I want also to thank you for bringing me to conferences, training me at doing oral presentations, presenting me to the neuroscientific community, giving me the chance to collaborate and to have a post-doc I really wanted to have, and for showing me how the research world works, such as getting fundings, publishing, supervising students, teaching, and doing scientific mediation. You taught me how to become a researcher. A huge thank you for helping me to build myself as a neuroscientist.

I would also like to thank ***Thérèse Collins***, who co-supervised my PhD. I think that you are an example for the scientific community. I have been impressed by the calm, the goodwill and the diplomacy, you deployed at work with everyone. It was a pleasure to work with you and to benefit from your great expertise in visual neurosciences.

Thank you to ***Florian Waszak***, director of the INCC, who accepted me in the center. Thanks to you, I have been able to do my PhD under good conditions despite the covid pandemic and the merge between universities!

I wish also to convey my gratitude to ***Ole Jensen***, who offered me to join his lab in Birmingham for a post-doc position after my PhD. It is an honor to have this position, and I am very happy about that!

I am also grateful to ***Rufin VanRullen***, who open the doors of the CerCo to me for an active collaboration on my TMS projects. Thank you for your time and your feedbacks. Thank you also to ***Samson Chota*** and ***Nathalie Vaiyssiere***, you helped me a lot for my experiments in Toulouse.

I am grateful to ***Gregor Thut*** and ***Frédéric Chavane*** for accepting to review this manuscript. Thank you also to ***Andrea Alamia***, ***Mathilde Bonnefond*** and ***Jean Lorenceau*** for being part of the jury of my thesis committee.

Carole, ***Sabine***, ***Aboubacar***, ***Francesca***, and ***Nate***, thank you very much for helping me to go through the meanders of the administration. It would have been very difficult without you!

Importantly, thanks to the ***Dugué Lab***! It was amazing to work with you. ***Laetitia***, ***Kirsten***, and ***David***, as post-doc, you truly helped me scientifically with your experience, for analyzing data, writing fundings and cover letters, and supervising students. ***Garance***, a special thank for you, if you did not get your own fundings to do your PhD, I would never have the chance to do my

PhD in the Dugué Lab. Last but not least, ***Laurie***! We did so many cigarette breaks together! It was so great to share with you all my joys and my difficult moments during this PhD. I really appreciated all the moments where we worked together and all the beers and lunches we shared. You are a true friend, and I give you all my courage to finish your PhD in your turn.

Thank you also to all my other colleagues from the INCC: ***Martina, Klara, Hamdi, Claire, Mark, Corentin, Jules, Louis, Louise, Flavia, Maxine, Marielle, etc***. It was great to share laboratory life with you.

I would also like to thank ***Roxane***, for her guidance and support during my PhD and before, when I was an M2 intern and a research assistant. You helped me to do all my PhD applications at this time, and I learned a lot by your side on scientific research. You also helped to manage my stress. Even now, I heard your voice telling me "*Ecoute Camille, ça va bien se passer*." I laugh a lot by your side, and you are a really good friend, as well as a brilliant neuroscientist. I am looking forward to running our own scientific project together.

Thank you, a lot, to ***la Salade Fraicheur***, my best friends since more than 10 years now. I love you guys, and my life would be so sad without you. Thank you for the holidays, the weekend, the drinks, the calls, that helped me to release pressure during the PhD!

I wish to convey my gratitude to ***my mother*** and ***my father***. Since I was little, you gave me the taste for science and good working. You always brought me your support and encourage me to do what I want in my studies. Thank you very much for your support and your love. I am fortunate to have you. Thank you also to my sister, ***Inès***, who welcomed me in Vichy to have some breaks during this PhD. I wish you to find your way in working, as I found mine.

Finally, I would like to thank ***Sonny Becker***, my partner. When we lived in Lyon, you told me that you will follow me everywhere for my PhD except in Paris. Of course, you followed me in Paris, and now, you will come with me to Birmingham for my post-doc. You always understood how much my career was important for me, and you always gave me your support. During my PhD, you were here to share my happiness, my accomplishments, and also all my stress, my doubts, my periods of feeling down, and my massive arguments! You always encourage me to do my best, and sometimes you forced me to take some rest! Thank you for being here for me during these 4 years of PhD. I can't imagine my life without you, and I am looking forward to living new adventures with you. I love you more than everything. Je t'aime plus que tout.

Abbreviations

BOLD: Blood Oxygen-Level Dependent.

ECoG: Electrocorticography.

EEG: Electroencephalography.

ERP: Event-Related Potentials.

FFT: Fast Fourier Transform.

IAF: Individual Alpha Frequency.

ICA: Independent Component Analysis.

ISI: Inter-Stimulus Interval.

ITI: Inter-Trial Interval.

LFP: Local Field Potentials.

MEG: Magnetoencephalography.

(f)MRI: (functional) Magnetic Resonance Imaging.

MT: Middle Temporal visual area.

MVPA: MultiVariate Pattern Analysis.

MUA: Multi-Unit Activity.

ROI: Region Of Interest.

RS: Resting State.

RT: Reaction Time.

SD: Standard Deviation.

SEM: Standard Error of the Mean.

SNR: Signal-to-Noise Ratio.

SO: Single Oscillator.

TMS: Transcranial Magnetic Stimulation.

V1: Primary visual area.

V2: Secondary visual area.

V4: Fourth visual area.

VEP: Visual Evoked Potential.

VSD: Voltage Sensitive Dye.

WCO: Weakly Coupled Oscillators.

Publications and Communications

Publications in peer-reviewed international journals

Fakche C., VanRullen R., Marque P., and Dugué L. (2022). *Alpha phase-amplitude tradeoffs predict visual perception*. eNeuro, 9:1, 1-16.

Manuscripts in preparation

Fakche C. and Dugué L. (2022). *Perceptual cycles travel across retinotopic space*. bioRxiv.

Galas L., **Fakche C.**, Baudouin, N., and Dugué L. (in preparation). *Spatial dynamics of perceptual rhythms.*

Scientific mediation

Fakche C. and Dugué L. (in preparation*). La perception visuelle change à travers le temps et l'espace*. The Conversation.

Communications at international conferences

Fakche C., Galas L., and Dugué L. (2022). *The spatio-temporal organization of alpha brain oscillations shape visual perception across the retinotopic space*. Accepted at the 44th European Conference on Visual Perception (ECVP), Nijmegen, Netherlands. **Oral presentation**.

Fakche C., VanRullen R., Marque P., and Dugué L. (2021). *Causal link between the phase and amplitude of spontaneous alpha oscillations, cortical excitability and visual perception*. 43rd ECVP, Online. **Poster presentation**.

Galas L., **Fakche C.**, Baudouin N. and Dugué L. (2021). *Investigating perceptual rhythms across retinotopic space.* 43rd ECVP, Online. **Poster presentation**.

Fakche C. and Dugué L. (2019). *Does the spatial organization of brain oscillations modulate perceptual rhythms?* 42nd ECVP, Leuven, Belgium. **Poster presentation**.

Communications at national conferences

Fakche C., VanRullen R., Marque P., and Dugué L. (2021). *Phase-amplitude tradeoffs of spontaneous alpha oscillations predict cortical excitability and visual perception*. Annual national meeting of the Research Group in Vision (GDR) Vision, Lille, France. **Oral presentation**.

Galas L., **Fakche C.**, Baudouin N. and Dugué L. (2021). *Spatial dynamics of perceptual rhythms.* Annual national meeting of the GDR Vision, Lille, France. **Poster presentation**.

Fakche C. and Dugué L. (2019). *Does the spatial organization of brain oscillations modulate perceptual rhythms?* Annual national meeting of the GDR Vision, Marseille, France. **Poster presentation**.

Invited talk

2022: *Brain oscillations: neural mechanism underlying perceptual rhythms*. Online presentation in Saskia Haegens' Brain rhythms Group.

Résumé substantiel

Les oscillations cérébrales ont été enregistrées chez l'Homme la première fois en 1929, par Hans Berger (Berger, 1929). Une oscillation cérébrale correspond à une activité rythmique du cerveau, qui croît et qui décroît de manière périodique au cours du temps. Elle se caractérise par sa période, i.e., la durée d'un cycle (exprimée en unité de temps), sa fréquence, exprimée en Hertz (s^{-1}), i.e. le nombre de cycles au cours d'une seconde, son amplitude, i.e., la distance entre le minimum et le maximum de l'activité cérébrale, et sa phase, i.e., la position sur le cycle à un moment donné (exprimée en radians ou en degrés, la phase varie entre 0° et 360°, 0 et 2π). A cette époque, Berger étudiait l'activité électrique du cerveau dans le Département de Psychiatrie et de Neurologie de Jena, en Allemagne, et son intérêt principal portait sur la télépathie, i.e., la capacité de communiquer d'esprit à esprit. Au lieu de prouver l'existence de la télépathie, il découvrit la présence d'une oscillation dans le cortex occipital, d'une amplitude de 150-200 microvolts, et de fréquence 10 Hz, lorsque les participants fermaient les yeux. Il nomma cette oscillation le rythme alpha. Dès cette découverte, Berger eut l'intuition que les oscillations cérébrales pourraient jouer un rôle fonctionnel sur la cognition. Il continua ses recherches durant les décennies qui suivirent et proposa une théorie décrivant que les oscillations alpha seraient associées à un état de repos, servant à inhiber les stimulations externes et internes, alors que les oscillations de hautes fréquences (42-90 Hz) seraient un corrélat de l'activité cérébrale (Quigley, 2021).

Le but de cette thèse est de contribuer à l'idée que Hans Berger a développée il y a presque un siècle sur le rôle fonctionnel des oscillations cérébrales dans la cognition humaine. De nombreuses études ont montré que les caractéristiques temporelles des oscillations, i.e., la phase et l'amplitude, modulaient les fonctions cognitives de manière indépendante. Dans cette thèse, nous faisons l'hypothèse que **nous pouvons mieux expliquer le rôle fonctionnel des oscillations cérébrales en prenant en compte les interactions entre les caractéristiques temporelles des oscillations, ainsi que leur organisation spatiale**. Nous nous sommes plus particulièrement intéressées au rôle des oscillations cérébrales dans la perception visuelle.

Depuis leur découverte en 1929, les oscillations cérébrales ont été classées en 5 bandes de fréquences : delta (0.1 – 3 Hz), theta (4 – 7 Hz), alpha (8 – 12 Hz), beta (13 – 30 Hz) et gamma (> 30 Hz). Les premières recherches ont associé les bandes de fréquences à des fonctions sensorimotrices ou cognitives spécifiques (Jensen et al., 2014). Récemment, cette

perception est devenue obsolète, de nombreuses fonctions cognitives sont associées à plusieurs fréquences oscillatoires, et une même bande de fréquence est associée à plusieurs fonctions. Pour cette raison, nous avons porté notre recherche sur le rôle fonctionnel de la phase et de l'amplitude des oscillations cérébrales sur la perception visuelle, ainsi que sur l'état d'excitabilité corticale associé.

L'**amplitude** des oscillations cérébrales de basses fréquences (delta, theta, alpha, beta) et de hautes fréquences (gamma) sont respectivement, négativement et positivement corrélée à la réponse hémodynamique et à l'activité neuronale (Logothethis et al., 2001 ; Brookes et al., 2005 ; Niessing et al., 2005 ; Mukamel et al., 2005 ; Goense and Logothethis, 2008 : Koch et al., 2009 ; Scheeringa et al., 2009 ; Yuan et al., 2010 ; Zumer et al., 2010 ; Singh et al., 2002 ; Scheeringa et al., 2011a ; Goldman et al., 2002 ; Laufs et al., 2003 ; Moosmann et al., 2003 ; Scheeringa et al., 2008 ; Manning et al., 2009 ; Haegens et al., 2011b ; Mukamel et al., 2005 ; Rasch et al., 2008 ; Ray et al., 2008a, 2008b ; Belitski et al., 2008 ; Ray and Maunsell, 2011; Zanos et al., 2012). Les oscillations gamma sont un indicateur de l'activité des neurones alors que les oscillations de basses fréquences semblent plutôt indiquer un rôle inhibiteur sur le cortex. Sur les performances perceptuelles, dans la modalité visuelle, il a été montré qu'une faible amplitude des oscillations cérébrales alpha dans les cortex pariéto-occipitales était associée à une plus grande probabilité de percevoir un stimulus visuel (Ergenoglu et al., 2004 ; Hanslmayr et al., 2007 ; Van Dijk et al., 2008 ; Wyart and Tallon-Baudry, 2009).

Concernant la **phase** des oscillations cérébrales, il a été montré que la réponse hémodynamique et à l'activité neuronale étaient modulée de manière périodique par la phase (Gray and Singer, 1989 ; Csicsvari et al., 2003 ; Lakatos et al., 2005 ; Rasch et al., 2008 ; Montemurro et al., 2008 ; Vinck et al., 2010 ; Haegens et al., 2011b ; Zanos et al., 2012 ; Scheeringa et al., 2011b ; Hanslmayr et al., 2013). De manière similaire, la perception visuelle fluctue rythmiquement en fonction de la phase des oscillations cérébrales delta, theta et alpha (Nunn and Osselton, 1974 ; Varela et al., 1981 ; Busch et al., 2009 ; Mathewson et al., 2009 ; Busch and VanRullen, 2010 ; Dugué et al., 2011a ; Fiebelkorn et al., 2013b ; Hanslmayr et al., 2013 ; Manasseh et al., 2013), i.e., on parle de **cycles perceptuels**. Certaines phases des oscillations sont associées à une haute probabilité de percevoir un stimulus visuel, i.e., phase optimale, alors que les phases opposées sont associées à des performances visuelles plus faibles, i.e., phase non-optimale.

Dans le premier projet de thèse, nous avons fait l'hypothèse qu'il existait un lien causal entre la phase et l'amplitude des oscillations, l'état d'excitabilité cortical, et la perception visuelle associée.

Dans le deuxième projet, nous avons étudié si les oscillations cérébrales pouvaient expliquer un phénomène de perception visuelle complexe, l'effet sériel.

Pour le moment, nous nous sommes concentrés majoritairement sur le rôle des caractéristiques temporelles des oscillations cérébrales, mais qu'en est-il de leur organisation spatiale ? Dès les années 1930, il a été montré que les oscillations cérébrales se propageaient à travers l'espace cortical (Adrian and Matthews, 1934b ; Adrian and Yamagiwa, 1935). La propagation de l'activité cérébrale se définit par un décalage constant du pic d'activité entre la source du signal et les positions plus éloignées (Sato et al., 2012 ; Muller et al., 2018). L'activité cérébrale peut être oscillatoire ou non-oscillatoire, ou encore évoquée par une stimulation ou spontanée. D'autre part, une distinction importante est faite entre la propagation de l'activité cérébrale *au sein d'une même aire cérébrale*, i.e. échelle mésoscopique, souvent enregistrée avec des méthodes invasives, et la propagation *entre plusieurs aires cérébrales*, i.e., échelle macroscopique, souvent mesurée avec l'électroencéphalographie (EEG), qui est non-invasif.

La **propagation mésoscopique des oscillations cérébrales** a été beaucoup observée chez l'animal (Stroh et al., 2013 ; Han et al., 2008 ; Townsend et al., 2015 ; Petsche and Stumpf, 1960 ; Adrian and Matthews, 1934 ; Arieli et al., 1995 ; Benucci et al., 2007 ; Freeman, 1978 ; Ketchum and Haberly, 1993 ; Besserve et al., 2015 ; Huang et al., 2010 ; Gabriel and Eckorn, 2003 ; Ylinen et al., 1995 ; Csicsvari et al., 2000 ; Patel et al., 2013 ; Wright and Sergejew, 1991 ; Prechtl et al., 1997 ; Lam et al., 2000, 2003 ; Muller et al., 2014 ; Lubenov and Siapas, 2009 ; Patel et al., 2012 ; Agarwal et al., 2014 ; Hernandez-Perez et al., 2020 ; Murthy and Fetz, 1996 ; Rubino et al., 2006 ; Takahashi et al., 2015 ; Zanos et al., 2015 ; Freeman and Baird, 1987 ; Freeman and Barie, 2000 ; Ray and Maunsell, 2011 ; Maris et al., 2013 ; Davis et al., 2020). Chez l'humain, seulement quelques études invasives chez des patients ont été réalisées (Takahashi et al., 2011 ; Zhang and Jacobs, 2015 ; Sreekumar et al., 2021), la faible résolution spatiale de l'EEG ne permettant pas d'observer l'activité cérébrale au sein d'une seule aire cérébrale. Les oscillations cérébrales se propagent à une vitesse moyenne de 0.58 m/s, sur une distance corticale moyenne de 12.5 mm, à l'échelle mésoscopique. Des études ont mis en évidence une corrélation entre la propagation de cette activité neuronale mésoscopique et certaines fonctions cognitives chez l'animal : la navigation spatiale (Agarwal et al., 2014),

l'attention (Maris et al., 2013), la mémoire (Han et al., 2008), la motricité (Rubino et al., 2006), les mouvements oculaires (Zanos et al., 2015), et la perception visuelle (Jancke et al., 2004 ; Zhang et al., 2012 ; Besserve et al., 2015 ; Rekauzke et al., 2016 ; Chemla et al., 2019 ; Davis et al., 2020). Chez l'humain, certaines études ont montré un rôle de la propagation de l'activité cérébrale non-oscillatoire sur la perception visuelle, grâce à la psychophysique (Wilson et al., 2001 ; Lee et al., 2005, 2007 ; Genç et al., 2015). En revanche, le rôle de la propagation mésoscopique des oscillations sur la perception visuelle humaine reste mal connu (voir Sokoliuk and VanRullen, 2016).

Dans le troisième projet de thèse, nous avons étudié le rôle de la propagation des oscillations mésoscopiques à travers l'espace rétinotopique sur la perception visuelle chez l'humain.

Inversement, la **propagation des oscillations cérébrales à l'échelle macroscopique** a été beaucoup observée chez l'humain grâce aux enregistrements EEG, sur des personnes au repos (Adrian and Yamagiwa, 1935 ; Cohn, 1948 ; Goldman et al., 1949 ; Von Leeuwen, 1964 ; Walter et al., 1966 ; Giannitrapani et al., 1966 ; Liske et al., 1967 ; Shaw and McLachlan, 1968 ; Hori et al., 1969 ; Barlow and Estrin, 1971 ; Hoovey et al., 1972 ; Hord et al., 1972, 1974 ; Suzuki, 1974 ; Inouye et al., 1983, 1995 ; Thatcher et al., 1986 ; Schack et al., 2003 ; Ito et al., 2005, 2007 ; Manjarrez et al., 2007 ; Nolte et al., 2008 ; Bahramisharif et al., 2013 ; Van Ede et al., 2015 ; Halgren et al., 2019 ; Alamia and VanRullen, 2019 ; Pang et al., 2020) ou réalisant une tâche cognitive : de mémoire (Alexander et al., 2006, 2008, 2009 ; Schack et al., 1999 ; Sauseng et al., 2002 ; Van Der Meij et al., 2012 ; Zhang et al., 2018) ou visuelle (Shaw and McLachlan, 1968 ; Barlow and Estrim, 1971 ; Brenner et al., 1981 ; Maclin et al., 1983 ; Burkitt et al., 2000 ; Shevelev et al., 2000 ; Schack et al., 2003 ; Srinivasan et al., 2006 ; Cottereau et al., 2011 ; Fellinger et al., 2012 ; Patten et al., 2012 ; Pang et al., 2020 ; Rodriguez et al., 1999 ; VanEde et al., 2015 ; Tsoneva et al., 2021 ; Thorpe et al., 2007 ; Alexander et al., 2013), par exemple. Les oscillations cérébrales se propagent à une vitesse moyenne de 5.2 m/s, sur une distance corticale allant de 5 à 25 cm, à l'échelle macroscopique. La propagation présente majoritairement une propagation antéro-postérieure ou postéro-antérieure, avec un décalage de phase allant de 30° à 240° entre les électrodes frontales et occipitales (Walter et al., 1966 ; Cohn, 1948 ; Hord et al., 1972, 1974 ; Suzuki, 1974 ; Burkitt et al., 2000 ; Ito et al., 2005 ; Zhang et al., 2018). De nombreuses études ont mis en évidence une corrélation entre le nombre et la direction des oscillations se propageant à travers le cortex, et des fonctions cognitives tel que la mémoire (Alexander et al., 2006 ; Ribary et al., 1991 ; Zhang et al., 2018 ; Sauseng et

al., 2002), l'attention (Alexander et al., 2008), les mouvements oculaires (Giannini et al., 2018) et la perception visuelle (Schack et al., 1999, 2003 ; Patten et al., 2012 ; Alamia and VanRullen, 2019 ; Pang et al., 2020 ; Shevelev et al., 2000 ; Fellinger et al., 2012 ; King and Wyart, 2021).

Dans le quatrième projet de thèse, nous faisons l'hypothèse qu'il est possible de manipuler la direction de propagation des oscillations cérébrales en manipulant la fonction cognitive engagée. D'autre part, nous allons tester s'il existe un lien causal entre la perception visuelle et la propagation postéro-antérieure des oscillations cérébrales.

Le but de cette thèse est de démontrer qu'en considérant les interactions entre les caractéristiques temporelles des oscillations cérébrales, ainsi que leur organisation spatiale, nous pouvons mieux expliquer leur rôle fonctionnel sur l'excitabilité corticale et la perception visuelle. Pour répondre à notre problématique, nous avons utilisé une approche multimodale comprenant de la **psychophysique**, de la **neuroimagerie** (EEG, IRM, oculométrie) et de la **stimulation non-invasive** (TMS), dans **4 grands projets**, chez l'humain sain.

Dans le **premier projet**, nous avons étudié si l'interaction entre la phase et l'amplitude des oscillations cérébrales spontanées alpha jouait un rôle fonctionnel sur l'excitabilité corticale et la perception visuelle, d'après les hypothèses formulées par la **théorie d'Inhibition Pulsée** (Jensen and Mazaheri, 2010 ; Klimesch et al., 2007 ; Mathewson et al., 2011). Cette théorie prédit que : 1) Une amplitude élevée des oscillations alpha induit de l'inhibition corticale à des phases spécifiques, associées à des performances perceptuelles faibles, alors qu'aux phases opposées, l'inhibition diminue (éventuellement, augmentation de l'excitation), et les performances perceptuelles augmentent. 2) Une amplitude faible des oscillations alpha est moins sujette à ces pulses d'inhibition périodiques, induit par la phase, entrainant des performances perceptuelles plus élevées en général. Pour tester ces prédictions, l'excitabilité corticale et la perception visuelle ont été évaluées chez l'humain avec la perception de phosphene, i.e., flash illusoire, induit par des pulses de TMS au niveau du cortex occipital, ainsi que l'activité cérébrale post-pulse, au cours d'un enregistrement EEG. Nous avons mis en évidence que la phase des oscillations spontanées alpha (~10 Hz) modulait la probabilité de percevoir un phosphene de manière périodique, avec une phase non-optimale pour la perception entre $-\pi/2$ et $-\pi/4$. Le rôle de la phase était sensiblement plus important lorsque l'amplitude des oscillations alpha était élevée (Fakche et al., 2022). **Notre étude supporte la théorie d'Inhibition Pulsée en montrant qu'il existe un lien causal entre la phase et l'amplitude**

des oscillations alpha, l'excitabilité corticale, et la perception visuelle associée (Fakche et al., 2022).

Dans le **second projet**, nous nous sommes intéressées au rôle des oscillations cérébrales dans **l'effet sériel**. L'effet sériel décrit que la perception d'un stimulus visuel est systématiquement biaisée par les précédentes perceptions visuelles (Fischer and Whitney, 2014 ; Liberman et al., 2014 ; Cicchini et al., 2014 ; Burr and Cicchini, 2014). Bien que l'effet sériel ait été beaucoup étudié au niveau comportemental, ses supports neuronaux reste mal défini. Nous avons réalisé une expérience d'effet sériel dans le cas de la perception d'un visage, qui est associée à de forts marqueurs neuronaux (Klopp et al., 1999 ; Hsaio et al., 2006 ; Rousselet et al., 2007 ; Sakihara et al., 2012 ; Tang et al., 2008 ; Torrence et al., 2021). En utilisant un algorithme de classification, il est possible de distinguer les essais où les participants perçoivent un visage comparé aux essais où ils perçoivent une maison (Haxby et al., 2001). L'algorithme de classification permet d'identifier l'activité cérébrale qui est associée à la perception d'un visage. Dans le cas de l'effet sériel, nous faisons l'hypothèse que l'activité cérébrale associée à la perception d'un visage sera identifiée dans les perceptions visuelles ambiguës biaisées vers la perception d'un visage. **Malheureusement, nos analyses n'ont pas permis de mettre en évidence un rôle fonctionnel des oscillations cérébrales dans l'effet sériel**.

Dans le **troisième projet**, nous avons testé si les oscillations cérébrales se propageaient à travers l'espace rétinotopique chez l'humain, entrainent des conséquences sur la perception visuelle. La propagation d'oscillations cérébrales au sein d'aires visuelles (V1, V2, V4, MT) a été mise en évidence avec des méthodes invasives chez l'animal (Sanchez-Vives and McCormick, 2000 ; Huang et al., 2004 ; Benucci et al., 2007 ; Han et al., 2008 ; Ray and Maunsell, 2011 ; Maris et al., 2013 ; Stroh et al., 2013 ; Muller et al., 2014 ; Zanos et al., 2015 ; Townsend et al., 2015 ; Davis et al., 2020). Pour des raisons éthiques, l'utilisation de méthodes d'enregistrements invasifs est limitée aux patients chez l'humain, ce qui a pour conséquence une étude plus difficile de la propagation des oscillations cérébrales à l'échelle mésoscopique. Pour surmonter cette limitation, nous avons mis au point une expérience de psychophysique, basée sur celle de Sokoliuk and VanRullen (2016), qui fait appel à nos connaissances sur le rôle de la phase dans la perception visuelle (Busch et al., 2009 ; Mathewson et al., 2009 ; Varela et al., 1981 ; Dugué et al., 2011a, 2015 ; Samaha et al., 2015, 2017 ; Fakche et al., 2022 ; Merholz et al., 2021 ; pour revue VanRullen 2016 ; Kienitz et al., 2021) et à l'organisation rétinotopique de V1, associée à un enregistrement EEG. **Nous avons mis en évidence que la perception**

visuelle était modulée de manière périodique à travers le temps et l'espace par la phase d'un stimulus périodique, suggérant que les oscillations alpha induites voyagent à travers l'espace rétinotopique pour moduler la perception, et ceci à une vitesse de propagation comprise entre 0.2-0.4 m/s (Fakche and Dugué, 2022, bioRxiv ; Galas, Fakche, Baudouin and Dugué, en préparation).

Dans le **quatrième projet**, nous avons étudié le rôle fonctionnel de la propagation des oscillations cérébrales alpha à l'échelle macroscopique dans la cognition humaine. En effet, des études récentes ont montré que la direction de propagation des oscillations était modulée durant les processus mnésiques (Sauseng et al., 2002 ; Zhang et al., 2018) et de perception visuelle (Shevelev et al., 2000 ; Schack et al., 1999, 2003 ; Patten et al., 2012 ; Alamia and VanRullen, 2019 ; Pang et al., 2020). Dans une première étude, nous avons testé si nous pouvions changer la direction de propagation des oscillations alpha en modulant la fonction cognitive engagée. Plus précisément, nous faisons l'hypothèse que durant le déploiement de l'attention endogène, la propagation est antéro-postérieure, et que cette propagation s'inverse lors de la perception visuelle. Nos premiers résultats valident cette hypothèse. **Nous observons une propagation des oscillations alpha des électrodes frontales vers celles occipitales durant le déploiement de l'attention endogène, et une inversion de cette propagation des électrodes occipitales vers celles frontales durant la perception d'une stimulation visuelle**.

Dans une deuxième étude, nous avons fait l'hypothèse qu'un pulse de TMS appliqué au niveau de V1 déclenchait de manière causale une oscillation se propageant des électrodes occipitales à celles frontales, à sa fréquence naturelle. De plus, cette propagation serait modulée par la perception d'un phosphene. Malheureusement, cette étude étant réalisée à Toulouse, en collaboration avec Rufin VanRullen, l'acquisition des données a été grandement retardée à cause de la pandémie du covid et de délais administratifs. **Nos résultats sur un participant suggèrent qu'un pulse de TMS appliqué au niveau du cortex occipital permet d'induire des oscillations cérébrales à leur fréquence naturelle, seulement lorsque le phosphene est perçu.** C'est un premier résultat encourageant pour tester notre hypothèse sur un lien causal entre la propagation postéro-antérieure des oscillations cérébrales induit par un pulse de TMS et la perception visuelle.

Ensemble, les différentes études réalisées au cours de cette thèse montrent que **les interactions entre les caractéristiques temporelles des oscillations cérébrales, ainsi que leur organisation spatiale, jouent un rôle important sur la perception visuelle humaine.**

A l'avenir, de nombreuses questions sur le rôle fonctionnel de l'organisation spatio-temporelle des oscillations cérébrales restent encore à élucider.

Tout d'abord, nous ferons toujours face aux limitations éthiques des enregistrements invasifs chez l'humain pour étudier la propagation des oscillations cérébrales, privilégiant des mesures en EEG, qui souffrent d'une résolution spatiale faible. Un élégant moyen de surmonter cette limitation est de développer des modèles. Grâce à nos connaissances, il est possible de modéliser l'activité spatio-temporelle d'une oscillation se propageant au sein d'une même aire, et entre plusieurs aires cérébrales, au niveau du cortex directement, i.e., sources neurales. Ces sources neurales peuvent ensuite être projetées sur les capteurs EEG. Il est alors ensuite possible de comparer des données EEG empiriques à celles prédites par le modèle. Cette approche, actuellement en développement dans notre équipe (Grabot et al., en préparation), permet d'étudier la propagation des oscillations cérébrales directement dans le cortex avec une méthode non-invasive.

Dans cette thèse, nous avons étudié la propagation d'une unique oscillation cérébrale à l'échelle mésoscopique et macroscopique. Mais le cerveau présente une activité oscillatoire spontanée, et reçoit de multiples stimulations internes et externes au même moment. Il est très probable que de multiples oscillations cérébrales voyagent au même moment, et donc interagissent ensemble. Mais quelle est la nature de cette interaction ? A l'échelle mésoscopique, des études chez l'animal suggèrent que deux oscillations se propageant peuvent : 1) Avoir un effet suppressif les unes sur les autres, 2) Fusionner, 3) Rester séparer. Nous aimerions étudier à l'avenir comment ces interactions entre les oscillations cérébrales jouent sur la perception.

Enfin, une question reste au jour d'aujourd'hui un grand mystère à titre personnel. Quel est le lien entre les oscillations à l'échelle mésoscopique et celles à l'échelle macroscopique ? Pour explorer cette question, nous aimerions à l'avenir développer une étude où les oscillations mésoscopiques et macroscopiques seront enregistrées de manière simultanée.

Pour conclure, **cette thèse a permis de contribuer aux recherches sur le rôle fonctionnel des oscillations cérébrales dans la cognition humaine**, bien que de nombreuses questions restent encore à explorer dans le futur.

Tables of contents.

Part 1. General Introduction.

Chapter 1. Brain oscillations, ubiquitous in the brain.

The first evidence of human brain oscillations was provided by Hans Berger in 1929 (**Figure 1.1**). At that time, Berger worked in the Department of Psychiatry and Neurology, in Jena, Germany, on brain's electrical activity. His main interest was the study of telepathy, i.e., the ability to communicate from mind to mind without any physical or sensorial means. Instead of showing that telepathy was a true phenomenon, he described for the first time a human oscillatory activity, mainly present in the occipital region, while participants were at rest. In his paper (Berger, 1929; **Figure 1.2**), he wrote: "The electroencephalogram represents a continuous curve with continuous oscillations in which […] one can distinguish larger first order waves with an average duration of 90 milliseconds and smaller second order waves of an average duration of 35 milliseconds. The larger deflections measure at most 150 to 200 microvolts […]." Berger called the first order waves of approximately 10 Hz, mainly induced by the closure of the eye, the alpha rhythm, because it was the first discovered; and the second order waves, more present when the eyes were open, the beta rhythm. Since this publication, Berger has had the intuition that brain oscillations could represent a reliable marker of brain activity that would be modulated by cognition, e.g., modulated by sensory stimulation, mental processing, vigilance state (awake, sleep, anesthetized) (Quigley, 2021). He continued his research for the following decades until he proposed a final version of his theory describing that the alpha rhythm was associated to rest, inhibited during sensory stimulation and mental tasks, and that high-frequencies (42-90 Hz, referred to as gamma later) would be a correlate of active brain activity (Quigley, 2021).

Figure 1.1: Hans Berger, the father of electroencephalography.

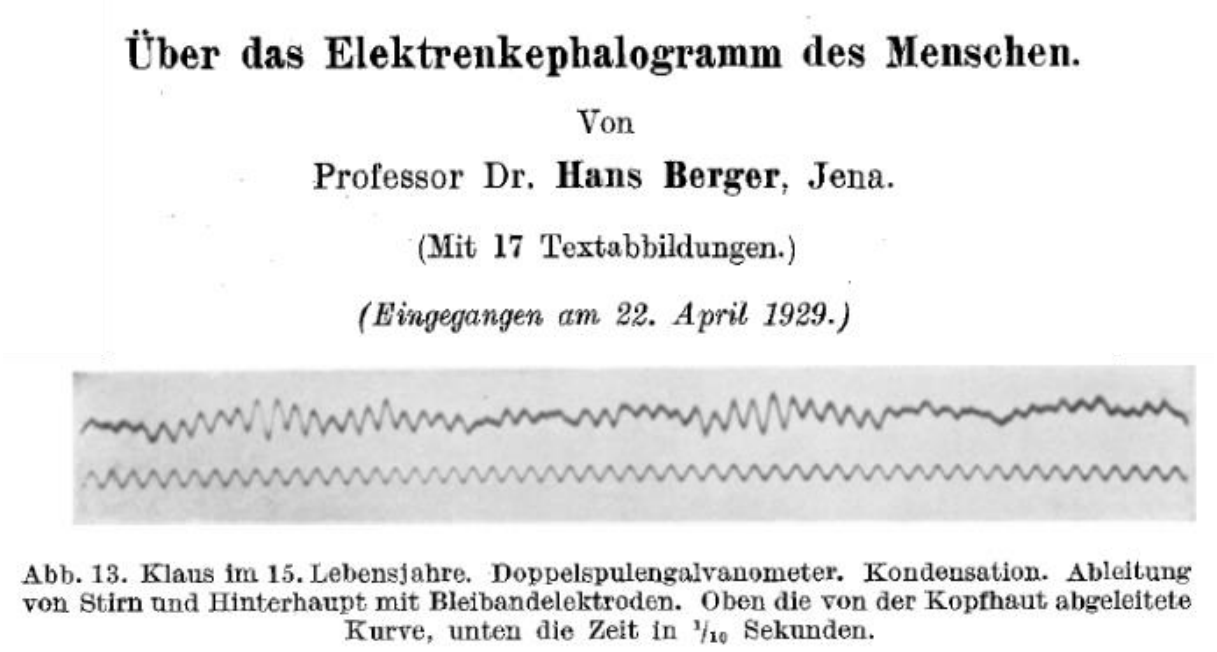

Über das Elektrenkephalogramm des Menschen.

Von

Professor Dr. **Hans Berger**, Jena.

(Mit 17 Textabbildungen.)

(Eingegangen am 22. April 1929.)

Abb. 13. Klaus im 15. Lebensjahre. Doppelspulengalvanometer. Kondensation. Ableitung von Stirn und Hinterhaupt mit Bleibandelektroden. Oben die von der Kopfhaut abgeleitete Kurve, unten die Zeit in $^1/_{10}$ Sekunden.

Figure 1.2: The first recording of alpha brain oscillations, from Berger, 1929. *Upper panel, title of the paper published by Berger in 1929. Translation: About the human electroencephalogram. Lower panel, upper line corresponds to the first recording of alpha brain oscillations, lower line, an alpha sinusoid at 10 Hz. Translation: Figure 13. Klaus at the age of 15. Double coil vanometer. Condensation. Derivation of the forehead and back with lead electrodes. Above, the curve derived from the scalp, below, the time in 1/10 second.*

This PhD work aims to contribute to the issues raised by Hans Berger almost a century ago concerning the functional role of brain oscillations on human cognition. In the **Introduction (Part 1)**, we will see that during the last decades, the features of brain oscillations (frequency, phase, amplitude; defined below) have been associated to cognitive functions, mainly *independently* from each other (**Part 1, Chapter 1**), i.e., the role of one specific frequency, the phase, or the amplitude, on one cognitive function. First, my PhD work investigates the *interaction* between the phase and amplitude on cognition, under a general physiological framework of alpha brain oscillations that could be applied to many different cognitive functions (**Part 2, Chapter 4**). In addition, we use a recent methodology to decode the spatial pattern of brain activity across time, i.e., classification algorithm, and associate these dynamics in cortical activity to human cognition (**Part 2, Chapter 5**). Second, my PhD work focus on the role of the spatio-temporal organization of brain oscillations on cognitive functions. Indeed, although the spatial dynamics of brain activity have been often observed *within* and *between* brain regions, their functional role has been poorly studied (**Part 1, Chapter 2**). We propose that not only the temporal aspect of brain oscillations but also their spatial

organization must be considered when investigating their functional role on cognition (**Part 2, Chapter 6 and Chapter 7**). To summarize, this PhD aims to demonstrate that **taking into account the spatio-temporal organization of brain oscillations** simultaneously, and in their entirety, i.e., the dynamics of the phase and amplitude across time and space, will allow us to **better understand their functional role on cognition** (**Part 1, Chapter 3**). Human cognition encompasses many brain functions, such as perception, attention, memory, consciousness, etc. Here, we decided to study **visual perception**, because of the important knowledge of the scientific community on vision, at a physiological, anatomical, and functional level. In addition, we aim to identify **causal links** between brain oscillations and cognitive functions. To do so, we use a non-invasive interventional technique, the transcranial magnetic stimulation. In sum, in this PhD work, we use a **multimodal approach** including **psychophysics**, **neuroimaging** (EEG, MRI, oculometry), and **non-invasive stimulation** (TMS), to investigate the causal, functional, role of the spatio-temporal organization of brain oscillations on visual perception.

Before going further, let us define what a brain oscillation is. A brain oscillation describes a brain activity that waxes and wanes periodically across time. It is characterized by its period, i.e., the duration of one oscillatory cycle, expressed in time units (**Figure 1.3.A**), its frequency, i.e., the speed of the oscillation, expressed in Hertz (s^{-1}) (**Figure 1.3.A**), its amplitude, i.e., the distance between the minimum and the maximum activity (**Figure 1.3.A**; note that the power corresponds to the amplitude squared), and by its phase, which describes the position along the oscillatory cycle at a given time point (**Figure 1.3.A**), expressed in degrees or in radians along the trigonometric cycle, i.e., the phase varies from 0° to 360°, from 0 to 2π (**Figure 1.3.B**).

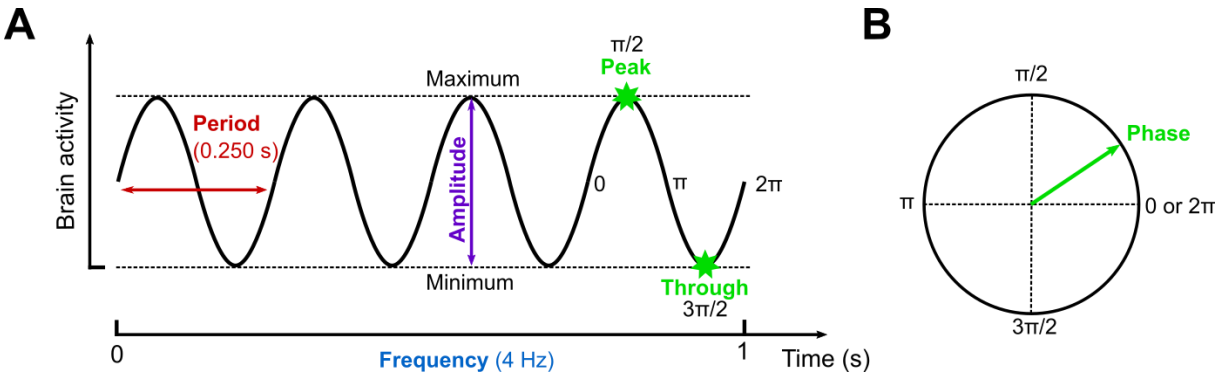

Figure 1.3: Oscillation's features. A. *A 4 Hz oscillation is represented. Its period corresponds to the duration of one cycle, 250 ms. Its amplitude corresponds to the distance between the minimum and the maximum activity. The phase varies from 0 to 2 π along one cycle, with the*

peak and the through corresponding to the maximum and the minimum activity, respectively. ***B.*** *Phase expressed along the trigonometric cycle.*

1. Functional role of brain oscillations

1.1. A frequency, a function?

Since their discovery in 1929, brain oscillations have been categorized into 5 frequency bands: delta (0.1 – 3 Hz), theta (4 – 7 Hz), alpha (8 – 12 Hz), beta (13 – 30 Hz) and gamma (> 30 Hz) (**Table 1**). At the beginning, the scientific community investigated whether these different frequency bands were associated to specific cognitive or sensorimotor functions (Jensen et al., 2014). But recently, this way of seeing the role of brain oscillation's frequency has been challenged. Instead of associating one cognitive function to one frequency band, several theories emerged to associate oscillatory frequency bands to more general brain processes, meaning that one frequency band would underlied different cognitive functions requiring a same underlying mechanism (Harmony, 2013; Buzsáki and Tingley, 2018; Klimesch et al., 2007a; Jensen and Mazaheri, 2010; Mathewson et al., 2011; Spitzer and Haegens, 2017; Merker, 2013; Fries, 2009). In addition, numerous studies highlighted that many frequency bands were involved in a same cognitive function.

I will present some functions that have been associated to each frequency bands, and recent theories on their general physiological role. I will then discuss the occurrence of specific frequency band oscillations for a same cognitive function.

Delta oscillations are well known to emerge during the slow waves sleep, the deeper stage of sleep where people are less sensitive to the environmental stimuli and high-level processes are inactive (Loomis et al., 1935). During state of awakening, the amplitude of delta oscillations increases in frontal regions during tasks which require internal cognition and simultaneously inhibition of the external environment, such as mental calculation, working memory, response inhibition (Harmony, 2013). Delta oscillations have thus been proposed to support **internal mentation** processes, i.e., the manipulation of internal representation, such as solving problems or reflect upon the past or the future, by inhibiting the external or irrelevant internal stimuli during sleep and awake states (Harmony, 2013).

Theta oscillations, more precisely, the hippocampal (and para-hippocampal) theta oscillations, have been largely involved in spatial navigation, time representation, and episodic memory function (Korotkova et al. 2018; Buzsáki and Tingley, 2018; Herweg et al., 2020).

Theta oscillations have a beneficial role on episodic memory, i.e., the memory of our past personal experiences, that implies the encoding of the spatio-temporal dimension, and the associated perceptual or emotional contents (Klimesch et al., 1997; Osipova et al., 2006; Guderian et al., 2009; Hanslmayr et al., 2011; Staudigl and Hanslmayr, 2013).

The role of the hippocampal theta in coding the spatial dimension came originally from the phenomenon of place cells, observed in rats (Burgess et al., 1992; Skaggs et al., 1996). The theta phase precession effect describes that there is a systematic relation between the rat's position in a given place field, the phase of the theta rhythm, and the firing rate of the associated place cells (Burgess et al., 1992; Skaggs et al., 1996). In humans, researchers found an equivalent of place cells in the hippocampus and an increase in the amplitude of theta oscillations during spatial navigation (Kahana et al., 1999; Ekstrom et al., 2003, 2005).

Theta oscillations seem to also contribute to the coding of the temporal dimension, through the activation of time cells. The firing pattern of time cells depends on events that occur reliably at particular moments in time, independently of the spatial information and of the behavior (MacDonald et al., 2011; Kraus et al., 2013). Interestingly, the theta phase precession effect observed in place cells also occurred in time cells (Pastalkova et al., 2008).

Regarding the role of hippocampal theta in space, time, and memory, Buzsáki and Tingley proposed that theta oscillations would act as **sequential generator** (Buzsáki and Tingley, 2018). Hippocampal theta oscillations would be an internal 'timer' in the brain, whose units can be modulated (space or time), shrunk and expanded, according to the external stimuli. According to this theory, the "episodic memory is simply an ordered sequence of translationally invariant *whats* and their related context (another *what*), with no explicit internal *representation* of space or time" (**Figure 1.4**; Buzsáki and Tingley, 2018).

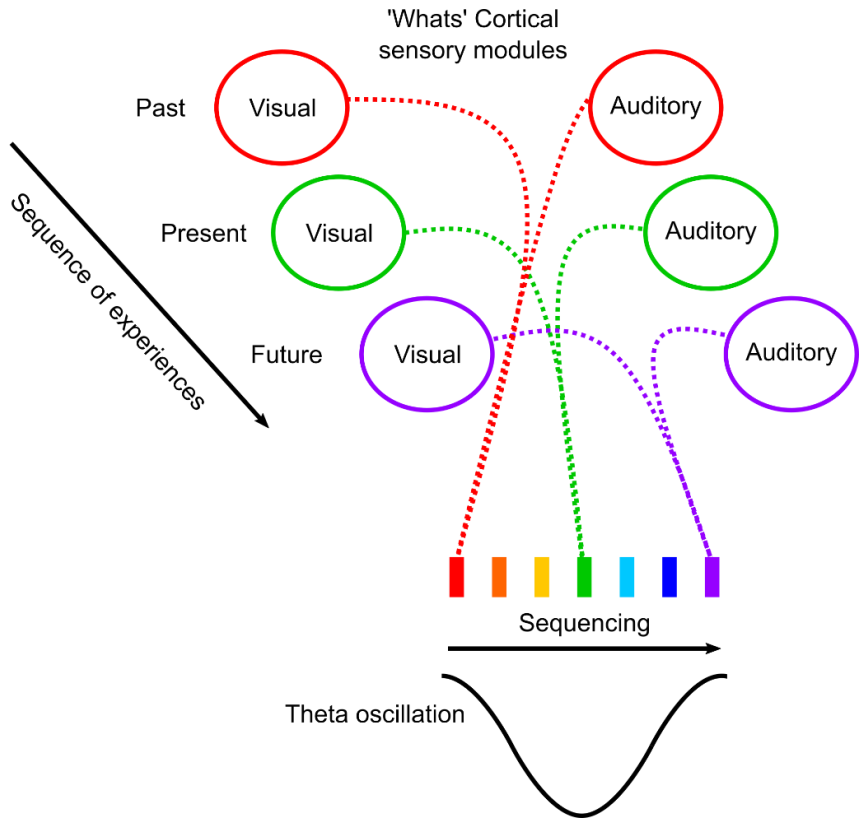

Figure 1.4: Theta hippocampal rhythm, a sequential generator, adapted from Buzsáki and Tingley, 2018. *Cortical sensory modules ('whats') are sequenced by the theta oscillations in the hippocampus, allowing to preserve the ordinal structure over which the multisensory experiences occur.*

Alpha oscillations have been associated with cortical idling in early EEG research, because the brain is firing spontaneously and synchronously at 10 Hz when participants are at rest (Berger, 1929; Adrian and Mathews, 1934a). Similarly, the suppression of alpha oscillations has been correlated to an increase in performance in various cognitive tasks (Pfurtscheller and Da Silva, 1999; Klimesch et al., 2007a), some involving memory functions (Sterman et al., 1996; Klimesch et al., 1996), and others attentional processes (Boiten et al., 1992; Dujardin et al., 1993).

Later, some studies suggested that alpha oscillations allowed to prevent the processing of incoming stimuli irrelevant to ongoing memory task (Klimesch et al., 1999; Jensen et al., 2002; Sauseng et al., 2005a; Cooper et al., 2003). The hypothesis of cortical idling was challenged. Alpha oscillations seem to have a **functional inhibition** role, i.e., their amplitude increases in order to inhibit the brain regions unrelated to the ongoing cognitive task, allowing the related-task brain areas to be fully active (**Figure 1.5**; Klimesch et al., 1999; Jensen et al., 2002). Indeed, a low amplitude of alpha oscillations in occipital regions have been associated

to higher visual performance (Ergenoglu et al., 2004; Hanslmayr et al., 2007; Van Dijk et al., 2008). During spatial visual attention tasks, the amplitude of alpha oscillations decreases in the visual hemisphere contralateral to the attended stimuli, while the amplitude of alpha increases in the ipsilateral hemisphere, to inhibit the unattended incoming stimuli (**Figure 1.6,** alpha lateralization effect; Worden et al., 2000; Sauseng et al., 2005b; Thut et al., 2006; Händel et al., 2011). The functional inhibition of alpha oscillations has been proposed to act in a pulsed, phasic manner. This hypothesis has been called the **Pulsed Inhibition theory** (Klimesch et al., 2007a; Jensen and Mazaheri, 2010; Mathewson et al., 2011), and will be further developed in **Chapter 4**.

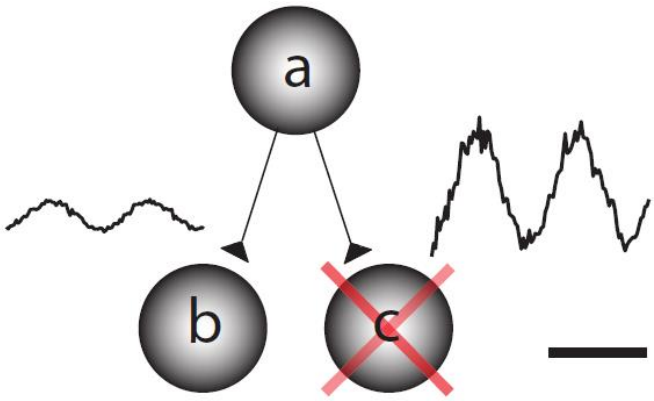

Figure 1.5: Gating by alpha inhibition, from Jensen and Mazaheri, 2010. *Here is a situation in which relevant information has to be transferred from cortical node a to cortical node b, but not from cortical node a to cortical node c. The node c is actively suppressed by functional inhibition, allowing to gate the information flow from node a to node b. The functional inhibition is reflected by alpha brain oscillations.*

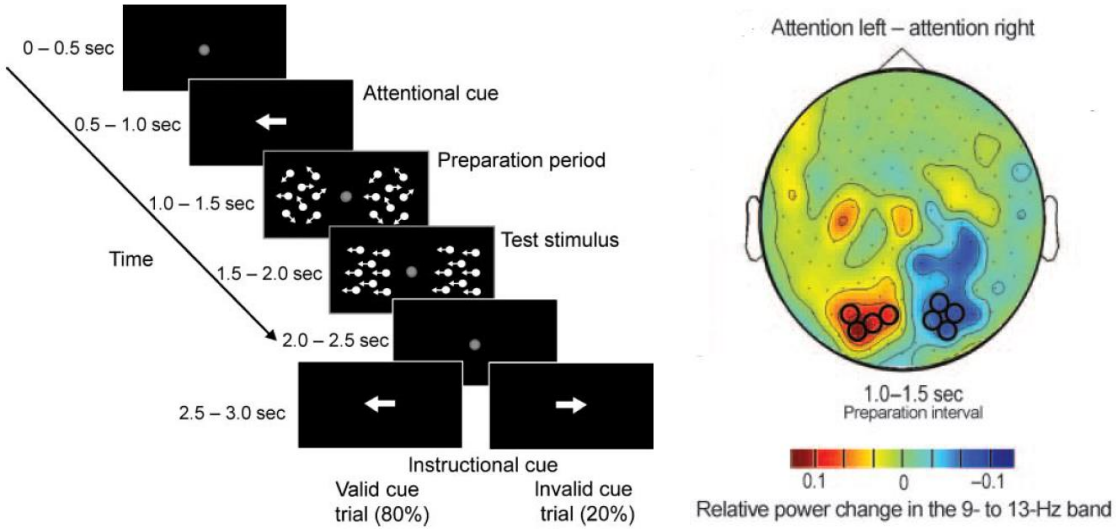

Figure 1.6: The alpha lateralization effect induced during a visual attention task, from Händel et al., 2011. *Left panel, Experimental paradigm. After a fixation period, an attentional cue indicates to participants whether they have to orient their attention to the left or to the right*

visual hemifield. The cue is followed by random dot kinematograms (RDK), i.e., an ensemble of moving dots, with an incoherent motion during the preparation period; and with a coherent motion to the left or to the right during the test period, that could differ between the two RDKs. After a delay, an instructional cue indicates to the participants the motion of the RDK they have to report. The instrucional cue could indicate the same visual hemifield as the attentional cue, it is a valid trial, or the opposite visual hemifield, it is an invalid trial, participants have to reorient their attention. Right panel, Topography of the alpha (9-13 Hz) amplitude, plotted as the difference between trials in which attention was focused on the left hemifield compared with attention focused on the right hemifield, during the preparation period. When attention is focused on the left hemifield compared to the right hemifield, we observe an increase in alpha amplitude in the ipsilateral hemisphere of the occipital cortex, and a decrease in the controlateral hemisphere.

Beta oscillations have been widely involved in sensorimotor functions (Kilavik et al., 2013), i.e., during tactile stimulation (Cheyne et al., 2003), movement execution (Cassim et al., 2000; Crone et al., 1998; Pfurtscheller et al., 1996), motor imagery (McFarland et al., 2000), movement observation (Babiloni et al., 2002).

Beta oscillations also play a role in cognitive processes, especially in working memory and decision-making tasks (Spitzer and Haegens, 2017). The amplitude of beta oscillations over fronto-parietal areas increases during the maintenance of information into working memory (Tallon-Baudry et al., 1998; Wimmer et al., 2016; Deiber et al., 2007; Chen and Huang, 2016; Honkanen et al., 2015). Some studies highlighted that the increased amplitude in the beta band was not sustained throughout the entire delay of memory retention, but only for the late several hundreds of milliseconds, presumably when the information retained into working memory has to be endogenously reactivated (Spitzer and Blankenburg, 2011; Spitzer et al., 2014; Wimmer et al., 2016). Several studies also showed that beta oscillations are involved in decision making processes (Haegens et al., 2011a; Herding et al., 2016; Stanley et al., 2018).

Beta oscillations in sensorimotor and cognitive functions have been proposed to reflect the maintenance of a status-quo, when no change is expected (Engel and Fries, 2010). Indeed, beta oscillations are widely expressed in the brain during the maintenance of a motor command (Baker et al., 1997; Chakarov et al., 2009) and during the retention of memory information (Tallon-Baudry et al., 1998; Wimmer et al., 2016; Deiber et al., 2007; Chen and Huang, 2016). Later, Spitzer and Haegens (2017) proposed that beta oscillations could play a key role in the **endogenous re-activation** of cortical representations through top-down attentional control (**Figure 1.7**). This hypothesis is coherent with the results observed in working memory and decision-making tasks, where beta oscillations occur in short-time windows, during the recall

of past information in order to provide a response to the task (Spitzer and Blankenburg, 2011; Spitzer et al., 2014; Wimmer et al., 2016; Haegens et al., 2011; Herding et al., 2016; Stanley et al., 2016).

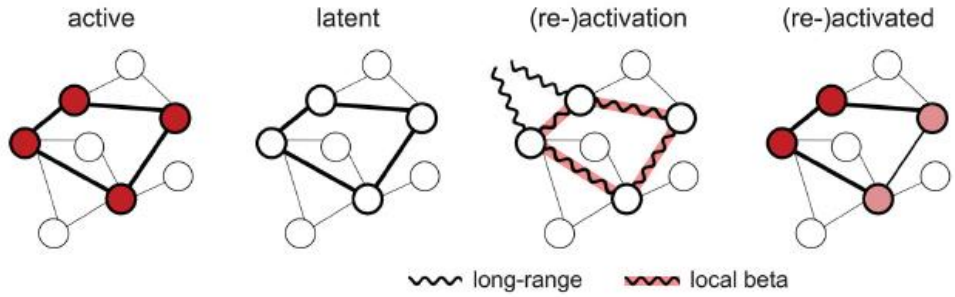

Figure 1.7: The endogenous content (re-)activation, from Spitzer and Haegens, 2017. *Left, Active cortical representations, characterized by spiking activity (symbolized in red) in neuronal ensembles. Second from left, Relevant information are maintained in latent memory representations, without spiking activity. Second from right, Endogenously driven (re-) activation of neuronal ensembles according to a brief increase in beta oscillations, under the control of long-range top-down connections. Right, (Re-)activated content representations, characterized by spiking activity in the neuronal ensemble, similar but not necessarily exactly identical to cortical representations in the left panel.*

Gamma oscillations have been linked to many high-level cognitive functions, including attention, memory, visual perception, sensorimotor integration, multisensory integration, language, and consciousness (Tallon-Baudry, 2009; Uhlhaas et al., 2011; Merker, 2013). The involvement of gamma oscillations in such a variety of cognitive and sensorimotor functions strongly suggests that these oscillations have a role in a more general physiological process.

Gamma oscillations appear to reflect **neural activity**. There is a strong relation between gamma oscillations and the hemodynamic response, i.e., cerebral blood flow measured by the blood oxygen-level dependent (BOLD) (Mukamel et al., 2005; Niessing et al., 2005, Lachaux et al., 2007; Zaehle et al., 2009; Conner et al., 2011; Ossandón et al., 2011). The amplitude of gamma oscillations is positively correlated with BOLD changes (Mukamel et al., 2005; Niessing et al., 2005; Lachaux et al., 2007; Zaehle et al., 2009; Conner et al., 2011), and the amplitude in the gamma band decreases with BOLD deactivation in the default mode network (**Figure 1.8**; Ossandón et al., 2011). Gamma oscillations are also related to spiking activity. Animal studies showed that single and multiple spiking activity was correlated with gamma oscillations in the local field potential (**Figure 1.9;** Eckhorn et al., 1988; Gray and Singer, 1989; Friedman-Hill et al., 2000; Maldonado et al., 2000; Wang, 2010).

It has been proposed that gamma oscillations play a key role to regulate the pattern of firing activity by acting as a mechanism of rhythmic **gain modulation** (Merker, 2013; Fries et al., 2009). Considering that the gain is modulated cyclically by 40-80 Hz gamma oscillations, the gain cycle is relatively short (12-25 ms), leading to rapid alternance between excitatory and inhibitory cortical states. Consequently, the input integration would strongly depend on the precision and the phase of the synchronization between the timing of input occurrence and the gain cycle. Following these considerations, new theory emerged, suggesting a role of **gamma oscillations synchrony** between neuronal or cortical structures (Fries et al., 2009).

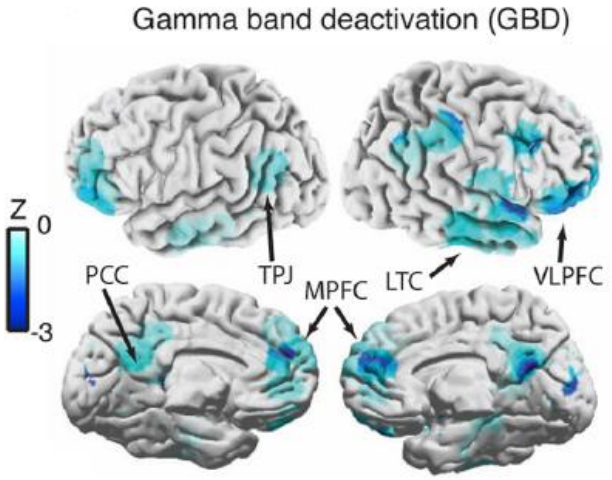

Figure 1.8: Gamma oscillations' amplitude decreases during visual search, from Ossandón et al., 2011. *A significant broad-band gamma (60-140 Hz) suppression is observed in regions involved in the default mode network.*

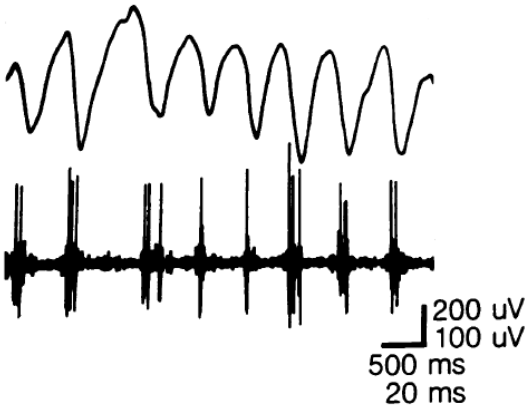

Figure 1.9: Multi-Unit Activity (MUA) and Local Field Potentials (LFP) recorded from area 17 in cats to the presentation of oriented light bar moving across the receptive field, from Gray and Singer, 1989*. Oscilloscope recordings of a single trial showing the response to the preferred direction of movement. Upper trace, neuronal oscillations (35-45 Hz) in the LFP. Lower trace, rhythmic MUA synchronized in phase with the LFP.*

In sum, several theories now associate oscillatory frequency bands to general brain processes (**Table 1**; Harmony, 2013; Buzsáki and Tingley, 2018; Klimesch et al., 2007a; Jensen and Mazaheri, 2010; Mathewson et al., 2011; Spitzer and Haegens, 2017; Merker, 2013; Fries, 2009).

Critically, some cognitive functions are supported by oscillations in a broad range of frequency bands. Numerous studies showed that delta, alpha, and beta oscillations over the fronto-parietal areas are involved in memory function. An increase in amplitude of these oscillations is associated with memory load and the maintenance of multisensorial information in working memory (**delta**: Harmony, 2013; **alpha**: Klimesch et al., 1999; Jensen et al., 2002; Sauseng et al., 2005a; Cooper et al., 2003; **beta**: Tallon-Baudry et al., 1998; Wimmer et al., 2016; Deiber et al., 2007; Chen and Huang, 2016; Honkanen et al., 2015). Hippocampal **theta** oscillations play a crucial role in episodic memory (Klimesch et al., 1997; Osipova et al., 2006; Guderian et al., 2009; Hanslmayr et al., 2011).

Similarly, for the motor function, we observe a decrease in mu, i.e., sensorimotor alpha, and beta oscillations over the parietal cortices during motor preparation, movement execution, motor imagery, and motor observation (**mu**: Neuper et al., 2006; **beta**: Kilavik et al., 2013; Cassim et al., 2000; Crone et al., 1998; Pfurtscheller et al., 1996; McFarland et al., 2000; Babiloni et al., 2002).

Finally, some studies have observed the emergence of oscillations in different frequency bands during the deployment of endogenous attention. When the attention is deployed at a given spatial location, **alpha** oscillations are observed (Worden et al., 2000; Sauseng et al., 2005b; Thut et al., 2006; Händel et al., 2011) while in tasks with stimuli displayed at multiple locations, the emergence of **theta** oscillations is observed (Dugué et al., 2015a, b, 2019; Landau & Fries, 2012; Fiebelkorn et al., 2013a; Song et al., 2014; Huang et al., 2015; Fiebelkorn et al., 2018; Helfrich et al., 2018; VanRullen, 2016a; Dugué & VanRullen, 2017).

Frequency Band	Frequency Range	Associated cognitive functions	General process
Delta (δ)	0.1 – 3 Hz	Slow Waves Sleep, Mental calculation, Working memory, Response inhibition	**Internal mentation** (Harmony, 2013)
Theta (θ)	4 – 7 Hz	Spatial navigation, Time representation, Episodic memory, Attention	**Sequential generator** (Buzsáki and Tingley, 2018)
Alpha (α)	8 – 12 Hz	Memory, Visual perception, Attention, Motor function	**Functional inhibition** (Klimesch et al., 2007a; Jensen and Mazaheri, 2010 Mathewson et al., 2011)
Beta (β)	13 – 30 Hz	Sensorimotor process, Working memory, Decision making	**Endogenous content (re) activation** (Spitzer and Haegens, 2017)
Gamma (γ)	> 30 Hz	Many cognitive and sensorimotor functions	**Neural activity, Gain modulation, Synchrony** (Merker, 2013; Fries, 2009)

Table 1: The relation between oscillatory frequency bands and general physiological brain process.

Because of these considerations, the association between cognitive functions and different oscillatory frequency bands seems now obsolete. Although the identification of one oscillatory frequency band involved in a cognitive process is still informative, it should be considered with caution. It is also important to identify the localization of brain oscillations, e.g., hippocampal, and neocortical theta oscillations appear to have completely different roles. Lastly, more and more studies turn their focus on the other characteristics of brain oscillations, the amplitude and the phase, which are going to be discussed in the two following sections. The aim of this PhD is to study the functional role of brain oscillations in perception. For this reason, we focus on studies showing a relation between amplitude and phase of brain oscillations and perceptual processes.

1.2. Changes in amplitude, changes in brain dynamics and perception.

The amplitude of brain oscillations has been associated with cortical activity, indexed directly by the measure of neuronal spiking activity, or indirectly by the measure of the cerebral blood flow with the blood oxygen-level dependent contrast measure obtained with functional magnetic resonance imagery (fMRI), i.e., the fMRI-BOLD response.

The hemodynamic responses covaried in localization and in timing, positively with gamma oscillations, and negatively with lower frequency oscillations (delta, theta, alpha, and beta) (**Figure 1.10**) (Logothethis et al., 2001; Brookes et al., 2005; Niessing et al., 2005; Mukamel et al., 2005; Goense and Logothethis, 2008: Koch et al., 2009; Zumer et al., 2010; Yuan et al., 2010; Singh et al., 2002; Goldman et al., 2002; Laufs et al., 2003; Moosmann et al., 2003; Scheeringa et al., 2009, 2008, 2011a). Similarly, the neuronal spiking activity was negatively correlated with the amplitude of oscillations in low frequency bands (delta, theta, and alpha), and positively correlated with the amplitude of high-frequency (gamma) oscillations (Manning et al., 2009; Haegens et al., 2011b; Mukamel et al., 2005; Rasch et al., 2008; Ray et al., 2008a, 2008b; Belitski et al., 2008; Ray and Maunsell, 2011; Zanos et al., 2012).

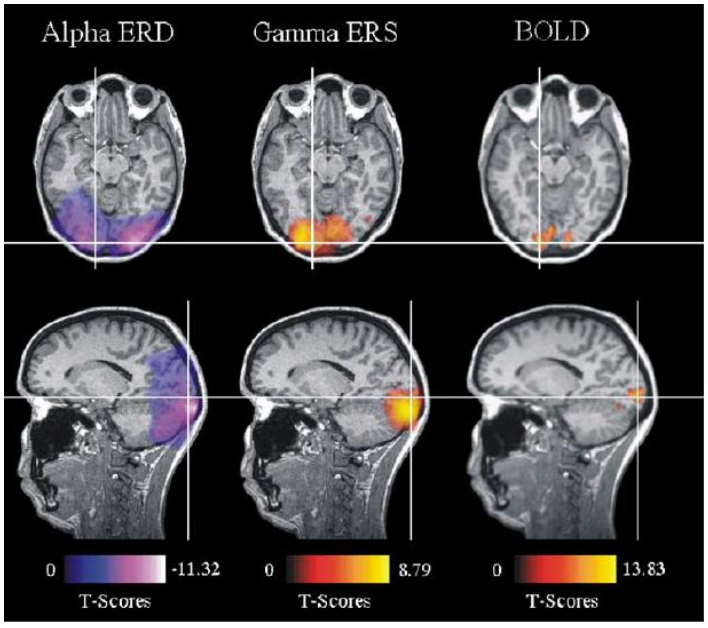

Figure 1.10: The spatial distribution of alpha event-related desynchronization, gamma event-related synchronization, and BOLD signals, from Brookes et al., 2005. *Alpha and gamma oscillatory activity was recorded with MEG. Blue color, decreased activity. Orange color, increased activity. Increased activity of BOLD signal in the visual cortex was associated to an increased oscillatory response in the gamma band, and a decreased oscillatory response in the alpha band.*

Interestingly, the correlation between the amplitude of brain oscillations and cortical activity are in line with the functional role of amplitude on perception.

The role of brain oscillations' amplitude on perceptual performance has been widely studied in the **visual modality**. A low amplitude of alpha oscillations localized in the parieto-occipital cortices was associated to a higher probability to perceive a subsequent visual stimulus (Ergenoglu et al., 2004; Hanslmayr et al., 2007; Van Dijk et al., 2008; Wyart and Tallon-Baudry, 2009). This facilitatory effect has also been found during the deployment of endogenous spatial attention, i.e., a low amplitude of alpha oscillations in the cortical hemisphere contralateral to an attended stimulus was associated with higher perceptual performance (Worden et al., 2000; Sauseng et al., 2005b; Thut et al., 2006; Händel et al., 2011). In addition, in a fusion effect task, i.e., two visual stimuli are presented with one or no tactile stimulation, low alpha amplitude predicted the perception of indeed two visual stimuli, while high alpha amplitude led to the misperception of a single stimulus (Lange et al., 2013). The authors proposed that instead of improving visual perception per se, lower alpha amplitude would reflect an increase in cortical excitability in the visual cortex (Lange et al., 2013). Concerning high-frequency oscillations, a high amplitude of gamma oscillations has been associated with a higher probability of stimulus perception (Wyart and Tallon-Baudry, 2009; Lange et al., 2013).

Several studies also revealed a crucial role of spontaneous oscillations over somatosensory cortices in **tactile perception**. The amplitude of alpha and beta oscillations is negatively correlated with the subsequent tactile perception (Linkenkaer-Hansen et al., 2004; Schubert et al., 2009; Jones et al., 2010; Zhang and Ding, 2010; Van Ede et al., 2012; Weisz et al., 2014). The decreased in alpha and beta oscillatory amplitude would account for 29% of the improvement in tactile perception (Van Ede et al., 2012).

Finally, the amplitude of brain oscillations has been associated to the **auditory modality**. As for visual perception, a decreased amplitude of alpha and beta band oscillations over the auditory cortices lead to an increase in the strength of auditory perception (Leske et al., 2014). A low amplitude of alpha oscillations over the auditory cortices is on the contrary associated to an increase in phantom sound sensation (i.e., tinnitus illusion) (Weisz et al., 2005; Müller et al., 2013a), and in the perception of illusory music (Müller et al., 2013b).

To summarize, numerous studies highlighted the role of brain oscillation's amplitude on perception in different modalities (visual, sensorimotor, auditory). A reduced amplitude in low frequency oscillations (delta, theta, alpha, beta) is associated to a higher state of cortical excitability, i.e., increased hemodynamic response and increased neuronal spiking activity, leading to better perceptual performance. Inversely, a lower amplitude of gamma oscillations is associated to weaker state of cortical excitability and reduced perception ability.

1.3. Rhythmicity in the brain, rhythmicity in perception: the role of phase.

A few studies have investigated the modulation of the fMRI-BOLD response by the phase of brain oscillations. Scheeringa et al., (2011b) used fMRI coupled with a simultaneous EEG recording to study the role of alpha phase on cortical activity at the onset of a brief visual stimulus. They showed a strong modulation of the BOLD response by the phase of alpha oscillations in the early visual areas (e.g., V1/V2), with a larger BOLD response when the onset of the visual stimulus was presented at the trough of the alpha cycle compared to the visual stimulus presented at the peak (Scheeringa et al., 2011b). Similarly, Hanslmayr et al. (2013) found that the BOLD response was modulated periodically by the phase of theta (7 Hz) oscillations in the intra-parietal sulcus (IPS), with a lower BOLD response at the trough of the theta cycle (Hanslmayr et al., 2013) (**Figure 1.11**).

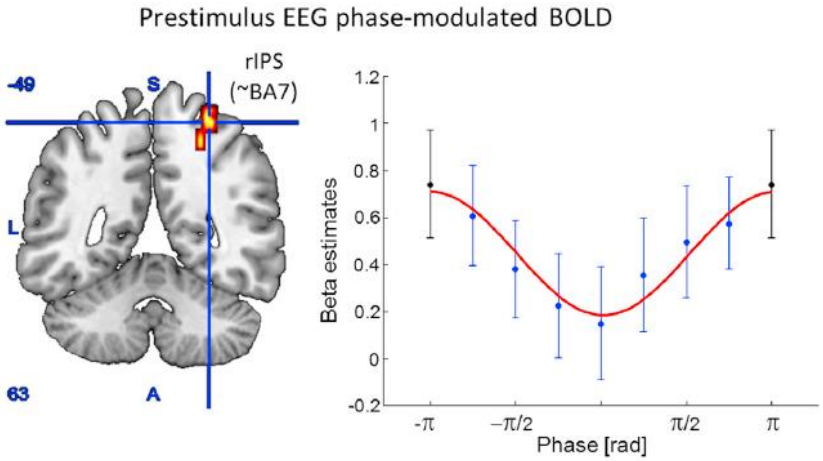

Figure 1.11: The phase of theta oscillations modulates the BOLD response, from Hanslmayr et al., 2013. *Beta estimates of the BOLD response were assigned to eight phase bins of the EEG oscillations in the right IPS at 7 Hz, -250 ms before stimulus onset. The data were fitted to an inverted cosine function. Error bars, standard error of the mean.*

Numerous studies found that the likelihood of neuronal firing, assessed with multiple spiking activity (MUA), depends on the instantaneous phase of low (delta, theta, alpha) and high-frequency (gamma) brain oscillations recorded with LFP (Gray and Singer, 1989; Csicsvari et al., 2003; Lakatos et al., 2005; Rasch et al., 2008; Montemurro et al., 2008; Vinck et al., 2010; Haegens et al., 2011b; Zanos et al., 2012). Whittingstall and Logothetis (2009) even showed that the phase of delta oscillations at the cortical surface, i.e., measured with EEG, modulated the spiking activity, with an optimal phase for neuronal firing at the trough of the delta cycle, around π (**Figure 1.12**).

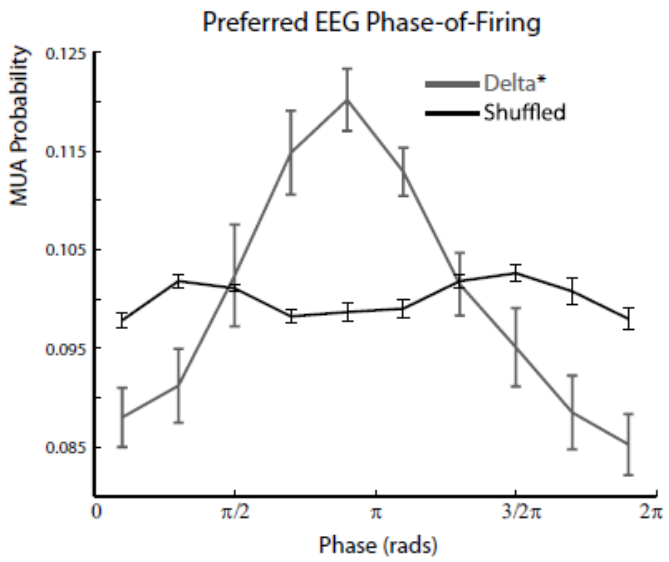

Figure 1.12: Multi-Unit Activity (MUA) is modulated by the phase of delta EEG oscillations, from Whittingstall and Logothetis, 2009. *MUA, recorded in visual areas of alert monkeys during natural movies displayed, was assigned to ten phase bins of the delta oscillation. Error bars, standard error of the mean. Shuffled data showed no significant tuning to MUA activity.*

Cortical activity is periodically modulated by the phase of brain oscillations. Thus, if the phase has a functional role on perception, our perceptual performance will fluctuate periodically, as cortical activity does.

The idea of perceptual cycles emerged a few centuries ago with the notion of discrete perception (VanRullen & Koch, 2003). The discrete perception theory describes that, although the integration of our environment seems continuous, in reality, we do not experience our world continuously, but as a series of discrete "moments," similar to the sequence of snapshots in movies. In the past decades, the notion of discrete perception has evolved to the notion of rhythmic (also called periodic or cyclic) perception. Rhythmic perception implies that the integration of our world is continuous, but perception would be facilitated during favorable

"moments" and inhibited at non-favorable "moments" (VanRullen, 2016a). The consequence of rhythmic perception is to produce **perceptual cycles**. According to the cyclic nature of brain oscillations, neuroscientists thought that they are the ideal candidate to be the neural support of rhythmic perception. There should be an optimal phase, associated with higher states of cortical excitability, that leads to better perceptual performance, and an opposite, non-optimal phase associated with more inhibitory cortical states, leading to impaired perceptual performance.

Numerous studies showed that perceptual performance fluctuated rhythmically according to the phase of low frequency brain oscillations. In visual detection tasks, the same stimuli lead to differential perceptual outcomes (e.g., perceived vs unperceived) according to the instantaneous phase of spontaneous low frequency (delta, theta, alpha) brain oscillations (**Figure 1.13**) over the fronto-occipital areas (Nunn and Osselton, 1974; Varela et al., 1981; Busch et al., 2009; Mathewson et al., 2009; Busch and VanRullen, 2010; Dugué et al., 2011a; Fiebelkorn et al., 2013b; Hanslmayr et al., 2013; Manasseh et al., 2013). The trial-by-trial perceptual variability explained by the phase of spontaneous oscillations is on average below 20% (Dugué et al., 2011a; VanRullen, 2016a).

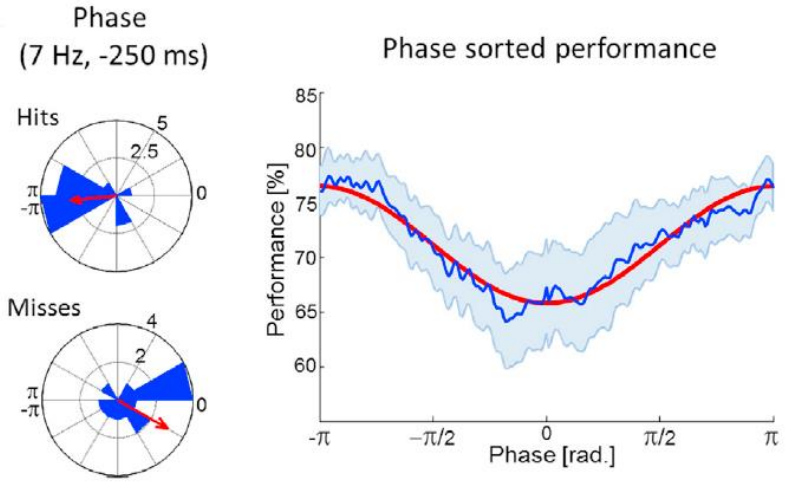

Figure 1.13: Perceptual performance is modulated periodically by the phase of theta brain oscillations, from Hanslmayr et al., 2013. *Participants performed a contour detection task simultaneously of an EEG recording. Left panel, phase of spontaneous oscillations averaged across participants. The phase is uniformly distributed around π for hits, whereas the phase is uniformly distributed around 0 for misses. Right panel, hits sorted according to the pre-stimulus phase at 7 Hz, -250 ms. Shaded area, standard error of the mean. Red curve, fit to an inverted cosine function.*

Because the phase of low frequency brain oscillations shapes visual perception, differences in the frequency of occipital oscillations should influence the temporal resolution

of visual perception. If two stimuli are presented during the same alpha cycle, they should be perceived as a single stimulus, resulting in a lower temporal resolution for perception for lower alpha frequencies (**Figure 1.14**). This hypothesis has been tested by Samaha and Postle (2015). They used a two-flash fusion threshold experiment: two spatially overlapping light flashes are presented successively with varying interstimulus interval (ISI), the shortest ISI allowing to discriminate the two flashes corresponds to the temporal resolution of visual perception. They found that participants with higher alpha frequency had significantly lower two-flash fusion threshold, meaning that they could discriminate two flashes at an ISI at which participants with lower alpha frequency perceived a single stimulus (Samaha and Postle, 2015). This study highlighted the crucial role of the phase of spontaneous brain oscillations in the temporal framing of visual perception. In visual search experiments, i.e., participants have to find a target among distractors, it has been showed that the frequency of the attentional cycles increased with the complexity of the task (Merholz et al., 2022). When participants had to find a + sign among L, the sampling frequency was at 7 Hz, whereas when the target was a T among L, the stimuli were sampled at 9.7 Hz (Merholz et al., 2022). These results suggest that the sampling frequency structure the temporal dynamics of neural activity as a function of the cognitive demand.

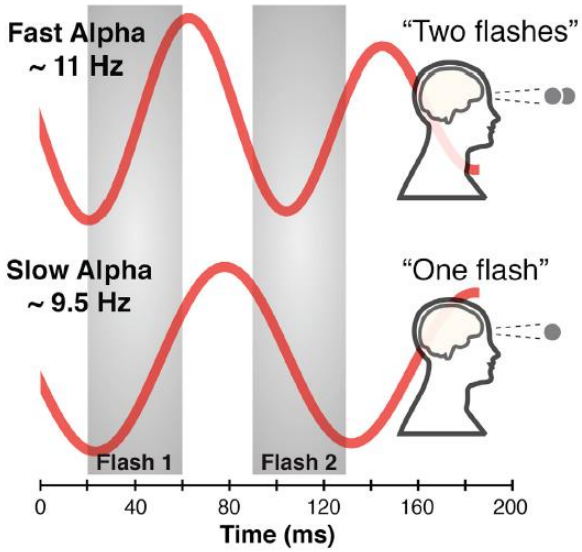

Figure 1.14: The frequency of alpha occipital brain oscillations predicts the temporal resolution of visual perception, from Samaha and Postle, 2015. *A fast alpha is associated with a better temporal resolution, i.e., participants perceived two flashes while the participants with a slower alpha perceived a single flash under the same experimental conditions.*

Similarly, one study used the flash-lag effect, i.e., the perceived location of a moving stimuli at the onset of a brief flash is delayed, to test whether the conscious updating of the

visual environment is cyclic (Chakravarthi and VanRullen, 2012). They found that the phase of low frequency brain oscillations (theta, alpha, beta) predicted the duration of the misperception induced by the flash-lag effect. These results suggest that the updating of the visual environment depend on the phase of brain oscillations (Chakravarthi and VanRullen, 2012).

Some studies demonstrated the presence of perceptual cycles with only psychophysical measurements (i.e., no electrophysiological recordings). They showed that participants sampled their visual environment periodically at a theta rhythm, in tasks where participants have to focus their attention sequentially on different visual stimuli (e.g., visual search experiment) (Landau & Fries, 2012; Fiebelkorn et al., 2013a; Song et al., 2014; Huang et al., 2015; Dugué et al., 2015b, 2017; Senoussi et al., 2019; Michel et al., 2021; for review, see Kienitz et al., 2021).

Finally, the role of phase on visual perception has been revealed through visual illusions, the most famous one being the wagon-wheel illusion, i.e., an impression that moving objects, as a wagon-wheel, reverse spontaneously their motion direction in movies because of the temporal subsampling of a discrete system, e.g., a video camera (**Figure 1.15**). Interestingly, the wagon-wheel illusion can also be observed in continuous light, suggesting a discrete sampling of the human visual system (Purves et al., 1996). By varying the rotation speed of a wheel, studies revealed that illusory reversal occurred preferentially around 10 Hz, suggesting that motion perception come from discrete sampling in the visual system every 100 ms (VanRullen et al., 2005, 2006, 2007; Reddy et al., 2011). Indeed, neuroimagery recordings showed that the wagon-wheel illusion was associated with brain oscillations at 13 Hz over the right parietal regions (VanRullen et al., 2006; Reddy et al., 2011).

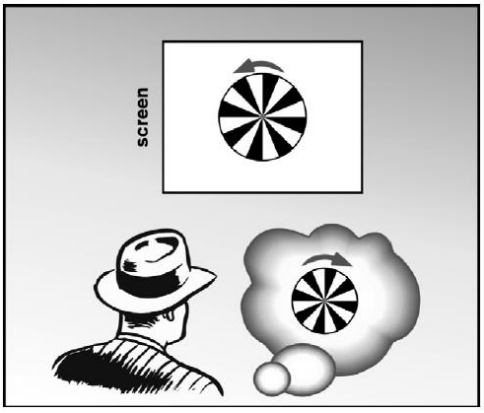

Figure 1.15: The wagon-wheel illusion, from VanRullen, 2007. *A rotating wheel is perceived as if it moves backward because of temporal subsampling of a discrete system, i.e., video camera, visual system.*

The role of oscillatory phase on perception has been widely studied in the visual modality, but some studies showed perceptual cycles in other sensory modalities. In the tactile modality, the probability of near-threshold stimulus detection depends on the phase of very slow (0.01 – 0.1 Hz) EEG oscillations, with a variability explained between the optimal ($-\pi/2$) and the non-optimal ($\pi/2$) phase as large as 55% (Monto et al., 2008), and on the phase of spontaneous alpha and beta oscillations (Ai and Ro, 2014; Baumgarten et al., 2015).
Similarly, the perception of near-threshold auditory stimulation was modulated by the phase of delta (Zoefel and Heil, 2013; Herrmann et al., 2016), theta (Ng et al., 2012) and alpha oscillations (Rice and Hagstrom, 1989). In addition, theta and alpha oscillations are involved in syllable perception (Ten Oever and Sack, 2015) and speech processing (Luo and Poeppel, 2007; Strauß et al., 2015).

Brain oscillations, according to their rhythmic nature, lead to an alternation between excitatory and inhibitory states of cortical activity, along with their phase. They are the neuronal support of perceptual cycles. This phenomenon describes our ability to perceive the world in a periodic manner, i.e., how our perceptual performance change periodically between favorable and less favorable moments. Indeed, perceptual performance in different sensory modalities (visual, tactile, auditory) is modulated by the phase of brain oscillations in wide range of low frequencies (very slow, delta, theta, alpha), with an optimal phase for perception that predicts better perceptual performance, and an opposite, non-optimal phase, leading to impaired performance.

In these first sections, we saw that the different features of brain oscillations, i.e., the frequency, the amplitude, and the phase, influence cortical excitability and the subsequent perceptual performance across multiple sensory modalities.

2. Ubiquity of brain oscillations across scales and species

To close this first chapter on brain oscillations, I would like to emphasize the importance of studying brain oscillations. Oscillations are recorded at various brain scales, i.e., cellular, local network, brain network, and they are observed in a wide range of species. Consequently, neuronal oscillations represent the most promising tool to combine findings from multiple disciplines within neurosciences, from studies at a molecular level to the ones on healthy humans with EEG. First, we will highlight that brain oscillations are present at different scales

of the brain (for review, see Wang, 2010). Then, we will look to the different species in which brain oscillations have been recorded.

2.1. Pacemaker neurons

Pacemaker neurons present intrinsic oscillatory membrane properties, allowing them to produce a spontaneous, rhythmic, activity, without the intervention of any electrical or chemical stimulation. This spontaneous rhythmic activity depends on voltage-gated membrane ion channel, that are at the origin of a succession of depolarizing and hyperpolarizing currents, leading to an oscillatory activity of the membrane potential (Ramirez et al., 2004). Pacemaker neurons have been mostly identified in the thalamus (Steriade and Deschene, 1984; MacCormick and Pape, 1990), and in the hippocampus (Maccaferri and McBain, 1996; Schweitzer et al., 2003; Hu et al., 2002) of mammalians. For example, the dorso-lateral geniculate nucleus, a thalamic relay of the visual pathway, presents a subpopulation of pacemaker neurons that generates a bursting activity at 2 Hz. This oscillatory activity depends on the interaction of two ionic currents: It and Ih (**Figure 1.16**; McCormick and Pape 1990). At approximatively -65 mV, the low threshold calcium current It continuously depolarizes the membrane potential, i.e., the associated ion channels are open and let calcium ions that have a positive charge enter into the neuron (Brown et al., 1990), until the threshold for a burst of action potentials (between -50 and -55 mV) is reached. The action potential inactivates the It current, that let enter cations, i.e., ion with positive charge, into the neuron, and the Ih current, another ion channel permeable to cations, leading to a repolarization of the membrane potential followed by a hyperpolarization. The state of hyperpolarization activates the Ih current, at approximatively -80 mV (Brown et al., 1990), cations enter into the neuron, until the membrane potential reaches again the threshold value of -65 mV to see the activation of the current It, leading to a new cycle.

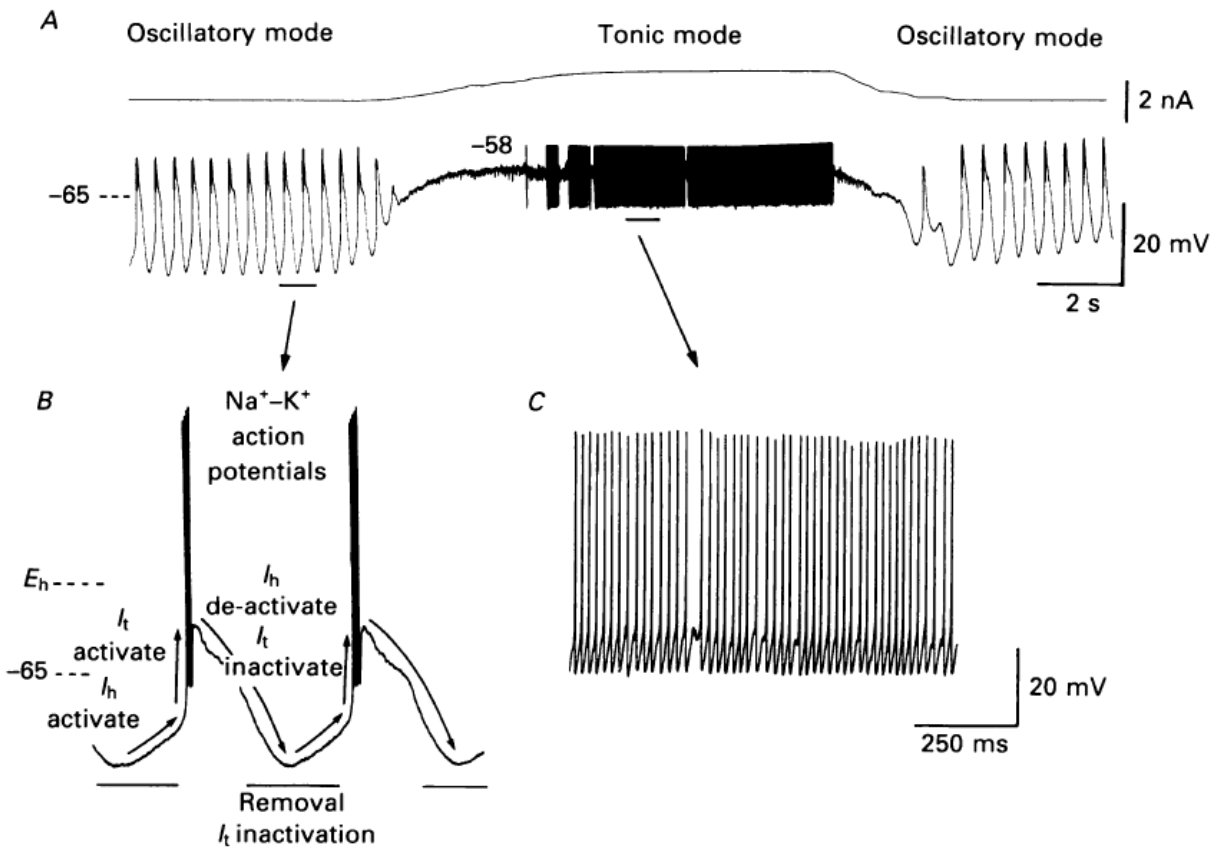

Figure 1.16: Pacemaker activity in the dorso-lateral geniculate nucleus neurons, from MacCormick and Pape, 1990. A. *The dorso-lateral geniculate nucleus neuron presents an oscillatory activity at a frequency of about 2 Hz, and a tonic mode of action potential generation after a pharmacological stimulation.* ***B.*** *The oscillatory activity would depend on two ionic currents, It and Ih. Activation of the current It depolarizes the membrane potential until it reaches the threshold for generating a burst of action potentials. The depolarization entrains a deactivation of the current It and Ih, leading to a repolarization followed by a hyperpolarization. The hyperpolarization state activates the current Ih that depolarize the neuron membrane potential until the current It is reactivated.* ***C.*** *Burst of action potentials during the tonic mode.*

The pacemaker activity of single neurons is modulated by the excitatory and inhibitory synapses, and by neuromodulators, in a population of neurons (Ramirez et al., 2004). In addition, they can transfer their rhythmic activity to other neuronal population. The presence of pacemaker neurons in a neural network will have a role on the entire oscillatory activity of the network.

2.2. Brain oscillations: from neurons to local networks

Invasive and modelling experiments proposed some neural mechanisms explaining the emergence of brain oscillations at the level of a neural network.

First, the inhibitory-inhibitory model relies on interactions between GABAergic synapses in a neuronal network exclusively composed of interneurons. We consider one interneuron, with an auto-regulator negative feedback, i.e., membrane repolarization after an excitatory input. According to this property, a tonic excitatory input would entrain a cyclic depolarization/hyperpolarization of the interneuron, according to the kinetics of the GABA receptor, which typically lasts from 10 to 20 ms. By considering a neural network exclusively composed of interneurons firing in phase, we can observe the emergence of gamma oscillations at 50 to 100 Hz (**Figure 1.17.A**) (Van Vreeswijk et al., 1994; Whittington et al., 2000; Jensen et al., 2014). The inhibitory-inhibitory model is involved in the generation of hippocampal gamma oscillations (Whittington et al., 1995; Traub et al., 1996).

Another plausible mechanism is the excitatory-inhibitory model. This model involves a mutual communication between an excitatory and an inhibitory population of neurons. The excitatory population sends excitatory inputs to the inhibitory population, leading to their firing. The activation of the inhibitory population would, in turn, send inhibitory inputs to the excitatory population, silencing the excitatory neurons. When the inhibition is released, the excitatory population fires, leading to a new cycle of mutual excitation/inhibition between the two neuronal populations. Here, the frequency of the oscillations depends on the communication delays between the two populations (**Figure 1.17.B**) (Ermentrout and Kopell, 1998; Whittington et al., 2000; Jensen et al., 2014). The excitatory-inhibitory model explains the origin of beta and gamma oscillations (Traub et al., 1999).

The two models presented above do not depend on pacemaker neurons but result from neuronal interactions in a local network, and they explain well the emergence of gamma and beta oscillations. Concerning the generation of alpha oscillations, they would depend on a population of pacemaker neurons in the thalamus, the high-threshold bursting (HTB) neurons. The HTB neurons are bursting in the alpha range (2-13 Hz), in synchrony with alpha oscillations (Hughes and Crunelli, 2005). Modeling and invasive studies suggest that the HTB neurons entrain thalamic interneurons at the alpha frequency that in turn, project to the primary visual cortex through relay-mode thalamocortical neurons, leading to the emergence of alpha oscillations in the cortex (**Figure 1.17.C**) (Lorincz et al., 2009; Vijayan and Kopell, 2012; Jensen et al., 2014). Theta and delta oscillations would also be supported by interactions between several brain regions, composed of inhibitory and excitatory populations, sometimes including pacemaker neuronal populations (Terman et al., 1996; Buzsaki, 2002; Jensen et al., 2014).

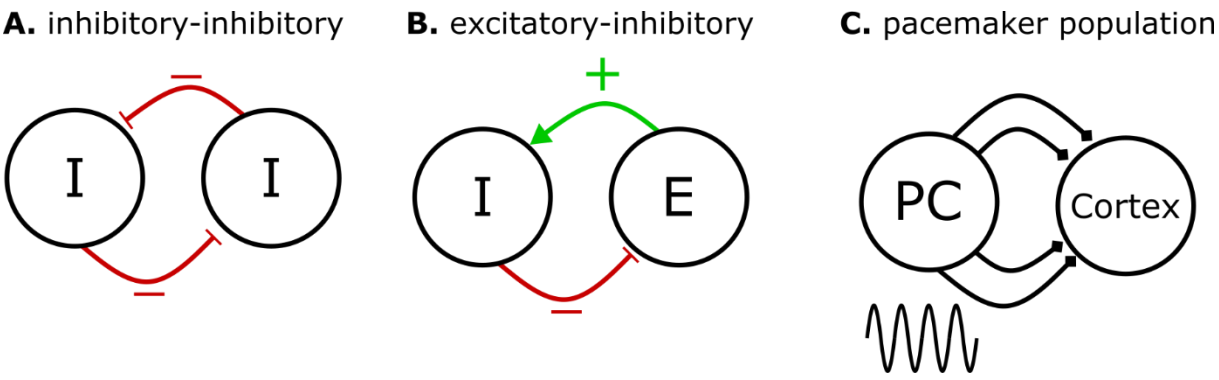

Figure 1.17: Brain oscillations models. A. *The inhibitory-inhibitory model. A tonic stimulation on an inhibitory neuronal population lead to a cyclic depolarization/hyperpolarization of the neurons according to the inhibitory neurotransmitter kinetics.* ***B.*** *The excitatory-inhibitory model. Cycles of mutual excitation/inhibition.* ***C.*** *A population of pacemaker neurons project its oscillatory intrinsic activity to another neuronal population, making it oscillates.*

2.3. Global oscillatory network

Brain oscillations in a wide range of frequencies are observed in every cortical and subcortical brain region. Interestingly, some studies showed that brain oscillations, in different regions and frequencies, can share coupling properties: phase-phase coupling, phase-amplitude coupling, or amplitude-amplitude coupling (Canolty and Knight, 2010; Hyafil et al., 2015). Theses subcategories of cross-frequency coupling always involved two brain oscillations, in distinct or in the same brain regions.

The phase-phase coupling mechanism reflects a phase synchronization between two oscillations with different frequencies. They play a role in memory. A phase synchronization between occipital theta and gamma oscillations is positively correlated to a matching process between the memory representation and the visual inputs revealing an integrative mechanism between the internal representation and the environment (Sauseng et al., 2008; Holz et al., 2010). A phase synchronization between theta and gamma oscillations has also been observed in the hippocampus and seems to play a role in spatial navigation (Belluscio et al., 2012; Zheng et al., 2016).

The phase-amplitude coupling mechanism describes a modulation in oscillatory amplitude as a function of the phase of another oscillation. Numerous studies showed that the amplitude of gamma oscillations, an index of firing activity, is phase-locked to the phase of theta/alpha oscillations (Canolty et al, 2006; Demiralp et al., 2007; Osipova et al., 2008; Bonnefond and Jensen, 2015). Slow oscillations could modulate windows of excitability, at which information

are processing, through the modulation of fast, gamma oscillations (Jensen and Colgin, 2007; Osipova et al., 2008; Bonnefond and Jensen, 2015).

The amplitude-amplitude coupling mechanism corresponds to a negative or a positive correlation between the amplitude envelopes of two oscillations with different frequencies. During motor imagery, beta oscillations over the precentral cortex are negatively coupled with gamma oscillations in the occipital cortex, suggesting an interaction between motor and visual areas during the formation of a movement (De Lange et al., 2008). In an attentional task, posterior alpha oscillations are negatively correlated with frontal theta oscillations. This pattern has been interpreted as a functional connectivity between attention control located in the frontal areas, and sensory systems, here the visual ones, in posterior areas (Mazaheri et al., 2009, 2010).

Oscillations are present from the single cell to the global network level. Their mechanisms begin to be understood thanks to animal and modeling studies, but we still do not know much on the neurophysiological mechanisms that link brain oscillations at the different scales.

2.4. Ubiquity of brain oscillations across species

Brain oscillations are ubiquitous: there are present in a wide range of species. Here, we are particularly interested in oscillations in humans, because this PhD work is exclusively composed of experiments on humans, but brain oscillations have been widely studied in animals, frequently in mammals (rats, monkeys, cats, mice; see **Table 2 and Table 3**). In addition, brain oscillations have been recorded in reptiles (Jaggard et al., 2021; Gaztelu et al., 1991; Prechtl, 1994; Gonzalez et al., 1999); fish, birds, and insects (Jaggard et al., 2021; Gutierrez et al., 2021). Brain oscillations appear to be a crucial mechanism for brain functioning, that has been conserved through evolution. This specificity of brain oscillations allows the scientific community to create bridges across different species, and to perform reliable studies at the molecular and cellular level with invasive studies in animals.

3. Summary

In this **Chapter 1**, we saw that since the discovery of brain oscillations in humans at the surface of the scalp, recorded with the first EEG system, the scientific community found the presence of brain oscillations at multiple brain scales, from the neuron to the whole brain, in multiples species, as in insects, fish, birds, reptiles, and non-human mammalians. Brain

oscillations are ubiquitous, and I think they have the possibility to bring the research in neuroscience to great discoveries.

The different parameters of brain oscillations, i.e., phase, amplitude, and frequency, have been associated to a broad range of cognitive functions. The first studies tried to associate one frequency band to one cognitive function, but this view is now obsolete. On the other hand, the great majority of studies investigated separately the role of phase and amplitude on cognition and cortical excitability. In this PhD work, we focus on the Pulsed Inhibition theory, that proposes a general physiological mechanism for alpha brain oscillations that could be applied to many cognitive functions, and a way the phase and the amplitude could jointly influence visual perception and cortical excitability (**Chapter 4**). In addition, we use a recent methodology that estimates the spatial pattern of brain activity across time, i.e., classification algorithm, and then associates these dynamics in cortical activity to different features of visual perception (**Chapter 5**).

Chapter 2. Cortical traveling waves.

In the previous chapter, we focused on the role of the temporal dynamics of brain oscillations on cognition and cortical excitability. What about the role of the spatial organization of brain oscillations? For decades, neuroscientists separated space and time, while in physics, the spacetime notion appeared at the beginning of the XXth century, and led to emergence of the spatial and the general relativity theories by Albert Einstein, who revolutionized research in theoretical physics and astrophysics. In our lab, we hypothesize that the spatial component of brain oscillations plays a crucial role on our cognitive functions. Consequently, we developed in this PhD several experiments to better understand the role of the spatio-temporal organization of brain oscillations on perception (**Chapter 6 and Chapter 7**).

Interestingly, the propagation of spontaneous brain oscillations across the cortex has been observed since 1935, by Adrian and Yamagiwa. They recorded brain activity with three oscillographs connected to pairs of electrodes placed at the surface of the scalp (**Figure 2.1**). They observed that the peaks and the troughs of alpha cycle did not coincide between the three oscillographs, suggesting that the oscillation "moves" across the cortex (**Figure 2.2**).

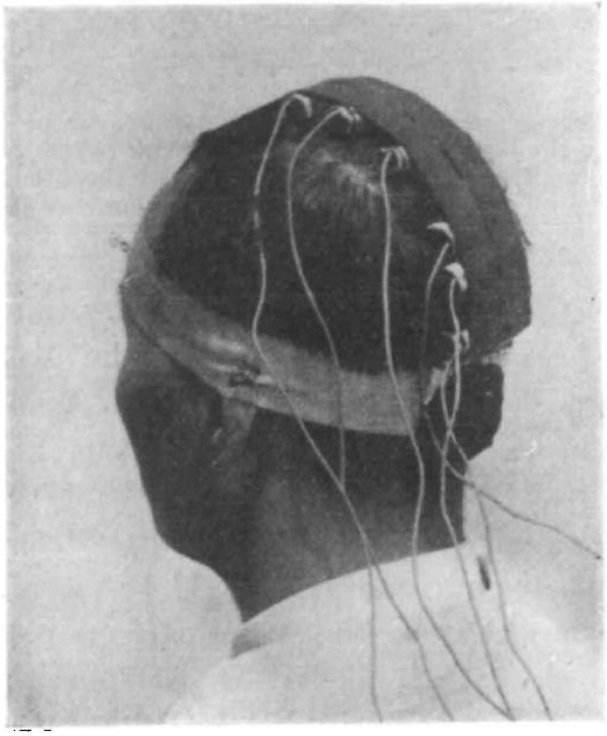

Figure 2.1: The EEG system used by Adrian and Yamagiwa, 1935.

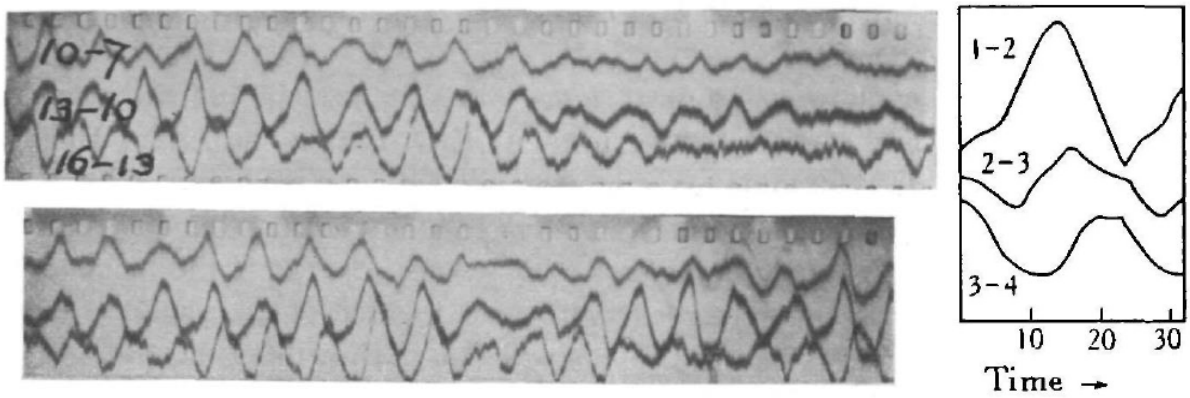

Figure 2.2: Brain oscillations "move" across the scalp, from Adrian and Yamagiwa, 1935.

One year before, Adrian and Matthews (1934b) described the propagation of brain oscillations across a short distance, only a few mm, in anesthetized rabbits. They recorded brain electrical activity with electrodes directly positioned at the surface of the neocortex, which was exposed to a drug allowing to stimulate spontaneous oscillatory activity in the brain. As you can see in **Figure 2.3**, the peak of latency is progressively delayed from one pair of electrodes to the other, suggesting the presence of a traveling activity.

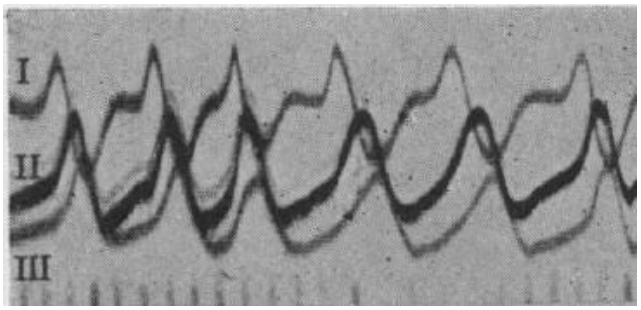

Figure 2.3: Brain oscillations travel on a short distance, from Adrian and Matthews, 1934b.

In this Chapter, we will present a review of the literature on traveling waves in various species and in response to diverse stimulations. We will be particularly interested in publications testing for a functional role of this propagating activity on cognitive functions, and we will see that at the moment, the functional role of traveling waves is poorly understood.

1. Definition of a traveling wave

A traveling wave is the propagation of neural activity with a constant shift in the peak latency between the origin of the signal and more distal positions, and frequently, a decrease in

amplitude (Sato et al., 2012; Muller et al., 2018). A traveling wave implies that brain activity emerges from a specific cortical location and then propagates through neuronal connections to include distant cortical populations. By opposition, a standing wave involves a fixed number of populations whose neuronal activity is synchronized across time, i.e., the peak is aligned across every cortical position (Benucci et al., 2007) (**Figure 2.4**).

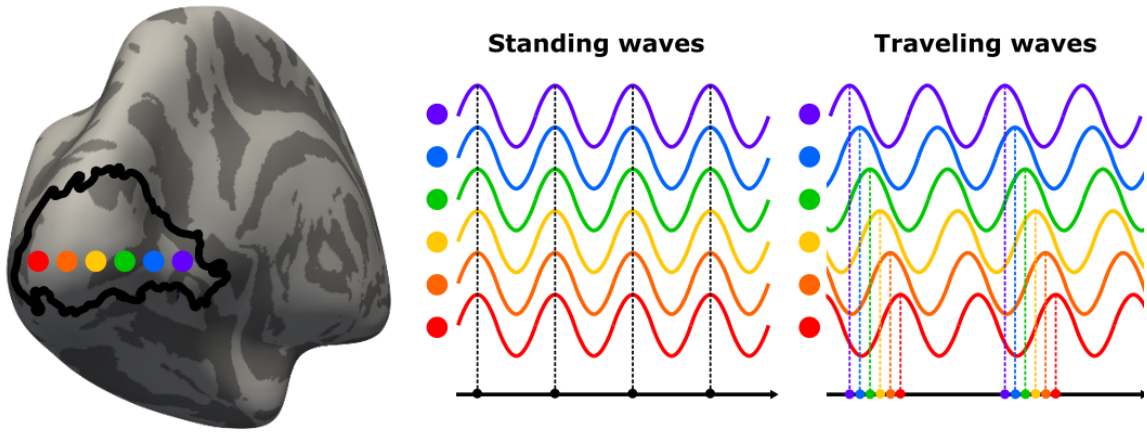

Figure 2.4: Traveling vs standing waves. *Six neuronal populations are considered within the cortical area V1. The source of neuronal activity is in purple. In a standing wave, the six cortical populations present an activity in synchrony, with no delay between them. In a traveling wave, the activity of each neuronal population is delayed with a constant shift according to their relative position to the origin of the signal. Note that here is represented an oscillatory brain activity, but the distinction between traveling and standing waves can also be applied to non-oscillatory brain signal.*

Traveling waves have been recorded at the macroscopic scale level, i.e., whole-brain scale. In this case, neural activity is propagating between cortical areas. **Macroscopic traveling waves** are usually recorded with non-invasive techniques, allowing for a high temporal resolution (EEG and MEG), but a low spatial resolution. The electrocorticography (ECoG) technique has both a high spatial and temporal resolution, but it is invasive, and can only be used in drug-resistant epileptic patients and animals (Muller et al., 2018).

The use of optical and electrophysiological invasive techniques with a high spatio-temporal resolution showed the presence of traveling waves at the mesoscopic scale level, i.e., between microscopic and macroscopic scales, corresponding to cortical or subcortical regions spanning several millimeters to centimeters. **Mesoscopic traveling waves** are propagating through a single brain area or nucleus. They are usually recorded with invasive

electrophysiological (LFP, MUA, intraEEG) and optical (calcium imaging, VSD, i.e., voltage sensitive dye) techniques (Muller et al., 2018).

Traveling waves are often observed on spatial maps representing the dynamics of peak latency or amplitude across the y and x space coordinates. According to this representation, standing and traveling waves can be modeled as displayed in **Figure 2.5**.

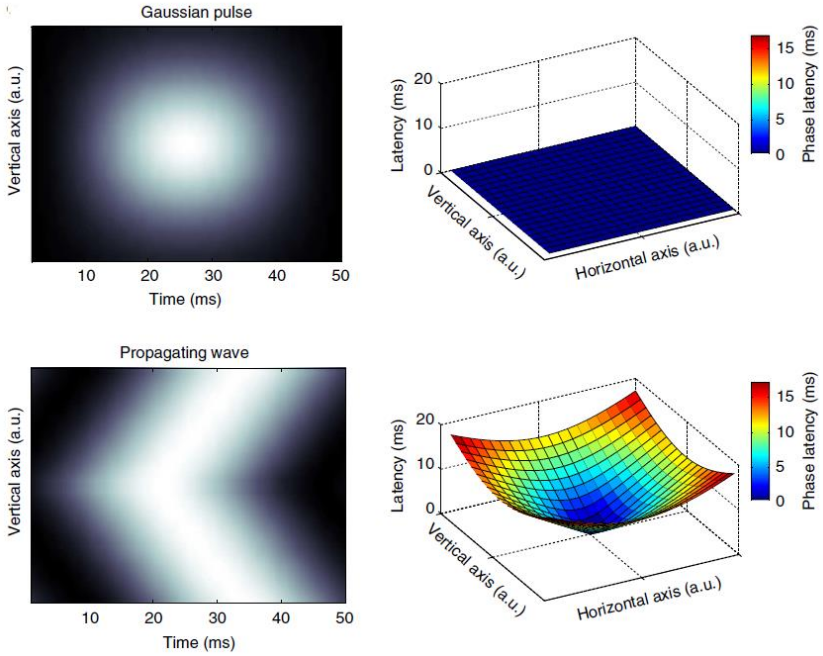

Figure 2.5: Standing vs traveling waves, from Muller et al., 2014. *Upper panel, a standing wave is modeled by a Gaussian pulse, the phase latency is constant across time and space (in arbitrary units). Lower panel, a traveling wave is defined by a constant shift of the phase latency across time and space.*

Both macroscopic and mesoscopic traveling waves are characterized by their **speed** of propagation and their **distance** of travel. Macroscopic traveling waves are also characterized by their **direction** of propagation.

In addition, they can be evoked by a stimulus or spontaneously present in the brain (**evoked vs. spontaneous**).

Finally, we make the distinction between the propagation of **non-oscillatory vs. oscillatory** brain activity. The non-oscillatory traveling activity is defined by its amplitude and its peak latency, while the oscillatory traveling activity is characterized by its frequency, its amplitude, and its phase.

In the following sections, we will characterize separately mesoscopic and macroscopic traveling waves, discuss their potential functional role on cognition, and present some neurophysiological plausible models explaining their underlying neural mechanisms.

2. Mesoscopic traveling waves

2.1. From anesthetized animals to humans

Mesoscopic traveling waves have been recorded since the 1950s in anesthetized cats and monkeys (Burns, 1950; Chang, 1951; Lilly and Cherry, 1954). The propagation of neural activity within single brain regions has been observed in response to electrical (Burns, 1950; Chang, 1951; **Figure 2.6**) and auditory stimulation (Lilly and Cherry, 1954).

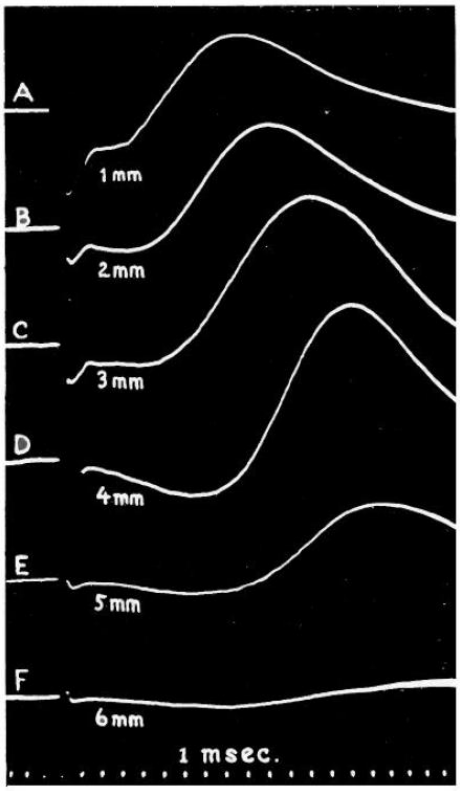

Figure 2.6: Propagation of neural activity within area 5 of anesthetized monkeys, from Chang, 1951. *Invasive electrophysiological recordings from six points on the cortical surface of area 5, each point being 1 mm farther distant from the stimulating electrode than the previous one. A shift of the peak latency is clearly observable as a function of the distance between the stimulating electrode and the site of recording.*

This result has then been replicated many times (**Table 2**).

The propagation of neural **non-oscillatory** activity has been observed in **animals** (**Figure 2.7**), in a wide range of species (rat, cat, monkey, guinea pig, salamander, ferret, zebrafish), under **anesthesia**, in response to **electrical** (Chang, 1951; Orbach and Cohen, 1983;

Cinelli and Kauer, 1995; Civillico and Contreras, 2006; Xu et al., 2007; Gao et al., 2012), **visual** (Grinvald et al., 1994; Kitano et al., 1995; Arieli et al., 1996; Bringuier et al., 1999; Jancke et al., 2004; Xu et al., 2007; Sharon et al., 2007; Lippert, Takagaki et al., 2007; Takagaki et al., 2008; Nauhaus et al., 2009, 2012; Gao et al., 2012; Rekauzke et al., 2016), **auditory** (Lilly and Cherry, 1954; Fukunishi et al., 1992; Taniguchi et al., 1992; Uno et al., 1993; Bakin et al., 1996; Tsytsarev et al., 2004; Song et al., 2006; Nishimura et al., 2007; Reimer et al., 2011), **somatosensory** (London et al., 1989; Derdikman et al., 2003; Petersen et al., 2003a, b; Civillico and Contreras, 2006; Lippert, Takagaki et al., 2007; Takagaki et al., 2008) and **olfactory stimulation** (Cinelli et al., 1995; Friedrich and Korsching, 1998), and during **spontaneous** activity (Volgushev et al., 2006; Lippert, Takagaki et al., 2007; Luczak et al., 2007; Takagaki et al., 2008; Nauhaus et al., 2009, 2012).

Mesoscopic non-oscillatory traveling waves have also been identified in **slice and in vitro preparations** in numerous experiments (Schwartzkroin and Prince, 1978; Grinvald et al., 1982; Voskuyl and Albus, 1985; Knowles et al., 1987; Chervin et al., 1988; Miles et al., 1988; Novak and Wheeler, 1989; Holsheimer and Da Silva, 1989; Chagnac-Amitai and Connors, 1989; Albowitz et al., 1990; Albowitz and Kuhnt, 1991, 1993; Wadman and Gutnick, 1993; Sugitani et al., 1994; Tanifuji et al., 1994; Sutor et al., 1994; Nelson and Katz, 1995; Yuste et al., 1997; Tsau et al., 1998; Fleidervish et al., 1998; Demir et al., 1999; Laaris et al., 2000; Contreras and Llinas, 2001; Wu et al., 2001; Tucker and Katz, 2003; Song et al., 2006).

Finally, mesoscopic traveling waves have been identified in **passive awake animals**, presented with visual, auditory, or somatosensory stimulation (Petersen et al., 2003b; Ferezou et al., 2006, 2007; Witte et al., 2007; Sit et al., 2009; Reynaud et al., 2012; Zhang et al., 2012; Yang et al., 2015) or at rest, or freely behaving (Ferezou et al., 2006; Luczak et al., 2007).

Importantly, only a few studies recorded mesoscopic traveling waves in **awake monkeys performing a task**, in the visual modality (Slovin et al., 2002; Chen et al., 2006; Chemla et al., 2019).

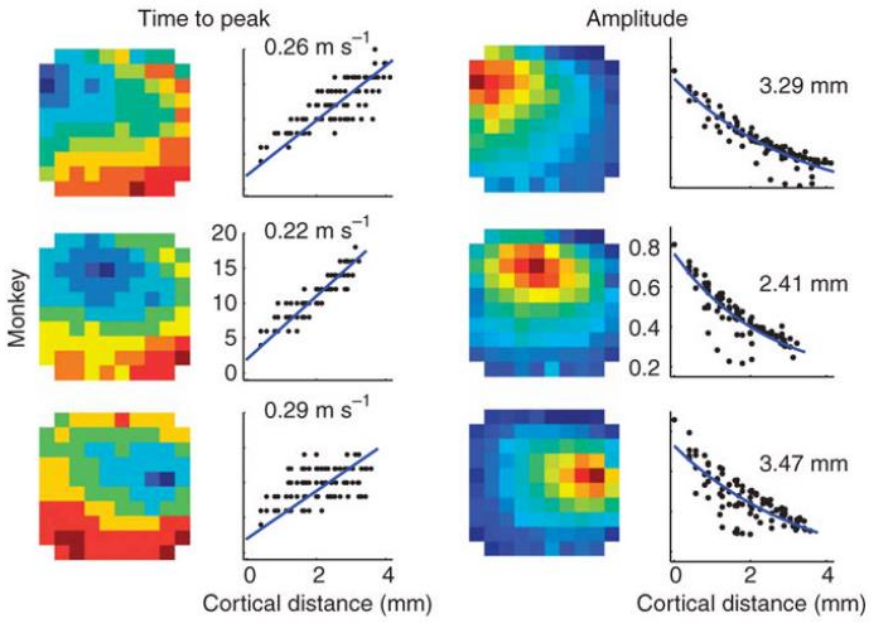

Figure 2.7: Mesoscopic traveling waves recorded with LFP technique, from Nauhaus et al., 2009. *Spontaneous traveling waves time-locked to an initial spiking activity, recorded in area V1 of anesthetized monkeys. Each rows correspond to traveling waves triggered by a single spike location. Left panels, the peak of neural activity is plotted as a function of the cortical distance from the triggering spike. The velocity of spontaneous mesoscopic traveling wave is on average 0.26 m/s. Right panels, the amplitude of neural activity is plotted as a function of cortical distance, with reddish colors corresponding to the ones with the maximum amplitude. The darkest red-saturated pixels correspond to the position of the initial spiking activity. The traveling waves spread over, on average, 3 mm of cortex.*

Similarly, **oscillatory** traveling activity has been recorded in many brain regions in response to diverse stimulations and in different **animal** species (**Figure 2.8**) (rat, cat, monkey, turtle, rabbit, ferret, mollusk, zebrafish).

The propagation of **very slow, delta, theta, alpha, beta, and gamma cortical oscillations** have been recorded in **anesthetized animals** (**very slow** (<1 Hz): Stroh et al., 2013; **delta**: Han et al., 2008; Townsend et al., 2015; **theta**: Petsche and Stumpf, 1960; **alpha**: Adrian and Matthews, 1934; Arieli et al., 1995; Benucci et al., 2007; **gamma**: Freeman, 1978; Ketchum and Haberly, 1993; Besserve et al., 2015; **multiple frequency bands**: Huang et al., 2010) as well as **in slice and in vitro preparations** (**very slow** (<1 Hz): Kleinfeld et al., 1994; Delaney et al., 1994; Gervais et al., 1996; Sanchez-Vives and McCormick, 2000; Nikitin and Balaban, 2000; **alpha**: Wu et al., 1999; **beta**: Prechtl et al., 2000; Friedrich et al., 2004; **multiple frequency bands**: Huang et al., 2004).

We will also note that some studies found mesoscopic oscillatory traveling waves in **subcortical structures** (thalamic nuclei: Verzeano and Negishi, 1960; Andersen et al., 1966; Kim et al., 1995; Neuenschwander and Singer, 1996; Contreras et al., 1996, 1997; Stroh et al., 2013).

Mesoscopic oscillatory traveling waves have also been observed in **awake animals**, **passive** (**gamma**: Freeman, 1978; Gabriel and Eckorn, 2003; **ripple** (100-200 Hz): Ylinen et al., 1995; Csicsvari et al., 2000; Patel et al., 2013; **multiple frequency bands**: Wright and Sergejew, 1991; Prechtl et al., 1997; Lam et al., 2000, 2003; Muller et al., 2014), **freely behaving** (**theta**: Lubenov and Siapas, 2009; Patel et al., 2012; Agarwal et al., 2014; Hernandez-Perez et al., 2020), or **performing (visuo-) motor** (**beta**: Murthy and Fetz, 1996; Rubino et al., 2006; Takahashi et al., 2015; Zanos et al., 2015), **olfactory** (**gamma**: Freeman and Baird, 1987), **auditory** (**gamma**: Freeman and Barie, 2000), **somatosensory** (**gamma**: Freeman and Barie, 2000), or **visual tasks** (**gamma**: Freeman and Barie, 2000; **multiple frequency bands**: Ray and Maunsell, 2011; Maris et al., 2013; Davis et al., 2020).

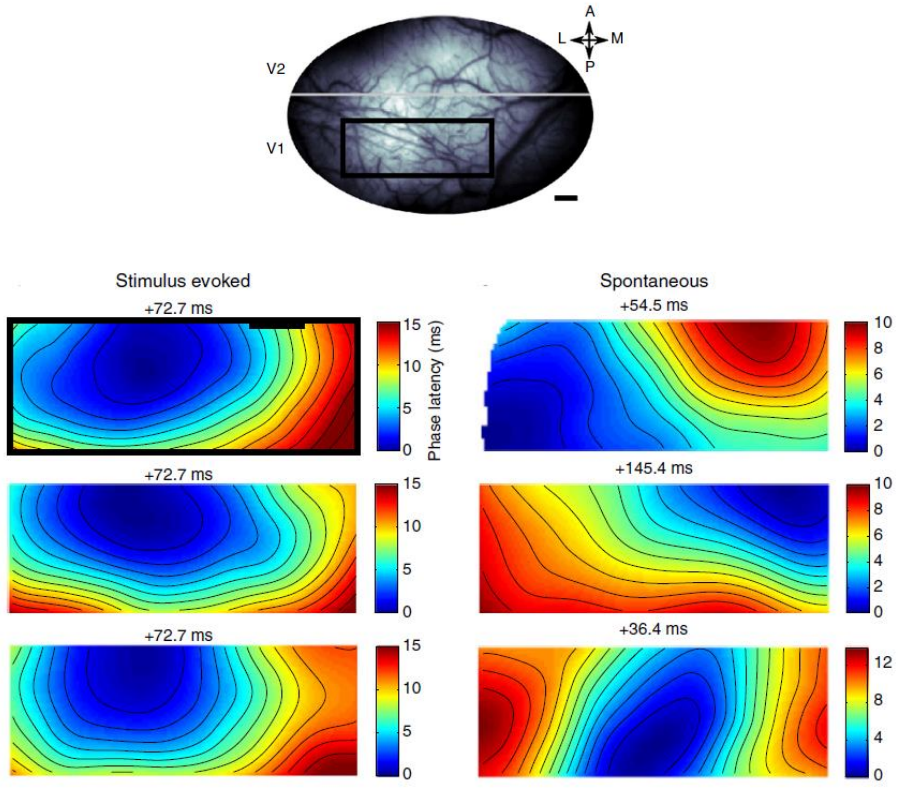

Figure 2.8: Mesoscopic traveling waves recorded with VSD technique, from Muller et al., 2014. *Phase-latency maps of the V1 region of monkeys delimited in the black box of the upper panel, recorded after a visual stimulation, or during resting state.*

In **humans**, only a few numbers of studies investigated the presence and the role of mesoscopic traveling waves. This limitation is mainly due to the fact that invasive recordings in humans is only possible in patients, and non-invasive recordings (EEG, MEG) suffer for a poor spatial resolution.

In patients, invasive recordings allowed to observe the propagation of **theta and alpha** traveling waves during a **memory task** (Zhang and Jacobs, 2015; Sreekumar et al., 2021). Similarly, **beta oscillations** have been recorded during **resting state** and **motor tasks** (Takahashi et al., 2011). In epileptic patients, the **ictal discharges** (in the gamma frequency) also act as traveling waves (Smith et al., 2016; Liou et al., 2017).

Mesoscopic traveling waves have also been observed with psychophysics experiment, sometimes coupled with fMRI recordings (Wilson et al., 2001; Lee et al., 2005, 2007; Knapen et al., 2007; Genç et al., 2015; Sokoliuk and VanRullen, 2016).

2.2. Mesoscopic traveling waves: propagation speed, spatial extent, and other properties

Mesoscopic **non-oscillatory** traveling waves are propagating at an **average speed of 0.24 m/s**, ranging from 0.001 to 2 m/s (Burns, 1950; Chang, 1951; Lilly and Cherry, 1954; Grinvald et al., 1982, 1994; Voskuyl and Albus, 1985; Knowles et al., 1987; Chervin et al., 1988; Miles et al., 1988; London et al., 1989; Holsheimer and Lopes da Silva, 1989; Novak and Wheeler, 1989; Chagnac-Amitai and Connors, 1989; Albowitz et al., 1990; Albowitz and Kuhnt, 1991, 1993; Wadman and Gutnick, 1993; Tanifuji et al., 1994; Sutor et al., 1994; Nelson and Katz, 1995; Yuste et al., 1997; Tsau et al., 1998; Fleidervish et al., 1998; Bringuier et al., 1999; Laaris et al., 2000; Wilson et al., 2001; Contreras and Llinas, 2001; Wu et al., 2001; Slovin et al., 2002; Derdikman et al., 2003; Peterson et al., 2003a, b; Tucker and Katz, 2003; Jancke et al., 2004; Lee et al., 2005; Song et al., 2006; Witte et al., 2007; Lippert, Takagaki, et al., 2007; Xu et al., 2007; Takagaki et al., 2008; Sit et al., 2009; Nauhaus et al., 2009, 2012; Reynaud et al., 2012; Gao et al., 2012; Yang et al., 2015; Rekauzke et al., 2016; Chemla et al., 2019), over a cortical distance from 0.4 to 12 mm, with an **average cortical distance of 3.2 mm** (Burns, 1950; Chang, 1951; Schwartzkroin and Prince, 1978; Miles et al., 1988; Chagnac-Amitai and Connors, 1989; Holsheimer and Lopes da Silva, 1989; Albowitz and Kuhnt, 1991; Fukunishi et al., 1992; Wadman and Gutnick, 1993; Tanifuji et al., 1994; Grinvald et al., 1994; Nelson and Katz, 1995; Contreras and Llinas, 2001; Wu et al., 2001; Slovin et al., 2002; Tucker and Katz, 2003: Petersen et al., 2003b; Song et al., 2006; Chen et al., 2006; Volgushev et al., 2006;

Lippert, Takagaki, et al., 2007; Sit et al., 2009; Nauhaus e al., 2009, 2012; Reimer et al., 2011; Reynaud et al., 2012; Yang et al., 2015; Rekauzke et al., 2016; Chemla et al., 2019).

For mesoscopic **oscillatory** traveling waves, the **propagation speed is on average 0.58 m/s**, ranging from 0.001 to 7 m/s (Adrian and Matthews, 1934; Petsche and Stumpf, 1960; Freeman, 1978; Freeman and Baird, 1987; Wright and Sergejew, 1991; Kleinfeld et al., 1994; Contreras et al., 1997; Prechtl et al., 1997, 2000; Wu et al., 1999; Nikitin and Balaban, 2000; Sanchez-Vives and Cormick, 2000; Freeman and Barrie, 2000; Lam et al., 2000, 2003; Friedrich et al., 2004; Rubino et al., 2006; Benucci et al., 2007; Han et al., 2008; Lubenov and Siapas, 2009; Ray and Maunsell, 2011; Patel et al., 2012, 2013; Stroh et al., 2013; Muller et al., 2014; Agarwal et al., 2014; Takahashi et al., 2011, 2015; Zhang and Jacobs, 2015; Zanos et al., 2015; Besserve et al., 2015; Smith et al., 2016; Liou et al., 2017; Davis et al., 2020; Hernandez-Perez et al., 2020; Sreekumar et al., 2021), over a cortical distance from 1 to 121 mm, with an **average cortical distance of 12.5 mm** (Adrian and Matthews, 1934; Murthy and Fetz, 1996; Wright and Sergejew, 1991; Wu et al., 1999; Freeman and Barrie, 2000; Prechtl et al., 2000; Lam et al., 2000; 2003; Gabriel and Eckorn, 2003; Friedrich et al., 2004; Rubino et al., 2006; Lubenov and Siapas, 2009; Ray and Maunsell, 2011; Patel et al., 2012, 2013; Maris et al., 2013; Muller et al., 2014; Zanos et al., 2015; Smith et al., 2016).

When considering the propagation of oscillatory traveling waves, we can also ask the number of cycles which propagates within a single brain area, and whether there is a link between the propagation speed and the frequency.

By considering the average propagation speed (0.58 m/s) and the average cortical distance travelled (12.5 mm), oscillatory traveling waves seem to propagate during on average 20 ms. Knowing that from frequency from 1 Hz to 50 Hz, one oscillatory cycle lasts from 1,000 ms to 20 ms, it appears that only **one cycle of oscillation is propagating within a single brain region**. Indeed, studies found that theta oscillations have a propagation of 28-49° across the whole human hippocampus (Zhang and Jacobs, 2015), and that one cycle of beta oscillations was propagating in V4 (Zanos et al., 2015).

In addition, several studies observed a **positive correlation between the propagation speed and the frequency of the oscillatory traveling waves** (**Figure 2.9**; Petsche and Stumpf, 1960; Freeman and Barrie, 2000; Zhang and Jacobs, 2015).

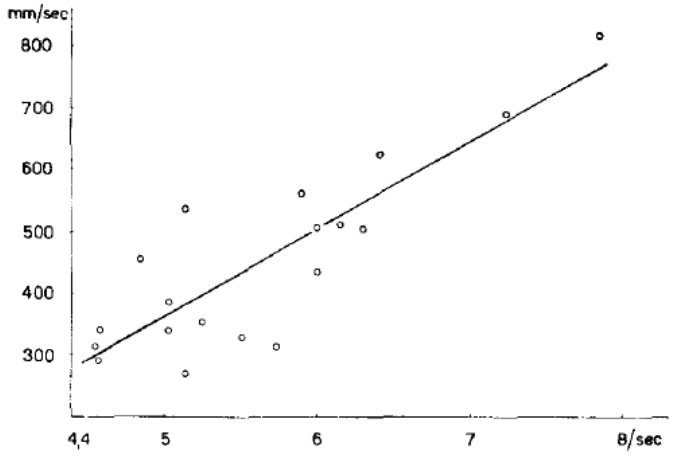

Figure 2.9: Relation between the propagation speed and the frequency of traveling waves recorded in the hippocampus, from Petsche and Stumpf, 1960.

The propagation of one traveling wave across a single brain area has been widely studied, but this view is likely a simplification of the spatio-temporal organization of cortical activity. The cortex received continuously numerous perceptual inputs at the same time. Consequently, **multiple traveling waves** should happen within single brain area at the same time, and interact with each others. Some studies found that two traveling waves that are both triggered at the same time propagate horizontally trough several mm of cortex, until they collide. At the moment of the collision, they would exert a suppressive mechanism on each other (Grinvald et al., 1994; Wu et al., 1999; Contreras and Llinas, 2001; Civillico and Contreras, 2006; Reynaud et al., 2012; Chemla et al., 2019). In other cases, traveling waves can remain segregated at two distant positions of the brain region, and not interact with each other (Contreras and Llinas, 2001).

Gao et al. (2012) investigated this question in-depth. They presented two visual stimuli, placed approximatively 2 mm away from each other in the retinotopic space of V1, and which both triggered a traveling wave (**Figure 2.10.A-B**). They studied the interaction between the two waves by changing the inter-stimulus interval (ISI) between the two stimuli. They showed that at an ISI of 300 ms or longer, traveling waves did not interact with each other. The brain activity evoked by the second stimulus was not affected by the first one, because the first-evoked wave propagated through the entire V1 area before the second stimulus triggered the second wave (**Figure 2.10.C**, top). When the ISI was between 100 and 300 ms, the second traveling wave was largely suppressed, because the V1 area was still affected by the propagation of the first wave (**Figure 2.10.C**, middle). Finally, at an ISI below 30 ms, the second-wave was triggered before the first-wave met the retinotopic position of the second

stimulus, leading to a fusion of cortical activity, and a unique traveling wave (**Figure 2.10.C**, down). Interestingly, the amplitude of the brain signal did not increase when the fusion occurred, suggesting that the neuronal population involved was the same that the one involved in the generation of independent traveling waves. The different interaction between two evoked traveling waves according to the ISI are summarized in **Figure 2.10.D**. In their paper, they also showed that these interactions were maintained between a traveling wave evoked by a visual stimulus, and spontaneous traveling waves (Gao et al., 2012). In most experiments, it is difficult to disentangle the evoked and the spontaneous brain activity, and we see with this study that it is crucial to investigate how they interact with one another.

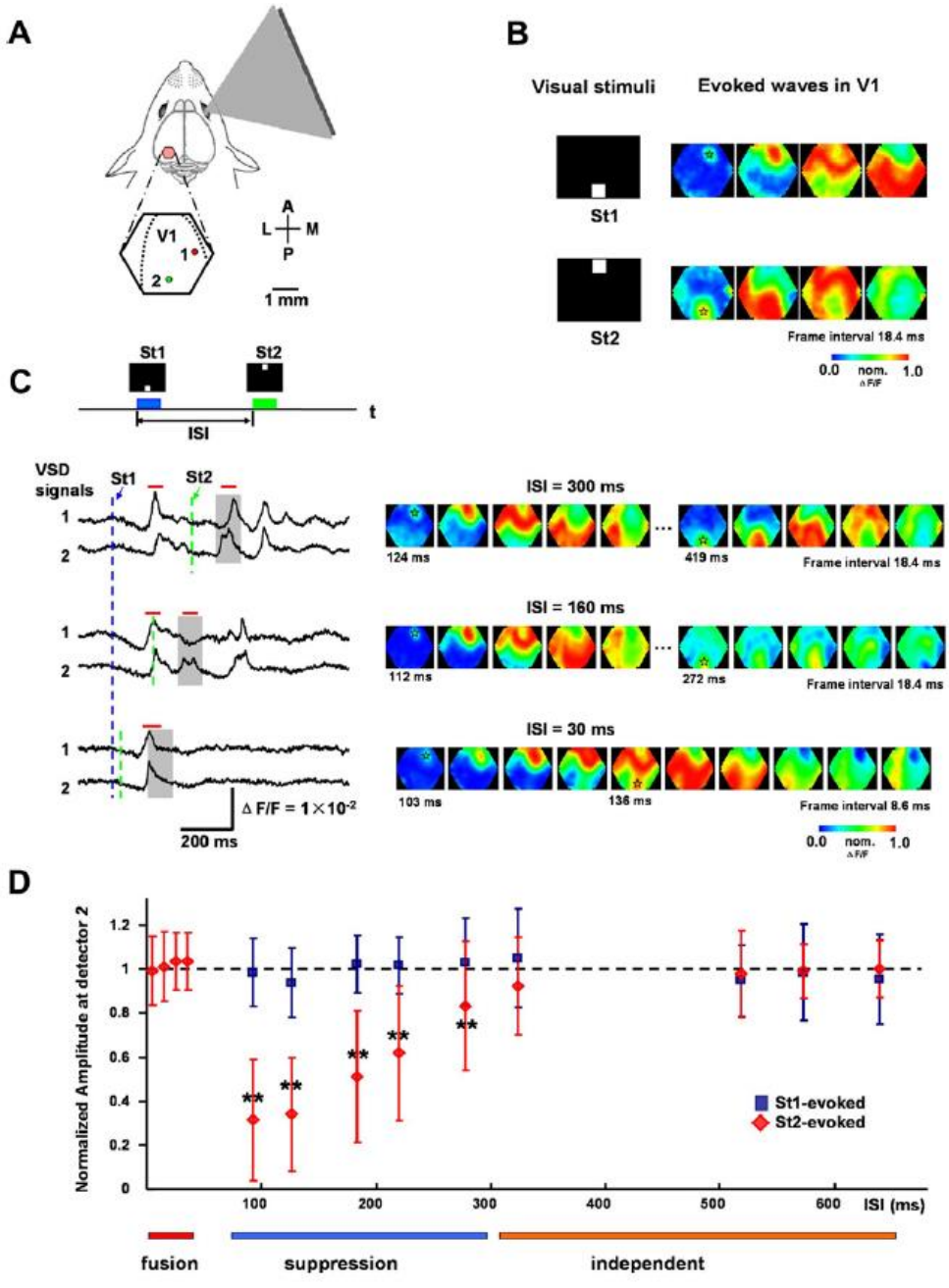

Figure 2.10: Interaction between traveling waves in V1, from Gao et al., 2012. A. *and* ***B.*** *VSD recordings were used in rats to investigate the interaction between traveling waves evoked by two visual stimuli, an upper and a lower square.* ***C.*** *and* ***D.*** *According to the inter-stimulus interval (ISI), we observe either a fusion, a suppression, or no interaction between the two traveling waves.*

Here, we are interested in mesoscopic traveling waves, i.e., that propagate within a single brain region. Each brain region is, however, adjacent to one another, and there is a myriad of dendritic and axonic connections between them. Thus, we wonder how **mesoscopic traveling waves in adjacent regions are behaving**? This question has begun to be studied in the visual cortex. More specifically, some studies were interested in the propagation of traveling waves within V1 and V2. They found that a single visual stimulation evoked traveling waves both in V1 and V2, that could be delayed between the two regions (Slovin et al., 2002), or that propagated synchronously (**Figure 2.11**, Muller et al., 2014). The propagation of traveling waves seems also to be reduced and slower at the border between V1 and V2 (Slovin et al., 2002; Xu et al., 2007).

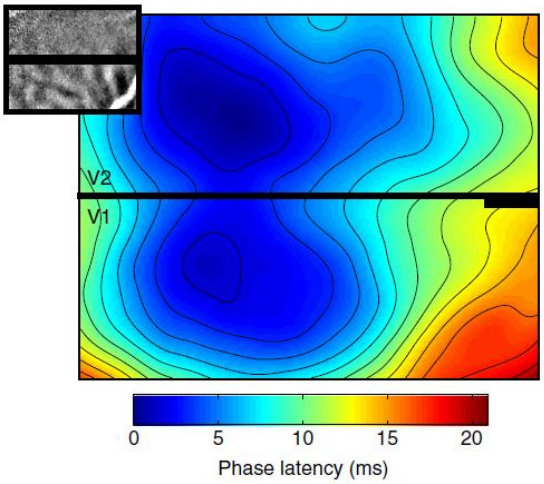

Figure 2.11: Simultaneous propagation of mesoscopic traveling waves in V1 and V2, from Muller et al., 2014.

Eventually, different shapes of traveling waves have been observed. Most of them are planar, but we will note that some studies found the presence of spiral waves, with a correspondence between the cycle of rotation, and the cycle of one oscillation (**Figure 2.12**, Huang et al., 2004).

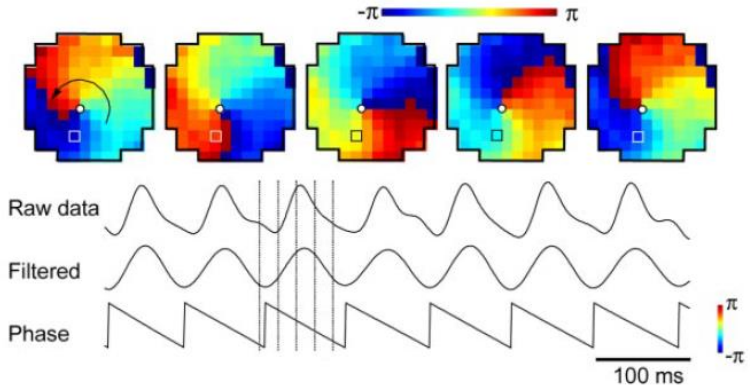

Figure 2.12: Spiral waves, from Huang et al., 2004. *VSD applied on rat neocortical slices (visual cortex).*

2.3. A possible role of mesoscopic traveling waves on cortical excitability and cognitive functions?

In the previous chapter, we saw that the phase of brain oscillations influences the state of cortical excitability. Here, we are interested in traveling waves, i.e., in brain oscillations presenting a constant phase shift across the cortex. Several studies highlighted that the **spiking activity** of neurons was correlated with the phase of oscillatory traveling waves (Roland et al., 2006; Lubenov and Siapas, 2009; Patel et al., 2012; Maris et al., 2013; Takahashi et al., 2015; Zang et al., 2015; Desserve at al., 2015; Hernandez-Perez et al., 2020; Davis et al., 2020; Sreekumar et al., 2021), as well as gamma bursting activity (Wu et al., 2001; Sreekumar et al., 2021) (but see Friedrich et al., 2004).

Traveling waves have also been correlated with a broad range of cognitive functions.

Theta traveling waves in the hippocampus appear to code for rat's position in space (Agarwal et al., 2014), in accordance with an important literature showing that hippocampal theta oscillations have a role in **spatial navigation**.

One study observed that the pattern of traveling waves was modulated by the attentional demand, in the brain area V4, during a visuo-attentional task (Maris et al., 2013), suggesting a relation between **attention** and traveling waves.

In 2008, Han et al. suggested that mesoscopic traveling waves could also play a role in visual **memory**. They observed that a training session significantly increased the proportion of spontaneous delta traveling waves in the visual cortex. Interestingly, these spontaneous traveling waves had the same initiation site and propagation as the visually-evoked traveling waves during the training. They proposed that this phenomenon of replaying the neural pattern of activity once the sensorial stimulation is over could be involved in the formation of visual short-term memory (Han et al., 2008).

In **motricity**, one study showed a correlation between the features of beta traveling waves and the position of the target in a reaching motor task (Rubino et al., 2006), suggesting that the phase and the amplitude of oscillatory traveling waves in the motor cortices provided task-related information.

One study revealed that oscillatory traveling waves in V4 were correlated with **saccadic eye movements**. They showed that the traveling waves triggered by a saccade led to a progressive phase reset from the center to the periphery of V4, entraining a synchronization between the probability of neuronal firing and the phase shift of oscillatory traveling waves. Those results suggest that traveling waves could reflect a mechanism used by the oculomotor system to control visuomotor processing (Zanos et al., 2015).

In **visual perception**, it has been shown that mesoscopic traveling waves explain illusory motion (Jancke et al., 2004; Zhang et al., 2012; Rekauzke et al., 2016; Chemla et al., 2019). Motion illusions are generated by presenting successively two identical stimuli according to a delay, at different positions in the visual field, relatively close to each other. Instead of perceiving two distinct stimuli, our brain perceives a single stimulus moving from the first to the second position in the visual field. It has been shown that this temporal sequence led to a first traveling wave propagating from the first stimulus to the second, and a second traveling wave propagating from the second to the first stimulus. The action of the first wave delayed and reduced the brain response at the onset of the second stimulus, and the second wave attenuates the brain response to the first stimulus. Importantly, the second suppressive traveling wave dampened the cortical representation of the first stimulation for the benefit of the second stimulus processing, leading to the representation of only one stimulus at a time, and the perception of the apparent motion illusion (Chemla et al., 2019). Another study demonstrated

that the mesoscopic traveling waves evoked by a moving stimulus was similar to the propagating activity evoked by illusory motion (Jancke et al., 2004; **Figure 2.13**).

Traveling waves seem also to communicate to specific neuronal populations the presence of visual features that are salient for the sending neuron (Besserve et al., 2015). Indeed, it has been showed that waves propagation was modulated between two neuronal population as a function of their tuning for visual features, i.e., in response to a visual stimulus, a traveling wave was more likely to propagate when the sending neuronal population was tuned to the feature of the visual stimulus; and the wave propagation is enhanced when the receiving neuron was less activated by the visual stimulation (Besserve et al., 2015).

Finally, a recent study demonstrated that spontaneous traveling waves predicted visual perception and the associated evoked-responses. Indeed, visual detection performance was modulated by the alignment of the phase of spontaneous traveling waves at stimulus onset (Davis et al., 2020).

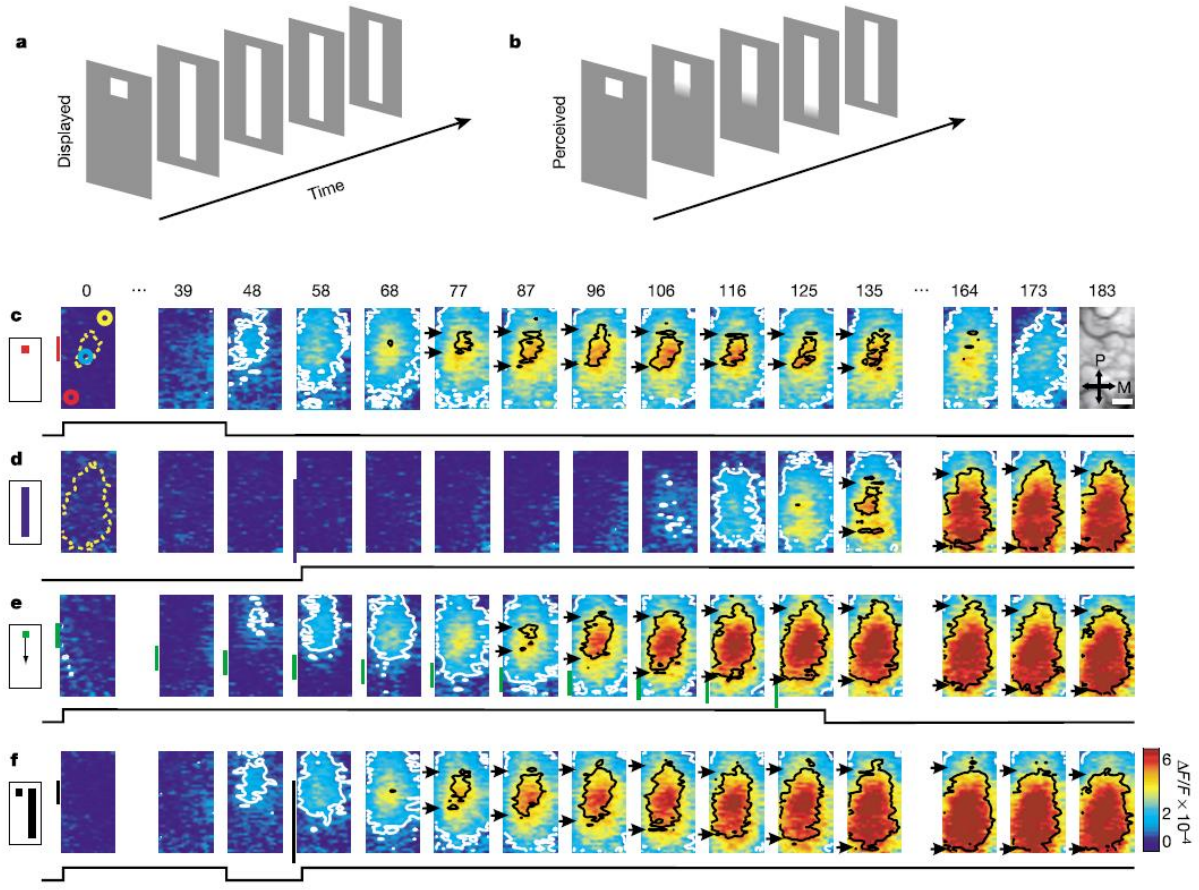

Figure 2.13: Propagating activity evoked by stationary, moving, and illusory moving stimuli, from Jancke et al., 2004. a. *Experimental paradigm: A square is presented shortly before a bar stimulus,* ***b.*** *creating an illusory perception of motion, i.e., the line-motion illusion.* ***c-f.***

Cortical activity recorded with intracellular electrodes and VSD in anesthetized cat's Brodmann area 18. At time 0 ms, the yellow dotted contours delimited the retinotopic representation of the stimuli. The color scale corresponds to changes in fluorescence across time, i.e., the neural activation. We observed traveling waves evoked by ***c.*** *a stationary square stimulus,* ***d.*** *a stationary bar stimulus,* ***e.*** *a moving square,* ***f.*** *the illusory motion. The propagating activity by the moving square and the illusory motion are very similar.*

The previous results come from invasive recordings. Some studies inferred a functional role of traveling waves on visual perception with psychophysics experiments, sometimes coupled with fMRI recordings. It appears that mesoscopic traveling waves in early visual areas support the phenomenon of binocular rivalry (Wilson et al., 2001; Lee et al., 2005). Binocular rivalry experiments rely on the presentation of two contradictory stimuli on each eye, leading to an alternation between the two percepts. To induce perceptual traveling waves, two moving gratings with opposite directions and contrast were displayed. When the perception of one moving grating was dominant, participants perceived a traveling wave that emerged locally and spread progressively, as a perceptual traveling wave, rendering the other grating invisible (**Figure 2.14**). Interestingly, the speed of the cortical traveling wave, recorded in the retinotopic map of V1, V2, and V3, with fMRI, corresponded to the subjective speed of the perceptual traveling wave (Lee et al., 2005, 2007). In addition, when a distracting stimulus was presented simultaneously of the binocular rivalry task, the traveling waves in V2 and V3 were altered (Lee et al., 2007), suggesting a role of attention on traveling waves in early visual areas triggered by visual perception. It has also been found that the propagation of traveling waves was correlated with the surface of the area V1 and V2, but not V3 (Genç et al., 2015).

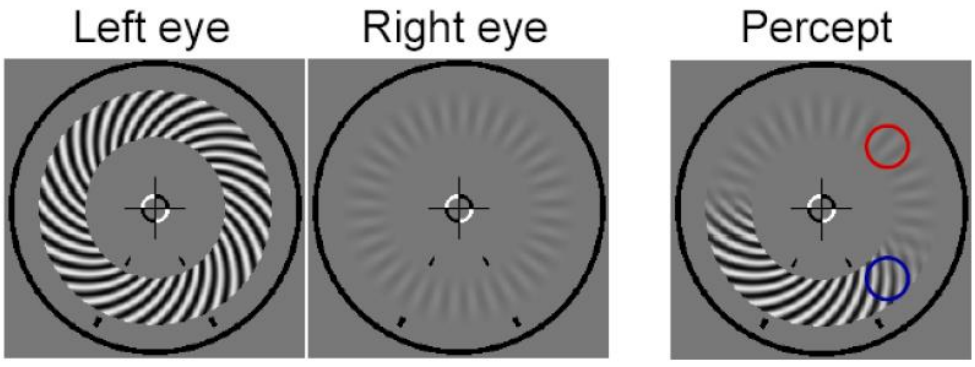

Figure 2.14: Perceptual traveling waves triggered by binocular rivalry in humans, from Lee et al., 2005.

Only one study using psychophysics demonstrated a functional role of oscillatory mesoscopic traveling waves at 5 Hz and 10 Hz on visual perception (Sokoliuk and VanRullen, 2016). The theoretical basis of this study will be explained in more details in **Chapter 6**.

2.4. What can be the neural support of mesoscopic traveling waves?

In a review, Ermentrout and Kleinfeld (2001) proposed three mechanisms allowing to explain the recording of traveling waves. (1) One single neuronal oscillator, i.e., a population of pacemaker neurons, can excite neighboring neuronal populations with an increasing delay (**Figure 2.15.a**). This mechanism lead to a fictive traveling wave, that does not rely on a true physiological process. (2) One single neuronal oscillator generates an output exciting activity that propagates along a chain of neuronal populations (**Figure 2.15.b**). This mechanism explains a true traveling wave, whose propagation's characteristics depend on the transmission between each neuronal population. (3) This final mechanism relies on a network of weakly coupled oscillators, i.e., each neuronal population can produce their own, intrinsic oscillatory activity, that propagates sequentially to the neighboring neuronal populations with a constant phase delay (**Figure 2.15.c**).

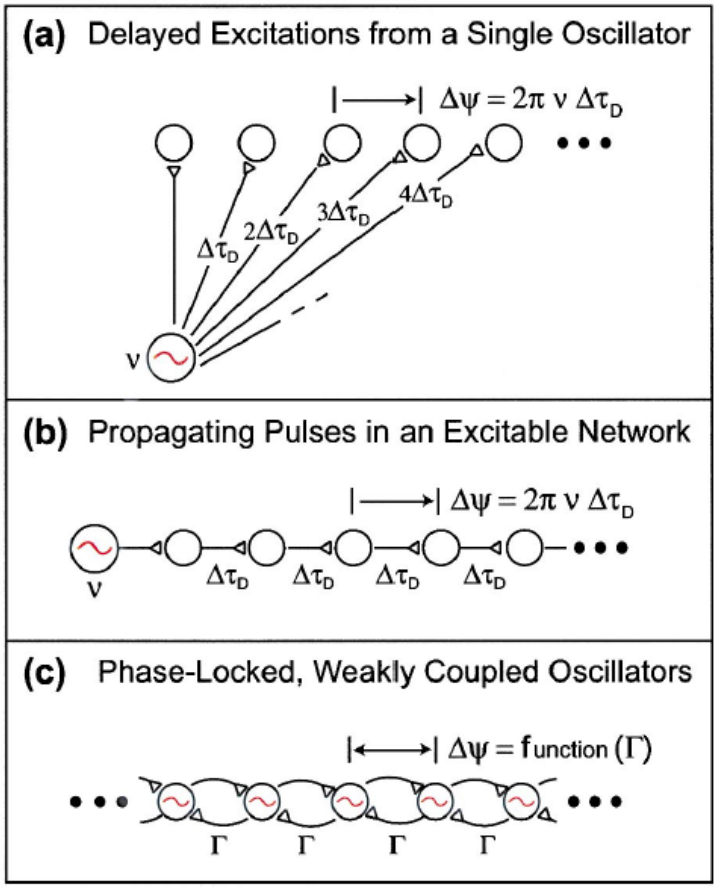

Figure 2.15: Neurophysiological models generating traveling waves, from Ermentrout and Kleinfeld, 2001.

Two mechanisms are physiologically plausible: the single oscillator (SO, **Figure 2.15.b**) and the weakly coupled oscillators (WCO, **Figure 2.15.c**). In the WCO model, the propagation of neuronal activity depends on a phase shift between the neuronal population, rather than time delays. Consequently, according to the WCO model, the propagation speed of traveling waves should be correlated with the frequency of the oscillation. Inversely, in the SO model, the propagation of neuronal activity depends on the axonal conduction delays. Because these conductions are fixed, the propagation of traveling waves should not correlate with the oscillatory frequency. Based on this rationale, few studies are in favor of a WCO model (Zhang and Jacobs, 2015; Hernadez-Pérez et al., 2020).

In both the SO and WCO models, the propagation of traveling waves is mediated by a communication between neuronal populations. Numerous studies suggest that this communication is supported by the unmyelinated long-horizontal fibers present in the superficial layers (II-III) of the cortex (Tanifuji et al., 1994; Nelson and Katz, 1995; Bringuier et al., 1999; Wu et al., 2001; Contreras and Llinas, 2001; Peterson et al., 2003a; Tucker and Katz, 2003; Ferezou et al., 2006; Song et al., 2006; Knapen et al., 2007; Nauhaus et al., 2009; Reynaud et al., 2012; Muller et al., 2014; Besserve et al., 2015; Davis et al., 2020). Indeed, 1) these connections spread over several millimeters of the cortical areas, 2) their speed, measured in vitro, is in the range of those estimated from recordings, and 3) VSD signal measured mostly the membrane potential of neural structures disposed in layers I-III. In addition, the fact that traveling waves have been recorded in cortical slices (**Table 2**) confirm that the propagation of cortical activity is supported by an intrinsic cortical circuitry.

For a long time, we thought that the horizontal fibres in V1 was connected preferentially to neurons with similar preferred orientation, i.e., like-to-like bias. A recent review suggests that the like-to-like bias occurs across short distance (a hypercolumn), and that a like-to-all bias emerges at long horizontal distance (Chavane et al., 2022), allowing the propagation of mesoscopic traveling waves across the entire V1 area.

3. Macroscopic traveling waves

3.1. A brain pattern mainly recorded in humans

The first macroscopic traveling waves have been recorded in 1935 (Adrian and Yamagiwa, 1935), in healthy humans, at rest. This result has then been replicated many times (**Table 3**).

In **humans**, **macroscopic oscillatory traveling waves** have been recorded in a broad range of frequency bands and during various cognitive tasks (**Figure 2.16**).

During **sleep**, studies observed that **very slow** oscillations (<1 Hz; Massimini et al., 2004, 2007; Nir et al., 2011), **delta** oscillations (Giannitrapani et al., 1966; Murphy et al., 2009; Hangya et al., 2011) and **spindles**, i.e., alpha activity (7-14 Hz) occurring during the second stage of sleep (Hughes et al., 1995; Muller et al., 2016), were propagating across the cortex.

Similarly, during **resting state**, the well-known **alpha** rhythm acted as macroscopic traveling waves (Adrian and Yamagiwa, 1935; Cohn, 1948; Goldman et al., 1949; Von Leeuwen, 1964; Walter et al., 1966; Giannitrapani et al., 1966; Liske et al., 1967; Shaw and McLachlan, 1968; Hori et al., 1969; Barlow and Estrin, 1971; Hoovey et al., 1972; Hord et al., 1972, 1974; Suzuki, 1974; Inouye et al., 1983, 1995; Thatcher et al., 1986; Schack et al., 2003; Ito et al., 2005, 2007; Manjarrez et al., 2007; Nolte et al., 2008; Bahramisharif et al., 2013; Van Ede et al., 2015; Halgren et al., 2019; Alamia and VanRullen, 2019; Pang et al., 2020).

Macroscopic traveling waves of **delta, theta, alpha** and **gamma** oscillations have been recorded while participants were performing a **memory task** (**delta**: Alexander et al., 2008, 2009, **theta**: Alexander et al., 2006; Sauseng et al., 2002; **alpha**: Schack et al., 1999; Sauseng et al., 2002; **multiple**: Van Der Meij et al., 2012; Zhang et al., 2018), a **visual task** (**theta**: Patten et al., 2012; Alexander et al., 2013; **alpha**: Shaw and McLachlan, 1968; Barlow and Estrim, 1971; Brenner et al., 1981; Maclin et al., 1983; Burkitt et al., 2000; Shevelev et al., 2000; Schack et al., 2003; Srinivasan et al., 2006; Cottereau et al., 2011; Fellinger et al., 2012; Patten et al., 2012; Van Ede et al., 2015; Pang et al., 2020; **gamma**: Rodriguez et al., 1999; VanEde et al., 2015; Tsoneva et al., 2021; **multiple**: Thorpe et al., 2007; Alexander et al., 2013), an **auditory task** (**delta**: Alexander et al., 2008, 2009; **alpha**: Darrow and Hicks, 1965; Shaw and McLachlan, 1968; **gamma**: Ribary et al., 1991; **multiple**: Giannitrapani, 1970), a **(oculo-) motor task** (**theta**: Giannini et al., 2018; **alpha**: Cooper and Mundy-Castle, 1960; Alexander et al., 2013), a **somatosensory task** (**alpha**: Shaw and McLachlan, 1968), a **temporal order judgement task** (**delta**: Kösem et al., 2014), **mathematical computation** (**theta**: Inouye et al.,

1994; **alpha**: Shaw and McLachlan, 1968; Hughes et al., 1995), and during **emotion and pain perception** (**alpha**: Hughes et al., 1995).

Some studies also found that **echoes** (10 Hz), electrical signals obtained from the cross-correlation between the EEG signal and a white-noise luminance stimulus, also propagated across the cortex (Lozano-Soldevilla and VanRullen, 2019; Alamia and VanRullen, 2019).

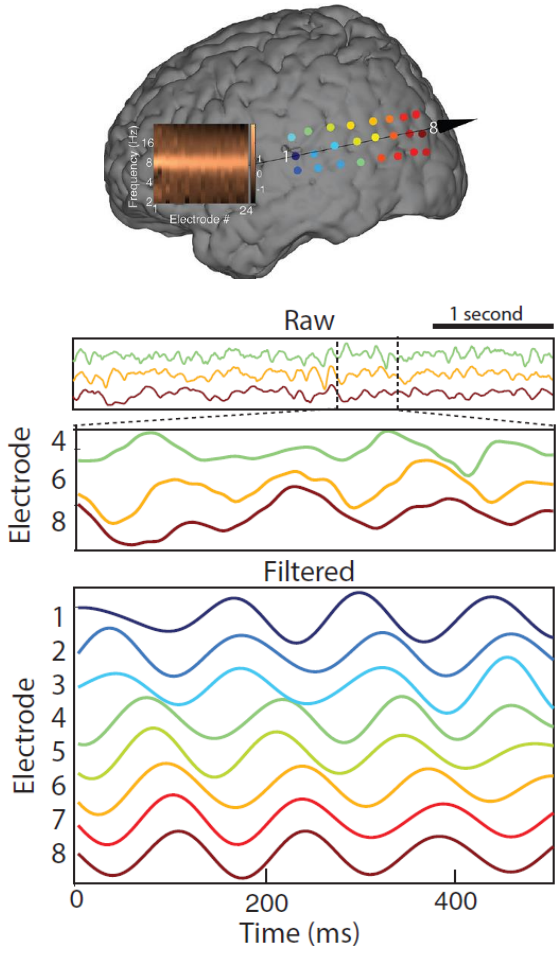

Figure 2.16: Macroscopic oscillatory traveling waves of alpha oscillations recorded in one patient with ECoG, from Zhang et al., 2018. *Raw (upper panel) and filtered (lower panel) brain signal for ECoG electrodes ordered in an anterior-to-posterior axis. Each electrode shows a clear brain oscillation, and we observe a shift of the phase from the anterior to the posterior electrodes, suggesting the presence of a macroscopic oscillatory traveling wave.*

Some studies found that **non-oscillatory** evoked responses also propagated in humans, after visual and somatosensory stimulations, and motor movements (Cracco et al., 1972; Childers et al., 1977; Gevins et al., 1989; Hughes et al., 1992; Klimesch et al., 2007b; Zauner et al., 2014; King and Wyart, 2021).

Macroscopic traveling waves have been less study in **animals**, likely because the use of invasive recordings in animal models allows to have a high spatial resolution, and is consequently better suited to investigate mesoscopic traveling waves. Still, we will note the recording of **delta** and **alpha** macroscopic traveling waves in animals (Roelfsema et al., 1997; Vyazovskiy et al., 2009).

Finally, in both **humans and animals**, MRI studies revealed that the **hemodynamic signals** in very low frequency range (0.01-0.1 Hz) also propagated across the cortex (Mitra et al., 2015; Matsui et al., 2016).

3.2. Macroscopic traveling waves: propagation speed, spatial extent, and other properties

Macroscopic traveling waves are propagating at a **speed of on average 5.2 m/s**, ranging from 0.4 to 20 m/s (Cooper and Mundy-Castle, 1960; Hughes et al., 1992, 1995; Burkitt et al., 2000; Schack et al., 2003; Massimini et al., 2004; Klimesch et al., 2007b; Manjarrez et al., 2007; Murphy et al., 2009; Hangya et al., 2011; Patten et al., 2012; Fellinger et al., 2012; Bahramisharif et al., 2013; Zauner et al., 2014; Muller et al., 2016; Zhang et al., 2018; Giannini et al., 2018; Halgren et al., 2019; Alamia and VanRullen, 2019; Tsoneva et al., 2021), over a **cortical distance of 5 to 25 cm**, for an average of 16.3 cm (Adrian and Yamagiwa, 1935; Brenner et al., 1981; Thatcher et al., 1986; Srinivasan et al., 2006; Thorpe et al., 2007; Zauner et al., 2014; Zhang et al., 2018; Tsoneva et al., 2021).

When considering the propagation of oscillatory traveling waves, we wonder what the phase shift between brain regions is, and whether there is a link between the propagation speed and the frequency.

The **phase shift** between occipital and frontal areas appears to range from 30° (Walter et al., 1966) to 145° - 180° (**Figure 2.17**; Cohn, 1948; Hord et al., 1972, 1974; Suzuki, 1974; Burkitt et al., 2000; Ito et al., 2005). One paper also found a larger phase shift of 240° (Zhang et al., 2018). As for mesoscopic traveling waves, it appears that only **one cycle of oscillation is propagating across the whole brain.**

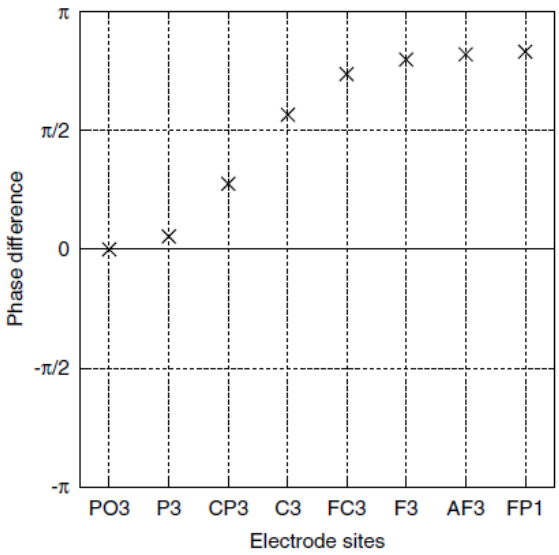

Figure 2.17. Phase shift between occipital and frontal electrodes, from Ito et al., 2005. *The phase difference between the occipital and the frontal electrodes gradually increases from 0 to almost 180°.*

The **propagation speed of oscillatory traveling waves is positively correlated to the frequency,** i.e., the higher the frequency, the faster the propagation speed (**Figure 2.18**; Patten et al., 2012; Zhang et al., 2018; Tsoneva et al., 2021). For example, Patten et al., (2012) showed in the same experiment that theta traveling waves were propagating at 4 m/s, while alpha traveling waves were propagating at 6.5 m/s (Patten et al., 2012).

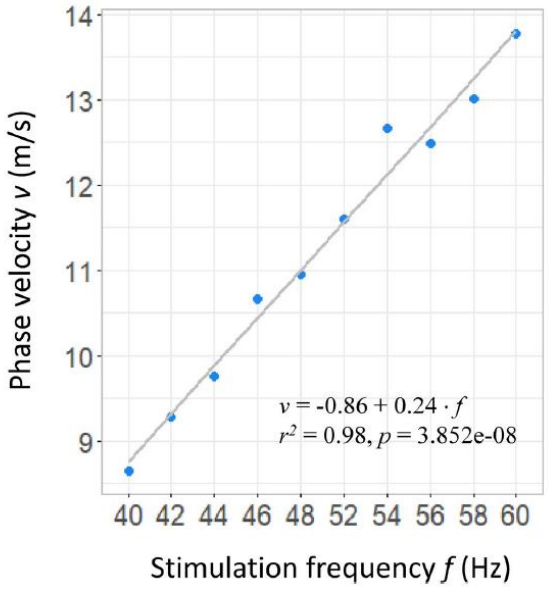

Figure 2.18: The propagation speed is positively correlated with the frequency of oscillatory traveling waves, from Tsoneva et al., 2021.

Macroscopic traveling waves are propagating across the whole brain, consequently, we wonder what **their direction** is. They mostly propagate in an anterior-to-posterior and in a posterior-to-anterior direction (Adrian and Yamagiwa, 1935; Cohn, 1948; Cooper and Mundy-Castle, 1960; Von Leeuwen, 1964; Walter et al., 1966; Shaw and McLachlan, 1968; Giannitrapani, 1970; Barlow and Estrim, 1971; Cracco, 1972; Hord et al., 1972; Suzuki, 1974; Childers, 1977; Inouye et al., 1983, 1994, 1995; Thatcher et al., 1986; Hughes et al., 1992, 1995; Ribary et al., 1991; Schak et al., 1999, 2003; Burkitt et al., 2000; Sauseng et al., 2002; Massimini et al., 2004; Ito et al., 2005, 2007; Alexander et al., 2006, 2008, 2009, 2013; Srinivasan et al., 2006; Klimesch et al., 2007b; Nolte et al., 2008; Murphy et al., 2009; Cottereau et al., 2011; Patten et al., 2012; Matsui et al., 2016; Zhang et al., 2018; Giannini et al., 2018; Alamia and VanRullen, 2019; Halgren et al., 2019; Lozano-Soldevilla and VanRullen, 2019; Pang et al., 2020; King and Wyart, 2021; Tsoneva et al., 2021).

The presence of rotating waves has also been observed (Goldman, 1949; Muller et al., 2016), as well as traveling waves propagating between the left and the right hemispheres (Liske et al., 1967; Giannitrapani, 1970; Hoovey et al., 1972; Schack et al., 2003; Ito et al., 2007), and from the midline to the periphery or toward the midline (Hughes et al., 1995).

Finally, multiple traveling waves can propagate across the scalp at the same time, and interact with each other. Only one study investigated this question. They triggered alpha traveling waves of echoes in the visual cortices, with a left and right stimulus displayed at the same time. They found that both waves appeared simultaneously and were superimposed on the scalp (**Figure 2.19**; Lozano-Soldevilla and VanRullen, 2019). However, at the moment, the way macroscopic traveling waves interact with each other remain ill-defined.

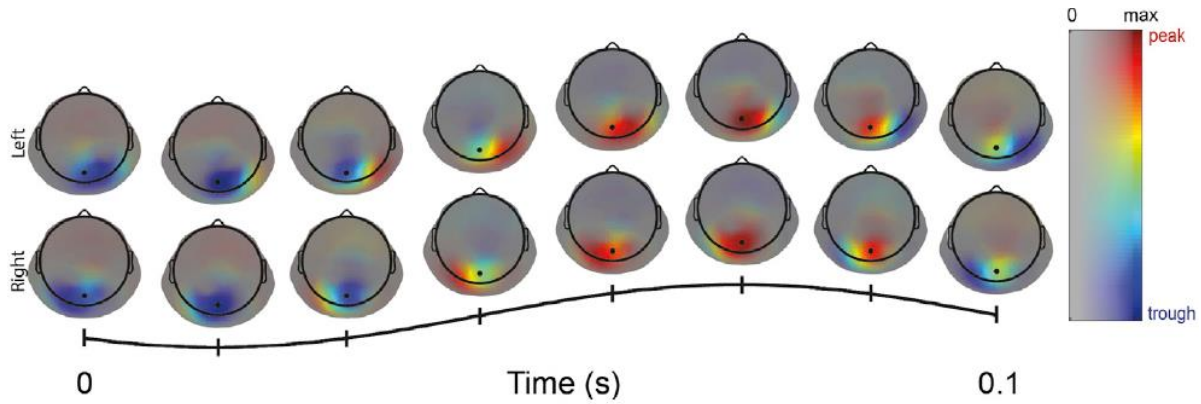

Figure 2.19: Simultaneous propagation of perceptual echoes triggered by a left and a right visual stimulus, from Lozano-Soldevilla and VanRullen, 2019. *Both echoes act as a traveling wave propagating from the occipital to the frontal cortices, with a phase shift across the scalp, and they were overlapping.*

3.3. A functional role of macroscopic traveling waves on cognitive functions and cortical excitability?

Some studies demonstrated that **gamma bursts** propagated according to the phase of oscillatory traveling waves, suggesting that cortical excitability followed the propagation of brain oscillations (Bahramisharif et al., 2013; Muller et al., 2016).

Concerning the functional role of macroscopic traveling waves on cognition, numerous studies found a correlation between their features and various cognitive functions.

Some studies have shown a functional role of macroscopic traveling waves in **memory** functions. A study comparing the performance between healthy and memory impaired elderly people during a working memory task demonstrated that the amount of traveling waves activity was correlated with behavioral and cognitive performance. Indeed, the behavioral performance of patients, indexed by the reaction times, was positively correlated with the strength of the spatio-temporal waves. In addition, a decreased posterior-to-anterior traveling wave activity was associated with a higher verbal learning deficit (Alexander et al., 2006). This is in line with an older study showing that the spatial organization of traveling waves was impaired in people with dementia (Ribary et al., 1991). Similarly, an ECoG study in drug-resistant epileptic patients demonstrated that the performance during a work memory task depends on traveling waves maintaining their optimal propagation direction, ant not on a change in the propagation speed or in the oscillating frequency (Zhang et al., 2018). In a task involving working and long-term memory systems, it has been shown that the memory performance was associated with the timing of change of traveling waves' direction, from the anterior-posterior trajectory, supposed to reflect working memory processes, to a posterior-to-anterior trajectory, expected to account for long-term memory processes (Sauseng et al., 2002).

Traveling waves seem also to be involved in **attention**. In Attention Deficit Hyperactivity Disorder (AHDH) children, the amount of traveling waves activity is reduced and negatively correlated with higher hyperactivity score (Alexander et al., 2008).

In **time perception**, one study revealed that a phase shift of an induced delta traveling wave during an audio-visual lag-adaptation, then predicted the participant's shifts of subjective audio-visual simultaneity (Kosem et al., 2014).

The propagation of oscillatory traveling waves seems to have a role in **visual perception**. The speed of alpha traveling waves was negatively correlated to reaction times in a visual categorization task, suggesting that slow alpha waves were associated with image categorization (Fellinger et al., 2012). A correlation between the propagation speed of prestimulus alpha traveling waves and reaction times have also been found in a visual go-no go task (Patten et al., 2012). Similarly, the speed and the direction of alpha traveling waves appeared to differ between the processing of concrete vs abstract words, suggesting a role of the propagation activity during word processing (Schak et al., 2003). During illusory perception, it appeared that the direction of traveling waves predicts the visual illusion perceived (Shevelev et al., 2000). One study suggested that non-oscillatory traveling brain activity encoded and communicated visual information trough the cortical hierarchy (**Figure 2.20**; King and Wyart, 2021). Finally, several studies observed a change in the direction of alpha traveling waves, from frontal to occipital cortices during resting state, to occipital to frontal cortices during visual perception, presumably to communicate visual information from the sensory cortex to higher-order level brain areas (**Figure 2.21**; Schack et al., 1999; Patten et al., 2012; Alamia and VanRullen, 2019; Pang et al., 2020).

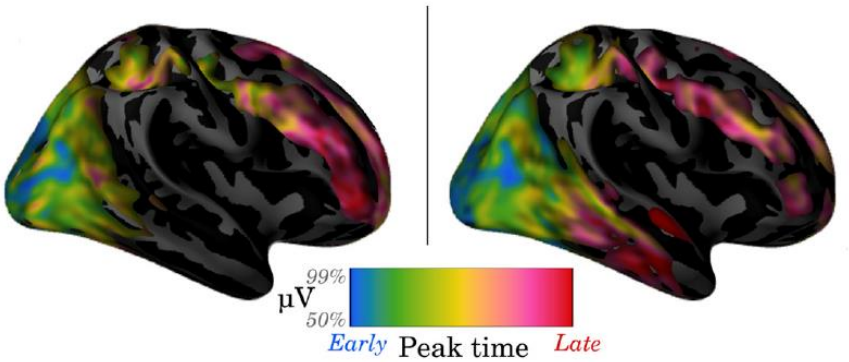

Figure 2.20: Visual representations propagate from low to higher-level areas, from King and Wyart, 2021. *Left panel, Orientation of the Gabor patches. Right panel, Changes in orientation. For both low-level visual information, the spatial pattern peaked in the occipital electrodes and then propagated towards anterior electrodes.*

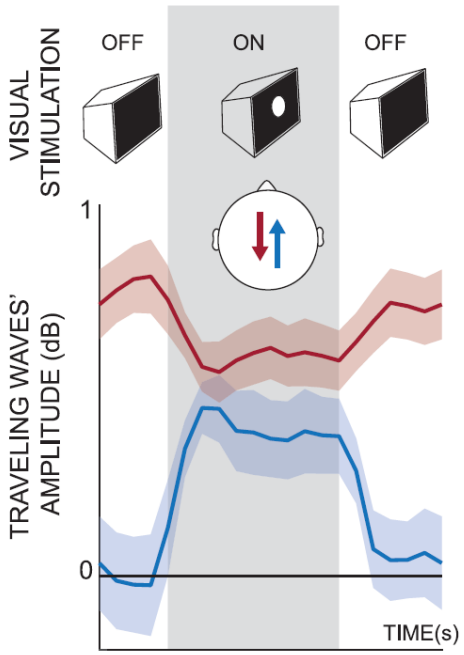

Figure 2.21: The direction of alpha traveling waves shifts according to on and off changes of visual stimulation, from Pang et al., 2020. *When the visual stimulus is off, alpha traveling waves propagate mainly in an anterior-to-posterior direction (in red), while when the visual stimulus if on, they mainly propagate in the posterior-to-anterior direction (in blue).*

Traveling waves have been associated to **saccadic eye movements**. In a freely viewing task, the spatial organization of traveling waves predicted saccade direction (Giannini et al., 2018).

A study also suggests a role of traveling waves in **semantic and lexical access** (Zauner et al., 2014).

Finally, some studies suggest that traveling waves could reflect the underlying **connectivity** between brain regions. Indeed, in schizophrenic patients that present a hypofrontality, i.e., a reduced connectivity between frontal regions and other brain regions, it has been shown that the patients presented less traveling waves activity with an anterior-to-posterior gradient (Alexander et al., 2009).

In conclusion, numerous studies found a correlation between various cognitive functions and changes in the **number and the direction of traveling waves** (Hughes et al., 1995; Alamia and VanRullen, 2019).

3.4. Models of macroscopic traveling waves

Macroscopic traveling waves are mainly recorded with EEG, an electrophysiological technique allowing to measure the global dynamics of large population of neurons. However, the EEG suffer from a low spatial resolution, impacted by a strong space averaging due to volume conduction effect, mainly induced by the physical separation between the neuronal sources and the sensors, i.e., the cerebrospinal fluid and the skull present conductivity that differ from the cortex. For these reasons, the best way to explain the emergence of macroscopic traveling waves, from the neuronal populations to the scalp, is to develop biophysiological models.

In a series of publications, Nunez developed a model based on the global theory of EEG (Nunez, 1974, 1981, 1989, Nunez and Srinivasan, 2006). This theory proposed that the EEG activity emerged from a coupling between cortical columns connected by short range intra-cortical fibers and long range cortico-cortical fibers. The model developed by Nunez relies on the propagation of action potential along the cortico-cortical fibres, that generate post-synaptic fields activity, mainly excitatory because the inhibitory interactions are frequently observed in the intra-cortical interactions, and with a spatio-temporal organization that depends on the location of the underlying firing activity (Nunez, 1989). This model predicted traveling waves that propagate across the entire cortical circumference, and with a phase velocity of approximatively 10 m/s, which is the range of velocities measured in humans (Nunez, 1989).

Alamia and VanRullen (2019) proposed a model of traveling waves based on the predictive coding framework. According to this framework, the brain is composed of high-level areas that predict the activity of low-level areas. These predictions are then compared to the actual brain activity in the low-level areas, and the unexplained residuals, also called the prediction errors, are communicated from the low-level to high-level areas (**Figure 2.22**). The predictive coding model proposes a mechanism which is cyclic by nature, and that relies on feedback and feedforward communications between areas, rendering this model plausible to explain the emergence of traveling waves (Alamia and VanRullen, 2019). Indeed, the model displays feedforward traveling waves, i.e., that propagate with a posterior-to-anterior direction, in the alpha range, in response to white-noise stimulus; and feedback traveling waves, i.e., that propagate in an anterior-to-posterior direction, in the alpha range, in response to an endogenous stimulus (Alamia and VanRullen, 2019).

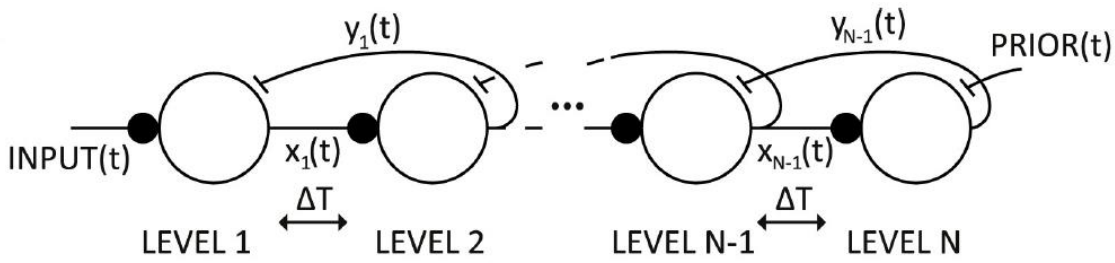

Figure 2.22: Predictive coding model, from Alamia and VanRullen, 2019. *The hierarchically higher levels (LEVEL2, LEVEL N) make predictions y(t) about the input received by the lower level (LEVEL 1, LEVEL N-1), and the residuals x(t), which corresponds to the prediction errors, are used to update the next prediction. ΔT is a constant representing the communication delay between two levels.*

Similarly, King and Wyart (2021) developed a model explaining traveling waves, in lines with the predictive coding framework. Their model was a 10-layer hierarchy of two variables, y, that represent the retention of stimulus information over time, and x, corresponding to the update of these representations. Each layer was interconnected with recurrent feedforward and/or feedback connections. They showed that the low-visual features propagated across a neuronal chain of negative feedback loops, recruited after the onset of the stimulus, to update the brain representation of the visual stimulus, and after the offset of the stimulus, to maintain the visual information over time, presumably to generate predictions concerning the future visual features (King and Wyart, 2021).

Interestingly, Hindriks et al., (2014) showed that macroscopic traveling waves recorded with EEG could be explained by the slow propagation of mesoscopic traveling waves over small cortical distance, mediated by intra-cortical axons, at a propagation speed of 0.3 m/s (Hindriks et al., 2014). According to this model, the high propagation speed of macroscopic traveling waves recorded on the scalp would be a consequence of the local curvature of the cortex, that entrains high angular velocities of the electrical activity (**Figure 2.23**; Hindriks et al., 2014).

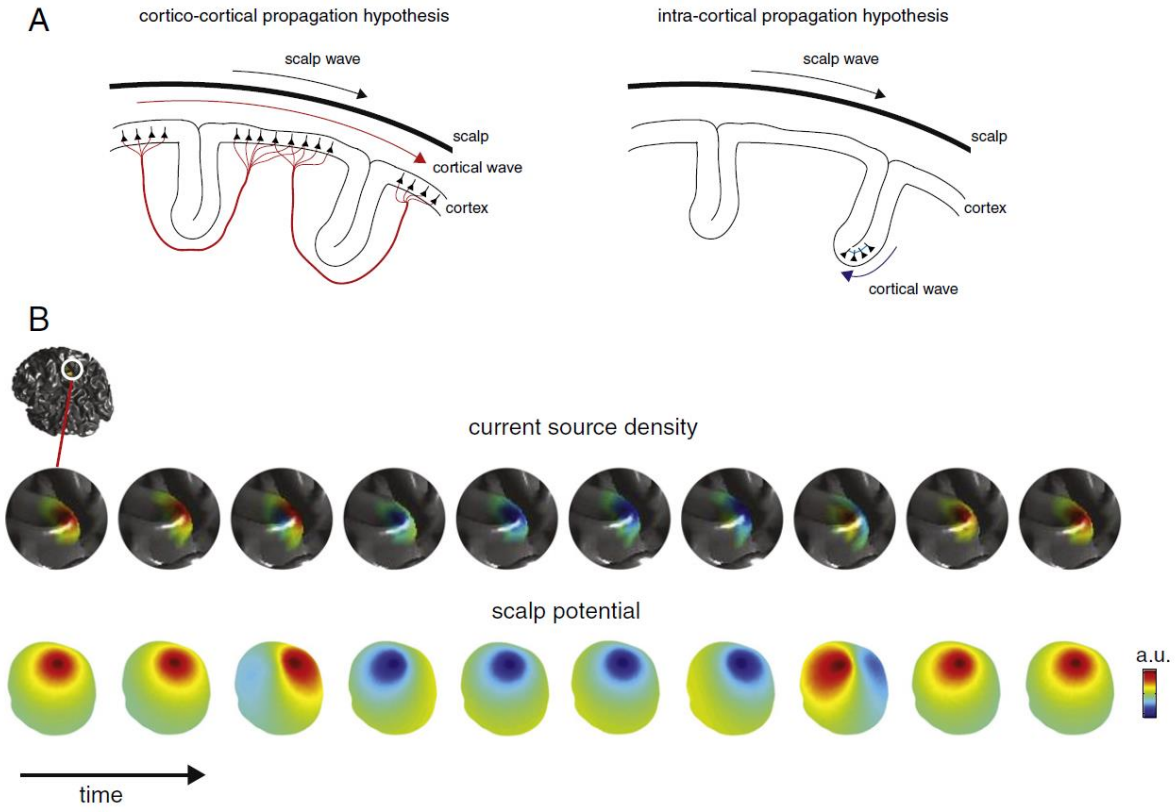

Figure 2.23: Cortico-cortical vs intra-cortical propagation, form Hindriks et al., 2014. A. *Left, Representation of the cortico-cortical propagation. Macroscopic traveling waves propagate through the neocortex via cortico-cortical axons. Right, Representation of the intra-cortical propagation. Macroscopic traveling waves result from localized mesoscopic traveling waves, mediated by intra-cortical axons.* ***B.*** *Top, Current source densities of a simulated mesoscopic traveling waves that propagate over a cortical gyrus. Bottom, Induced electrical activity at the surface of the scalp. The scalp potential behaves like a macroscopic traveling waves.*

Different models have been proposed to explain the emergence of macroscopic traveling waves. Further works is needed to better understand the physiological mechanism underlying macroscopic traveling waves.

4. Summary

The propagation of neuronal activity has been observed since the beginning of the EEG with Adrian and Mathews (1934a) and Adrian and Yamagiwa (1935).

Mesoscopic traveling waves have been mainly recorded in in vitro preparation and in anesthetized animals, with invasive recordings. They correspond to the propagation of a transient or an oscillatory activity across a single brain area, at a propagation speed between

0.24 and 0.58 m/s, over a short cortical distance (a few mm). Mesoscopic traveling waves are presumably supported by an intrinsic cortical circuitry, the unmyelinated long-horizontal fibers present in the superficial layers (II-III) of the cortex. Some studies suggest that this propagating activity could have a role in cognitive functions, but this question has been poorly studied. In this PhD, we wonder whether alpha oscillations can propagate across the retinotopic space and influence visual perception across space, in healthy humans (**see Chapter 6**).

Macroscopic traveling waves have been mainly recorded in humans, with non-invasive recordings methods with low spatial resolution (MEG/EEG). They propagate at a speed of 5.2 m/s, over a large cortical distance from 5 to 25 cm, and could be oscillatory or non-oscillatory activity. Numerous studies found a correlation between various cognitive functions and changes in the number and the direction of traveling waves. However, their direct, functional role on cognitive function remains ill-defined. In this PhD, we want to better understand the causal and functional role of macroscopic traveling waves on cognition (**see Chapter 7**).

Study	Date	Method	Human/ Animal	Awake/ Anesthetized/In vitro	Frequency	Modality	Task	Speed (m/s)	Distance (mm)	Cortical area
Non-oscillatory										
Animals										
Albowitz et al.	1990	VSD	Guinea pig	Slice	_	_	Elec., Che.	0.013-0.265	_	Sensory cortex
Albowitz and Kuhnt	1991	VSD	Guinea pig	Slice	_	_	Elec., Che.	0.069-0.538	1.2	Hippocampus
Albowitz and Kuhnt	1993	VSD	Guinea pig	Slice	_	_	Elec.	0.095-0.675	_	Visual cortex
Arieli et al.	1996	VSD, LFP	Cat	Anesthetized	_	Visual	Vis., RS	_	_	V1
Bakin et al.	1996	VSD	Rat, Guinea pig	Anesthetized	_	Auditory	Aud.	_	few	Auditory cortex
Bringuier et al.	1999	Microelectrodes	Cat	Anesthetized	_	Visual	Vis.	0.1	_	V1
Burns	1950	Microelectrodes	Cat	In vitro	_	_	Elec., RS	0.015-2	1	Visual cortex
Chagnac-Amitai and Connors	1989	Microelectrodes	Rat	Slice	_	_	Che.	0.002-0.1	2	S1
Chang	1951	Microelectrodes	Cat, Monkey	Anesthetized	_	_	Elec.	0.6-1	5	Parietal cortex
Chemla et al.	2019	VSD	Monkey	Awake	_	Visual	Two-step apparent motion	0.26	3	V1
Chen et al.	2006	VSD	Monkey	Awake	_	Visual	Detection task	_	1.54-2.2	V1
Chervin et al.	1988	LFP	Rat, Cat	Slice	_	_	Elec.	0.06-0.09	few	S1, M1, V1
Cinelli et al.	1995	VSD	Salamander	Anesthetized	_	Olfactory	Olf., Elec.	_	_	Olfactory bulb
Cinelli and Kauer	1995	VSD, Microelectrodes	Salamander	Anesthetized	_	_	Elec.	_	_	Olfactory bulb and cortex
Civillico and Contreras	2006	VSD, LFP	Mouse	Anesthetized	_	Somatosensory	Sens., Elec.	_	_	Somatosensory cortex

Contreras and Llinas	2001	VSD, intraEEG	Guinea Pig	Slice	_	_	Elec.	0.181-0.217	1-2	Visual and Somatosensory cortices
Demir et al.	1999	VSD	Rat	Slice	_	_	Elec.	_	_	Olfactory cortex
Derdikman et al.	2003	VSD	Rat	Anesthetized	_	Somatosensory	Sens.	0.3-0.45	_	Somatosensory cortex
Ferezou et al.	2006	VSD	Mouse	Awake and Anesthetized	_	Somatosensory	Sens., Freely behaving	_	_	Barrel cortex
Ferezou et al.	2007	VSD	Mouse	Awake and Anesthetized	_	Somatosensory	Sens., Elec., RS	_	_	Somatosensory and Motor cortex
Fleidervish et al.	1998	Microelectrodes	Mouse	Slice	_	_	Che.	0.004	_	Barrel cortex
Friedrich and Korsching	1998	VSD	Zebrafish	Anesthetized	_	Olfactory	Olf., Elec.	_	_	Olfactory bulb
Fukunishi et al.	1992	VSD	Guinea pig	Anesthetized	_	Auditory	Aud.	_	1.8	Auditory cortex
Gao et al.	2012	VSD	Rat	Anesthetized	_	Visual	Vis., Elec.	0.065	_	Visual cortex
Grinvald et al.	1982	VSD	Rat	Slice	_	_	Elec.	0.1	_	Hippocampus
Grinvald et al.	1994	VSD	Monkey	Anesthetized	_	Visual	Vis.	0.09-0.25	1.5-2.7	V1
Holsheimer and Da Silva	1989	Microelectrodes	Guinea pig	Slice	_	_	Che., Elec.	0.1-1.8	1	Hippocampus
Jancke et al.	2004	VSD, intraEEG	Cat	Anesthetized	_	Visual	Illusory motion	0.09	_	V1
Kitano et al.	1995	LFP	Cat	Anesthetized	_	Visual	Vis.	_	_	Visual cortex
Knowles et al.	1987	Microelectrodes	Guinea pig	Slice	_	_	Che., Elec.	0.13-0.21	_	Hippocampus
Laaris et al.	2000	VSD, LFP	Mouse	Slice	_	_	Elec., Che.	0.04	_	Somatosensory cortex
Lilly and Cherry	1954	Microelectrodes	Cat	Anesthetized	_	Auditory	Aud.	0.06-0.96	_	Auditory cortex
Lippert, Takagaki et al.	2007	VSD, LFP	Rat	Anesthetized	_	Visual and Somatosensory	Vis., Sens., RS	0.2	4	Visual and Barrel cortices

London et al.	1989	VSD	Rat	Anesthetized	_	Somatosensory	Sens., Elec.	0.6	_	Somatosensory cortex
Luczak et al.	2007	Microelectrodes	Rat	Anesthetized and Awake	_	_	RS	_	_	Somatosensory cortex
Miles et al.	1988	LFP	Guinea Pig	Slice	_	_	Che.	0.15	10	Hippocampus
Nauhaus et al.	2009, 2012	LFP, MUA	Monkey, Cat	Anesthetized	_	Visual	Vis., RS	0.09-0.3	2.1-5.8	V1
Nelson and Katz	1995	VSD	Ferret	Slice	_	_	Elec.	0.16	1	Visual cortex
Nishimura et al.	2007	VSD	Guinea Pig	Anesthetized	_	Auditory	Aud.	_	_	Auditory cortex
Novak and Wheeler	1989	Microelectrodes	Rat	Slice	_	_	Che.	0.29-0.41	_	Hippocampus
Orbach and Cohen	1983	VSD, LFP	Salamander	Anesthetized, In vitro	_	_	Olfactory nerve stimulation	0.2	_	Olfactory bulb
Petersen et al.	2003a	VSD, whole-cell recordings	Rat	Anesthetized	_	Somatosensory	Sens.	0.033-0.06	_	Barrel cortex
Petersen et al.	2003b	VSD, Microelectrodes	Rat, Mouse	Awake and Anesthetized	_	Somatosensory	Sens., RS	0.1	0.5-1.5	Somatosensory cortex
Rekauzke et al.	2016	VSD	Cat	Anesthetized	_	Visual	Vis.	0.13-0.2	1.2-3	V1
Reimer et al.	2011	LFP	Rat	Anesthetized	_	Auditory	Aud.	0.00001-0.00002	4	Auditory cortex
Reynaud et al.	2012	VSD	Monkey	Awake	_	Visual	Vis.	0.01-0.37	2-8	V1
Schwartzkroin and Prince	1978	Microelectrodes	Guinea pig	Slice	_	_	Che.	_	2 -3	Hippocampus
Sharon et al.	2007	VSD, Microelectrodes	Cat	Anesthetized	_	Visual	Vis.	_	_	Visual cortex
Sit et al.	2009	VSD	Monkey	Awake	_	Visual	Vis.	0.4	2.75	V1
Slovin et al.	2002	VSD	Monkeys	Awake	_	Visual	Vis., Saccadic eye movement task	0.15-0.19	6.5-9	V1, V2

Song et al.	2006	VSD	Guinea Pig	Anesthetized, In vitro	_	Auditory	Aud., Elec.	0.26-0.38	3	A1
Sugitani et al.	1994	VSD	Guinea pig	Slice	_	_	Elec.	_	_	Olfactory cortex
Sutor et al.	1994	VSD, LFP	Rat	Slice	_	_	Che.	0.078	_	Frontal cortex
Takagaki et al.	2008	VSD	Rat	Anesthetized	_	Visual and Somatosensory	Vis., Sens., RS	0.2-0.32	_	Visual, Somatosensory and Associative cortices
Tanifuji et al.	1994	VSD	Rats	Slice	_	_	Elec.	0.06	0.9	Visual cortex
Taniguchi et al.	1992	VSD	Guinea pig	Anesthetized	_	Auditory	Aud.	_		Auditory cortex
Tsau et al.	1998	VSD, Microelectrodes	Rat	Slice	_	_	Che.	0.031	_	Neocortex
Tsytarev et al.	2004	Optics, Microelectrodes	Cat	Anesthetized	_	Auditory	Aud.	_	_	A1
Tucker and Katz	2003	VSD, intraEEG	Ferret	Slice	_	_	Elec.	0.24	0.4-2	Visual cortex
Uno et al.	1993	VSD	Guinea pig	Anesthetized	_	Auditory	Aud.	_	_	Auditory cortex
Volgushev et al.	2006	LFP, Microelectrodes	Cat	Anesthetized	_	_	_	_	4-12	Somatosensory cortex
Voskuyl and Albus	1985	Microelectrodes	Rat	Slice	_	_	Che.	0.01-0.5	_	Hippocampus
Wadman and Gutnick	1993	Microelectrodes	Guinea Pig	Slice	_	_	Elec.	0.008-0.15	3	Neocortex
Witte et al.	2007	Microelectrodes	Cat	Awake	_	Auditory	Aud.	0.05-0.2	few	Auditory cortex
Wu et al.	2001	VSD, LFP	Rat	Slice	_	_	Elec.	0.001-0.02	0.8	Auditory and Somatosensory cortices
Xu et al.	2007	VSD	Rat	Anesthetized	_	Visual	Vis., Elec.	0.05-0.07	_	V1, V2
Yang et al.	2015	VSD	Monkey	Awake	_	Visual	Vis.	0.023-0.03	5	V1, V2

Yuste et al.	1997	VSD	Rat	Slice	_	_	Elec.	0.001	_	Visual cortex
Zhang et al.	2012	VSD	Rat	Awake	_	Visual	Apparent motion	_	_	V1
Humans										
Knapen et al.	2007	Psychophysics	Human	Awake	_	Visual	Binocular rivalry	_	_	V1
Lee et al.	2005	Psychophysics, fMRI	Human	Awake	_	Visual	Binocular rivalry	0.16-0.22	_	V1
Lee et al.	2007	Psychophysics, fMRI	Human	Awake	_	Visual	Binocular rivalry	_	_	V1, V2, V3
Genç et al.	2015	Psychophysics, MRI	Human	Awake	_	Visual	Binocular rivalry	_	_	V1, V2, V3
Wilson et al.	2001	Psychophysics	Human	Awake	_	Visual	Binocular rivalry	0.224-0.44	–	V1
Oscillatory										
Animals										
Adrian and Matthews	1934	ECoG	Rabbit	Anesthetized	Alpha (10 Hz)	_	Che.	0.01	4	Neocortex
Agarwal et al.	2014	MUA, LFP	Rat	Awake	Theta (8-9 Hz)	_	Freely behaving	0.01	_	Hippocampus
Andersen et al.	1966	Microelectrodes	Cat	Anesthetized	Spindle (7-14 Hz)	_	_	_	_	Thalamic nuclei
Arieli et al.	1995	VSD; Microelectrodes	Cat	Anesthetized	Alpha (7-14 Hz)	Visual	Vis.	_	few	Visual cortex
Benucci et al.	2007	VSD	Cat	Anesthetized	Alpha (10 Hz)	Visual	SSVEP	0.2-0.5	_	V1
Besserve et al.	2015	LFP, MUA	Monkey	Anesthetized	Gamma (50-80 Hz)	Visual	Vis., RS	0.36	few	V1
Contreras et al.	1996	LFP	Cat	Anesthetized	Spindle (7-14 Hz)	_	_	_	_	Thalamus
Contreras et al.	1997	Microelectrodes	Cat	Anesthetized, In vitro	Spindle (7-14 Hz)	Sleep	Elec., RS	0.001-0.003	–	Thalamus

Csicsvari et al.	2000	MUA, LFP	Rat	Awake	Ripple (80-250 Hz)	Sleep	_	_	_	Hippocampus
Davis et al.	2020	MUA, LFP	Monkey	Awake	Multiple (10-30 Hz)	Visual	Detection task, Natural vision	0.1-0.6	_	Middle Temporal visual area
Delaney et al.	1994	VSD	Mollusk	In vitro	1 Hz	Olfactory	Old., RS	_	_	Olfactory organ
Freeman	1978	MUA	Cat and Rabbit	Awake and Anesthetized	Gamma (38-80 Hz)	Olfactory	Olf., Elec.	0.45-7.36	few	Olfactory bulb and cortex
Freeman and Baird	1987	Microelectrodes	Rabbit	Awake	Gamma (39-90 Hz)	Olfactory	Discrimination task	1.72-1.87	_	Olfactory bulb
Freeman and Barrie	2000	Microelectrodes	Rabbit	Awake	Gamma (20-80 Hz)	Visual, Auditory, Somatosensory	Discrimination task	0.5-4	5-20	Visual, Auditory and Somatosensory cortices
Friedrich et al.	2004	LFP, VSD	Zebrafish	In vitro	Beta (20-30 Hz)	Olfactory	Olf.	0.45	2	Olfactory bulb
Gabriel and Eckorn	2003	MUA, LFP	Monkey	Awake	Gamma (30-90 Hz)	Visual	Vis.	_	7	V1
Gervais et al.	1996	VSD, Microelectrodes	Mollusk	In vitro	0.7 Hz	Olfactory	Olf.	_	_	Olfactory organ
Han et al.	2008	VSD	Rat	Anesthetized	Delta (0.5-4 Hz)	Visual	Vis., RS	0.01-0.016	few	Visual cortex
Hernandez-Perez et al.	2020	LFP, MUA	Rat	Awake	Theta (~8 Hz)	_	Freely behaving	0.08-0.18	_	Medial Entorhinal cortex
Huang et al.	2004	VSD	Rat	Slice	Multiple (4-15 Hz)	_	Che.	_	few	Visual cortex
Huang et al.	2010	VSD, Microelectrodes	Rat	Anesthetized	Multiple (3-22 Hz)	Sleep	Che., Sleep	_	_	Visual cortex
Ketchum and Haberly	1993	LFP	Rat	Anesthetized	Gamma (54 Hz)	_	Elec.	_	_	Olfactory cortex

Kim et al.	1995	Microelectrodes	Ferret	Slice	Spindle (7-14 Hz)	Sleep	Elec., RS	0.0003-0.0015	–	Thalamic nuclei
Kleinfeld et al.	1994	LFP, VSD	Mollusk	In vitro	1 Hz	_	_	0.001	_	Olfactory organ
Lam et al.	2000, 2003	VSD, LFP	Turtle	Awake	14.1 Hz (rostral), 6.6 Hz (caudal)	Olfactory	Olf.	0.12-0.18	2	Olfactory bulb
Lubenov and Siapas	2009	LFP, MUA	Rat	Awake	Theta (4-10 Hz)	_	Freely behaving	0.08-0.1	11.1-14.9	Hippocampus
Maris et al.	2013	LFP, MUA	Monkey	Awake	Theta (3-4 Hz), Alpha (9-13 Hz), Gamma (35-75 Hz)	Visual	Visual attentional task	–	<1	V4
Muller et al.	2014	VSD	Macaque	Awake	Multiple (5-20 Hz)	Visual	Vis., RS	0.25-1.35	7	V1, V2
Murthy and Fetz	1996	LFP	Monkeys	Awake	Beta (20-40 Hz)	Motor	Motor task	_	15	Motor cortex
Neuenschwander and Singer	1996	MUA	Rabbit	Anesthetized	Gamma (81 Hz)	Visual	Vis.	_	_	Thalamic nuclei
Nikitin and Balaban	2000	Microelectrodes, VSD	Mollusk	In vitro	0.6-0.8 Hz	Olfactory	Old., RS	0.003	_	Procerebral lobe
Patel et al.	2012	LFP, MUA	Rat	Awake	Theta (5-10 Hz)	_	Freely behaving, Sleep	0.16	10	Hippocampus
Patel et al.	2013	LFP	Rats	Awake	Ripple (140-180 Hz)	Sleep	Sleep	0.35	4-8	Hippocampus
Petsche and Stumpf	1960	Microelectrodes	Rabbits	Anesthetized	Theta (4-7 Hz)	_	Elec., Che., Sens.	0.19-0.5	few	Neocortex, Hippocampus, Diencephalon
Prechtl et al.	1997	VSD, LFP	Turtle	Awake	Multiple (5-23 Hz)	Visual	Vis.	0.05-0.09	_	Visual cortex
Prechtl et al.	2000	LFP	Turtle	In vitro	Beta (20 Hz)	Visual	Vis.	0.2-0.4	2	Visual cortex

Ray and Maunsell	2011	MUA	Monkey	Awake	Multiple (3-90 Hz)	Visual	Detection task	0.25-0.49	2	V1
Rubino et al.	2006	LFP	Monkeys	Awake	Beta (10-45 Hz)	Motor	Reaching and choice task	0.12-0.28	10	M1 and Dorsal Premotor cortex
Sanchez-Vives and Cormick	2000	Microelectrodes	Ferret	Slice	0.1-0.5 Hz	_	_	0.01	_	Visual and Prefrontal cortices
Stroh et al.	2013	Optogenetics, LFP	Mouse	Anesthetized	< 1 Hz	Visual	Optogenetics, Vis.	0.037	few	V1, Frontal area, Thalamic nuclei
Takahashi et al.	2015	LFP, MUA	Monkey	Awake	Beta (15-40 Hz)	Motor	Motor task	0.23-0.26	_	M1
Townsend et al.	2015	MUA, LFP	Monkey	Anesthetized	Delta (1-4 Hz)	Visual	Vis.	_	_	Middle Temporal visual area
Verzeano and Negishi	1960	Microelectrodes	Cat	Anesthetized	Spindle (7-14 Hz)	Visual	Vis.	_	_	Thalamic nuclei
Wright and Sergejew	1991	Microelectrodes	Cat	Awake	Multiple (1-32 Hz)	_	RS	0.1-0.29	7	Occipito-parietal cortex
Wu et al.	1999	VSD, LFP	Rat	Slice	Alpha (7-10 Hz)	_	_	0.3	> 5	Somatosensory cortex
Ylinen et al.	1995	MUA	Rat	Awake	Ripple (150-200 Hz)	Sleep	Sleep	_	_	Hippocampus
Zanos et al.	2015	LFP	Macaque	Awake	Beta (20-40 Hz)	Visual	Saccades	0.31	121	V4
Humans										
Liou et al.	2017	intraEEG	Human	Awake	Ictal Discharge (80-150 Hz)	–	–	0.229-0.472	–	Temporal cortex
Smith et al.	2016	intraEEG	Human	Awake	Ictal Discharge (< 50 Hz)	–	–	0.21	5.67	Associative cortex
Sokoliuk and VanRullen	2016	Psychophysics	Human	Awake	5 Hz and 10 Hz (SSVEP)	Visual	SSVEP	_	few	V1

Sreekumar et al.	2021	intraEEG	Human	Awake	Multiple (2-14 Hz)	Memory	Memory task	0.11	_	Temporal cortex
Takahashi et al.	2011	intraEEG	Human	Awake	Beta (15-18 Hz)	Motor	Motor task, RS	0.15-0.35	_	Motor cortex
Zhang and Jacobs	2015	intraEEG	Human	Awake	Theta (2-8 Hz)	Memory	Memory task	1-5	_	Hippocampus

Table 2. Publications on mesoscopic traveling waves. *VSD: Voltage Sensitive Dye. MUA: Multi-Unit array. LFP: Local Field Potential. intraEEG: intra Electroencephalography. (f)MRI: (functional) Magnetic Resonance Imaging. Elec.: Electrical Stimulation. Che.: Chemical Stimulation. Olf.: Olfactive Stimulation. Sens.: Sensory Stimulation. Vis.: Visual Stimulation. Aud.: Auditory Stimulation. RS: Resting State. SSVEP: Steady State Visual Evoked Potential. V1: Primary Visual Cortex. S1: Primary Somatosensory Cortex. A1: Primary Auditory Cortex. M1: Primary Motor Cortex.*

Study	Date	Method	Human/ Animal	Awake/ Anesthetized	Oscillatory	Modality	Task	Speed (m/s)	Distance (cm)	Direction
Non-oscillatory										
Humans										
Childers	1977	EEG	Human	Awake	VEP	Visual	Vis.	_	_	AP
Cracco	1972	EEG	Human	Awake	SEP	Somatosensory	SensMot	_	_	AP
Gevins et al.	1989	EEG	Human	Awake	ERP	Visuomotor	Visuomotor task	_	_	_
Hughes et al.	1992	EEG	Human	Awake	VEP	Visual	SSVEP	3.9-6.7	_	AP and PA
King and Wyart	2021	EEG	Human	Awake	_	Visual	Vis.	_	_	PA
Klimesch et al.	2007	EEG	Human	Awake	VEP	Visual	Vis.	3	_	PA
Zauner et al.	2014	EEG	Human	Awake	VEP	Visual	Semantic task	5-6	8	_
Oscillatory										
Animals										
Matsui et al.	2016	HemoS	Mouse	Anesthetized	0.045 Hz	_	RS	_	_	AP
Roelfsema et al.	1997	Microelectrodes	Cat	Awake	Alpha (7-13 Hz)	_	RS	_	_	_
Vyazovskiy et al.	2009	LFP	Rat	Awake	Delta (0.5-4 Hz)	Sleep	Sleep	_	_	_
Humans										
Adrian and Yamagiwa	1935	EEG	Human	Awake	Alpha (10 Hz)	_	RS	_	5	PA
Alamia and VanRullen	2019	EEG	Human	Awake	Echoes, Alpha	Visual	Vis., RS	2.2	_	PA and AP
Alexander et al.	2006	EEG	Human: memory impairments and healthy	Awake	Theta (6 Hz)	Memory	Mem.	_	_	PA (mostly)

Alexander et al.	2008	EEG	Human: ADHD and healthy	Awake	Delta (1 Hz)	Auditory, Visual	Aud., Mem.	_	_	PA
Alexander et al.	2009	EEG	Human: schizophrenia and healthy	Awake	Delta (2-4 Hz)	Auditory, Visual	Aud., Mem.	_	_	AP
Alexander et al.	2013	MEG/ EEG/ ECoG	Human	Awake	MEG: Delta, Alpha; EEG: Theta, Alpha; ECoG: Alpha.	MEG: audio-visual; EEG: visual; ECoG: motor.	MEG: Vis.; EEG: Vis.; ECoG: SensMot.	–	–	MEG: AP-SI; EEG: PA; ECoG: SI.
Bahramisharif et al.	2013	ECoG	Human	Awake	Alpha (8-10 Hz)	_	RS	0.7-2.1	_	_
Barlow and Estrin	1971	EEG	Human	Awake	Alpha (9-10 Hz)	Visual	RS, SSVEP	_	_	PA
Brenner et al.	1981	MEG	Human	Awake	Alpha (13 Hz)	Visual	SSVEP	_	8	_
Burkitt et al.	2000	EEG	Human	Awake	Alpha (10 Hz)	Visual	SSVEP	7-11	_	PA
Cohn	1948	EEG	Human	Awake	Alpha (10 Hz)	_	RS	_	_	AP/PA
Cooper and Mundy-Castle	1960	EEG	Human	Awake	Alpha (8-11 Hz)	Motor	SensMot	1-20	_	AP and PA
Cottereau et al.	2011	MEG	Human	Awake	Alpha (7.5, 15 Hz)	Visual	Vis.	_	_	PA
Darrow and Hicks	1965	EEG	Human	Awake	Alpha (10 Hz)	Auditory	Aud.	_	_	_
Fellinger et al.	2012	EEG	Human	Awake	Alpha (8-12 Hz)	Visual	Vis.	6-12	_	posterior-to-lateral
Giannini et al.	2018	EEG	Human	Awake	Theta (6.5 Hz)	Oculomotor	Natural scenes	3	_	PA-IS
Giannitrapani et al.	1966	EEG	Human	Awake	Alpha, Delta (4 Hz)	_	RS, Sleep	_	_	_
Giannitrapani	1970	EEG	Human: children.	Awake	Multiple (8-24 Hz)	Auditory	RS, Aud.	_	_	AP/PA, LR/RL
Goldman et al.	1949	EEG	Human	Awake	Alpha	_	RS	_	_	rotating

Halgren et al.	2019	ECoG	Human	Awake	Alpha (7-13 Hz)	_	RS	1	_	AP-SI and PA
Hangya et al.	2011	ECoG	Human	Awake	Delta (0.5-2 Hz)	Sleep	Sleep	3.3	_	_
Hoovey et al.	1972	EEG	Human	Awake	Alpha	_	RS	_	_	LR/RL
Hord et al.	1972	EEG	Human	Awake	Alpha (10 Hz)	_	RS	_	_	PA
Hord et al.	1974	EEG	Human	Awake	Alpha (9-10.5 Hz)	_	RS	_	_	_
Hori et al.	1969	EEG	Human	Awake	Alpha	_	RS	_	_	_
Hughes et al.	1995	EEG	Human	Awake	Alpha, Spindles	_	RS, Sleep, Math., Emotion and Pain perception	3.1-3.8	_	toward-midline, from-midline, AP, PA
Inouye et al.	1983	EEG	Human	Awake	Alpha (7-13 Hz)	_	RS	_	_	AP
Inouye et al.	1994	EEG	Human	Awake	Theta (6-7 Hz)	_	Math.	_	_	AP/PA
Inouye et al	1995	EEG	Human	Awake	Alpha (7-14 Hz)	_	RS	_	_	PA
Ito et al.	2005	EEG	Human	Awake	Alpha (8-13 Hz)	_	RS	_		PA
Ito et al.	2007	EEG	Human	Awake	Alpha (8-13 Hz)	_	RS	_	_	AP and LR
Kosem et al.	2014	MEG	Human	Awake	Delta (1 Hz)	Audio-visual	Temporal order judgment task	_	_	_
Liske et al.	1967	EEG	Human	Awake	Alpha (10 Hz)	_	RS	_	_	LR/RL
Lozano-Soldevilla and VanRullen	2019	EEG	Human	Awake	Echoes	Visual	Vis.	_	_	PA
Maclin et al.	1983	MEG	Human	Awake	Alpha (13 Hz)	Visual	SSVEP	_	_	_
Manjarrez et al.	2007	EEG	Human	Awake	Alpha (10 Hz)	_	RS	2.1	_	multiple
Massimini et al.	2004	EEG	Human	Awake	< 1 Hz	Sleep	Sleep	1.2-7	_	AP (mostly) and PA
Massimini et al.	2007	EEG	Human	Awake	<1 Hz	Sleep	TMS pulses	_	_	_

Mitra et al., 2015	2015	MRI	Human	Awake	<1 Hz	Sleep	Sleep, RS	_	_	AP
Muller et al.	2016	ECoG	Human	Awake	Spindles (11-15 Hz)	Sleep	Sleep	2-5	_	temporal-to-parietal-to-frontal
Murphy et al.	2009	EEG	Human	Awake	Delta	Sleep	TMS pulses	0.4 - 6.3	_	AP and PA
Nir et al.	2011	ECoG	Human	Awake	<1 Hz	Sleep	Sleep	_	_	_
Nolte et al.	2008	EEG	Human	Awake	Alpha (10 Hz)	_	RS	_	_	AP
Pang et al.	2020	EEG	Human	Awake	Alpha (8-13 Hz)	Visual	Vis., RS	_	_	PA and AP
Patten et al.	2012	EEG	Human	Awake	Theta (4-8 Hz), Alpha (8-12 Hz)	Visual	Vis.	4-6.5	_	PA and AP
Ribary et al.	1991	MEG	Human: memory impairments and healthy	Awake	Gamma (40 Hz)	Auditory	SSAEP	_	_	AP
Rodriguez et al.	1999	EEG	Human	Awake	Gamma (36-40 Hz)	Visual	Vis.	_	_	_
Sauseng et al.	2002	EEG	Human	Awake	IAF -6/+4 Hz, IAF -4/+2 Hz	Memory	Mem.	_	_	AP and PA
Schack et al.	1999	EEG	Human	Awake	Alpha (8-10 Hz)	Memory	Mem.	_	_	PA
Schack et al.	2003	EEG	Human	Awake	Alpha (8-10 Hz)	Visual	RS, Vis.	10	_	PA, LR, RL
Shaw and McLachlan	1968	EEG	Human	Awake	Alpha	_	RS, Aud., Vis., SensMot., Math.	_	_	AP/PA
Shevelev et al.	2000	EEG	Human	Awake	Alpha (IAF)	Visual	SSVEP	_	_	multiple
Srinivasan et al.	2006	EEG	Human	Awake	Alpha (11-13 Hz)	Visual	SSVEP	_	12-25	PA
Suzuki	1974	EEG	Human	Awake	Alpha (8-10 Hz)	_	RS	_	_	PA

Thatcher et al.	1986	EEG	Human: Children.	Awake	Delta (0.5-3.5 Hz), Theta (3.5-7 Hz), Alpha (7-13 Hz), Beta (13-22 Hz)	–	RS	_	20	PA and AP
Thorpe et al.	2007	EEG, MEG	Human	Awake	Theta (4-8 Hz), Alpha (10-14 Hz)	Visual	SSVEP	_	20-25	_
Tsoneva et al.	2021	EEG	Human	Awake	Gamma (40-60 Hz)	Visual	SSVEP	8-14.	21.6-23.5	PA
van DerMeij et al.	2012	ECoG	Human	Awake	Multiple (2-16 Hz)	Memory	Mem.	_	_	_
van Ede et al.	2015	MEG	Human	Awake	Alpha (8-12 Hz), Gamma (50-70 Hz)	Visual	Vis., RS	_	_	_
Von Leeuwen	1964	EEG	Human	Awake	Alpha (10 Hz)	_	RS	_	_	PA
Walter et al.	1966	EEG	Human	Awake	Alpha (11 Hz)	_	RS	_	_	PA
Zhang et al.	2018	ECoG	Human	Awake	Multiple (2-15 Hz)	Memory	Mem.	0.55	11.7	AP and PA

Table 3. Publications on macroscopic traveling waves. *EEG: Electroencephalography. MEG: Magnetoencephalography. ECoG: Electrocorticography. HemoS: Hemodynamic signal. MRI: Magnetic Resonance Imaging. LFP: Local Field Potential. VEP: Visual Evoked Potential. SEP: Somatosensory Evoked Potential. IAF: Individual alpha frequency. SSVEP: Steady State Visual Evoked Potential. SSAEP: Steady State Auditory Evoked Potential. Vis.: Visual task. SensMot.: Sensorimotor task. Aud.: Auditory task. Mem. Memory task. Math.: Mathematical computation. TMS: Transcranial Magnetic Stimulation. AP: Anterior-to-posterior. PA: Posterior-to-anterior. LR: Left-to-right. RL: Right-to-left. SI: Superior-to-inferior. IS: Inferior-to-superior.*

Chapter 3. Aim of this PhD.

The temporal features of brain oscillations (phase, amplitude) can predict perception, e.g., perception is modulated periodically by the phase of low-frequency brain oscillations. This phase effect only account for less than 20% of the trial-by-trial variability in perceptual performance (e.g., Busch et al., 2009; Dugué et al., 2011a; Hanslmayr et al., 2013; Samaha et al., 2015). In this PhD, we hypothesize that if brain oscillations are the support of perception, they should explain a larger portion of the variance observed in empirical data. We propose that we can better characterize the functional role of brain oscillations on perception by considering the interaction between the temporal features and the spatial organization of brain oscillations.

We decided to study **visual perception**, a modality that has been widely studied by the scientific community, at a physiological, anatomical, and functional level.

One of the main advantages of the visual system is the phenomenon of **retinotopy**, i.e., elements close to each other in the visual field are encoded by two neuronal populations close to each other in the cortex (**Figure 3.1**). This topographical mapping of the spatial structure and the distance between elements in the visual field appears between the retina and area V1, but also in other cortical visual areas higher in the hierarchy, such as V2, V3, V4. The representation of the visual scene is distorted. The visual information that appears in the fovea has a larger cortical representation compared to the periphery, associated to a higher spatial resolution. This distortion between the actual visual stimulation and its representation in the cortex is done through a factor of **cortical magnification**.

It is also possible to **individually map participants' retinotopic cortex** using fMRI. Cortical representation of eccentricity is performed by displaying a ring filled with a checkerboard that extends from the center to the periphery. Cortical representation of visual polar angles is performed by displaying a wedge filled with a checkerboard that is rotating around a point in the center of the screen. This experimental method allows the identification of the early visual regions in each individual (**Figure 3.2**) (Dougherty et al., 2003; Larsson and Heeger, 2006; Dugué et al., 2020). Retinotopic mapping is useful to study the spatial organization of brain oscillations in humans.

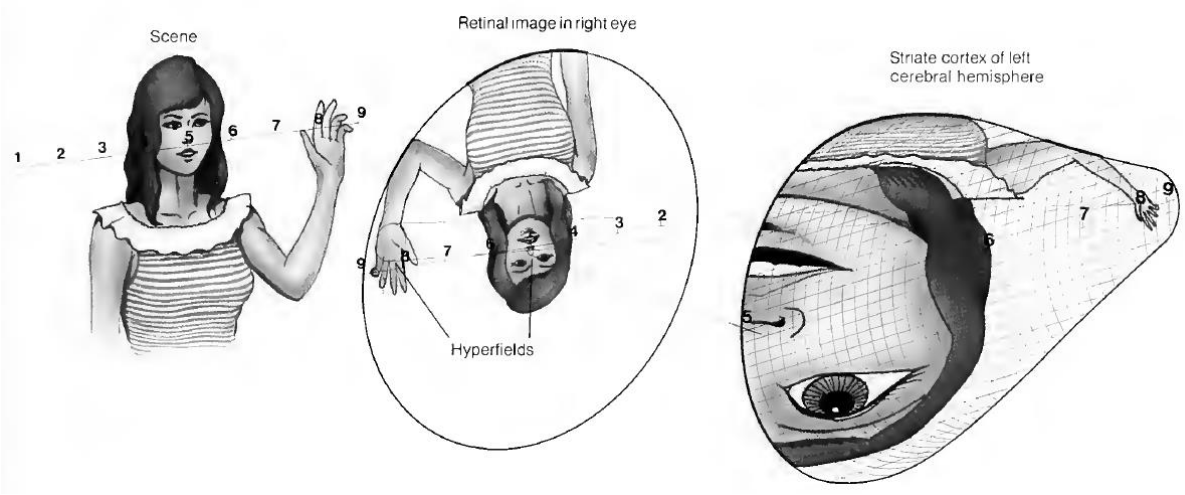

Figure 3.1: Image inversion and distortion, from Frisby, 1979. *At the stage of the retina, the image of the visual object is inverted in an upside-down manner. At the stage of the primary visual cortex, the image is still inverted, but also disproportionate. The visual information received in the fovea has a greater representation in the brain.*

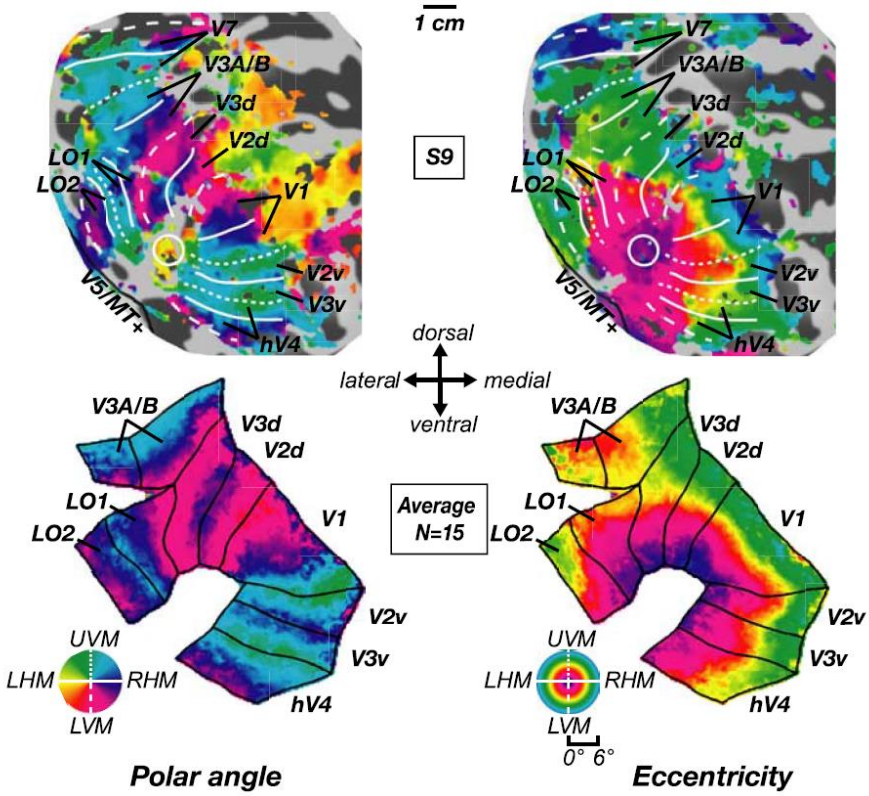

Figure 3.2: Retinotopic mapping, from Larsson and Heeger, 2006. *Up, retinotopic map of one participant. Down, retinotopic maps averaged across all participants (n=15).*

In this PhD, we also want to test **causal links** between brain oscillations and visual perception. To this aim, we use a non-invasive interventional technique, the **transcranial magnetic stimulation (TMS)**. TMS was first proposed as a tool to stimulate the brain by

Barker, in 1985 (Barker et al., 1985). They showed that a pulse of TMS applied over motor cortices led to the stimulation of the peripheral nerve, followed by a muscle contraction.

Magnetic stimulation relies on the Faraday's law of electromagnetism induction that describes the interaction between magnetic and electric fields (Faraday, 1832). Electromagnetism induction states that a changing electric current produces a changing magnetic field, that, in turn, induces a secondary electric current (Epstein, 2008). In the case of TMS, the magnetic stimulator, i.e., a capacitive high-voltage, high-current charge-discharge system, is going to produce and store an electric current, that will be transfer to the magnetic stimulation coil to produce a magnetic field (Wagner et al., 2007). By applying the coil on the human scalp, the induced magnetic field entrain a secondary electric current that spreads over neural and non-neural tissues, according to their conduction properties (Wagner et al., 2009). The direction of the electrical current induced in the brain tissue is perpendicular to the surface of the coil (Valero-Cabre et al., 2017). This electrical field influences the electrical state of neuronal population in the brain region targeted by the coil. To place the TMS coil with a high spatial precision, it is possible to use online stereotaxic neuronavigation systems. These systems are able to track in real time the position of the TMS coil in space, and allow an online visualization of the coil's position on a 3D reconstruction of individual MRI head-brain volume (Valero-Cabre et al., 2017). The resulting electric field induced by TMS on the cortex can be modeled from anatomical MRI images (Thielscher et al., 2015; **Figure 3.3**).

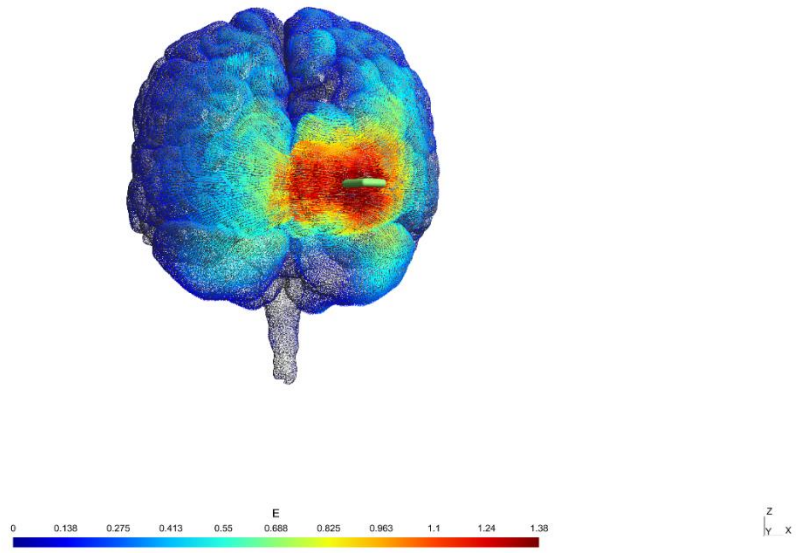

Figure 3.3: Modeling of the electrical current induced by a single-pulse TMS applied over the visual cortex, with SimNIBS (Thielscher et al., 2015). *The 3D head model was constructed from individual MRI images provided in SimNIBS. A Magstim 70 mm figure-of-eight coil was*

selected and placed over the right visual cortex. Its position and direction are represented in green. The electric field (V/m) induced by a single-pulse TMS is represented on the 3D head model.

This PhD aims to demonstrate that **taking into account both the spatial and the temporal organization of brain oscillations** simultaneously, and in their entirety, i.e., **the dynamics of the phase and amplitude across time and space**, will allow us to **better understand their functional role on visual perception**.

To achieve our objectives, we developed **4 projects** and used a multimodal approach including **psychophysics**, **neuroimaging** (EEG, MRI, oculometry), and **TMS**, and collected, and analyzed, data from healthy human participants.

In the first project, we tested whether there is a causal, joint relation between the amplitude and the phase of brain oscillations, the state of cortical excitability and the subsequent visual perception. Single pulses of TMS applied over V1/V2 elicit an illusory percept called phosphene. Phosphene perception depends on the ongoing cortical state, and allows testing for causal relation between spontaneous brain oscillations, cortical excitability, and the associated visual perception. Studies using this paradigm showed that the probability to perceive a phosphene is higher when the amplitude of spontaneous alpha oscillations is low (Romei et al., 2008; Samaha et al., 2017), and fluctuates along with the alpha phase (Dugué et al., 2011a; Samaha et al., 2017). In addition, phosphene perception leads to a higher event-related potential (ERP) than the absence of percept (Dugué et al., 2011a; Taylor et al., 2010; Samaha et al., 2017), allowing to quantify the modulation in cortical excitability. Here, we studied the causal interaction between the amplitude and the phase of brain oscillations according to the predictions made by the Pulsed Inhibition theory (Jensen and Mazaheri, 2010). Cortical excitability and visual perception were assessed with phosphene perception (and their evoked activity) induced by single pulses of TMS over the occipital cortex, with simultaneous EEG recording to measure spontaneous brain oscillations.

In the second project, we asked whether the temporal dynamics of the spatial pattern of brain oscillations can predict a complex phenomenon of visual perception, serial dependance. The behavioral phenomenon of serial dependance describes that visual perception is biased toward perceived stimuli in the recent past, i.e., the construction of visual perception depends on both prior and present visual inputs (Fischer and Whitney, 2014; Collins,

2019, 2020). Serial dependance occurs for various visual features, including, orientation (Fischer and Whitney, 2014), face perception (Liberman et al., 2018), and numerosity (Fornaciai and Park, 2019), suggesting an important principle of visual perception. However, the neural dynamics of serial dependance is poorly understood. In our project, we hypothesize that serial dependance is underlied by brain oscillations. We developed a serial dependance task on face perception associated with EEG recordings. A classification algorithm was then applied to investigate whether the spatio-temporal pattern of brain activity associated with face perception can be found in visual stimuli biased toward the previous perception of a face stimulus.

In the third project, we tested the hypothesis that brain oscillations travel across the retinotopic space, i.e., mesoscopic traveling waves, leading to perceptual consequences. Visual perception is modulated periodically by the phase of low-frequency oscillations, with periods associated to a high probability of stimulus perception, i.e., optimal phases (Busch et al., 2009; Mathewson et al., 2009; Varela et al., 1981; Dugué et al., 2011a). The phase effect accounts for less than 20% of trial-by-trial variability in perceptual performance (Busch et al., 2009; Dugué et al., 2011a, 2015). We hypothesized that by considering the spatial organization of brain oscillations, we can better explain the functional role of brain oscillations on visual perception. Psychophysics experiments associated with EEG recording were developed to test our hypothesis.

In the fourth project, we studied the functional role of the propagation direction of macroscopic oscillatory traveling waves. Alpha brain oscillations can propagate between cortical areas along the antero-posterior axis (e.g., Sauseng et al., 2002; Zhang et al., 2018; Alamia and VanRullen, 2019; Pang et al., 2020). We hypothesized that manipulating cognition will manipulate traveling wave's direction of propagation. To this aim, we developed an experiment manipulating both visual perception and endogenous spatial attention during EEG recordings. We hypothesized that endogenous attention is associated with traveling waves propagating from the frontal-to-occipital areas, and that during visual perception, the propagation direction is reversed from the occipital-to-frontal areas.

We also tested whether visual perception causally triggers a traveling wave in the anterior-to-posterior direction with a study including EEG recordings and single pulses of TMS applied over V1 to induce phosphene perception.

Part 2. Experimental Work.

Chapter 4. Causal link between the phase and amplitude of spontaneous alpha oscillations, cortical excitability and visual perception.

The amplitude and the phase of brain oscillations in low frequency bands (theta, alpha) influence both cortical excitability and visual perception, independently. In this chapter, we studied the role of alpha phase-amplitude tradeoffs on cortical excitability and visual perception, according to the predictions made by the Pulsed Inhibition theory (Jensen and Mazaheri, 2010; Klimesch et al., 2007a; Mathewson et al., 2011).

To this aim, we assessed cortical excitability and visual perception in healthy humans using phosphene perception induced by single pulses of TMS, and its post-pulse evoked activity recorded with simultaneous EEG. A first study was developed, unfortunately, we cannot continue it, for practical reasons, i.e., unfeasibility of the experiment, and the covid pandemic. Consequently, we reanalyzed data already published (Dugué et al., 2011a) to test our hypothesis. This last study provided strong causal evidence in favor of the Pulsed Inhibition theory.

1. The Pulsed Inhibition theory

For a long time, alpha brain oscillations were interpreted as “cortical idling” (for review Pfurtscheller & Silva, 1999). Several studies highlighted the key role of alpha oscillations in various cognitive functions, and proposed that they act as a functional inhibitor (VanRullen, 2016a; Dugué and VanRullen, 2017; Clayton et al., 2018; Samaha et al., 2020; Kienitz et al., 2021). Considering that alpha brain activity is an oscillatory phenomenon, and that the phase of the alpha cycle strongly influences both cortical excitability and perception (Varela et al., 1981; Busch et al., 2009; Mathewson et al., 2009; Dugué et al., 2011a; Scheeringa et al., 2011b; Hagens et al., 2011b; Samaha et al., 2015), the functional inhibition exerted by alpha oscillations is probably periodic. Indeed, it was proposed that “alpha activity produces boots of inhibition repeated every ~100 ms” (Mazaheri and Jensen, 2010). The Pulsed Inhibition theory describes a physiological proposal on how the amplitude of alpha oscillations influences the phase effect (Jensen and Mazaheri, 2010; Klimesch et al., 2007a; Mathewson et al., 2011), i.e., the alternation between states of cortical excitation and inhibition, as a function of the alpha phase, leading to rhythmicity in performance. This theory makes two clear predictions. (1) High

alpha amplitude induces cortical inhibition at specific phases, associated with low perceptual performance, while at opposite phases, inhibition decreases (potentially increasing excitation) and perceptual performance increases. (2) Low alpha amplitude is less susceptible to these phasic (periodic) pulses of inhibition, leading to overall higher perceptual performance (**Figure 4.1**).

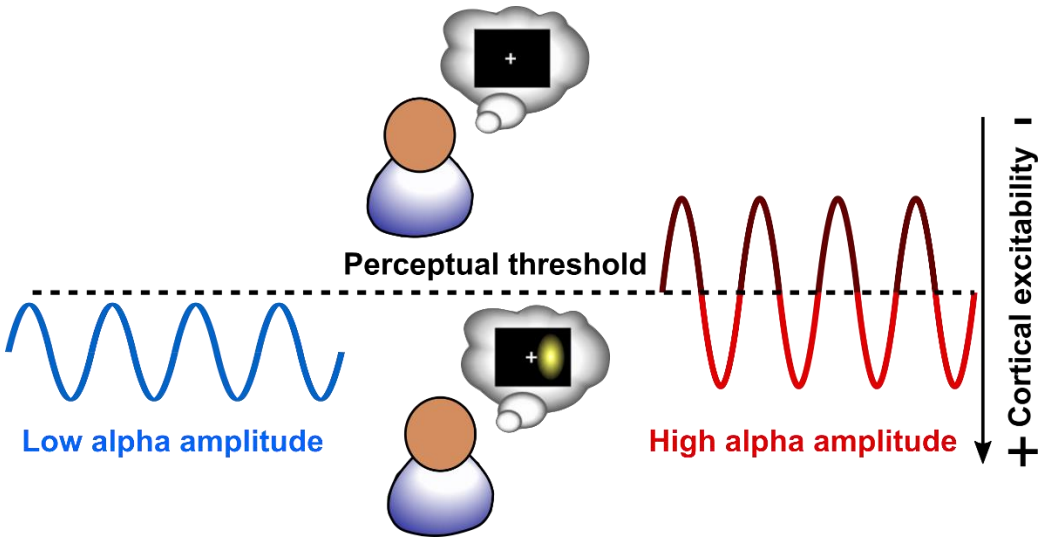

Figure 4.1: The Pulsed Inhibition theory*. When alpha amplitude is low, the level of cortical excitability is high and always above the perceptual threshold. All incoming stimuli are processed and perceived. When alpha amplitude is high, the level of cortical excitability fluctuates along with the phase, between excitatory and inhibitory states, above and below the perceptual threshold. This leads to a periodicity in perception. Incoming stimuli are processed and perceived only at optimal phases, during excitatory states.*

The basic principles of the Pulsed Inhibition theory can be illustrated by considering the level of excitation in three different pyramidal excitatory cells and the phase of the brain oscillations (**Figure 4.2**; Klimesch et al., 2007a). A pyramidal cell with a basal level of excitability sufficiently high overrides the inhibition induced by the oscillatory activity and fires tonically when the amplitude is low (Cell 1 in **Figure 4.2.1**). For the same amplitude, pyramidal cells with a lower basal level of excitability are firing periodically (Cells 2 and 3 in **Figure 4.2.1**). Crucially, when the amplitude of the oscillatory activity increases, all pyramidal cells fire periodically (Cell 1 in **Figure 4.2.2**) and the time-windows for neural firing become more precise (Cells 2 and 3 in **Figure 4.2.2**). Thus, alpha oscillations would represent a functional timing mechanism. According to the oscillations' amplitude, the time-window for neural processing becomes shorter or longer.

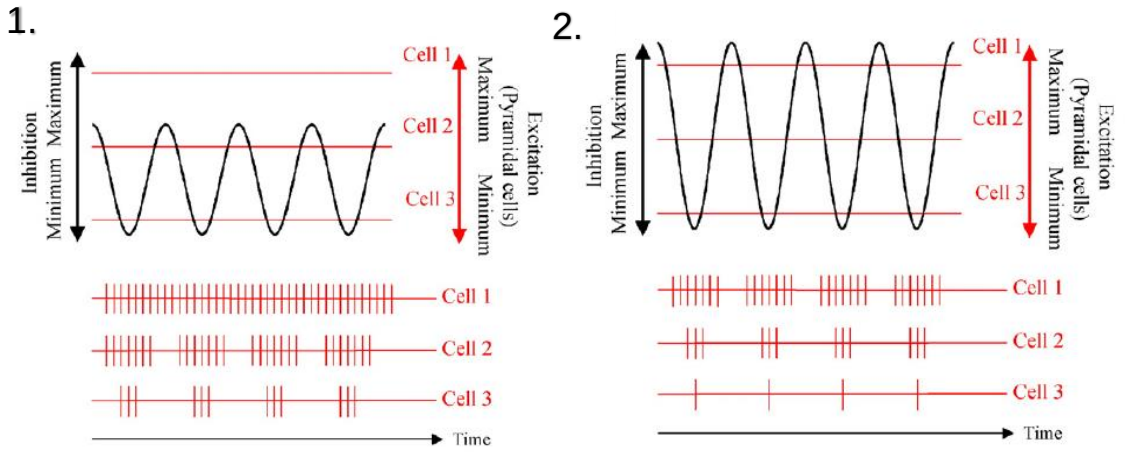

Figure 4.2: The basic principles of the Pulsed Inhibition theory, from Klimesh et al., 2007a. *According to the basal level of excitation of three different pyramidal excitatory cells and the amplitude of the oscillation, two different firing patterns occur.* ***1.*** *The amplitude of the oscillation is low, a pyramidal cell with a high basal level of excitation fires tonically, while pyramidal cells with a low basal level of excitation fire periodically.* ***2.*** *The amplitude of the oscillation is high, all pyramidal cells are firing periodically according to the phase of the oscillations. Their basal level of excitation determines the length of the integrative time-windows.*

2. A role of endogenous attention?

In their proposal on the role of alpha oscillations as an active inhibitory process, Klimesch et al. (2007a) and Mathewson et al. (2011) evoked that the amplitude of alpha oscillations in the occipital regions could be controlled by top-down processes from fronto-parietal areas. Recent studies highlighted that brief interferences induced by repetitive TMS over frontal areas disrupt the emergence and the modulation of alpha oscillations in the visual cortex during a visual attention task. In addition, this absence of alpha modulation caused by the alteration of the brain activity in the frontal regions was associated to altered perceptual performance (Capotosto et al., 2009; Marshall et al., 2015). Indeed, several authors have proposed that alpha oscillations carry information from frontal to sensory areas through feedback connections (Michalareas et al., 2016; van Kerkoerle et al., 2014). In the framework of the Pulsed Inhibition theory, frontal areas would exercise a key role in the timing of cortical activation in visual areas; through their top-down influence on the amplitude of alpha oscillations, they would enhance or reduce the effect of alpha phase on perception. Indirectly, frontal areas could play a role in the emergence of inhibitory and excitatory moments (Klimesch et al., 2007a).

To investigate this hypothesis, we designed an experiment with a visuo-spatial attention task. During the deployment of endogenous, top-down, covert, attention in space, we observed the phenomenon of alpha lateralization (Worden et al., 2000; Sauseng et al., 2005b; Thut et al., 2006; Händel et al., 2011). According to the Pulsed Inhibition theory, we expect to observe a phase effect on cortical excitability and visual perception in the occipital hemisphere ipsilateral to the attended visual hemifield, i.e., where the amplitude of spontaneous alpha oscillations increases. The role of phase should be less important or absent in the occipital hemisphere contralateral to the attended visual hemifield, i.e., where the amplitude of spontaneous alpha oscillations decreases.

In 2010, Busch and VanRullen proposed an alternative hypothesis. Indeed, they found that visual performance fluctuates along with the phase of spontaneous oscillations at 7 Hz only for attended stimuli, i.e., for lower alpha amplitude. Interestingly, they found that the phase and the amplitude effect on visual perception occurred at different frequencies (7 Hz and 12 Hz, respectively), and presented different EEG topographies (fronto-central and posterior, respectively). They theorized that the role of phase and amplitude on perception would be independent and rely on different oscillatory mechanisms (Busch and VanRullen, 2010). This goes against the predictions made by the Pulsed Inhibition theory, which predicts a periodicity in perception mainly for unattended stimuli, i.e., where the endogenous attention is not focused and needs to be reoriented.

In a study, we aimed at disentangling these two contradictory hypotheses. We worked on this project in collaboration with Rufin VanRullen from the Brain and Cognition Research Center (CerCo, Toulouse, France) in the team Neuronal Dynamics of Vision: Perception, Attention and Consciousness. Unfortunately, we will see that we were unable to optimize the experiment, due to technical issues.

2.1. Procedure

Participants. The data from one pilot participant was recorded and analyzed in this study. They fulfilled the standard inclusion criteria for TMS experiment (Rossi et al., 2009), and gave their written informed consent. The study was approved by the local French ethics committee “Sud-Ouest et Outre-Mer I” (IRB # 2009-A01087-50) and followed the Declaration of Helsinki.

TMS apparatus and EEG recording. Participant seated in a dark room, 57 cm from a computer screen (36.5° * 27° of visual angles). Their head was maintained using a chinrest and a headrest. Two 70-mm figure-of-eight coils were placed over the right and the left occipital poles (V1/V2; ~1 cm above the inion and ~2 cm away from the midline). Biphasic TMS pulses were applied with a Magstim Rapid2 stimulator of 3.5 Tesla (Magstim, Spring Garden Whitland, Great Britain). EEG was recording simultaneously with a 64-channels BrainAmp system (Brain Products GmbH) with reference and ground electrodes placed respectively at AFz and FCz locations.

Stimuli. Stimuli were generated with Matlab R2014b 32bit (The MathWorks, Natick, MA) and the PsychToolbox 3.0.11. They were displayed on a 1920 * 1080 pixels screen with a 120 Hz refresh rate. We used a fixation cross with arms of 0.2° (degrees of visual angles) length and 0.05° width. An expansion of the lower left or right arm of the fixation cross associated to color change from grey to white was used, respectively, as left or right endogenous cue. A neutral cue was also designed, where the two lower arms of the fixation cross become white and bigger.

Phosphene screening and titration. The participant was selected based on their ability to perceive TMS-induced phosphenes in both the left and the right visual field. A train of 7 pulses at 20 Hz and 70% of the TMS machine output intensity, i.e., suprathreshold, was applied over the right and left occipital poles (i.e., V1/V2; Dugué et al., 2011a, b, 2016, 2019) while participant kept fixating at a central fixation. Participant was asked to draw their right and left phosphene as precisely as possible by pressing the mouse-button to delimit the outlines of the phosphenes. They could check the location and shape of their drawings and repeat the procedure as many times they want. The phosphene drawing was then used in the experiment (see **Figure 4.3** for phosphene's drawing examples). An individual phosphene perception threshold at 75% was determined for each visual field, by applying single pulses of TMS at varying intensities and asking the participant to report whether they perceived a phosphene or not. Similarly, a one-up/two-down staircase procedure was performed for the left and the right phosphene's drawing to reach a perceptual threshold of 75%, by varying the stimulus contrast. A grey fixation cross was presented during 300 ms, followed by a neutral cue during 60 ms. After a random inter-stimulus interval (ISI) between 1500 and 2000 ms, the phosphene's drawing was displayed. The participant had to indicate whether they perceived the stimulus on the left or on

the right side of the screen, or if they did not perceive it, with keyboard keys, after a GAP of 500 ms. There was a random inter-trial interval (ITI) ranging from 1500 to 2500 ms, with a 100 ms step, between each trial.

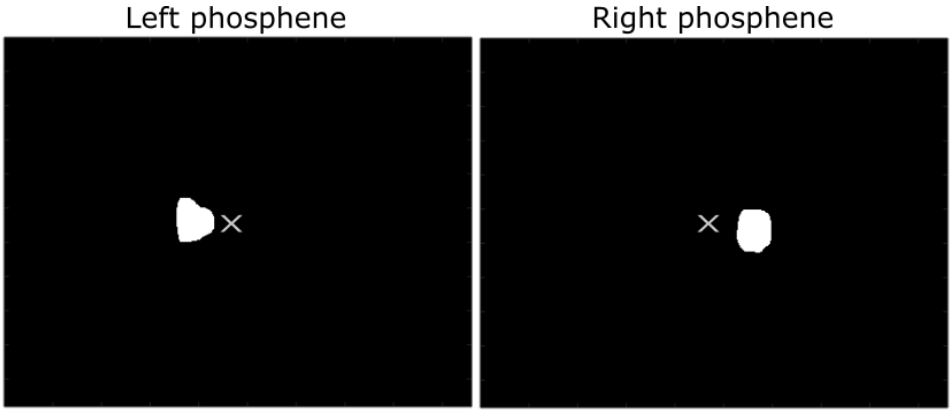

Figure 4.3: Left and right phosphene's drawings.

Experimental session. The experiment was split in two sessions of 1000 trials, divided into 20 blocks of 50 trials, composed of 80% of TMS trials and 20% of catch trials. Each trial begun with a fixation cross for 300 ms. Then, a left or right cue for 60 ms was presented to indicate participants to orient their attention, respectively, to the left or to the right side of the screen. After a random delay between 1500 and 2000 ms, single pulses of TMS were applied at 75% threshold in the TMS condition, and phosphene's drawing was displayed for 60 ms at 75% threshold in the catch condition. Trials could be valid (70%) if the phosphene was presented in the attended side of the screen, or invalid (30%) if the phosphene was displayed on the unattended side, requiring the participant to reorient their attention. After a 500 ms delay, the fixation cross became blue instructing the participant to indicate whether they perceived a phosphene on the left or on the right, or not, with the left or right arrow, or space, respectively. For the catch trials, the fixation cross became red or green for 500 ms, to indicate whether they were incorrect or correct, respectively. This feedback was used to keep participants motivated to use the endogenous cues and allowed an efficient attentional deployment. Each trial was separated by a random ITI between 1500 and 2500 ms, with a 100 ms step. The percentage of correct responses was monitored for the TMS and catch conditions at the end of each block. The staircase procedures were repeated if needed to maintain perceptual thresholds around 75% (**Figure 4.4**). Note that for the pilot session, we recorded only 7 blocks.

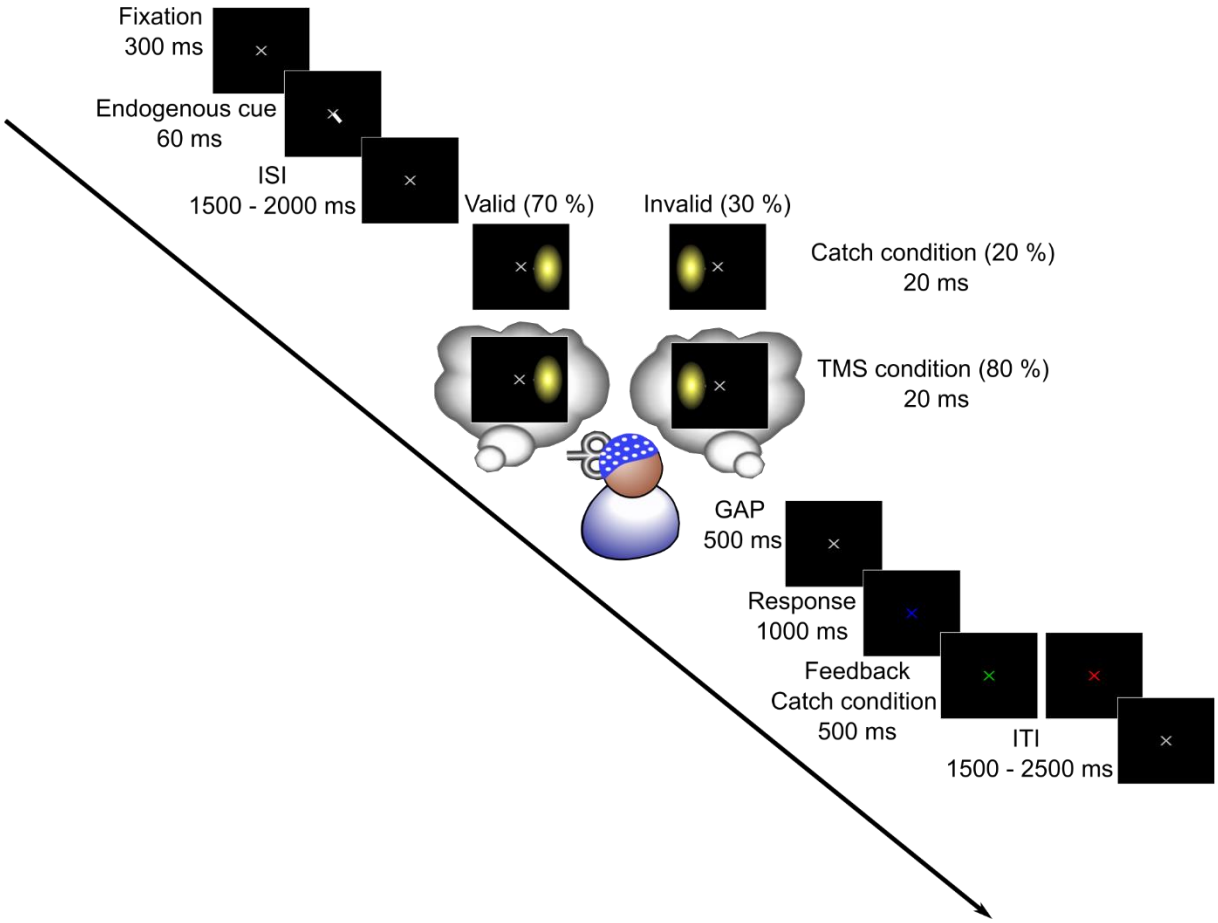

Figure 4.4: Experimental procedure. *A grey fixation cross was displayed for 300 ms, followed by a left or right endogenous cue for 60 ms, used to orient participant's endogenous spatial attention. After a random delay between 1500 and 2000 ms, single-pulse TMS was applied in the TMS condition, and phosphene's drawing was displayed for 60 ms in the catch condition. Trials could be valid (70%) if the phosphene was presented in the attended side of the screen, or invalid (30%) if the phosphene was displayed on the unattended side. The fixation cross became blue after a 500 ms delay instructing the participant to answer. For the catch condition, they received feedback on their performance, the fixation cross become red or green for 500 ms, to indicate whether they were incorrect or correct, respectively. Each trial was separated by a random ITI between 1500 and 2500 ms, with a 100 ms step.*

Behavioral analyses. Behavioral analyses were done with Matlab R2014b (The MathWorks, Natick, MA). The hit rate, i.e., participant correctly reported the presence of the phosphene, the false alarm ratio, i.e., participant reported either the absence of the phosphene, or a wrong phosphene position, the dprime, and the median reaction times for the correct responses, were computed for valid and invalid trials, both for the TMS and catch conditions.

EEG analyses. EEG analyses were performed with EEGLAB 13.6.5 (Swartz Center for Computational Neuroscience, UC San Diego, California; Delorme & Makeig, 2004) and custom software written in Matlab R2014b (The MathWorks, Natick, MA).

Preprocessing. EEG data and channel localizations were imported into EEGLAB. EEG data were downsampled to 512 Hz, and re-reference to average reference. Visual inspection allowed identification of bad signal-to-noise ratio electrodes, that were interpolated.

Alpha lateralization. Data was epoched from -1000 ms to +2600 ms from the onset of the cue. Epochs were manually inspected and rejected if artifacts were detected. A time-frequency transform (Hanning tapers) was computed on single trials with the *timefreq* function from EEGLAB. The "cycles" parameter was set to 3. The "freqs" parameter was set to [4, 20], producing frequencies that increase from 4 to 20 Hz. The amplitude was extracted for each trial and electrode, and transformed into a Z-score value according to a baseline time window from -500 ms to -200 ms according to the cue onset.

Z-score = amplitude – mean (baseline amplitude) / std (baseline amplitude)

Z-scores values were averaged separately between left and right cued trials, and we computed the difference left minus right cued trials. Time frequency map and topography of the difference were plotted to investigate the presence of alpha lateralization.

2.2. Preliminary results

Behavior. Dprime and median reaction times were computed separately for valid and invalid trials, both for the TMS and the catch conditions, on the pilot participant. The dprime was higher and the median reaction times lower, in valid compared to invalid trials, for both TMS and catch conditions (**Figure 4.5**). Visuo-spatial endogenous attention was successfully manipulated, with no speed-accuracy tradeoff.

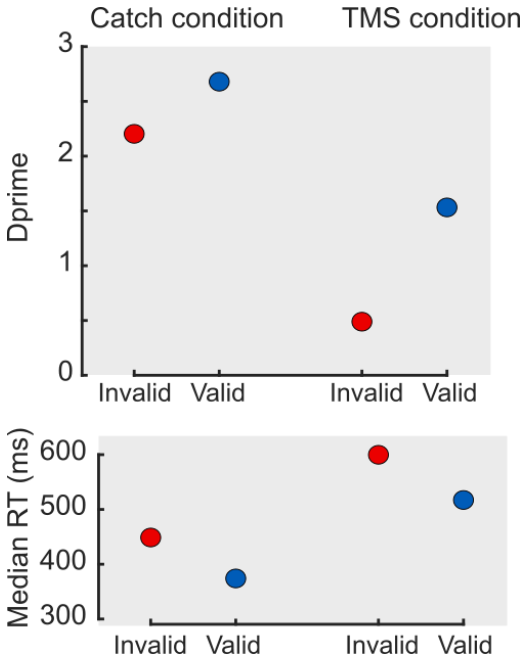

Figure 4.5: Visuo-spatial endogenous attention was successfully manipulated. *Dprime and median reactions from one pilot participant, for both catch and TMS conditions, valid (blue dots) and invalid (red dots) trials.*

Alpha lateralization. The topography of the amplitude of the difference between left and right cued trials showed an increase in the amplitude of alpha brain oscillations in the occipital cortex ipsilateral to the attended visual field, and a decrease in the amplitude in the contralateral occipital cortex (**Figure 4.6**). The alpha lateralization pattern was observed in the pilot participant suggesting a successful manipulation of spatial endogenous attention.

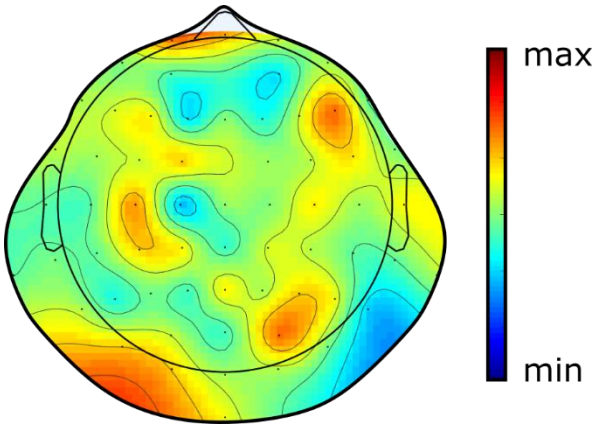

Figure 4.6: Alpha lateralization topography. *The amplitude of alpha oscillations increased in the ipsilateral hemisphere to the attended position, i.e., left one, and decreased in the contralateral hemisphere, i.e., right one.*

2.3. Optimization of the procedure

During data collection, we were able to record only 7 experimental blocks over the 20 intended in a single session. We realized that the experimental set-up time, i.e., the EEG and the two TMS set-ups, was too long. Consequently, we re-designed the experiment to use only one TMS, to reduce the experiment set-up time.

In addition, the number of unperceived phosphene in the invalid trials for the TMS condition was low (120 trials) and would probably entrain an underestimation of the phase during the EEG analyses. Consequently, we tried to increase the number of invalid trials for the TMS condition while keeping an appropriate balance between valid and invalid trials across all conditions to allow the deployment of endogenous attention.

We increased the number of invalid trials in the TMS condition from 30% to 50%, so, associated to a decrease in the number of valid trials in the TMS condition to 50%. To obtain an adequate balance between valid (70%) and invalid (30%) trials across the whole experiment, the validity in the catch condition was set to 80% valid – 20% invalid, and there was twice as many trials of catch condition than trials of TMS condition. The experiment was divided into two sessions with approximatively 1500 trials (1000 catch trials + 500 TMS trials). Half of the session was performed with TMS applied over the right occipital pole, and the other half with TMS applied over the left occipital pole. The use of only one TMS involved some adjustments. When the TMS was applied over the left occipital pole, the participant could perceive only a phosphene in the right visual hemifield. For every endogenous cue orienting to the right visual hemifield, the trials were systematically valid, and for every endogenous cue orienting to the left visual hemifield, the trials were systematically invalid (and vice-versa for TMS applied over the right occipital pole). In addition, for the catch condition, we use the drawing of the phosphene perceived and its mirror image.

Despite the changes implemented to optimize the experiment, we realized that we were still not able to perform the experiment when we tried to record the data of a pilot participant. The set-up of the EEG system and one TMS take time, and we cannot reduce the number of trials without losing a reliable estimation of the phase. Finally, the experiment was really long and tiring for the participant.

In addition, at this moment of my PhD, the covid pandemic arrived in France, preventing us for performing experiments in human participants for several months. Consequently, we

decided to analyzed data already published (Dugué et al., 2011a) to test our hypothesis on the causal interaction between the phase and amplitude of alpha oscillations on cortical excitability and visual perception.

3. PUBLICATION: Fakche, VanRullen, Marque & Dugué. Alpha phase-amplitude tradeoffs predict visual perception.

eNeuro

Research Article: New Research

Cognition and Behavior

α Phase-Amplitude Tradeoffs Predict Visual Perception

Camille Fakche,[1] Rufin VanRullen,[2] Philippe Marque,[3,4] and Laura Dugué[1,5]

https://doi.org/10.1523/ENEURO.0244-21.2022

[1]Université de Paris, Integrative Neuroscience and Cognition Center Unité Mixte de Recherche 8002, Centre National de la Recherche Scientifique, Paris F-75006, France, [2]Centre National de la Recherche Scientifique, CerCo, Centre de Recherche Cerveau et Cognition, Unité Mixte de Recherche 5549, Université de Toulouse, Toulouse F-31052, France, [3]Toulouse NeuroImaging Center, Unité Mixte de Recherche 1214, INSERM Institut National de la Santé et de la Recherche Médicale, Toulouse F-31024, France, [4]Médecine Physique et de Réadaptation, Centre Hospitalier Universitaire Rangueil, Toulouse F-31059, France, and [5]Institut Universitaire de France (IUF), Paris F-75005, France

Visual Abstract

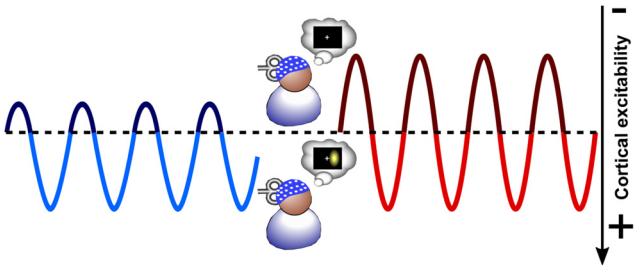

Spontaneous α oscillations ($\sim$10 Hz) have been associated with various cognitive functions, including perception. Their phase and amplitude independently predict cortical excitability and subsequent perceptual performance. However, the causal role of α phase-amplitude tradeoffs on visual perception remains ill-defined. We aimed to fill this gap and tested two clear predictions from the pulsed inhibition theory according to which α oscillations are associated with periodic functional inhibition. (1) High-α amplitude induces cortical inhibition at specific phases, associated with low perceptual performance, while at opposite phases, inhibition decreases (potentially increasing excitation) and perceptual performance increases. (2) Low-α amplitude is less susceptible to these phasic (periodic) pulses of inhibition, leading to overall higher perceptual performance. Here, cortical excitability was assessed in humans using phosphene (illusory) perception induced by single pulses of transcranial magnetic stimulation (TMS) applied over visual cortex at perceptual threshold, and its postpulse evoked activity recorded with simultaneous electroencephalography (EEG). We observed that prepulse α phase modulates the probability to perceive a phosphene, predominantly for high-α amplitude, with a nonoptimal phase for phosphene perception between $-\pi/2$ and $-\pi/4$. The prepulse nonoptimal phase further leads to

Significance Statement

The pulsed inhibition theory predicts that the functional inhibition induced by high-α oscillations' amplitude is periodic, with specific phases decreasing neural firing and perceptual performance. In turn, low-α oscillations' amplitude is less susceptible to phasic moments of pulsed inhibition leading to overall higher perceptual performance. Using transcranial magnetic stimulation (TMS) with simultaneous electroencephalography (EEG) recordings in humans, we found that specific phases of spontaneous α oscillations ($\sim$10 Hz) decrease cortical excitability and the subsequent perceptual outcomes predominantly when α amplitude is high. Our results provide strong causal evidence in favor of the pulsed inhibition theory.

an increase in postpulse-evoked activity [event-related potential (ERP)], in phosphene-perceived trials specifically. Together, these results show that α oscillations create periodic inhibitory moments when α amplitude is high, leading to periodic decrease of perceptual performance. This study provides strong causal evidence in favor of the pulsed inhibition theory.

Key words: α oscillations; cortical excitability; EEG; phase-amplitude tradeoffs; TMS; visual perception

Introduction

α Brain oscillations (8–12 Hz) play a role in various cognitive functions, including visual perception (VanRullen, 2016a; Dugué and VanRullen, 2017; Clayton et al., 2018; Samaha et al., 2020; Kienitz et al., 2021), and are proposed to support active functional inhibition (Pfurtscheller and Lopes da Silva, 1999). Specifically, low parieto-occipital α amplitude recorded in human is correlated with a higher probability to perceive a near-threshold visual stimulus (Ergenoglu et al., 2004; Sauseng et al., 2005; Thut et al., 2006; van Dijk et al., 2008; Händel et al., 2011). Similarly, specific α phases lead to better detection performance while opposite phases lead to impaired performance (Varela et al., 1981; Busch et al., 2009; Mathewson et al., 2009; Dugué et al., 2011a; Samaha et al., 2015). Perception fluctuates periodically over time, along with the phase of α oscillations.

α Oscillations' amplitude and phase further seem to predict cortical excitability. Spiking activity recorded in macaques is higher at the trough of the α cycle, and for lower α amplitude (Bollimunta et al., 2008; Haegens et al., 2011, 2015; van Kerkoerle et al., 2014). Moreover, functional magnetic resonance imaging studies have shown that the cortical blood oxygenation level-dependent response fluctuates along with the phase of α oscillations in visual cortex (V1/V2; Scheeringa et al., 2011), and increases when α amplitude decreases (Goldman et al., 2002; Moosmann et al., 2003). Critically, transcranial magnetic stimulation (TMS) studies went beyond such correlational evidence. When applied over V1/V2, single-pulse TMS can elicit phosphenes (illusory percepts) depending on cortical state, i.e., when cortical excitability is sufficiently high. Phosphene perception leads to a higher event-related potential (ERP) than the absence of percept (Taylor et al., 2010; Dugué et al., 2011a; Samaha et al., 2017). Interestingly, studies have shown that phosphene perception is higher for low prepulse α amplitude (Romei et al., 2008; Samaha et al., 2017), and fluctuates according to α phase (Dugué et al., 2011a; Samaha et al., 2017). These studies independently suggest that both α oscillations' amplitude and phase modulate cortical excitability and causally predict visual perception. However, their joint causal effects are still ill-defined.

Here, we address this question in the framework of the pulsed inhibition theory (Klimesch et al., 2007; Jensen and Mazaheri, 2010; Mathewson et al., 2011), which makes two clear predictions regarding α phase-amplitude tradeoffs: (1) high-α amplitude exhibits states of cortical inhibition at specific phases associated with lower perceptual performance (nonoptimal phases); while (2) low-α amplitude is less susceptible to phasic pulsed inhibition, leading to high perceptual performance. A few studies have investigated the phase-amplitude tradeoffs (i.e., effect of the interaction between phase and amplitude) of low frequency oscillations on sensory perception and motor functions in human (Table 1). Although most of these studies observed a phase effect on task performance exclusively (or stronger) for high-α (or lower frequencies) amplitude (Mathewson et al., 2009; Ng et al., 2012; Ai and Ro, 2014; Bonnefond and Jensen, 2015; Herrmann et al., 2016; Spitzer et al., 2016; Kizuk and Mathewson, 2017; Hussain et al., 2019; Alexander et al., 2020), one found a phase effect for low-α amplitude exclusively (Busch and VanRullen, 2010), some found no difference between high-α and low-α amplitude (Milton and Pleydell-Pearce, 2016; Harris et al., 2018), and finally, some found no phase effect (Zoefel and Heil, 2013; Madsen et al., 2019). Importantly, most of these studies are correlational (Table 1). Only two (Hussain et al., 2019; Madsen et al., 2019) investigated the causal link between spontaneous α oscillations' amplitude and phase, cortico-spinal excitability, assessed with TMS to evoke a motor-evoked potential (MEP) on the hand muscle, and the subsequent motor performance. Other studies found a causal phase effect of spontaneous α oscillations on cortico-spinal excitability and the associated MEP for high-α amplitude, but used the absence of α oscillations as control thus not comparing phase-effects between a high-α and low-α amplitude condition (Schaworonkow et al., 2018, 2019; Stefanou et al., 2018; Zrenner et al., 2018; Bergmann et al., 2019).

We investigated the causal effect of spontaneous α phase-amplitude tradeoffs on cortical excitability and subsequent perceptual performance in the visual modality, and tested the predictions made by the pulsed inhibition theory using TMS and electroencephalography (EEG)

Received May 25, 2021; accepted January 16, 2022; First published January 1, 2022.

The authors declare no competing financial interests.

Author contributions: R.V. and L.D. designed research; P.M. and L.D. performed research; C.F. and L.D. analyzed data; C.F., R.V., and L.D. wrote the paper.

This work was supported by the European Research Council (ERC) under the European Union's Horizon 2020 Research and Innovation Programme Grant Agreement No. 852139 (to L.D.), the Agence Nationale de la Recherche (ANR)-Deutsche Forschungsgemeinschaft (DFG) Programme Grant Agreement No. J18P08ANR00 (to L.D.), and the ANR Programme Grant Agreement No. ANR-19-NEUC-0004 (to R.V.).

Acknowledgements: We thank Laetitia Grabot and Mehdi Senoussi for their useful comments on this manuscript.

Correspondence should be addressed to Camille Fakche at camille.fakche@gmail.com.

https://doi.org/10.1523/ENEURO.0244-21.2022

Table 1: Electro/magneto-encephalography (EEG/MEG) experiments investigating oscillations phase-amplitude tradeoffs on behavioral performance in human

Study	Method	Frequency band	Frequency	Oscillatory activity	Modality	Behavioral measure	Main results
Studies using TMS							
Visual modality							
Current study	EEG	α	10 Hz	Spontaneous	Visual	Near-threshold TMS-induced phosphene perception	Phase-amplitude effect on detection, stronger for high amplitude
Other modalities							
Hussain et al. (2019)	EEG	α, β	8–12 Hz, 13–30 Hz	Spontaneous	Motor	Supra-threshold TMS-induced MEP	Optimal phase (leading to increased MEP) reverses between low-α and high-α amplitude; no phase-amplitude effect for β
Madsen et al. (2019)	EEG	α	7–13 Hz	Spontaneous	Motor	Supra-threshold TMS-induced MEP	No phase-amplitude effect on MEP amplitude
Studies not using TMS							
Visual modality							
Alexander et al. (2020)	EEG	α	5.6–14.4 Hz	Spontaneous	Visual	Detection of near-threshold stimulus through eyes closed	Phase effect on detection for high amplitude
Bonnefond and Jensen (2015)	MEG	α	9–12 Hz	Stimulus-locked (retention interval)	Visual	Sternberg working memory task with supra-threshold stimuli	Phase effect on γ power for high amplitude
Busch and VanRullen (2010)	EEG	θ	7 Hz	Spontaneous (amplitude attentionally modulated)	Visual	Detection of spatially attended or unattended near-threshold visual stimulus	Phase effect on detection and GFP for low amplitude
Harris et al. (2018)	EEG	θ, α	5 Hz, 11–15 Hz	Stimulus-locked (α amplitude attentionally modulated)	Visual	Detection of spatially attended or unattended near-threshold visual stimulus	No phase-amplitude effect on detection
Kizuk and Mathewson (2017)	EEG	α	12 Hz	Entrained	Visual	Detection of spatially attended or unattended metacontrast masked stimulus (75% performance)	Tendency for phase-amplitude effect on detection, stronger for high amplitude
Mathewson et al. (2009)	EEG	α	10 Hz	Stimulus-locked	Visual	Detection of metacontrast masked stimulus (70% performance)	Phase effect on detection for high amplitude
Milton and Pleydell-Pearce (2016)	EEG	α	7.8–12.7 Hz	Spontaneous (amplitude attentionally modulated)	Visual	Simultaneity judgement of spatially attended or unattended stimulus (50% performance)	No phase-amplitude effect on simultaneity judgement
Other modalities							
Ai and Ro (2014)	EEG	α	8–12 Hz	Spontaneous	Somatosensory	Detection of near-threshold stimulus	Phase effect on detection for high amplitude
Herrmann et al. (2016)	MEG	δ	2 Hz	Entrained	Auditory	Detection of near-threshold stimulus	Phase effect on detection for high amplitude
Ng et al. (2012)	EEG	θ, α	2–6 Hz, 8–12 Hz	Entrained	Auditory	Detection of near-threshold stimulus	θ Phase-amplitude effect on detection, stronger for high amplitude; no phase-amplitude effect for α
Spitzer et al. (2016)	EEG	δ, θ, and α	3 Hz, 6.7 Hz, 11 Hz	Stimulus-locked	Visual, auditory, and somatosensory	Two-interval numerosity comparison task (80% performance)	δ Phase-amplitude effect on choice-predictive signals, stronger for high amplitude; no phase-amplitude effect for θ and α
Zoefel and Heil (2013)	EEG	δ	0.5 Hz	Entrained and spontaneous	Auditory	Detection of near-threshold stimulus	No phase-amplitude effect on detection neither for entrained nor for spontaneous oscillations

Note that studies independently investigating the phase and the amplitude of oscillations were not included in this table. We only selected studies specifically investigating the interaction between the instantaneous phase and the amplitude on behavioral performance. Entrained oscillations: oscillations with a nonrandom phase distribution induced by a repetitive stimulus presentation. Stimulus-locked oscillations: oscillations with a nonrandom phase distribution induced by a single stimulus. Spontaneous oscillations: oscillations with a random phase distribution. GFP, global field power; MEP, motor-evoked potential; TMS, transcranial magnetic stimulation.

in human. Cortical excitability was assessed using phosphene perception induced by single-pulse TMS applied over V1/V2 at perceptual threshold (~50% detection), and its postpulse evoked activity. Our results validate both predictions, demonstrating that α oscillations create periodic inhibitory moments when α amplitude is high, leading to lower perceptual performance. Critically, both simulations and ERP analyses confirmed that the obtained results were not a mere analysis confound in which the quality of the phase estimation covaries with the amplitude.

Materials and Methods

This study is a reappraisal of an early study from Dugué et al. (2011a), which focused on the causal link between the phase of ongoing α oscillations, cortical excitability, and visual perception. Here, we instead focused on the combined role of the phase and the amplitude of spontaneous α oscillations on the causal relation between cortical excitability and visual perception.

Participants

As in the original study, the data from nine participants (eight male, 20–35 years old) were analyzed (for inclusion/exclusion criteria, see Dugué et al., 2011a). All participants fulfilled the standard inclusion criteria for TMS experiment (Rossi et al., 2009), gave their written informed consent, and were compensated for their participation. Human participants were recruited in Toulouse, France. The study was approved by the local French ethics committee Sud-Ouest et Outre-Mer I (IRB #2009-A01087-50) and followed the Declaration of Helsinki.

TMS apparatus and EEG recording

Participants seated in a dark room, 57 cm from a computer screen (36.5° × 27° of visual angle). Their head was maintained using a chinrest and a headrest. A 70-mm figure-of-eight coil was placed over the right occipital pole (V1/V2; ~1 cm above the inion and ~2 cm away from the midline). The handle of the coil was oriented vertically, with the handle of the coil positioned dorsally to the coil itself, resulting in a ventral to dorsal electric current in the brain tissue. Biphasic TMS pulses were applied with a Magstim Rapid^2 stimulator of 3.5 Tesla (Magstim). EEG was acquired simultaneously with a 64-channels Active Two Biosemi system, with DC recording at a sampling rate of 1024 Hz. Additional electrodes, Common Mode Sense (CMS) and Driven Right Leg (DRL), were placed 2 cm under the eyes of the participants and were used as reference and ground, respectively, to minimize TMS-induced EEG artifact. Finally, horizontal, and vertical electro-oculograms were recorded using three additional electrodes placed around the eyes.

Experimental procedure

Phosphene screening and titration

Participants were selected based on their ability to perceive TMS-induced phosphenes in the left visual field. A train of seven pulses at 20 Hz and 70% of the TMS machine output intensity, i.e., suprathreshold, was applied over the right occipital pole (i.e., V1/V2; Dugué et al., 2011a; see also Dugué et al., 2016, 2019; Lin et al., 2021) while participants kept fixating at a central fixation. 24% of the participants did not perceive any phosphene (four out of 17) and were thus excluded from the main experiment. For each remaining participant, an individual phosphene perception threshold was determined by applying single pulses of TMS at varying intensities and asking them to report (with their dominant hand) whether they perceived a phosphene or not (left or right arrow on the computer keyboard, respectively).

Experimental session

Participants performed four blocks of 200 trials each, composed of 90% of test trials and 10% of catch trials (randomly interleaved). In the test trials, single-pulse TMS was applied at the perception threshold, on average across participants, phosphenes were perceived in 45.96 ± 7.68% of trials. In the catch trials, the stimulation intensity was kept the same, but instead of applying single pulses, double pulses (40-ms interval) were administered to monitor the validity of participants' responses (91.66 ± 8.81% of phosphene perceived). In other words, participants were presumably not pressing the button randomly; the selected cortical location did in fact lead to phosphene perception when stimulated. Adding a second pulse of TMS with a short delay between the two pulses has a cumulative effect on neural activity, leading to suprathreshold stimulation (Ray et al., 1998; Gerwig et al., 2005; Kammer and Baumann, 2010). The longer the delay between the two pulses, the most likely such cumulative effect disappears, which in the present case would lead for the participants to perceiving two pulses. Debriefing with each participant confirmed that this was never the case. Throughout the experiment, participants kept fixating a central dot and pressed a button to start the trial (Fig. 1). The delay between the button-press and the subsequent TMS pulse varied randomly between 1500 and 2500 ms. After a 600-ms delay following the pulse, a response screen was displayed instructing the participants to indicate whether they perceived a phosphene or not with the left or right arrow, respectively. The percentage of phosphene perceived was monitored every 20 trials. When above 75% or below 25% of phosphene perceived in the test trials, the experimenter repeated the threshold procedure to select an intensity so as to maintain a threshold around 50% of phosphene perceived.

EEG analyses

EEG analyses were performed with EEGLAB 13.6.5 (Swartz Center for Computational Neuroscience, University of California San Diego, California; Delorme and Makeig, 2004) and custom software written in MATLAB R2014b (The MathWorks).

EEG preprocessing

EEG data for test trials and channel localizations were imported into EEGLAB. EEG data were downsampled to 512 Hz, re-referenced to average reference, and epoched from −1500 to 1000 ms around the single-pulse of TMS. To minimize the artifact induced by the pulse, EEG data from

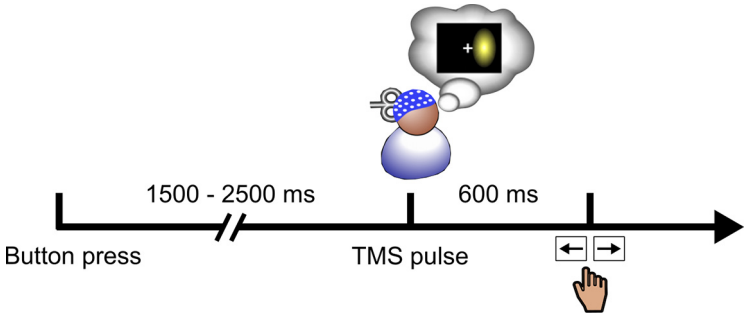

Figure 1. Experimental paradigm. Participants self-initiated the trial by pressing a button. After a random delay between 1500 and 2500 ms, a single (90% of trials) or a double (10% of trials) pulse of TMS was applied over V1/V2. After a 600-ms delay, participants indicated whether they perceived the phosphene or not with the left or right arrow, respectively.

−1 to 150 ms around the pulse was erased and replaced with a linear interpolation of the window boundaries. Epochs were finally manually inspected and rejected if artifacts (e.g., blinks) were detected. No electrode was rejected from the analysis.

Time-frequency decomposition

A time-frequency transform (morlet wavelets) was computed on single trials with the timefreq function from EEGLAB. The "cycles" parameter was set to [1, 15], the length of the filter increasing logarithmically from 1 to 15 cycles. The "freqs" parameter was set to [2, 100], producing frequencies that increase from 2 to 100 Hz.

Trial sorting by bin of amplitude

We then sorted the trials according to the amplitude of prepulse, spontaneous, α oscillations. The amplitude at each time-frequency point and for each trial, participant, and electrode was thus calculated. It corresponds to the absolute of the complex vector obtained from the time-frequency decomposition. For each trial and participant, we then averaged the amplitude across all electrodes (we had no a priori hypothesis regarding the electrode location of the effect) and time-frequency points selected based on the previous publication (Dugué et al., 2011a), i.e., time-frequency points at which a significant effect of the prepulse phase on phosphene perception was observed (from −400 to −50 ms before the pulse to avoid postpulse contamination on prepulse activity, and from 7 to 17 Hz). Trials were then sorted in three equally sized bins of low-amplitude, medium-amplitude, and high-amplitude trials. The percentage of phosphene perceived was computed for each bin of amplitude. Kruskal–Wallis test was used to test for significant difference in phosphene perception across bins. The next analyses were performed on the two extreme bins, i.e., low and high amplitude, exclusively, to clearly separate the low-α and high-α amplitude trials (with no possibility of overlap) using the least number of bins necessary to maximize the number of trials per condition. There were on average across the nine participants 108 ± 17.92 trials for the perceived-phosphene and 115.56 ± 15.86 trials for the unperceived-phosphene condition for the low-α amplitude trials, and 98.56 ± 30 trials for the perceived-phosphene and 126.11 ± 29.73 trials for the unperceived-phosphene condition for the high-α amplitude trials.

Phase-opposition

We calculated the phase-locking values (i.e., amount of phase concentration across trials), separately for low-α and high-α amplitude trials, and perceived-phosphene and unperceived-phosphene trials. The phase-locking value was obtained by, first, dividing the complex vectors obtained from the time-frequency decomposition by their length (i.e., instantaneous amplitude) thus normalizing for amplitude and keeping only the instantaneous phase (i.e., angle of the vectors). Second, the mean across trials of the normalized vectors was computed. The length of the average vector is now a measure of phase distribution, i.e., phase-locking across trials. For each amplitude condition, we subsampled the number of trials in the phosphene condition with the most trials to match the phosphene condition with the least trials. This subsampling procedure was repeated 100 times with a different subset of selected trials, and then we averaged the iterations. For each participant, phase-locking values were then summed across perceived-phosphene and unperceived-phosphene trials to obtain phase-opposition sums (POSs). POSs were then averaged across all electrodes, separately for low-α and high-α amplitude trials.

This measure of phase opposition is designed to give a low value when summing over two conditions both with uniform (random) phase distributions. On the other hand, POS is high when summing over two conditions both with strong phase-locked distributions across trials, as would happen when two conditions are associated with opposite phases. Since POS is computed on spontaneous (prepulse) activity, i.e., the phase distribution across all trials can be assumed to be uniform (see below for further statistics), if the phase is locked across trials for one specific condition (half of the overall trials) then the phase of the other condition (other half of the overall trials) would logically be locked in the opposite direction, leading to a high POS value.

This average was then compared with a surrogate distribution obtained with a permutation procedure (Dugué et al., 2011a, 2015; VanRullen, 2016b) consisting in shuffling the perceived-phosphene and unperceived-phosphene labels (5000 repetitions) and recalculating phase-locking values

(including subsampling) to obtain a surrogate phase-locking distribution under the null hypothesis that both perceived-phosphene and unperceived-phosphene trials have a uniform phase distribution, and further summed across the two surrogate distributions to compute a surrogate POS, characterized by a given mean and SEM (Standard Error of the Mean; separate procedure for low-α and high-α amplitude). *Z*-scores were computed by comparing the experimentally obtained POS to the mean and SEM of the surrogate POS: *Z*-scores = (POS − surrogate POS mean)/surrogate POS SEM.

False discovery rate (FDR) correction for multiple comparisons was further applied to *p*-values. A topographical analysis on the *z*-scores revealed two regions of interest (ROIs) involved in the phase-opposition effect (occipital and frontal). We repeated the previous analyses for these regions.

Specific time-frequency points were then selected for further analyses. We selected the time points separately for occipital and frontal electrodes/ROIs for which Dugué et al. (2011a) observed the maximal phase effect between perceived-phosphene and unperceived-phosphene conditions at electrodes PO3 (in occipital ROI: −77 ms) and AFz (in frontal ROI: −40 ms), respectively. We selected the 10.7-Hz frequency for both occipital and frontal electrodes/ROIs based on the fast Fourier transform (FFT) performed on prepulse ERPs (see below), this frequency is identical to the frequency obtained when performing FFTs on prepulse EEG time series (see below, FFT on prepulse EEG time series). Note that the frequency resolution differs between the wavelet decomposition and the FFT. Thus, for all wavelet decomposition related analyses, we used the closest frequency (10.7 Hz) to the peak observed in the FFT analyses (10.24 Hz).

We further ensured, at these selected time-frequency points, that the prepulse phase-opposition effect was not because of a contamination by the wavelet decomposition from the postpulse activity, separately for electrode PO3 and AFz. We thus tested whether the phase was uniformly distributed for both low-α and high-α amplitude trials. For each trial, phases were extracted and averaged across participants, separately for perceived-phosphene and unperceived-phosphene conditions, and the uniformity of the distribution across all trials was tested with a Rayleigh test from the Circular Statistics Toolbox (P. Berens, CircStat: A MATLAB Toolbox for Circular Statistics, Journal of Statistical Software, Volume 31, Issue 10, 2009 http://www.jstatsoft.org/v31/i10, Berens, 2009). For both amplitude conditions, and for both electrode PO3 (low-α amplitude trials: $p = 0.081657$, $\kappa = 0.1883$; high-α amplitude trials: $p = 0.22\,314$, $\kappa = 0.13\,517$) and electrode AFz (low-α amplitude trials, $p = 0.65\,929$, $\kappa = 0.076575$; high-α amplitude trials, $p = 0.19\,943$, $\kappa = 0.14\,016$), the tests did not reveal a significant effect suggesting that the phase was uniformly distributed across trials.

Finally, *post hoc* one-tailed *t* tests were performed to investigate whether POS, computed for each participant at the selected time-frequency points and averaged across electrodes for the occipital and the frontal ROI separately, differed significantly between low-α and high-α amplitude trials. This analysis was similarly performed for several versions of α amplitude binning (i.e., 2, 3, 4, and 5). On average across the nine participants, phosphene-conditions, and α-amplitude conditions, there were 167.94 ± 36.01 trials per bin in the two-bin version, 111.96 ± 24.29 trials in the three-bin version, 83.97 ± 18.41 trials in the four-bin version, and 67.18 ± 15.39 trials in the five-bin version.

FFT on prepulse EEG time series

To confirm further that the high-α as well as the low-α amplitude conditions both contained α oscillations, EEG time series from −600 to −1 ms were analyzed with an FFT (500 points zero padding), independently for the occipital and frontal ROI, for each α-amplitude condition, trial and participant. The resulting amplitude spectra were then averaged across trials and participants and plotted from 2 to 40 Hz. One-tailed *t* tests were used to compare individual 10.24-Hz peaks to their corresponding 1/f aperiodic component. The 10.24-Hz peaks were further compared between low-α and high-α amplitude conditions with one-tailed *t* tests. To ensure that the significant difference between the two conditions did not come from a difference in their aperiodic 1/f component, we also fitted the amplitude spectra to the 1/f component for each participant and compared the 1/f component at 10.24 Hz between low-α and high-α amplitude conditions with two-tailed *t* tests.

Simulations

The phase-opposition analysis between low-α and high-α amplitude trials could be because of an analysis confound, i.e., with decreasing amplitude, the robustness of the phase estimation decreases. Hence, a control procedure ensured that the phase estimation was not impacted by amplitude covariation, especially relevant when interpreting phase-opposition in low-α amplitude trials. A time-frequency decomposition and phase-opposition analysis, identical to the one described above (Fig. 2), was performed on a simulated dataset. Four electrophysiological datasets were simulated with similar properties as those observed in our empirical data: one for each experimental condition (300 trials each), i.e., perceived-phosphene and unperceived-phosphene for low-α and high-α amplitude conditions. Specifically, each trial was created as a sum of sine waves from 2 to 40 Hz. The amplitude of the simulated signal was determined based on the empirical data. For frequencies from 2 to 7 and 13 to 40 Hz, an amplitude of 100 arbitrary units (au) was chosen. For frequencies from 8 to 12 Hz, amplitudes varied depending on the simulated condition. For the low-α amplitude condition, we selected amplitudes of 280 au and 320 au for perceived-phosphene and unperceived-phosphene condition, respectively. For the high-α amplitude condition, we selected amplitudes of 580 and 620 au for perceived-phosphene and unperceived-phosphene conditions, respectively. A random phase between 0 and 2π was selected for frequencies from 2 to 7 and 13 to 40 Hz. For frequencies from 8 to 12 Hz, the phase varied depending on the simulated condition, i.e., [0 π] for perceived-phosphene for both low-α and high-α amplitude

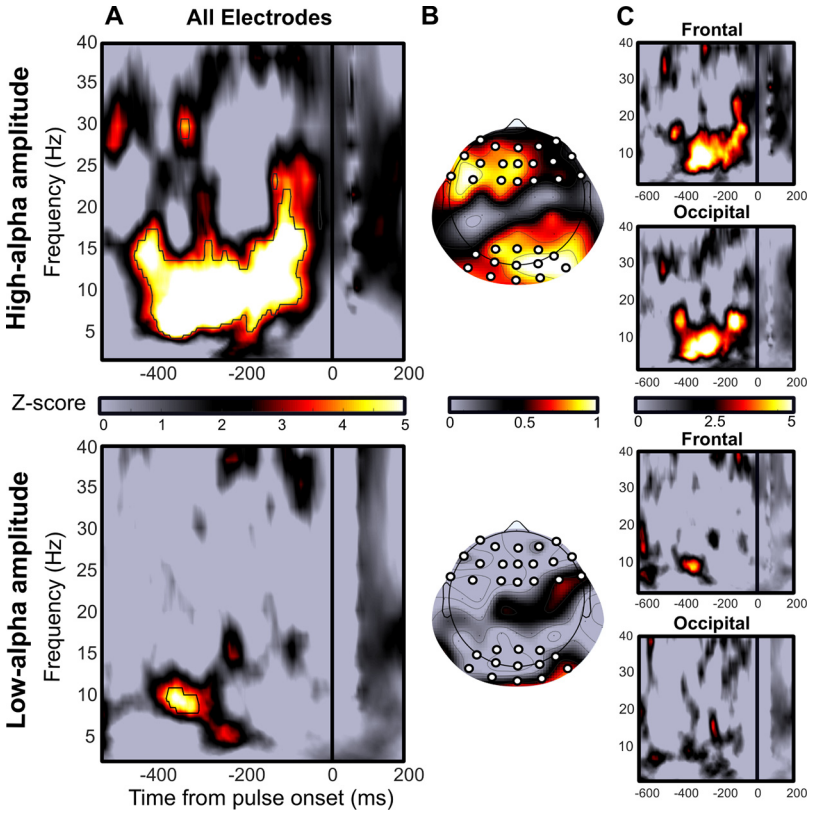

Figure 2. The phase of spontaneous α oscillations predicts phosphene perception mainly for high-α amplitude. This figure is supported by Extended Data Figures 2-1, 2-2, 2-3. Upper panel, Phase-opposition computed, respectively, on high-α amplitude trials. Lower panel, Low-α amplitude trials. ***A***, *Z*-scores map of phase-opposition between perceived-phosphene and unperceived-phosphene conditions averaged across nine participants and all 64 electrodes. Colormap, *Z*-scores. Black outline, significant phase-opposition FDR corrected for multiple comparisons (FDR = 0.01, corresponding to *p*-values threshold of 2.08×10^{-5} for low-α amplitude condition, and 1.96×10^{-5} for high-α amplitude condition). There is a significant phase-opposition from -400 to -50 ms before the pulse, between 5 and 18 Hz when α amplitude is high. The effect is less extended across time and frequencies when α amplitude is low. ***B***, *Z*-scores topographies averaged across the time-frequency window identified in panel ***A*** for high-α amplitude. The effect is maximal in a frontal and an occipital ROI when α amplitude is high. The topography is less clear when α amplitude is low. White dots, electrodes of interest within each ROI. ***C***, *Z*-scores maps of phase-opposition computed separately for the frontal ROI (upper panel) and the occipital ROI (lower panel).

conditions, and $[\pi\ 2\pi]$ for unperceived-phosphene for both low-α and high-α amplitude conditions. This phase distribution was applied to 80% of trials. In the other 20% of trials, a random phase between 0 and 2π was selected. Finally, white noise (VanRullen, 2016b) was added to all simulated datasets (amplitude: 4000 au) to match the empirically observed averaged *z*-score of phase-opposition (Fig. 2).

ERPs. Previously preprocessed EEG data were further cleaned from the power line noise by applying a notch filter at 50 Hz (band-stop at 47–53 Hz) before epoching. ERPs, centered on the pulse onset, were computed as the average of trials for each α-amplitude condition, phosphene-perception condition, and participant. The difference of ERPs between perceived-phosphene and unperceived-phosphene conditions was computed, separately for low-α and high-α amplitude conditions. The ERP differences were then compared against zero with repeated measures one-tailed *t* tests (from 350 to 800 ms). Correction for multiple comparisons was applied following a cluster procedure. For each participant, surrogate ERPs were obtained by shuffling the perceived and unperceived phosphene labels (500 repetitions). *t* tests were recomputed similarly as before, and the number of consecutive significant time points (surrogate cluster size) for each repetition was stored. The *p*-value for each empirical cluster was then computed as the proportion of surrogate clusters that were larger than the empirical cluster. Using an α level of 0.05, we considered an empirical cluster significant if its size was larger than at least 95% of the surrogate clusters.

FFT on prepulse ERPs

The use of TMS to induce phosphene perception rather than an external stimulation allows for direct access to the instantaneous state of the spontaneous brain oscillations. In other words, one can directly compute the prepulse ERP differences (time before pulse onset) between perceived-phosphene and unperceived-phosphene conditions, to assess spontaneous oscillatory activity. In this case, when comparing ERP differences between perceived-phosphene and unperceived-phosphene conditions, separately for low-α and high-α (presorted)

amplitude trials, there is no analysis confound coming from a less accurate phase estimation when α amplitude is low. ERP differences from -400 to 0 ms were then analyzed with an FFT (500 points zero padding), independently for electrodes PO3 and AFz, for each α-amplitude condition and for each participant. The resulting amplitude spectra were then averaged across participants and plotted from 2 to 40 Hz (a peak at 10.24 Hz was observed for both electrodes and for each α-amplitude condition). We then performed the following steps to test for a difference between high-α and low-α amplitude trials in the resulting amplitude spectra: (1) difference of the averaged amplitude spectra between high-α and low-α amplitude trials; (2) fit of this difference to the 1/f component; (3) removing of the 1/f component; (4) Gaussian fit of the resulting amplitude spectra to extract the frequency window showing a difference between high-α and low-α amplitude trials; (5) statistical comparison of the amplitude spectra (uncorrected for 1/f) between high-α and low-α amplitude trials conditions with a one-tailed *t* test. To ensure that the obtained significant difference between low-α and high-α amplitude conditions was not because of a difference in their 1/f aperiodic components, we fitted the amplitude spectra to their 1/f component and computed the area under the curve, for each participant, separately for low-α and high-α amplitude conditions, for both electrodes PO3 and AFz. The area under the curve of the low-α amplitude condition was compared with the one of the high-α amplitude condition with a two-tailed *t* test.

Finally, an FFT (500 points zero padding) was performed separately for the ERP of perceived-phosphene and unperceived-phosphene conditions on each participant. We then computed phase-locking values across participants to assess the interindividual variability at 10.24 Hz for low-α and high-α amplitude trials separately (frequency at which a peak of amplitude was observed in the amplitude spectra of the ERP difference between phosphene perceived and unperceived conditions). The sum of phase-locking values across participants of perceived-phosphene and unperceived-phosphene conditions was computed, for low-α and high-α amplitude trials separately, and evaluated statistically with a permutation procedure. *P*-values were estimated by comparing these POSs to the mean and SEM of the surrogate distribution obtained by shuffling the perceived-phosphene and unperceived-phosphene labels (repeated 500 times), for low-α and high-α amplitude trials separately, before replicating the previous analysis on the surrogate ERPs.

FFT on postpulse ERPs

As mentioned above, the advantage of the present TMS procedure is that it allows for direct access to the instantaneous state of the spontaneous brain oscillations. In other words, prepulse spontaneous activity is readily observable on the ERP. To ensure that postpulse ERPs were not contaminated by spontaneous α oscillations (i.e., that the TMS pulse here reset α oscillations), an FFT (500 points zero padding) was performed on the ERPs of the perceived-phosphene and unperceived-phosphene conditions, from 400 to 800 ms, for electrodes PO3 and AFz separately, and for each α-amplitude condition and participant. One-tailed *t* tests against the aperiodic 1/f activity were used to test the significance of the 10.24-Hz peak.

Perceptual performance as a function of prepulse phase

Low-α and high-α amplitude trials were sorted in nine phase bins at the selected time-frequency points (see above, Phase-opposition), separately for the occipital ROI, as well as the specific electrode PO3 (-77 ms, 10.7 Hz), and the frontal ROI, as well as the specific electrode AFz (-40 ms, 10.7 Hz). The percentage of perceived-phosphene was computed for each phase bin, α-amplitude condition, electrode, and participant, and further averaged across participants and electrodes. The values were finally normalized by dividing the percentage of perceived-phosphene averaged across phase bins, separately for each α-amplitude condition. A two-way repeated-measures ANOVA was performed to test for the main effect of phase bin. The percentage of variance explained was computed as the difference between the optimal phase (maximum percentage of phosphene perceived) and the opposite one.

ERP amplitude as a function of prepulse phase

Bin sorting was applied as described in the previous section. Then, the ERP difference between perceived-phosphene and unperceived-phosphene conditions for each phase bin and α-amplitude condition was computed. The maximum perceived-unperceived ERP difference was selected in the time window in which an ERP difference between low-α and high-α amplitude was detected, according to repeated measures two-tailed *t* test for each time point from 350 to 800 ms (PO3: from 482 to 513 ms; AFz: from 605 to 728 ms). A two-way repeated-measures ANOVA was performed to test for a main effect of phase bin and interaction between phase bin and α-amplitude (results regarding the main effect of α-amplitude were not interpreted). Specifically, we tested the hypotheses that (1) the ERP difference between perceived-phosphene and unperceived-phosphene conditions depended on the phase of spontaneous α oscillation, and (2) that this phase effect is stronger for high-α amplitude trials. Finally, we calculated the maximum ERP amplitude of the perceived-phosphene and unperceived-phosphene conditions separately, independently for phase bin centered on $-\pi/4$ and $\pi/2$, corresponding, respectively, to the maximum and the minimum ERP difference, and low-α and high-α amplitude trials. For each α-amplitude condition, we fitted the data to a linear mixed-effect model with phase bins and phosphene conditions as fixed effects, and participants as random effects. *Post hoc* analyses were done with one-tailed *t* tests.

Results

Single-pulse TMS was applied over the right occipital cortex (V1/V2) in nine healthy participants, at threshold intensity (45.96 $\pm$ 7.68% of phosphene perceived across participants) while simultaneously recording EEG. Previous analysis of this dataset (Dugué et al., 2011a) revealed that the phase of spontaneous α oscillations in the time-

frequency window from −400 to −50 ms prepulse, and from 7 to 17 Hz, predicts the perceptual outcome. This phase effect explained ~15% of the variability in phosphene perception. Here, trials were split according to low-amplitude, medium-amplitude, and high-amplitude of the prepulse spontaneous α oscillations (within the same time frequency-window as in Dugué et al., 2011a). We tested the two predictions made by the pulsed inhibition theory: (1) high-α amplitude induces periodic inhibitory moments leading to poor perceptual performance; and (2) low-α amplitude is less susceptible to phasic inhibition, and lead to overall higher perceptual performance. We first analyzed phosphene detection for each α-amplitude condition. We observed that phosphene detection rate depends on α amplitude with the highest detection being in low-α (48.22 ± 4.88%) then medium-α (45.94 ± 7.92%), and high-α (43.75 ± 11.57%) amplitude trials (Kruskal–Wallis: $p = 0.0553$, Cohen's d (effect size) = 0.88). Note that the earlier study (Dugué et al., 2011a) was not optimized to test the predictions made by the pulsed inhibition theory. However, the present results argue in its favor, with higher phosphene perception when α amplitude is low (Romei et al., 2008). In the next analyses, we discarded the medium-α amplitude trials to concentrate on the low-α and high-α amplitude conditions. This allowed us to clearly separate the two types of amplitude trials, while maximizing the number of trials per condition (see also Extended Data Fig. 2-1 for further assessment of such amplitude binning procedure).

To investigate the potential joint effect of the amplitude and the phase of spontaneous α oscillations on phosphene perception, we calculated POS (see Materials and Methods), separately for low-α and high-α amplitude conditions. Specifically, this analysis assesses whether phosphene perception is modulated by significantly different phases of the α cycle by computing the sum of phase-locking values (i.e., the amount of phase concentration across trials) over the perceived-phosphene and unperceived-phosphene conditions (Dugué et al., 2011a,b, 2015; VanRullen, 2016b). Spontaneous activity is characterized by a uniform phase distribution across all trials. Thus, if the phase is locked across trials for the perceived-phosphene condition (approximately half of the overall trials) then the phase of the unperceived-phosphene condition (other half of the overall trials) will logically be locked in the opposite direction, leading to a strong POS. Conversely, a weak POS value can only be obtained if both perceived and unperceived-phosphene conditions have near-random phase distributions, i.e., if phase does not affect phosphene perception. For high-α amplitude (Fig. 2, top raw), this analysis revealed a strong phase-opposition between perceived-phosphene and unperceived-phosphene conditions across all participants and electrodes, from −400 to −50 ms prepulse, and in the frequency range from 5 to 18 Hz (Fig. 2*A*). This effect remained significant after FDR correction for multiple comparisons (FDR = 0.01, corresponding to a z-score threshold of 4.27, a p-value threshold of 1.96×10^{-5}, and a Cohen's d threshold approaching infinity). The corresponding topography revealed that the phase-opposition effect was maximal over occipital and frontal electrodes (Fig. 2*B*,*C*). The analysis was replicated on low-α amplitude trials (Fig. 2, bottom raw). The overall strength of the effect was less important, i.e., effect less extended across time and frequency, for low-α amplitude trials (remained significant after FDR correction, FDR = 0.01, corresponding to a z-score threshold of 4.26, a p-value threshold of 2.08×10^{-5}, and a Cohen's d approaching infinity), and showed a less informative topography of the effect. A *post hoc* analysis revealed that POS values, averaged across electrodes, separately for the occipital and frontal ROIs at the respective selected time-frequency points (see Materials and Methods), were significantly higher for high-α compared with low-α amplitude trials at (10.7 Hz, −77 ms) for the occipital ROI (one-tailed t test: $p = 0.0016$, Cohen's $d = 1.9645$, CI = [0.042; infinity]; Extended Data Fig. 2-1*B*) and at (10.7 Hz, −40 ms) for the frontal ROI (one-tailed t test: $p < 0.001$, Cohen's $d = 2.1165$, CI = [0.0457; infinity]; Extended Data Fig. 2-1*F*). Together, these results suggest that there is an optimal phase of spontaneous α oscillations that predicts phosphene perception. This phase effect is more robust across time and across frequencies and is significantly higher for high-α compared with low-α amplitude trials. Interestingly, Extended Data Fig. 2-1 further illustrates the impact of several binning versions of the previous analysis (from two to five bins). In all versions, there is a difference of POS between low-α and high-α amplitude trials (one-tailed t tests for all binning versions show ps < 0.004 and Cohen's ds > 1.27). However, increasing the number of bins decreases the number of trials in each bin. Consequently, all main analyses were performed on the three-bin version (excluding the middle bin) to clearly separate low-α and high-α amplitude trials while maximizing the number of trials per condition.

To ensure that the difference in phase effect observed between low-α and high-α amplitude trials does not depend on a poor estimation of the phase when α amplitude is low, we performed a control analysis based on simulations (Extended Data Fig. 2-2). The phase-opposition analysis displayed in Figure 2 was repeated on simulated data generated with the same parameters (amplitude ratio between low-α and high-α amplitude trials) than those observed in the empirical dataset (for more details, see Materials and Methods). The simulations show that in both the low-α and high-α amplitude conditions, POS between perceived-phosphene and unperceived-phosphene trials can be observed with similar time-frequency profiles. Thus, the effect observed in Figure 2 cannot be simply explained by an underpowered phase estimation in low-α amplitude trials but indeed reflects a functional neurophysiological brain process. In addition, we tested that α oscillations are actually present in prepulse, low-α amplitude trials (Extended Data Fig. 2-3). An FFT on the prepulse EEG activity revealed a peak at 10.24 Hz in the occipital ROI for both low-α (one-tailed t test against the 1/f aperiodic activity: $p = 0.0354$, Cohen's $d = 0.7371$, CI = [11.7481; infinity]) and high-α ($p = 0.0102$, Cohen's $d = 0.9999$, CI = [60.0927; infinity]) amplitude trials, and in

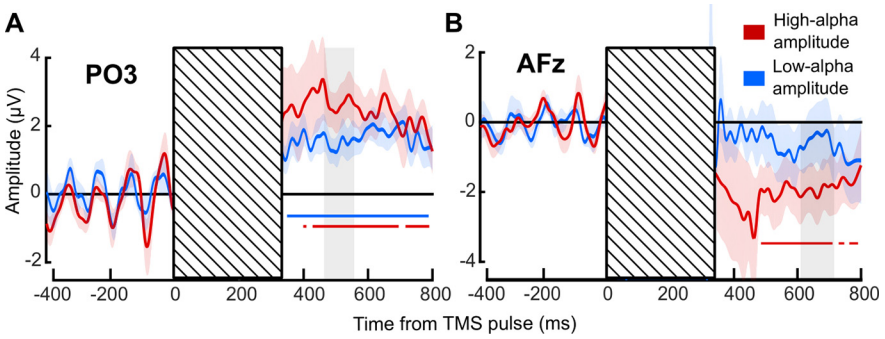

Figure 3. Difference between perceived-phosphene ERP and unperceived-phosphene ERP. This figure is supported by Extended Data Figure 3-1. ***A***, ERP difference at electrode PO3 between perceived-phosphene and unperceived-phosphene conditions averaged across nine participants. ***B***, ERP difference at electrode AFz. Red, high-α amplitude trials; blue, low-α amplitude trials. Colored shaded areas, SEM. Striped areas, mask the TMS-induced artifact. Colored solid horizontal lines, significant ERP difference against zero (significant cluster for PO3, low-α and high-α amplitude and AFz, high-α amplitude; $p < 0.001$). Gray shaded areas, selected time window of interest.

the frontal ROI for both low-α ($p = 0.0465$, Cohen's $d = 0.6668$, CI = [1.6258; infinity]) and high-α ($p = 0.0162$, Cohen's $d = 0.9527$, CI = [29.2137; infinity]) amplitude trials. This analysis confirms that estimating the phase in low-α amplitude trials is indeed neurophysiologically relevant. Additionally, the peak at 10.24 Hz was significantly higher for high-α compared with low-α amplitude trials, for both the occipital (one-tailed t tests: $p = 0.0268$, Cohen's $d = 0.2176$, CI = [6.8434; infinity]) and the frontal ($p = 0.0316$, Cohen's $d = 0.2485$, CI = [4.1668; infinity]) ROI. This difference was unlikely because of a difference in the 1/f aperiodic activity between low-α and high-α amplitude conditions, i.e., there was no significant difference in the 1/f component at 10.24 Hz between low-α and high-α amplitude conditions for the occipital (two-tailed t tests: $p = 0.2362$; Cohen's $d = 0.1893$, CI = [−9.8442; 34.4352]) and the frontal ($p = 0.0867$, Cohen's $d = 0.3361$, CI = [−2.5463; 30.6516]) ROI.

To further understand the link between prepulse spontaneous α oscillatory phase and amplitude, cortical excitability and phosphene perception, and address further a possible confound coming from a less accurate phase estimation when α amplitude is low (see Materials and Methods), we analyzed the ERP difference between perceived-phosphene and unperceived-phosphene conditions. Critically, the use of TMS to induce phosphene perception allows for direct access to the instantaneous state of the spontaneous brain oscillations. In other words, the prepulse ERP differences (time before pulse onset) between perceived-phosphene and unperceived-phosphene conditions, allows to assess spontaneous oscillatory activity. Thus, if there is an optimal phase for perception and an opposite, nonoptimal one, then for each participant the prepulse ERP for perceived-phosphene and for unperceived-phosphene should each oscillate in α, and so would the ERP difference. Additionally, if all participants share the same optimal phase, then the prepulse ERP difference averaged across participants should oscillate in α as well. We analyzed the ERP difference between perceived-phosphene and unperceived-phosphene conditions for electrodes PO3 and AFz (selected, respectively, in the occipital and frontal ROIs based on previous studies; Taylor et al., 2010; Dugué et al., 2011a; Fig. 3). For both electrodes and for both low-α and high-α amplitude trials, the ERP difference appeared periodic in the last 400 ms preceding the pulse (note that both low-α and high-α amplitude conditions show this effect). An FFT applied on the ERP difference of each participant in the prepulse period (−400–0 ms) showed a peak in amplitude for both electrode PO3 (10.24 Hz for both low-α and high-α amplitude; Fig. 4*A*) and electrode AFz (10.24 Hz for low-α and 9.22 Hz for high-α amplitude; Fig. 4*B*). Additionally, the amplitude of the prepulse oscillatory difference between perceived-phosphene and unperceived-phosphene was significantly higher for high-α amplitude compared with low-α amplitude trials, for the frequency window from 5.12 to 11.26 Hz for PO3 (one-tailed t test: $p = 0.044$, Cohen's $d = 0.361$, CI = [0.813; infinity]; see Materials and Methods), and from 7.16 to 10.24 Hz for AFz ($p = 0.039$, Cohen's $d = 0.241$, CI = [0.786; infinity]). This difference was unlikely because of a difference in the 1/f aperiodic activity between low-α and high-α amplitude conditions as their aperiodic activity did not differ significantly, neither for electrode PO3 (two-tailed t test: $p = 0.063$, Cohen's $d = 0.3131$, CI = [−13.8069; 414.8763]) nor AFz (two-tailed t test: $p = 0.806$, Cohen's $d = 0.0264$, CI = [−76.8006; 95.8066]). To further assess the interindividual variability, we calculated the sum of phase-locking values across participants at 10.24 Hz for perceived-phosphene and unperceived-phosphene conditions, separately for low-α and high-α amplitude trials, and for PO3 and AFz electrodes. In other words, we ask whether the prepulse ERP for each condition oscillates in-phase across all participants, and are in phase-opposition between perceived-phosphene and unperceived-phosphene conditions. We found that there is a phase-opposition between perceived-phosphene and unperceived-phosphene conditions for the electrode PO3, for high-α amplitude trials (permutation statistics: z-score = 1.9794, $p = 0.0239$, Cohen's $d = 1.756$), but not for low-α amplitude trials (z-score = 0.9856, $p = 0.1622$, Cohen's $d = 0.6957$), nor for AFz low-α (z-score = 0.2059, $p =$

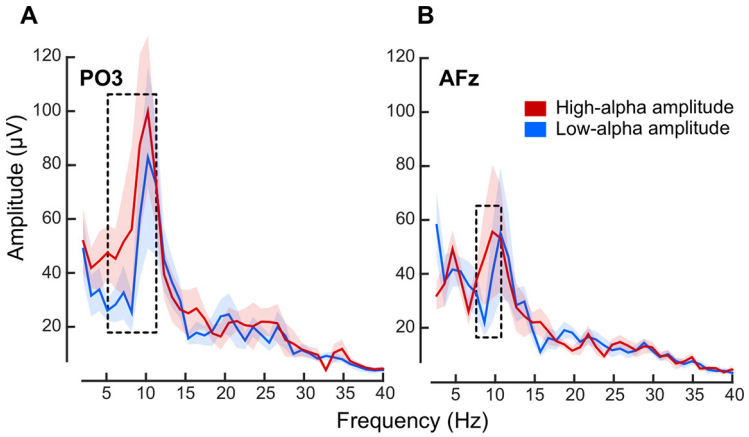

Figure 4. The prepulse ERP difference between perceived-phosphene and unperceived-phosphene conditions oscillates in α. ***A***, Frequency spectra computed on the ERP difference between perceived-phosphene and unperceived-phosphene conditions, on the prepulse period from −400 to 0 ms, respectively, for electrode PO3, and, ***B***, electrode AFz. Red color, high-α amplitude trials; blue color, low-α amplitude trials. Colored solid lines, frequency spectra averaged across the nine participants between 2 and 40 Hz. Shaded area, SEM. Dotted rectangle, significant difference between high-α and low-α amplitude trials averaged across frequency window from 5.12 to 11.26 Hz for electrode PO3, and from 7.16 to 10.24 Hz for electrode AFz (one-tailed *t* tests: $p = 0.044$ for PO3, $p = 0.039$ for AFz). Frequency peak at 10.24 Hz for both low-α and high-α amplitude for electrode PO3; at 10.24 Hz for low-α and 9.22 Hz for high-α amplitude for electrode AFz.

0.4184, Cohen's $d = 0.1375$) and high-α (z-score = 1.169, $p = 0.1212$, Cohen's $d = 0.8462$) amplitude. Phosphene perception depends on an optimal phase of α oscillation at the occipital electrode PO3, when α amplitude is high. Together, these analyses suggest that phosphene perception alternates between optimal and nonoptimal phases of the α (10.24 Hz) oscillations in the 400-ms window before the pulse, with all participants sharing a similar optimal phase. This phase effect is predominant in the occipital region, and stronger when the α amplitude is high.

Next, for each participant, we sorted low-α and high-α amplitude trials in nine bins according to the prepulse EEG phase, for the selected time-frequency points (occipital ROI: −77 ms, 10.7 Hz; frontal ROI: −40 ms, 10.7 Hz). Then, the percentage of phosphene perceived was calculated for each bin and averaged across participants (Fig. 5). A two-way repeated-measures ANOVA revealed a significant effect of the phase in both the occipital ($F_{(1,8)} = 2.117$, $p = 0.0467$, η^2 (effect size) = 20.93, square sum (SS) = 0.345) and frontal ($F_{(1,8)} = 3.360$, $p = 0.0028$, η^2 = 29.58, SS = 0.472) ROIs. There was no main effect of amplitude in either the occipital ($F_{(1,8)} = 1.818$, $p = 0.2145$, η^2 = 18.51, SS = 0.001) or the frontal ($F_{(1,8)} = 0.225$, $p = 0.6476$, $\eta^2 = 2.74$, SS < 0.001) ROIs, nor interaction in either the occipital ($F_{(1,8)} = 0.249$, $p = 0.9794$, SS = 0.048) or the frontal ($F_{(1,8)} = 0.462$, $p = 0.8781$, SS = 0.076) ROIs. Critically, the results show that the optimal phase for phosphene perception is centered on $\pi/2$ while the opposite phase, between $-\pi/2$ and $-\pi/4$, is nonoptimal. Finally, we observe that the percentage of variance explained by the phase is more important for high-α (occipital: 16.9% difference between $\pi/2$ and $-\pi/2$; frontal: 21.2%) compared with low-α (occipital: 13.3%; frontal: 17.6%) amplitude of spontaneous oscillations. We repeated this analysis for the individual electrodes PO3 and AFz and observed similar effects. A two-way repeated-measures ANOVA showed a significant effect of the phase for both electrodes PO3 ($F_{(1,8)} = 2.113$, $p = 0.0472$, η^2 = 20.89, SS = 0.937) and AFz ($F_{(1,8)} = 2.106$, $p = 0.0479$, η^2 = 20.84, SS = 0.908), no significant main effect of the amplitude for either electrode PO3 ($F_{(1,8)} = 0.461$, p = 0.5164, η^2 = 5.45, SS = 0.002) or AFz ($F_{(1,8)} = 0.002$, $p = 0.9633$, η^2 = 0.03, SS < 0.001), and no interaction for either electrode PO3 ($F_{(1,8)} = 0.612$, $p = 0.7648$, SS = 0.294) or AFz ($F_{(1,8)} = 0.389$, $p = 0.9224$, SS = 0.2).

To understand the role of spontaneous α oscillations phase-amplitude tradeoffs on cortical excitability and subsequent perceptual performance, we then focused on the postpulse evoked activity. Dugué et al. (2011a) previously observed a larger postpulse ERP in the perceived- than in the unperceived-phosphene trials, with a positive differential activity for PO3, and negative for AFz, between ∼300 and ∼600 ms. They interpreted these results as a physiological consequence of phosphene perception. Here, we computed the ERP difference between perceived-phosphene and unperceived-phosphene conditions, separately for low-α and high-α amplitude trials and observed a similar effect in both low-α and high-α amplitude conditions (Fig. 3; see also Extended Data Fig. 3-1 for ERPs on each condition separately). An FFT was computed from 400 to 800 ms after the pulse on the perceived-phosphene and unperceived phosphene ERP, separately for electrodes PO3 and AFz, and for low-α and high-α amplitude trials. There was no significant frequency peak at 10.24 Hz in the postpulse ERP amplitude spectra, in any of the conditions for both electrode PO3 (one-tailed *t* tests against the 1/f aperiodic component: low-α amplitude, perceived: $p = 0.9244$, Cohen's d = −0.4967, CI = [−28.6420; infinity]; unperceived: p = 0.6837, Cohen's d = −0.1176, CI = [−11.6204; infinity]; high-α amplitude, perceived: $p = 0.4279$, Cohen's d =

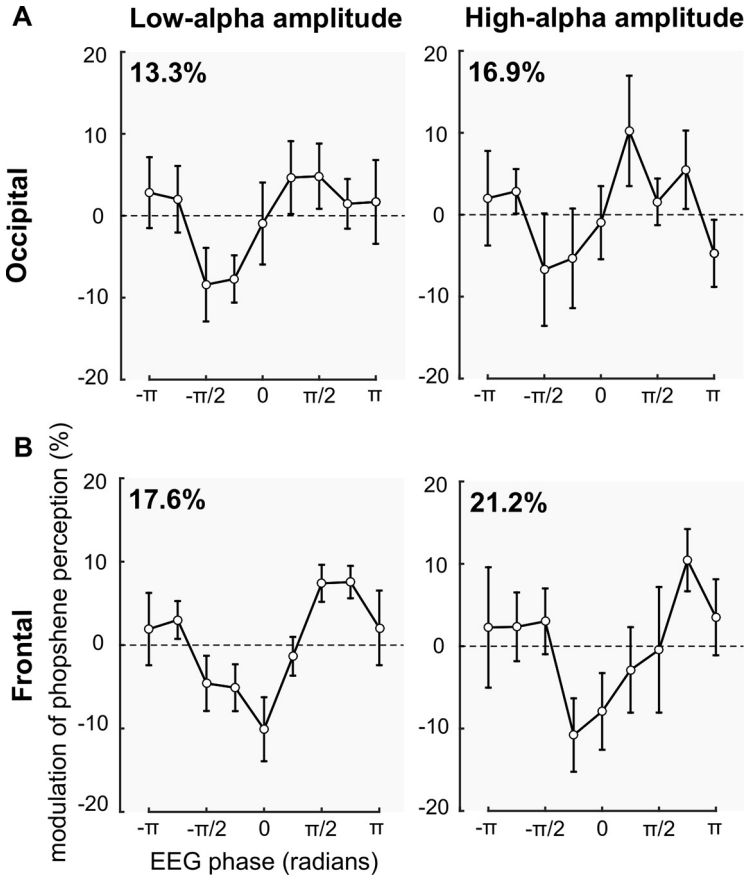

Figure 5. The phase $\pi/2$ of the α cycle is the optimal phase for phosphene perception. Left panels, Phosphene perception computed for nine phase bins (expressed in radians), normalized according to the average phosphene perception, and averaged across the nine participants and electrodes of interest, for low-α amplitude trials. Right panels, For high-α amplitude trials. Error bars, SEM. ***A***, Phosphene perception is plotted according to the instantaneous phase at -77 ms, 10.7 Hz, for the occipital ROI. Phosphene perception oscillates along with the α phase (two-way repeated-measures ANOVA: $F_{(1,8)} = 2.117$, $p = 0.0467$, $\eta^2 = 20.93$), with an optimal phase for phosphene perception at the phase $\pi/2$ of the α cycle. The percentage of variance explained by the phase is more important for high-α (16.9% difference between $\pi/2$ and $-\pi/2$) compared with low-α (13.3%) amplitude trials. ***B***, Phosphene perception is plotted according to the instantaneous phase at -40 ms, 10.7 Hz for the frontal ROI. Phosphene perception oscillates along with the α phase (two-way repeated-measures ANOVA: $F_{(1,8)} = 3.360$, $p = 0.0028$, $\eta^2 = 29.58$), with an optimal phase for phosphene perception at the phase $\pi/2$ of the α cycle. The percentage of variance explained by the phase is more important for high-α (21.2% difference between $\pi/2$ and $-\pi/2$) compared with low-α (17.6%) α amplitude trials.

0.0643, CI = [−17.1197; infinity]; unperceived: $p = 0.0971$, Cohen's $d = 0.3345$, CI = [−4.1354; infinity]) and AFz (low-α amplitude, perceived: $p = 0.9864$, Cohen's $d = -1.3376$, CI = [−36.8469; infinity]; unperceived: $p = 0.5615$, Cohen's $d = -0.0520$, CI = [−15.0938; infinity]; high-α amplitude, perceived: $p = 0.3038$, Cohen's $d = 0.0322$, CI = [−28.0728; infinity]; unperceived: $p = 0.1811$, Cohen's $d = 0.0610$, CI = [−17.3280; infinity]). Thus, the postpulse signal likely does not contain sufficient prepulse information to translate into a contamination of the postpulse ERP.

Finally, we investigated the link between the prepulse α phase and amplitude, and the postpulse evoked activity. For each participant, we sorted the low-α and high-α amplitude trials in nine bins, as previously described, separately for electrodes PO3 and AFz. For each phase bin and α-amplitude condition, the maximum perceived-unperceived ERP difference was computed on a selected time-window of interest (see Materials and Methods; Fig. 3, gray shaded areas). A two-way repeated-measures ANOVA on electrode PO3 (Fig. 6*A*) revealed a significant main effect of the phase ($F_{(1,8)} = 2.338$, $p = 0.0286$, $\eta^2 = 22.62$, SS = 430.66) and α-amplitude ($F_{(1,8)} = 13.623$, $p = 0.0061$, $\eta^2 = 63$, SS = 137.62; this is coherent with the selection of the ERP time window of interest and will not be further interpreted; see Materials and Methods), but no significant interaction ($F_{(1,8)} = 0.377$, $p = 0.9289$, SS = 61.76). The two-way repeated-measures ANOVA on electrode AFz (Fig. 6*C*) showed a significant main effect of the α-amplitude ($F_{(1,8)} = 12.749$, $p = 0.0073$, $\eta^2 = 61.44$, SS = 102.97; this is coherent with the selection of the ERP time window of interest and will not be further interpreted; see Materials and Methods), no significant effect of the phase ($F_{(1,8)} = 0.393$, $p = 0.9206$, $\eta^2 = 4.68$, SS = 161.37), and no interaction ($F_{(1,8)} = 0.376$, $p = 0.9297$, SS = 158.75). In other words, for both low-α and high-α amplitude, the phase of prepulse spontaneous α oscillations predicts the ERP difference exclusively for the occipital electrode

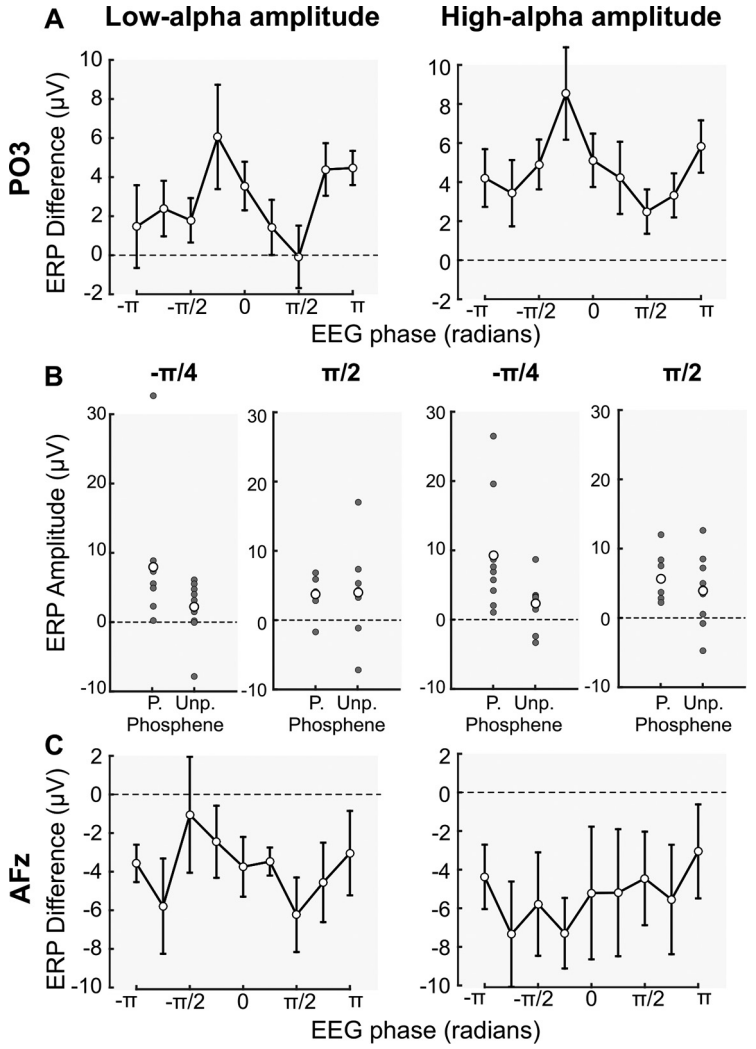

Figure 6. The ERP is higher for perceived-phosphene trials at the nonoptimal phase for phosphene perception, for the electrode PO3. Left panels, ERP difference between perceived-phosphene and unperceived-phosphene conditions computed for nine phase bins, and averaged across the nine participants, for low-α amplitude trials. Right panels, For high-α amplitude trials. ***A***, Single trials were sorted into nine phase bins according to the instantaneous phase at -77 ms, 10.7 Hz, for the electrode PO3. For each phase bin, the maximum perceived-unperceived ERP difference was computed. Errors bars, SEM. The ERP difference oscillates along with the α phase ($F_{(1,8)} = 2.338$, $p = 0.0286$, $\eta^2 = 22.62$). The ERP difference was higher at the phase $-\pi/4$. ***B***, ERP for the perceived-phosphene and unperceived-phosphene conditions, for the electrode PO3, for the phase $-\pi/4$ and $\pi/2$. P., perceived-; Unp., unperceived-phosphene conditions. Gray dots, maximum ERP for each participant; white dots, averaged ERP across the nine participants. The maximum ERP at the phase $-\pi/4$ for perceived-phosphene trials was significantly higher compared with unperceived-phosphene trials at the phase $-\pi/4$ for both low-α (one-tailed t test, $p = 0.0265$) and high-α ($p = 0.0074$) amplitude trials type, and compared with unperceived-phosphene trials at the phase $\pi/2$ for both low-α ($p = 0.0254$) and high-α ($p = 0.0253$) amplitude trials type. ***C***, Single trials were sorted into nine phase bins according to the instantaneous phase at -40 ms, 10.7 Hz, for the electrode AFz. For each phase bin, the maximum perceived-unperceived ERP difference was computed. Errors bars, SEM.

PO3. Specifically, we observed a higher ERP difference at $-\pi/4$, i.e., around the nonoptimal phase for phosphene perception (see Fig. 5*A*). This effect seems to come from an increased ERP in perceived-phosphene trials specifically. Indeed, we extracted the peak of the ERP for low-α and high-α amplitude trials, at $-\pi/4$ and $\pi/2$ phases of the α cycle, corresponding, respectively, to the maximum and the minimum ERP difference observed (see Fig. 5*A*), separately for perceived-phosphene and unperceived-ERPs, for the nine participants (Fig. 6*B*). We implemented two linear mixed effects models, one for each α-amplitude condition. In each model, we entered as fixed effects the phase ($-\pi/4$, $\pi/2$), the phosphene condition (perceived, unperceived), as well as their interaction. As random effect, we had participants' intercepts and slopes for the effect of phase and phosphene condition. We observed a significant effect of the phosphene condition for both low-α ($t_{(32)} = -3.1$, $p = 0.004$, estimate = -12.201 ± 3.935, SE) and high-α ($t_{(32)} = -3.252$, $p = 0.003$, estimate = -12.188 ± 3.748, SE) amplitude conditions, a significant effect of the phase for low-α ($t_{(32)} = -2.551$, $p = 0.0157$, estimate = -10.161 ± 3.983, SE) and high-α

($t_{(32)} = -2.313$, $p = 0.0273$, estimate = -8.833 ± 3.82, SE) amplitude conditions, and a significant interaction between the phosphene condition and the phase for both low-α ($t_{(32)} = 2.468$, $p = 0.0191$, estimate = 6.142 ± 2.489, SE) and high-α ($t_{(32)} = 2.237$, $p = 0.033$, estimate = 5.292 ± 2.369, SE) amplitude conditions. A *post hoc* analysis showed that the ERP difference at $-\pi/4$ for perceived-phosphene trials was significantly higher compared with unperceived-phosphene trials at $-\pi/4$ for both low-α (one-tailed *t* test, $p = 0.0265$, Cohen's $d = 0.809$, CI = [1.09; infinity]) and high-α ($p = 0.0074$, Cohen's $d = 1.069$, CI = [2.753; infinity]) amplitude conditions, and compared with unperceived-phosphene trials at $\pi/2$ for both low-α ($p = 0.0254$, Cohen's $d = 0.477$, CI = [0.747; infinity]) and high-α ($p = 0.0253$, Cohen's $d = 0.737$, CI = [0.984; infinity]) amplitude conditions. Thus, around $-\pi/4$ for both low-α and high-α amplitude, we observed a low percentage of perceived-phosphene (Fig. 5*A*) associated with a high ERP difference when the phosphene is perceived (Fig. 6*A*).

Discussion

In this study, we tested the two clear predictions of the pulsed inhibition theory (Klimesch et al., 2007; Jensen and Mazaheri, 2010; Mathewson et al., 2011): (1) high-α amplitude induces cortical inhibition at specific phases of the α cycle, leading to periodic perceptual performance; while (2) low-α amplitude is less susceptible to phasic (periodic) pulsed inhibition, leading to overall higher perceptual performance. Cortical excitability was assessed by both phosphene detection and postpulse evoked EEG activity. We showed that the prepulse phase of spontaneous α oscillations (~10 Hz) modulates the probability to perceive a phosphene (with a nonoptimal phase between $-\pi/2$ and $-\pi/4$). This phase effect was stronger for high-α amplitude trials. Moreover, the prepulse nonoptimal phase leads to an increase in postpulse evoked activity (ERP), in phosphene-perceived trials specifically. Together, our results provide strong evidence in favor of the pulsed inhibition theory by establishing a causal link between the amplitude and the phase of spontaneous α oscillations, cortical excitability, and subsequent perceptual performance.

α Phase-amplitude tradeoffs on perception

As previously described in the literature, we found that the phase of spontaneous oscillations in the α frequency range predicts whether a near-threshold stimulus would be successfully perceived (Busch et al., 2009; Mathewson et al., 2009; Dugué et al., 2011a; Samaha et al., 2015, 2017). The use of TMS to induce phosphene perception rather than an external stimulation allows for direct access to the absolute phase of spontaneous oscillations. We found that a phase between $-\pi/2$ and $-\pi/4$ was associated with inhibitory moments leading to lower perceptual performance while the opposite one ($\pi/2$) was optimal for perception. Critically, as predicted by the pulsed inhibition theory, our results are in line with some previous studies showing that the phase of spontaneous α oscillations better predicts perceptual performance for high than for low-α amplitude (Mathewson et al., 2009; Ng et al., 2012; Ai and Ro, 2014; Bonnefond and Jensen, 2015; Herrmann et al., 2016; Spitzer et al., 2016; Kizuk and Mathewson, 2017; Alexander et al., 2020) but not others (Busch and VanRullen, 2010; Zoefel and Heil, 2013; Milton and Pleydell-Pearce, 2016; Harris et al., 2018; Madsen et al., 2019). Other studies investigated the specific case in which a high-α amplitude condition is compared with the actual absence of α oscillations (Schaworonkow et al., 2018, 2019; Stefanou et al., 2018; Zrenner et al., 2018; Bergmann et al., 2019). They found periodic functional inhibition induced by μ oscillations (α oscillations recorded in the motor cortex) in the high-α amplitude condition (see next paragraph for more details). Here, we compared high-α amplitude trials to trials in which α oscillations were present but with a lower amplitude, and found a phase effect in both α-amplitude conditions, but strongest when α amplitude is high.

α Phase-amplitude tradeoffs on cortical excitability

We observed that the phase and the amplitude of spontaneous α oscillations influence cortical excitability, only when there is subsequent perception. Indeed, a phase between $-\pi/2$ and $-\pi/4$ led to higher ERP exclusively for phosphene perception trials. Interestingly, this phase was also associated with lower perceptual performance. The nonoptimal phase of the α oscillations (between $-\pi/2$ and $-\pi/4$) tends to create periodic inhibitory cortical states favoring the absence of phosphene perception, which leads to a greater ERP response when a phosphene is in fact perceived. It is important to notice that the paradigm developed by Dugué et al. (2011a) was designed to specifically investigate the role of the phase of α oscillations (and not the phase-amplitude tradeoffs). However, the results are compelling and in line with other studies observing similar effects (Bonnefond and Jensen, 2015; Hussain et al., 2019; and others comparing high-α amplitude to the absence of α oscillations: Schaworonkow et al., 2018, 2019; Stefanou et al., 2018; Zrenner et al., 2018; Bergmann et al., 2019). In the motor modality, they used single-pulse TMS over the motor cortex to induce MEPs allowing to estimate corticospinal excitability. They found an increase in corticospinal excitability and the subsequent MEP for high-μ amplitude oscillations (i.e., α oscillations observed in somatosensory and motor areas) and for specific μ phases (Schaworonkow et al., 2018, 2019; Stefanou et al., 2018; Zrenner et al., 2018; Bergmann et al., 2019; Hussain et al., 2019). Bonnefond and Jensen (2015) alternatively analyzed the power of high γ oscillations (80–120 Hz) considered to reflects neuronal firing (Ray et al., 2008). They showed that γ power was weaker at the trough of high-α amplitude oscillations (Bonnefond and Jensen, 2015). As predicted by the pulsed inhibition theory, high-α amplitude modulates cortical and corticospinal excitability periodically. Interestingly, although the pulsed inhibition theory (Jensen and Mazaheri, 2010) originally proposed asymmetrical pulsed inhibition (i.e., inhibition at one particular phase and no inhibition at the opposite one), Bergmann et al. (2019) argued in favor of asymmetrical pulsed facilitation. Indeed, they assessed the role of the GABAergic system, considered the main

source of inhibition in the brain (Ribak and Yan, 2000), on the amplitude and phase of μ oscillations, and did not observe any relation. The symmetry/asymmetry hypothesis was not explicitly assessed in the present study. Further investigation is thus necessary to disentangle the three possibilities: (1) symmetric pulsed inhibition and facilitation; (2) asymmetrical pulsed inhibition; or (3) asymmetrical pulsed facilitation.

α, A top-down process?

Our results show a potential functional link between the occipital and the frontal lobes. Several authors have proposed that α carries feedback information (van Kerkoerle et al., 2014; Michalareas et al., 2016) and that the amplitude of occipital α oscillations is modulated by top-down connections from frontoparietal regions (Klimesch et al., 2007; Mathewson et al., 2011). Here, we can speculate that the frontal region plays a role in the emergence of inhibitory and excitatory moments in occipital cortex. Specifically, their top-down influence on the amplitude of α oscillations would enhance or reduce locally the effect of the phase of occipital α oscillations on perceptual performance, thus explaining that the link between the phase and the amplitude of α oscillations and cortical excitability (ERP) was only present in the occipital ROI. In addition, the previous study from which the data originate (Dugué et al., 2011a) shows that the time at which the phase predicted the perceptual outcome differed by nearly one-half α-cycle between the occipital (-77 ms) and the frontal (-40 ms) ROI. This difference may reflect the delay for neural information to be transferred from one brain region to the other, consistent with previous observations of an α phase difference between occipital and frontal regions during visual perception (Burkitt et al., 2000; Patten et al., 2012; Alamia and VanRullen, 2019; Pang et al., 2020; Tsoneva et al., 2021). Further studies are warranted to investigate the functional interplay between the frontal and occipital cortex in the context of the pulsed inhibition theory.

In conclusion, our study provides strong causal evidence in favor of tradeoffs between the phase and the amplitude of α oscillations to create periodic inhibitory moments leading to rhythms in perception. As predicted by the pulsed inhibition theory, the effect of the phase of spontaneous α oscillations on perception increases for larger α amplitude.

References

Ai L, Ro T (2014) The phase of prestimulus alpha oscillations affects tactile perception. J Neurophysiol 111:1300–1307.

Alamia A, VanRullen R (2019) Alpha oscillations and traveling waves: signatures of predictive coding? PLoS Biol 17:e3000487.

Alexander KE, Estepp JR, Elbasiouny SM (2020) Effects of neuronic shutter observed in the EEG alpha rhythm. eNeuro 7: ENEURO.0171-20.2020– 14.

Berens P (2009) CircStat: a MATLAB toolbox for circular statistics. J Stat Softw 31:1–21.

Bergmann TO, Lieb A, Zrenner C, Ziemann U (2019) Pulsed facilitation of corticospinal excitability by the sensorimotor μ-alpha rhythm. J Neurosci 39:10034–10043.

Bollimunta A, Chen Y, Schroeder CE, Ding M (2008) Neuronal mechanisms of cortical alpha oscillations in awake-behaving macaques. J Neurosci 28:9976–9988.

Bonnefond M, Jensen O (2015) Gamma activity coupled to alpha phase as a mechanism for top-down controlled gating. PLoS One 10:e01286671.

Burkitt GR, Silberstein RB, Cadusch PJ, Wood AW (2000) Steady-state visual evoked potentials and travelling waves. Clin Neurophysiol 111:246–258.

Busch NA, VanRullen R (2010) Spontaneous EEG oscillations reveal periodic sampling of visual attention. Proc Natl Acad Sci USA 107:16048–16053.

Busch NA, Dubois J, VanRullen R (2009) The phase of ongoing EEG oscillations predicts visual perception. J Neurosci 29:7869–7876.

Clayton MS, Yeung N, Cohen Kadosh R (2018) The many characters of visual alpha oscillations. Eur J Neurosci 48:2498–2508.

Delorme A, Makeig S (2004) EEGLAB: an open source toolbox for analysis of single-trial EEG dynamics including independent component analysis. J Neurosci Methods 134:9–21.

Dugué L, VanRullen R (2017) Transcranial magnetic stimulation reveals intrinsic perceptual and attentional rhythms. Front Neurosci 11:1–7.

Dugué L, Marque P, VanRullen R (2011a) The phase of ongoing oscillations mediates the causal relation between brain excitation and visual perception. J Neurosci 31:11889–11893.

Dugué L, Marque P, VanRullen R (2011b) Transcranial magnetic stimulation reveals attentional feedback to area V1 during serial visual search. PLoS One 6:e19712.

Dugué L, Marque P, VanRullen R (2015) Theta oscillations modulate attentional search performance periodically. J Cogn Neurosci 27:945–958.

Dugué L, Roberts M, Carrasco M (2016) Attention reorients periodically. Curr Biol 26:1595–1601.

Dugué L, Beck AA, Marque P, VanRullen R (2019) Contribution of FEF to attentional periodicity during visual search: a TMS study. eNeuro 6:ENEURO.0357-18.2019–10.

Ergenoglu T, Demiralp T, Bayraktaroglu Z, Ergen M, Beydagi H, Uresin Y (2004) Alpha rhythm of the EEG modulates visual detection performance in humans. Brain Res Cogn Brain Res 20:376–383.

Gerwig M, Niehaus L, Kastrup O, Stude P, Diener HC (2005) Visual cortex excitability in migraine evaluated by single and paired magnetic stimuli. Headache 45:1394–1399.

Goldman RI, Stern JM, Engel J, Cohen MS (2002) Simultaneous EEG and fMRI of the alpha rhythm. Neuroreport 13:2487–2492.

Haegens S, Nácher V, Luna R, Romo R, Jensen O (2011) α-Oscillations in the monkey sensorimotor network influence discrimination performance by rhythmical inhibition of neuronal spiking. Proc Natl Acad Sci USA 108:19377–19382.

Haegens S, Barczak A, Musacchia G, Lipton ML, Mehta AD, Lakatos P, Schroeder CE (2015) Laminar profile and physiology of the α rhythm in primary visual, auditory, and somatosensory regions of neocortex. J Neurosci 35:14341–14352.

Händel BF, Haarmeier T, Jensen O (2011) Alpha oscillations correlate with the successful inhibition of unattended stimuli. J Cogn Neurosci 23:2494–2502.

Harris AM, Dux PE, Mattingley JB (2018) Detecting unattended stimuli depends on the phase of prestimulus neural oscillations. J Neurosci 38:3092–3101.

Herrmann B, Henry MJ, Haegens S, Obleser J (2016) Temporal expectations and neural amplitude fluctuations in auditory cortex interactively influence perception. Neuroimage 124:487–497.

Hussain SJ, Claudino L, Bönstrup M, Norato G, Cruciani G, Thompson R, Zrenner C, Ziemann U, Buch E, Cohen LG (2019) Sensorimotor oscillatory phase-power interaction gates resting human corticospinal output. Cereb Cortex 29:3766–3777.

Jensen O, Mazaheri A (2010) Shaping functional architecture by oscillatory alpha activity: gating by inhibition. Front Hum Neurosci 4:1–13.

Kammer T, Baumann LW (2010) Phosphene thresholds evoked with single and double TMS pulses. Clin Neurophysiol 121:376–379.
Kienitz R, Schmid MC, Dugué L (2021) Rhythmic sampling revisited: experimental paradigms and neural mechanisms. Eur J Neurosci. Advance online publication. Retrieved Oct 13, 2021. doi: 10.1111/ejn.15489.
Kizuk SAD, Mathewson KE (2017) Power and phase of alpha oscillations reveal an interaction between spatial and temporal visual attention. J Cogn Neurosci 29:480–494.
Klimesch W, Sauseng P, Hanslmayr S (2007) EEG alpha oscillations: the inhibition-timing hypothesis. Brain Res Rev 53:63–88.
Lin YJ, Shukla L, Dugué L, Valero-Cabré A, Carrasco M (2021) Transcranial magnetic stimulation entrains alpha oscillatory activity in occipital cortex. Sci Rep 11:18562.
Madsen KH, Karabanov AN, Krohne LG, Safeldt MG, Tomasevic L, Siebner HR (2019) No trace of phase: corticomotor excitability is not tuned by phase of pericentral mu-rhythm. Brain Stimul 12:1261–1270.
Mathewson KE, Gratton G, Fabiani M, Beck DM, Ro T (2009) To see or not to see: prestimulus alpha phase predicts visual awareness. J Neurosci 29:2725–2732.
Mathewson KE, Lleras A, Beck DM, Fabiani M, Ro T, Gratton G (2011) Pulsed out of awareness: EEG alpha oscillations represent a pulsed-inhibition of ongoing cortical processing. Front Psychol 2:99.
Michalareas G, Vezoli J, van Pelt S, Schoffelen J-M, Kennedy H, Fries P (2016) Alpha-beta and gamma rhythms subserve feedback and feedforward influences among human visual cortical areas. Neuron 89:384–397.
Milton A, Pleydell-Pearce CW (2016) The phase of pre-stimulus alpha oscillations influences the visual perception of stimulus timing. Neuroimage 133:53–61.
Moosmann M, Ritter P, Krastel I, Brink A, Thees S, Blankenburg F, Taskin B, Obrig H, Villringer A (2003) Correlates of alpha rhythm in functional magnetic resonance imaging and near infrared spectroscopy. Neuroimage 20:145–158.
Ng BSW, Schroeder T, Kayser C (2012) A precluding but not ensuring role of entrained low-frequency oscillations for auditory perception. J Neurosci 32:12268–12276.
Pang Z, Alamia A, VanRullen R (2020) Turning the stimulus on and off changes the direction of α traveling waves. eNeuro 7: ENEURO.0218-20.2020.
Patten TM, Rennie CJ, Robinson PA, Gong P (2012) Human cortical traveling waves: dynamical properties and correlations with responses. PLoS One 7:e38392.
Pfurtscheller G, Lopes da Silva FH (1999) Event-related EEG/MEG synchronization and desynchronization: basic principles. Clin Neurophysiol 110:1842–1857.
Ray PG, Meador KJ, Epstein CM, Loring DW, Day LJ (1998) Magnetic stimulation of visual cortex: factors influencing the perception of phosphenes. J Clin Neurophysiol 15:351–357.
Ray S, Crone NE, Niebur E, Franaszczuk PJ, Hsiao SS (2008) Neural correlates of high-gamma oscillations (60-200 Hz) in macaque local field potentials and their potential implications in electrocorticography. J Neurosci 28:11526–11536.
Ribak CE, Yan XX (2000) GABA neurons in the neocortex. In: GABA in the nervous system: the view at fifty years (Martin DL, Olsen RW, eds), pp 357–368. Philadelphia: Lippincott Williams and Wilkins.
Romei V, Brodbeck V, Michel C, Amedi A, Pascual-Leone A, Thut G (2008) Spontaneous fluctuations in posterior alpha-band EEG activity reflect variability in excitability of human visual areas. Cereb Cortex 18:2010–2018.
Rossi S, Hallett M, Rossini PM, Pascual-Leone A; Safety of TMS Consensus Group (2009) Safety, ethical considerations, and application guidelines for the use of transcranial magnetic stimulation in clinical practice and research. Clin Neurophysiol 120:2008–2039.
Samaha J, Bauer P, Cimaroli S, Postle BR (2015) Top-down control of the phase of alpha-band oscillations as a mechanism for temporal prediction. Proc Natl Acad Sci USA 112:8439–8444.
Samaha J, Gosseries O, Postle BR (2017) Distinct oscillatory frequencies underlie excitability of human occipital and parietal cortex. J Neurosci 37:2824–2833.
Samaha J, Iemi L, Haegens S, Busch NA (2020) Spontaneous brain oscillations and perceptual decision-making. Trends Cogn Sci 24:639–653.
Sauseng P, Klimesch W, Stadler W, Schabus M, Doppelmayr M, Hanslmayr S, Gruber WR, Birbaumer N (2005) A shift of visual spatial attention is selectively associated with human EEG alpha activity. Eur J Neurosci 22:2917–2926.
Schaworonkow NC, Gordon P, Belardinelli P, Ziemann U, Bergmann TO, Zrenner C (2018) μ-Rhythm extracted with personalized EEG filters correlates with corticospinal excitability in real-time phase-triggered EEG-TMS. Front Neurosci 12:1–6.
Schaworonkow N, Triesch J, Ziemann U, Zrenner C (2019) EEG-triggered TMS reveals stronger brain state-dependent modulation of motor evoked potentials at weaker stimulation intensities. Brain Stimul 12:110–118.
Scheeringa R, Mazaheri A, Bojak I, Norris DG, Kleinschmidt A (2011) Modulation of visually evoked cortical FMRI responses by phase of ongoing occipital alpha oscillations. J Neurosci 31:3813–3820.
Spitzer B, Blankenburg F, Summerfield C (2016) Rhythmic gain control during supramodal integration of approximate number. Neuroimage 129:470–479.
Stefanou MI, Desideri D, Belardinelli P, Zrenner C, Ziemann U (2018) Phase synchronicity of μ-rhythm determines efficacy of interhemispheric communication between human motor cortices. J Neurosci 38:10525–10534.
Taylor PCJ, Walsh V, Eimer M (2010) The neural signature of phosphene perception. Hum Brain Mapp 31:1408–1417.
Thut G, Nietzel A, Brandt SA, Pascual-Leone A (2006) Alpha-band electroencephalographic activity over occipital cortex indexes visuospatial attention bias and predicts visual target detection. J Neurosci 26:9494–9502.
Tsoneva T, Garcia-Molina G, Desain P (2021) SSVEP phase synchronies and propagation during repetitive visual stimulation at high frequencies. Sci Rep 11:1–13.
van Dijk H, Schoffelen JM, Oostenveld R, Jensen O (2008) Prestimulus oscillatory activity in the alpha band predicts visual discrimination ability. J Neurosci 28:1816–1823.
van Kerkoerle T, Self MW, Dagnino B, Gariel-Mathis M-A, Poort J, van der Togt C, Roelfsema PR (2014) Alpha and gamma oscillations characterize feedback and feedforward processing in monkey visual cortex. Proc Natl Acad Sci USA 111:14332–14341.
VanRullen R (2016a) Perceptual cycles. Trends Cogn Sci 20:723–735.
VanRullen R (2016b) How to evaluate phase differences between trial groups in ongoing electrophysiological signals. Front Neurosci 10:1–22.
Varela FJ, Toro A, Roy John E, Schwartz EL (1981) Perceptual framing and cortical alpha rhythm. Neuropsychologia 19:675–686.
Zoefel B, Heil P (2013) Detection of near-threshold sounds is independent of EEG phase in common frequency bands. Front Psychol 4:1–17.
Zrenner C, Desideri D, Belardinelli P, Ziemann U (2018) Real-time EEG-defined excitability states determine efficacy of TMS-induced plasticity in human motor cortex. Brain Stimul 11:374–389.

Extended Data

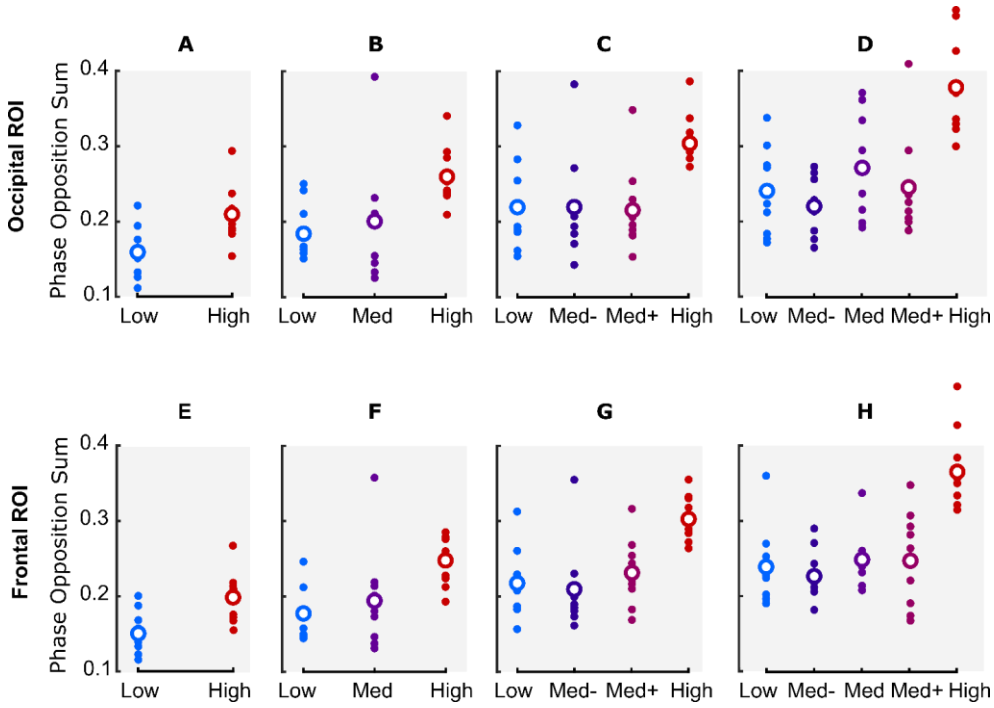

Extended Data Figure 2-1. The phase effect on phosphene perception is higher for high- compared to low-alpha amplitude trials. Phase-opposition sum computed for several binning versions of alpha amplitude trials, at 10.7 Hz and **A-D** at -77 ms pre-pulse, and averaged across electrodes within the occipital ROI, **E-H** at -40 ms pre-pulse, and averaged across the electrodes within the frontal ROI. Dots, POS for individual participants. Circles, POS averaged across the 9 participants. All following analyses were performed on the 3-bins condition (**B** and **F**), i.e., trials were binned in low-, medium- (med) and high-alpha amplitude trials, discarding the medium-alpha amplitude bin.

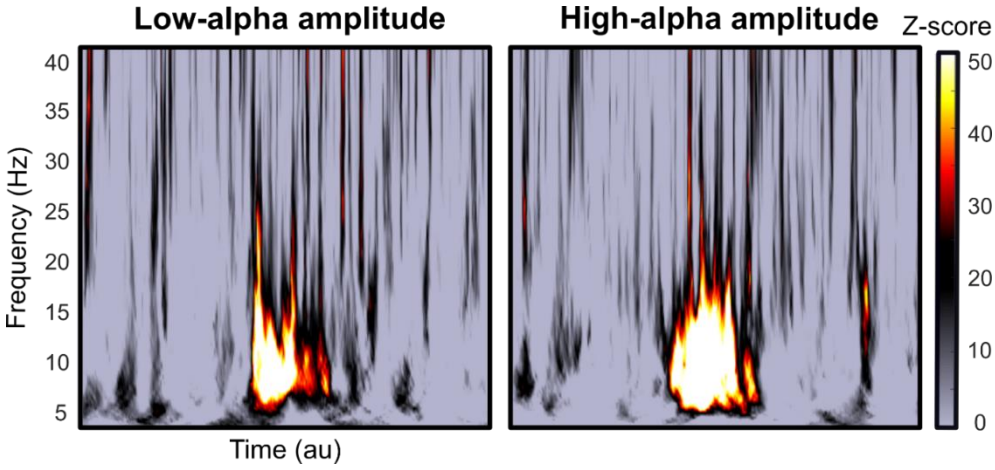

Extended Data Figure 2-2. Both low- and high-alpha amplitude oscillations simulated datasets show a similar phase effect on perception. Left panel, phase-opposition computed on simulated low-alpha amplitude trials. Right panel, simulated high-alpha amplitude trials. Z-scores maps of phase-opposition between perceived- and unperceived-phosphene conditions. Colormap, Z-

scores. Au, Arbitrary Unit. Between low- and high-alpha amplitude simulated trials, there is a comparable phase-opposition between perceived- and unperceived-phosphene conditions, from 5 to 18 Hz.

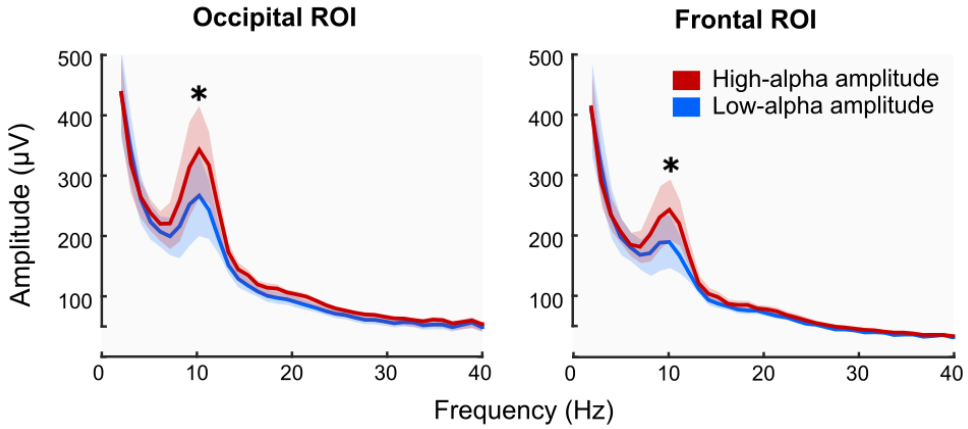

Extended Data Figure 2-3. Pre-pulse oscillatory activity in the alpha frequency band in both low- and high-alpha amplitude conditions. Amplitude spectra computed on the EEG time-series from -600 ms to -1 ms relative to pulse onset, for the occipital ROI (left panel) and the frontal (right panel) ROI. Red color, high-alpha amplitude condition. Blue color, low-alpha amplitude condition. Colored solid lines, amplitude spectra averaged across the 9 participants between 2 and 40 Hz. Colored shaded areas, standard error of the mean. *, significant difference at 10.24 Hz between low- and high-alpha amplitude conditions.

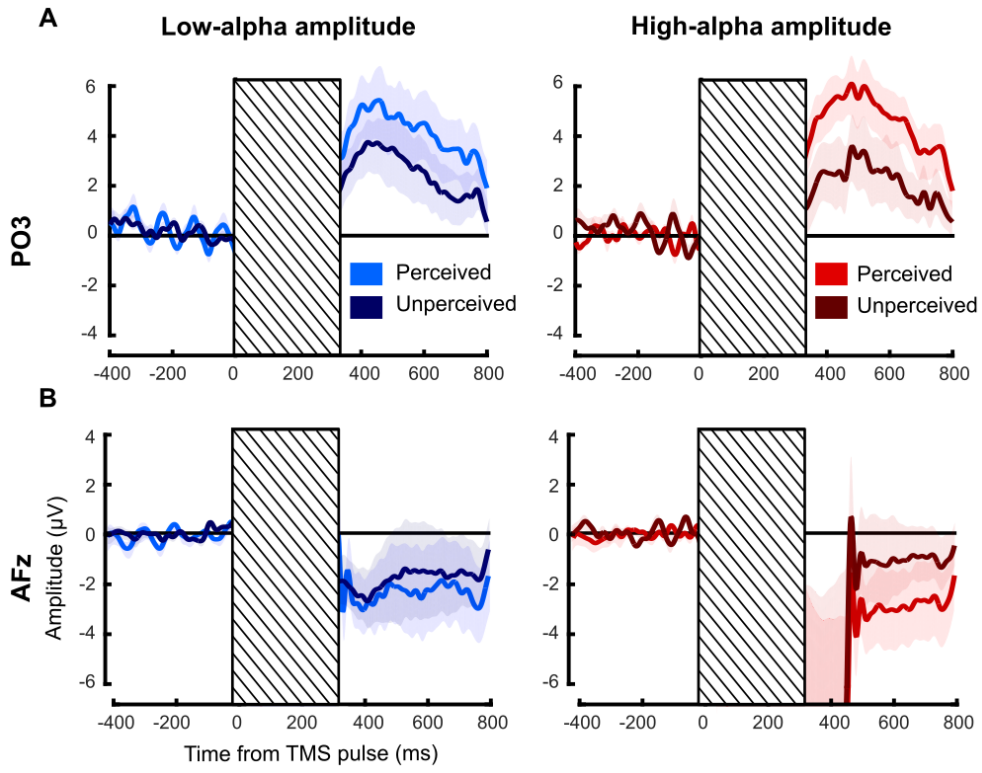

Extended Data Figure 3-1. ERPs for perceived- and unperceived-phosphene trials. **A.** ERPs at electrode PO3 for perceived- and unperceived-phosphene trials averaged across the 9

participants. **B.** ERPs at electrode AFz. Red, high-alpha amplitude condition. Blue, low-alpha amplitude condition. Light colors, perceived-phosphene condition. Dark colors, unperceived-phosphene condition. Colored shaded areas, standard error of the mean. Striped area, mask the TMS-induced artifact.

4. Summary and Discussion

In the first study, we wanted to investigate the role of endogenous attention on the phase effect according to the Pulsed Inhibition theory. In a visuo-spatial endogenous attention task, we expected to observe a phase effect on cortical excitability and the subsequent visual performance only for non-attended stimuli, i.e., associated with a high amplitude of alpha oscillations in the brain, and a reduced or an absence of phase effect for attended stimuli, i.e., associated with a low amplitude of alpha oscillations in the brain. On the other hand, the study from Busch and VanRullen (2010) suggested that the phase of brain oscillations would modulate visual perception only in the attended condition (Busch and VanRullen, 2010). We wanted to disentangle these two contradictory hypotheses with a combined EEG-TMS experiment. Unfortunately, the experiment we designed was not feasible in practical terms. The proposed experiment has to be improved or reshaped in order to establish a causal link between alpha phase-amplitude tradeoffs, cortical excitability, the subsequent visual perception, and the role of endogenous attention.

In the second study (Fakche et al., 2022), we provide strong evidence in favor of the Pulsed Inhibition theory by establishing a causal link between the amplitude and the phase of spontaneous alpha oscillations, cortical excitability, and subsequent perceptual performance. Two clear predictions of the Pulsed Inhibition theory (Jensen and Mazaheri, 2010; Klimesch et al., 2007; Mathewson et al., 2011) were tested: 1) high alpha amplitude induces an alternation between excitatory and inhibitory cortical states, according to optimal and non-optimal phases of brain oscillations, leading to rhythmicity in perceptual performance; and 2) low alpha amplitude induces overall higher cortical excitability, less susceptible to phasic (periodic) pulsed inhibition, and lead to overall higher perceptual performance. We showed that the phase of spontaneous alpha oscillations (~10 Hz) modulated the probability to perceive a phosphene, with non-optimal phases between $-\pi/2$ and $-\pi/4$. This phase effect was higher for high alpha amplitude trials.

Compared to previous non-invasive human studies which correlated EEG or MEG phase with amplitude and associated behavioral measure (Alexander et al., 2020; Bonnefond and Jensen, 2015; Busch and VanRullen, 2010; Harris et al., 2018; Kizuk and Mathewson, 2017; Mathewson et al., 2009; Milton and Pleydell-Pearce, 2016; Ai and Ro, 2014; Hermann et al., 2016; Ng et al., 2012; Spitzer et al., 2016; Zoefel and Heil, 2013), the use of TMS in this experiment allowed to investigate a *causal* link between alpha phase-amplitude tradeoffs, visual perception and cortical excitability. In addition, we had a direct access to the instantaneous phase of brain oscillations. Here, TMS-induced phosphene perception reflects the instantaneous excitatory state of the visual cortex and the instantaneous phase of brain oscillations.

5. Future research questions

The Pulsed Inhibition theory highlights the crucial role of the inhibitory processes in the brain mechanisms underlying cognitive functions, such as perception. Jensen and Mazaheri (2010) summarized this important idea in the following nice and elegant sentence: "In order to study the working brain as a network, it is crucial to understand not only how the task-relevant regions are engaged but also how the task-irrelevant regions are inhibited." They proposed that the inhibition induced by alpha brain oscillations would be under the control of the GABAergic interneurons network (Jensen and Mazaheri, 2010). It would be of great interest in the future to investigate the role of these interneurons on the pulses of inhibition induced by alpha oscillations on cortical excitability and cognitive functions.

Interestingly, although the Pulsed Inhibition theory (Jensen and Mazaheri, 2010) originally proposes asymmetrical pulsed inhibition (i.e., inhibition at one particular phase and no inhibition at the opposite one), Bergmann et al. (2019) argues in favor of asymmetrical pulsed facilitation. Further investigations are thus necessary to disentangle the three possibilities: (1) symmetrical pulsed inhibition and facilitation, (2) asymmetrical pulsed inhibition, or (3) asymmetrical pulsed facilitation.

The frontal regions seem to be involved in the emergence of inhibitory pulses in the occipital cortex, probably trough feedback connections underlying top-down mechanisms, such as endogenous attention. We could investigate in a novel paradigm whether there is functional connectivity between frontal and occipital regions, trough phase-to-phase or phase-to-

amplitude coupling, or by using dynamic causal modeling. We could also use TMS to perturb frontal regions and look at the causal consequences on the occipital alpha phase-amplitude tradeoffs on perception.

In addition, the time at which the phase predicted the perceptual outcome differed by nearly one-half alpha-cycle between the occipital (-77 ms) and the frontal (-40 ms) ROI (Fakche et al., 2022). This difference may reflect the delay for neural information to be communicated from one brain region to the other, consistent with previous observations of an alpha phase difference between occipital and frontal regions during visual perception, and suggesting a functional role of macroscopic traveling waves (Burkitt et al., 2000; Patten et al., 2012; Alamia and VanRullen, 2019; Pang et al., 2020; Tsoneva et al., 2021). This possibility should be explored in the future.

Chapter 5. Brain oscillations, the neural dynamics underlying serial dependance.

The functional role of brain oscillations in visual perception has been widely studied in simple visual processes. In visual detection tasks, the probability to perceive a threshold visual stimulus depends on the amplitude (Ergenoglu et al., 2004; Hanslmayr et al., 2007; Van Dijk et al., 2008; Wyart and Tallon-Baudry, 2009) and the phase (Nunn and Osselton, 1974; Varela et al., 1981; Busch et al., 2009; Mathewson et al., 2009; Busch and VanRullen, 2010; Dugué et al., 2011a; Fiebelkorn et al., 2013b; Hanslmayr et al., 2013; Manasseh et al., 2013) of low frequency brain oscillations. Other studies investigated visual perception during the deployment of spatial endogenous attention and found a functional role of the amplitude (Worden et al., 2000; Sauseng et al., 2005b; Thut et al., 2006; Händel et al., 2011) and the phase (Landau & Fries, 2012; Fiebelkorn et al., 2013a; Song et al., 2014; Huang et al., 2015; Dugué et al., 2015a; Dugué et al., 2017; Senoussi et al., 2019; Michel et al., 2021; for review, see Kienitz et al., 2021) of low frequency oscillations, once more.

In this project, we asked whether brain oscillations could underlie a more complex visual process, serial dependence.

1. Serial dependence in visual perception

In his book *Vision Science: Photons to phenomenology* (1999), Stephen E. Palmer proposes that "people's perception actually corresponds to the models their visual systems have constructed rather than (or in addition to) the sensory stimulations on which they are based." Visual perception is not simply the summation of the visual inputs received by our eyes; it depends on a construction built by the brain. In visual neuroscience, one of the most-questioned psychological constructs is the apparent stability of the visual world. Indeed, we continuously receive numerous visual inputs with a high variability due to internal noise (e.g., blinks, eyes, and head movements, that interrupt and disturb the retinal image several times per second) and external noise (e.g., changes in lighting). Despite this high variability, our phenomenological visual experience remains highly stable over time. A process that may contribute to this impression of stability is the continuity field, a spatiotemporal window that integrates present visual input and recent stimulus history. This integration is quantified by the phenomenon of serial dependence (Fischer and Whitney, 2014; Collins, 2019, 2020), i.e., visual perception is biased towards the previous visual inputs. In 2014, Fischer and Whitney developed a

psychophysical experiment to investigate visual serial dependence (Fischer and Whitney, 2014). In their study, participants performed an orientation judgement task of Gabor patches. They showed that the orientation perception of the input stimulus was systematically biased toward the stimuli seen in the recent past (up to ten seconds) (**Figure 5.1**, Fischer and Whitney, 2014). Then, several studies investigated the features of serial dependence in visual perception. However, the neural dynamics underlying serial dependence remain ill-defined.

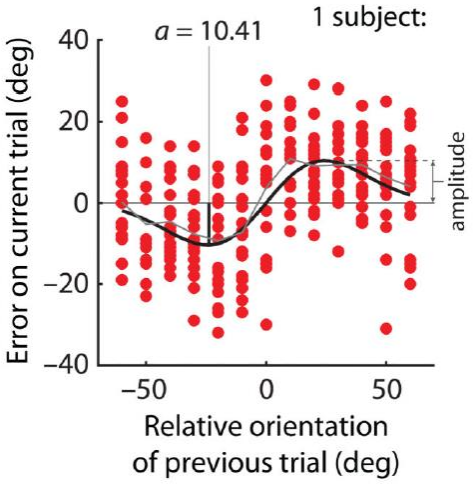

Figure 5.1: Serial dependence in orientation perception, from Fischer and Whitney, 2014*. Error plot for one participant. Values on the abscissa indicate the distance in degrees between the present Gabor patch and the previous one, with positive values corresponding to a more clockwise orientation of the previous patch relative to the present patch. Values on the ordinate indicate the participant's error when reporting the present Gabor orientation with a response cue, in degrees. Data were fitted with the 1st derivative of a Gaussian curve. The participant's errors in reporting the Gabor's orientation were biased toward the previous stimulus.*

2. The neural dynamics of serial dependence in face perception

2.1. Introduction

Serial dependence has been found to occur across many visual features, from basic attributes, such as orientation (Fischer and Whitney, 2014; Fritsche et al., 2017; Cicchini et al., 2017), position (Manassi et al., 2018; Collins, 2019), motion (Alais et al., 2017), and numerosity (Corbett et al., 2011; Cicchini et al., 2014; Fornaciai and Park, 2018a, b), to higher-level stimuli such as face perception (Liberman et al., 2014; Taubert et al., 2016; Xia et al., 2016) and visual scenes (Manassi et al., 2017).

The spatiotemporal window characterizing the continuity field appears to integrate visual information on a ten second time-window (Fischer and Whitney, 2014) and to be retinotopic, with a relatively large spatial extend up to 22 degrees of visual angle (John-Saaltink et al., 2016; Collins, 2019).

Although there is plenty of evidence showing that serial dependence occurs at the stage of perceptual processing (Fischer and Whitney, 2014; John-Saaltink et al., 2016; Fornaciai and Park, 2018a; Collins, 2020), it has also been proposed that serial dependence may bias visual perception at later decisional stages (Cicchini et al., 2017; Fritsche et al., 2017). Serial dependence presumably occurs at both early and late stages depending on the task and stimuli (Collins, 2021). The study of the neural dynamics underlying serial dependence allows to contribute to this debate, by identifying at which level of the cortical hierarchy serial dependence occurs.

Serial dependence has been widely studied at the perceptual level, and seems to be important for the visual processing of various attributes. Yet, the neural dynamics underlying visual serial dependence remains ill-defined. One study used an orientation judgement task coupled with fMRI recording to identify at which levels of the visual hierarchy serial dependence occurred (John-Saaltink et al., 2016). They showed that the orientation signal in V1, V2, and V3, was biased toward the orientation of the previous stimuli, just like at the perceptual level, in a retinotopic manner. These results suggest that serial dependence occurs at the perceptual level, by modulating the low-level sensory representations of the present stimulus according to the previous stimuli seen (John-Saaltink et al., 2016). However, MRI recordings suffer from a poor temporal resolution, leading to the impossibility to investigate the neural *dynamics*.

Recently, the neural dynamics of serial dependence have been investigated in numerosity, with EEG recordings (Fornaciai and Park, 2018a, 2020). First, they showed that the amplitude of the visual evoked potentials (VEP) induced by the present stimulus was modulated by the previously perceived stimulus, i.e., higher VEP amplitude when the previous stimulus had a greater numerosity compared to when the previous stimulus had a smaller numerosity. This effect occurred around 250-300 ms after the stimulus onset, and had an occipital topography. In addition, the modulation of the VEP was in accordance with the behavioral results, which showed a strong serial dependence effect (Fornaciai and Park, 2018a, 2020). They also demonstrated that the biased representation of visual inputs, due to serial dependence, was maintained in sensory memory (Fornaciai and Park, 2020).

Here, we studied the neural dynamics of serial dependence in face perception with EEG recordings. We chose to use face stimuli because their perception is associated with strong neural markers. Several studies have shown that the amplitude of brain oscillations from 5 to 45 Hz, localized over the parieto-occipital electrodes, increases between 0 and 200 ms after the onset of a face (Klopp et al., 1999; Hsaio et al., 2006; Rousselet et al., 2007; Sakihara et al., 2012). Face perception also evokes a component named N170, and studies have suggested that the oscillatory activity between 5 and 45 Hz correlates with the amplitude and latency of the N170 component (Tang et al., 2008; Sakihara et al., 2012; Torrence et al., 2021). The use of a classifier, i.e., a mathematical algorithm identifying spatial patterns of brain activity across time, is also able to distinguish between trials in which participants perceived a face compared to trials in which participants perceived a house (Haxby et al., 2001). The classification algorithm relies on the hypothesis that if two conditions, e.g., a house and a face, are represented by distinct patterns of brain activity, the classifier can, after training, associate each new trial to the corresponding condition according to the spatial pattern of brain activity contained in that trial.

In the context of serial dependence, the neural representation of previous stimuli seems to be encoded and maintained in early visual areas, leading to an alteration of the perception of the present visual input (John-Saaltink et al., 2016; Fornaciai and Park, 2018a, 2020).

We hypothesized that the spatial pattern of brain activity associated with face perception, i.e., the component N170 in the time domain, and the increase in amplitude from 5 to 45 Hz in the time-frequency domain, is maintained in the early visual areas after the presentation of a face, and that this neural representation is going to bias the following visual perception towards face perception. In our study, participants (n=26) performed a categorization task on non-ambiguous stimuli of cars, houses, and faces, and ambiguous stimuli consisting of morphs between car and house, car and face, and face and house, all interleaved. We hypothesized that the performance of a classifier trained to disentangle between faces and other objects would be able to identify face perception in morph trials preceded by a face. In other words, we proposed that the pattern of brain activity identified by the classifier during face perception would be found in trials biased towards a face representation due to serial dependence.

2.2. Materials and Methods

Participants. 26 participants (18 females, mean age: 25.7 years, ranging from 19 to 41 years) were included in the study. All participants were free from medication affecting the central nervous system, reported no history of psychiatric or neurological disorders, gave their written informed consent and were compensated for their participation. The study was approved by the local French ethics committee Ouest IV (IRB #2020-A00859-30) and followed the Declaration of Helsinki.

Stimuli. Stimuli were designed with PsychToolbox 3.0.12, running in Matlab R2014b 64-bit (The MathWorks, Natick, MA), and displayed with a ProPixx Projector (VPixx Technologies, Saint-Bruno, QC, Canada), on a 1890 * 1060 mm projection screen (1920 * 1080 pixels; 100 Hz refresh rate), at 101 cm distance. Fixation dots (diameter of 0.25 dva) were displayed at the center of a screen with a gray background associated with visual noise. 147 images were used: three were non-ambiguous images of face, car, and house, and the remaining images were gradual morphs between two conditions. There were 48 morphs of car and house, 48 morphs of car and face, and 48 morphs of house and face (**Figure 5.2**). Images were embedded in visual noise.

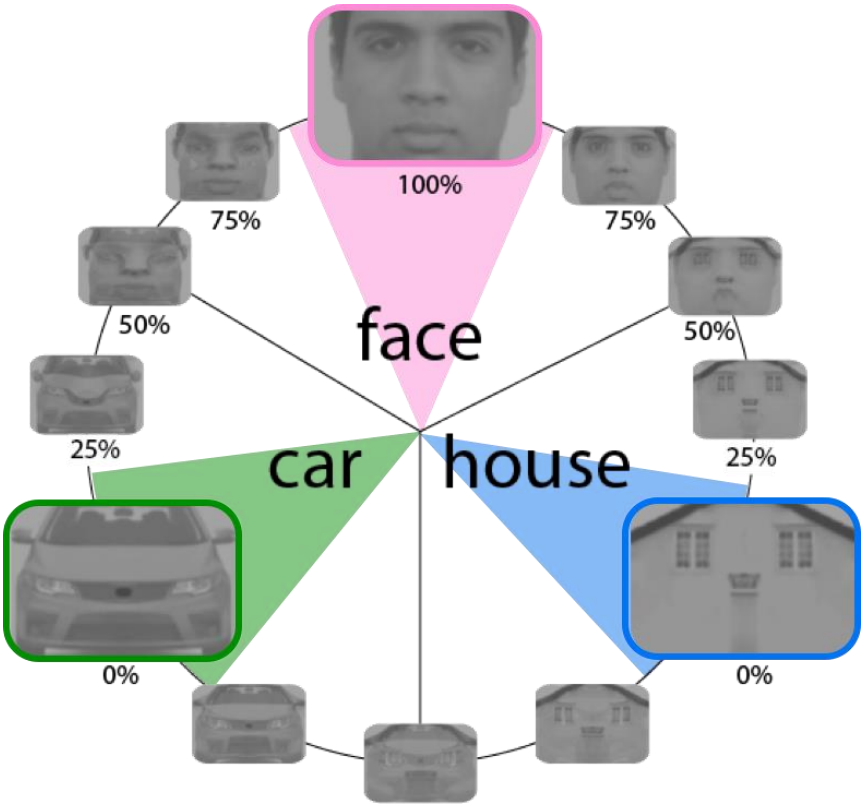

Figure 5.2: Morphs wheel used in the experiment. *The images were gradual morphs between face and house, face and car, and car and house. The percentages correspond to the amount of the face prototype included in each morph.*

Eye tracker. Participant's head was maintained with a chinrest. An infrared video-camera system (EyeLink 1000 plus 5.08, SR Research, Ottawa, Canada) was used to ensure that participants maintained their gaze on the fixation cross throughout the trial. The trial only started when participants were successfully maintaining fixation. When a gaze deviation of >1° from the center of the screen was detected or a blink, we considered that the participant broke fixation, and the trial was stopped and rerun at the end of the experiment.

EEG. EEG was recorded using a 128-channels actiChamp system (Brain Products GmbH). The ground was placed at the Fpz position, and the right mastoid was used as reference (DC recording; 1000 Hz sampling rate).

Procedure. Participants performed one EEG session composed of 1617 trials. Participants had the option to take a break every 100 trials. They were asked to fixate the central dot on the screen. Once correct detection was detected for 200 ms, the trial began. One of the 147 images was displayed embedded in noise during 300 ms, followed by noise only for at least 300 ms. Participants had to indicate whether they perceived a car, a face, or a house, with the left, up, and right arrows of the keyboard. The object category-key assignment was counterbalanced across participants. When participants gave their answer, a new trial began (**Figure 5.3**).

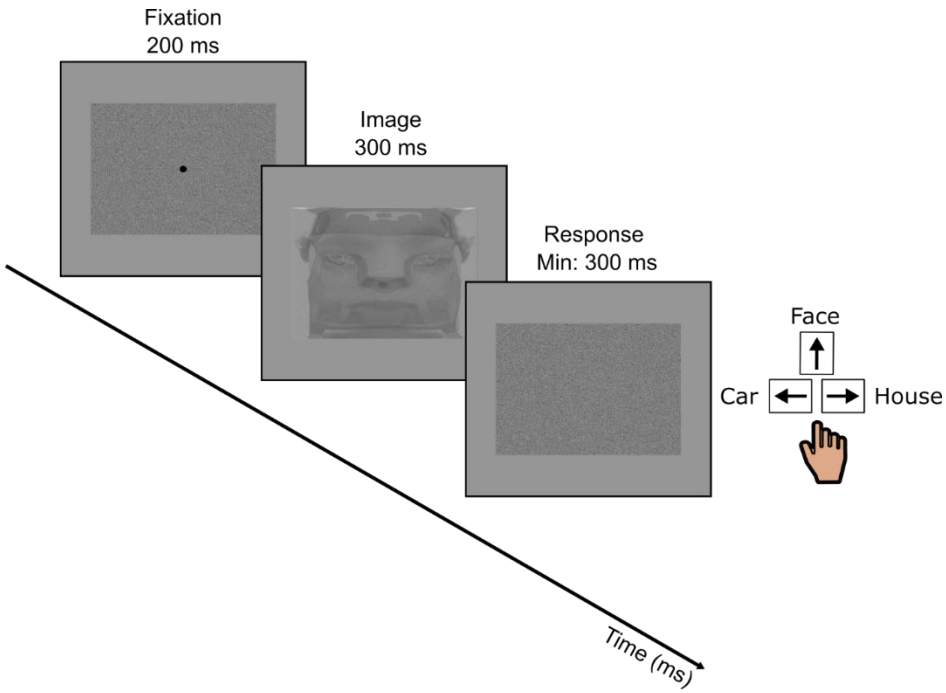

***Figure 5.3: Experimental protocol**. After fixation at screen center for 200 ms, a trial began. A morph embedded in noise was presented for 300 ms, followed by a response screen for at least 300 ms. Participants had to indicate whether they perceived a car, a face, or a house.*

Behavioral analyses. Behavioral performance was computed and plotted for each condition (car/face morphs, face/house morphs, house/car morphs), as a function of the previous stimulus. For example, for the 48 car/face morphs, the percentage of "face" responses was computed for each morph as a function of the preceding stimulus: preceded by a car versus preceded by a face. Individual psychometric curves were obtained by fitting the data to a sigmoid with the psignifit 3 toolbox (Schütt, H. H., Harmeling, S., Macke, J. H., & Wichmann, F. A. (2016). Painfree and accurate Bayesian estimation of psychometric functions for (potentially) overdispersed data. Vision research, 122, 105-123; https://github.com/wichmann-lab/psignifit/wiki). The point of subjective equality (PSE) was extracted for each participant, and we tested with t-tests whether the PSE was shifted between the performance preceded by the first vs the second condition, which is a marker of serial dependence. Indeed, we hypothesize that morphs preceded by a face will more often be categorized as a face, leading to a leftward shift of the psychometric function, relative to when they are preceded by a car. This logic can be extended to the two other morph continua (car/house and house/face).

In addition, we quantified serial dependence by computing the proportion of trials in which the errors were biased towards the previous trials, compared to the total number of errors. Because we had three different stimuli (car, house, face), the level of chance was at 33%. For ease of interpretation, 33% was subtracted, thus 0% corresponds to no serial dependence, positive values to a serial dependence, i.e., there are more errors towards the past, and negative values to a repulsive effect, i.e., there are more errors opposite to the previous stimuli. T-tests were performed to investigate whether serial dependence was significantly different from chance.

EEG analyses. EEG analyses were performed with Fieldtrip (Oostenveld et al., 2011; Donders Institute for Brain, Cognition and Behavior, Radboud University, Nijmegen, the Netherlands), EEGLAB 13.6.5 (Swartz Center for Computational Neuroscience, UC San Diego, California; Delorme & Makeig, 2004) and custom software written in Matlab R2014b (The MathWorks, Natick, MA).

Preprocessing. EEG data and channel location were imported into Fieldtrip. A high-pass filter at 0.1 Hz and a notch filter around 50 Hz was applied, to respectively remove slow drifts and 50 Hz electric noise. Visual inspection allowed to identify electrodes with a low signal-to-noise ratio, which were then interpolated. EEG data were re-reference to the average reference, and epoched from -200 ms to +300 ms according to the image onset.

Definition of ambiguous and non-ambiguous trials. Ambiguous and non-ambiguous morphs were defined separately for each participant, based on their psychometric function. We considered that the 10% of the upper and lower psychometric curves correspond to a non-ambiguous perception of the stimuli car, house, and face. Morphs between were considered ambiguous, i.e., morphs between car and house, house and face, and face and car. The three non-ambiguous categories are illustrated in **Figure 5.2** (green: unambiguous car; pink: unambiguous face; blue: unambiguous house; white: ambiguous morphs). Note that because we used individual psychometric functions, the extent of the ambiguous and non-ambiguous categories differed between individuals.

Event-related potentials (ERPs). ERPs, centered on the image onset, were computed as the average of trials for each non-ambiguous condition, face, car and house. ERPs were then average across participants and parieto-occipital electrodes, and plotted.

Time-frequency decomposition. A time-frequency transform (morelet wavelet) was computed on single epochs, with the *timefreq* function from EEGLAB. The "cycles" parameter was set to from 1 to 15. The "freqs" parameter was set to [5, 40], producing 50 frequencies that increase logarithmically from 5 to 40 Hz.

Amplitude analysis. The amplitude was extracted with *abs* function (from Matlab) from the time-frequency decomposition for each trial, electrode, and participant. Time-frequency maps were plotted on the difference between non-ambiguous trials of face perception (Face) and car or house (NonFace) perception, for data averaged across trials, electrodes, and participants.

Multivariate pattern analysis (MVPA) on EEG time series. MVPA were performed with MVPA-Light toolbox (Treder, M. S. (2020). *MVPA-Light: A Classification and Regression Toolbox for Multi-Dimensional Data*. Frontiers in Neuroscience, 14, 289. https://doi.org/10.3389/FNINS.2020.00289] (https://www.frontiersin.org/articles/10.3389/fnins.2020.00289/full)).

Classification analyses consist in training a classifier to distinguish two or more conditions on a set of training trials. After the training phase, the classifier is tested on a set of testing trials, composed of trials not used during the training. If the classifier is able to predict the condition of the testing trials, it means that the multivariate pattern of brain activity is able to associate a brain activity to one of the conditions. Cross-validation was performed to ensure unbiased

evaluation of classification performance, i.e., the dataset was split in k folds (k = 10), and in every iteration (repeat = 2), one of the k folds was used for the training, and the others k folds were used for the testing. We used a linear discriminant analysis (LDA) classifier algorithm. We performed classification across time, time generalization, i.e., the classifier was trained at a given time point t1, and then tested at all time points t2 in the trial; the procedure was repeated for every combination of training and testing time points, given a time*time matrix of classification, and searchlight analysis, i.e., classification across time at the sensors level.

For each classification analysis, we subsampled the number of trials in the condition with the most trials to match the condition with the fewest trials. This subsampling procedure was repeated 10 and 100 times, for the first and second analysis respectively (see below), with a different subset of selected trials, and then we averaged the iterations. Please note that we chose to perform only 10 and 100 repetitions because of time constraints, the analysis will be done with a higher number of repetitions in the near future.

In addition, classification analysis was performed at the individual level, and then the results of the classification were averaged across participants.

Multivariate pattern classification was first performed on non-ambiguous Face and NonFace conditions, to verify that face perception was associated with a specific brain activity pattern. We expected to be able to classify faces versus non-faces, replicating previous research (Haxby et al., 2001).

Second, we investigated whether the pattern of brain activity associated with face perception was found in ambiguous trials with a face morph more efficiently when the previous stimulus was a non-ambiguous face compared to a non-ambiguous car or house, due to serial dependence. The classifier was trained on Face and NonFace conditions, and then tested on face morphs preceded by a non-ambiguous face or a non-ambiguous car or house.

To evaluate the significance of the classification analysis, we computed permutations tests with 1000 repetitions, and applied a cluster correction.

2.3. Results

Behavior. Behavioral performance was computed for each condition (car/face, face/house, house/car) as a function of the previous stimulus. For the house/face condition, we observed a significant difference of the PSE between stimuli preceded by a house and stimuli preceded by a face (two-tailed t-tests: p-value = 0.0257; CI = [-2.0777; -0.1464]; Cohen's d = -0.4489), suggesting an effect of serial dependence. For the house/car and face/car conditions, the PSE

was not significantly different between stimuli preceded by the first or the second stimuli (house/car: p-value = 0.2471; CI = [-1.8975; 0.5113]; Cohen's d = -0.2997; face/car: p-value = 0.1875; CI = [-0.2701; 1.3093]; Cohen's d = 0.1719).

Serial dependence was further quantified by computing the proportion of trials in which the errors were biased towards the previous trials, compared to the total number of errors, for each of the three pairs of conditions (car/face, face/house, house/car). A significant serial dependence effect was observed for the face/house continuum (one-tailed t-test against 0%: p-value = 0.0162; Cohen's d = 0.6280; CI = [0.0198; +Infinity]) with a serial dependence of 8%, and house/car continuum (p-value = 0.0405; Cohen's d = 0.5045; CI = [0.0042; +Infinity]) with a serial dependence of 7%. Concerning the car/face continuum, the effect observed was not significantly different from chance (one-tailed t-test against 0%: p-value = 0.7595; Cohen's d = -0.1984; CI = [-0.0427; +Infinity]).

Together, the behavioral analysis suggested a reliable serial dependence of 8% and 7% for the house/face and house/car continuum, respectively.

ERPs. ERPs averaged across participants and parieto-occipital electrodes were plotted for non-ambiguous conditions. A negative component identified as the N170 was observed between 145 and 200 ms, for each condition, face, car, and house (**Figure 5.4**). The amplitude of the N170 was even higher for house compared to face and car stimuli. Consequently, contrary to our hypothesis, the N170 component was not a brain activity specifically associated with face perception in our data.

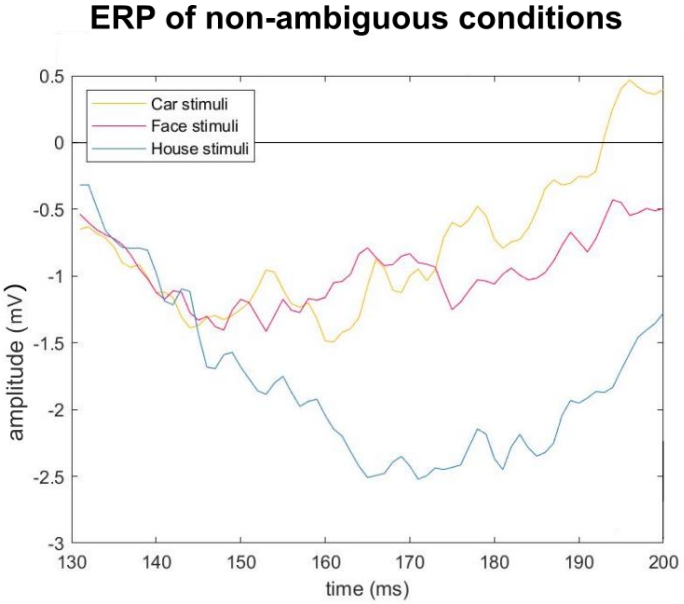

Figure 5.4: ERPs plotted for non-ambiguous stimuli*. ERPs were averaged across participants (n=26) and parieto-occipital electrodes, and plotted for the non-ambiguous conditions face,*

car, and house. A N170 was identified in face but also in house and car conditions. The highest N170 amplitude was found for the house condition. These results suggested that the N170 component was not a brain activity specifically associated with face perception in our experiment.

Time-frequency analysis. To investigate whether the amplitude of brain oscillations between 5 and 45 Hz was positively associated with face perception, we performed a time-frequency decomposition on Face and NonFace epochs and extracted the amplitude. Time-frequency map of the amplitude difference between Face and NonFace conditions was plotted for data averaged across trials, participants, and all or parieto-occipital electrodes (**Figure 5.5**). The amplitude in the time-frequency window from 40 to 90 ms after the image onset, between 16 to 26 Hz, slightly increased in response to face perception, but this effect was very low (~1 µV).

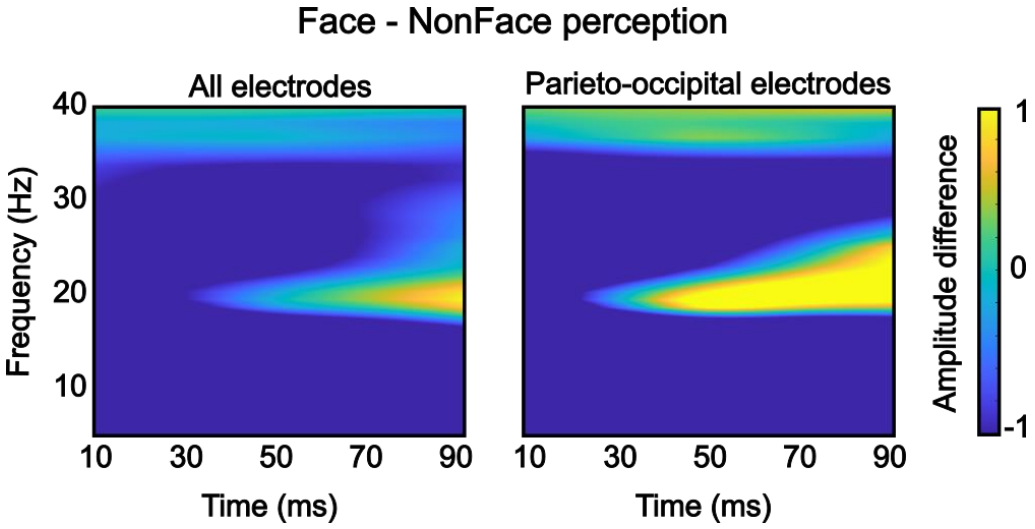

Figure 5.5: Face perception was associated with a slight increase in the amplitude of low-frequencies. *Right panel, Time-frequency maps of the difference in amplitude between Face and NonFace, averaged across participants (n=26) and all electrodes, Left panel, across parieto-occipital electrodes. A very slight difference (~1µV) was observed between 40 and 90 ms, from 16 to 26 Hz.*

MVPA on EEG time series. Multivariate pattern classification analysis (MVPA) was performed on the EEG time series epoched from -200 ms to 300 ms relative to morph onset, to investigate whether the classifier was able to distinguish between Face and NonFace perception. Classification performance across the time dimension was computed on the accuracy and on the area under the curve. The permutation tests indicated that the classification was significant (cluster corrected; $p<0.001$) from 130 to 300 ms after the image onset (**Figure 5.6.A**). The time

generalization was performed on both the accuracy and the area under the curve. The results are summarized in a matrix (**Figure 5.6.B**), with the x-and y- axis corresponding to the time points on which the classifier was tested and trained, respectively. The diagonal of the matrix is equivalent to the classification across the time dimension, i.e., the classifier was trained and tested at the same time point. The permutation tested showed that each classifier generalized over a transient time period only, corresponding to the diagonal of the time generalization matrix (cluster corrected; $p<0.001$). This result suggests that the pattern of brain activity encoding face perception was time specific. The searchlight analysis on accuracy showed that the relevant brain activity for face perception was localized in the occipital cortex (**Figure 5.6.C**).

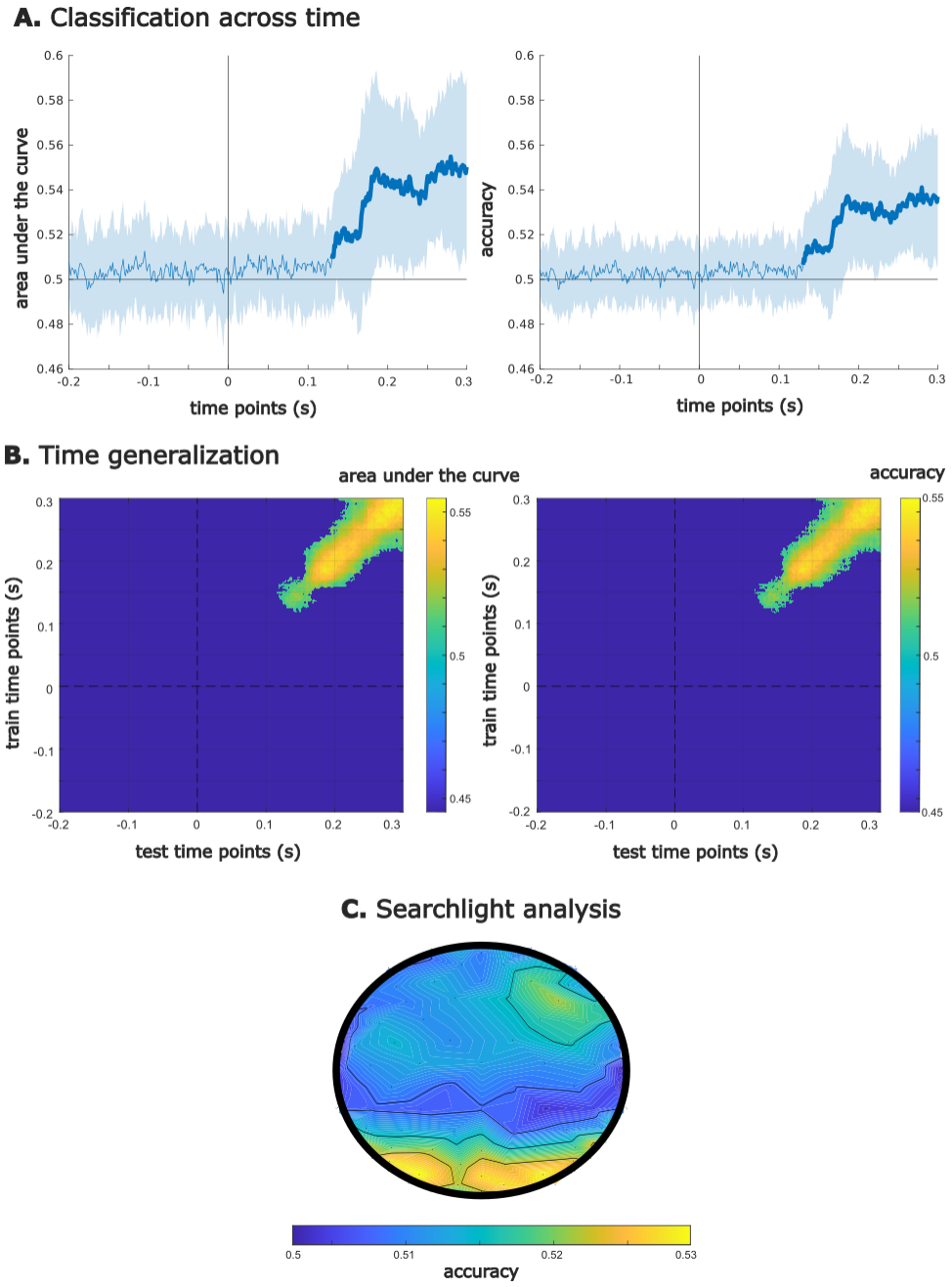

Figure 5.6: Face perception decoding. *MVPA analysis of Face vs NonFace perception averaged across the 26 participants.* ***A.*** *Classification across time, of the area under the curve and the accuracy metrics, on left and right panels, respectively. The performance was significantly higher from 130 to 300 ms.* ***B.*** *Time generalization matrix, of the area under the curve and the accuracy metrics, on left and right panels, respectively. Only the diagonal showed a significant pattern, suggesting that the brain activity pattern underlying face perception was transient.* ***C.*** *Searchlight analysis, on the accuracy. The relevant pattern of brain activity for face perception was in the occipital cortex.*

Second, the classifier was trained on Face and NonFace conditions, and tested on ambiguous morphs, preceded by a non-ambiguous face or by a non-ambiguous car or house. We hypothesized that the classifier would identify the pattern of brain activity associated with face perception, and be able to find this pattern in morphs more efficiently when the morph was preceded by a face compared to other objects. Classification performance across the time dimension was computed on the accuracy and the area under the curve. Both metrics were always at the chance level (50% for two conditions tested) (**Figure 5.7**). These results suggested that the classifier was not able to find the brain activity associated with face perception more efficiently in morphs preceded by a face stimulus.

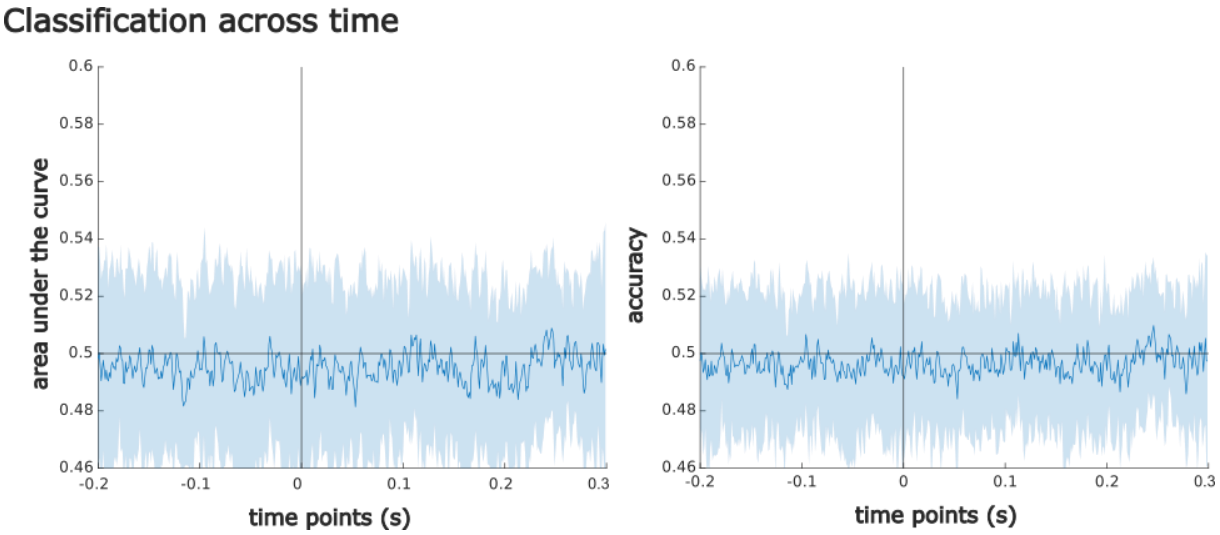

Figure 5.7: The classifier did not find the brain activity associated with face perception more efficiently in ambiguous morphs preceded by face perception. *MVPA analysis on ambiguous morphs preceded by a non-ambiguous face or a non-ambiguous car or house, averaged across the 26 participants. Classification across time, of the area under the curve and the accuracy metrics, on left and right panels, respectively. The performance was always at the chance level (50%), showing that the classifier did not distinguish a special pattern of brain activity between the two conditions tested.*

3. Summary and Discussion

In this study, we hypothesized that the pattern of brain activity identified by a classification algorithm specific to face perception (as opposed to the perception of other objects such as cars and houses) would also be found in trials with ambiguous objects whose perception was biased towards a face representation due to serial dependence.

To test our hypothesis, we designed a categorization task on non-ambiguous images of cars, houses, and faces, and ambiguous images consisting of morphs between car and house, car and face, and face and house. Previous experiments have found that serial dependence occurred for face perception (Liberman et al., 2014; Taubert et al., 2016; Xia et al., 2016). Our behavioral analysis also showed serial dependence, but only on the face/house morphs. This result suggests that serial dependence occurred for the perception of faces mixed with houses but not with cars, which is quite surprising. To better understand these results, we plan to examine the visual features, and notably the spatial frequency component, of each morph family. The different features of a visual image are processed relatively independently along the visual hierarchy. Any difference in the basic features between face-car and face-house morphs may explain why they are perceived differently.

At the electrophysiological level, face perception has been associated with a negative component N170 in the time domain, and with an increase in the amplitude of brain oscillations from 5 to 45 Hz in the time-frequency domain (Klopp et al., 1999; Hsaio et al., 2006; Rousselet et al., 2007; Tang et al., 2008; Sakihara et al., 2012; Torrence et al., 2021). Surprisingly, our ERP analysis showed that face, but also car and house perception evoked a N170 component. Similarly, the difference between faces and other objects in the time-frequency domain was associated with a very slight increase of the amplitude of brain oscillations from 16 to 26 Hz. Together, the electrophysiological analysis suggests that face perception was not associated with specific brain markers, neither in the time domain nor in the time-frequency domain, in our experiment.

We performed MVPA on the EEG time series to test whether the pattern of brain activity during face perception was significantly different from car or house perception. The pattern of brain activity in the occipital cortex from 130 to 300 ms after the image onset allowed us to decode face perception. The time generalization analysis showed that the neural code for face

perception was linear and time specific, and the searchlight analysis showed that the pattern of brain activity identified by the classifier was in the occipital cortex. Interestingly, the classifier was able to associate face perception with a specific pattern of brain activity while the ERP and time-frequency analysis did not. In addition, the pattern of brain activity associated with face perception appeared to emerge in the early visual areas, as shown by the occipital topography.

Finally, we tested whether a classifier trained to find the pattern of brain activity associated with face perception was able to find this brain activity in ambiguous morphs preceded by a face, i.e., morphs biased towards the face perception due to serial dependence. Unfortunately, the performance of the classifier was at the level of chance, i.e., the classifier was not able to find the brain activity associated with face perception more efficiently in face morphs preceded by a face stimulus.

Although we hypothesized that the pattern of brain activity underlying face perception would be oscillatory, we found no evidence in favor of this hypothesis in our data. Indeed, the time-frequency map of the difference between face and other objects perception showed a slight increase of the amplitude that was low (~1µV). In addition, the shape of the classification across time did not appear to present an oscillatory pattern. Similarly, the time generalization did not show any evidence of a periodicity in the neural code. In sum, our first analysis did show any evidence of a functional role of brain oscillations in serial dependence of face perception.

In this study, we hypothesized that the pattern of brain activity associated with face perception (and identified with a classification algorithm) would be found in stimuli biased towards face perception due to serial dependence. This hypothesis relies on the fact that: 1) Serial dependence occurs robustly in face perception, 2) Face perception is associated with a specific pattern of brain activity both in time and time-frequency domains. However, neither assumption was validated by our initial behavioral and electrophysiological results. Consequently, we cannot conclude that brain oscillations play a functional role in serial dependence in face perception at the moment. Further analysis will be performed soon to try to understand why we did not find a strong serial dependence in face perception at the behavioral level, as well as the absence of a specific pattern of brain activity associated with face perception.

4. Future research questions

Serial dependence is the phenomenon in which visual perception is strongly and systematically biased toward similar visual inputs from the recent past (Fischer and Whitney, 2014; Liberman et al., 2014; Cicchini et al., 2014; Burr and Cicchini, 2014). These perceptual consequences are in line with the ones describes by predictive coding theory. Predictive coding theory arises from the Bayesian brain framework, that postulates that the brain is performing probabilistic inference to generate an internal model of the external world. The probabilistic inferences are computed by the brain in two different steps: *Bayesian inference* and *Bayesian learning*. 1) The brain generates predictions about the external world according to its internal model, based on the past experience, i.e., *Bayesian inference*. 2) The brain updates its internal model by interacting with the external world: each novel input from the external world is used to update the internal model and generate new predictions, i.e., *Bayesian learning* (Friston et al., 2012; Lecaignard, 2016). In serial dependence, visual perception would be biased by the internal model of the external world constructed from the recent past inputs. The Bayesian brain framework implies a communication between brain areas, explained by the predictive coding theory. Predictive coding describes that the inferences computed by the Bayesian brain rely on the feedback communication of predictions and the feedforward communication of prediction errors. There is an exchange of information along the cortical hierarchy, in both directions, allowing the Bayesian brain to build and update its internal model of the external world (Rao & Ballard, 1999; Friston et al., 2005; Bastos et al., 2012; Fontolan et al., 2014; Lecaignard, 2016). Brain oscillations have been proposed to be the neural support of the communication between brain areas along the cortical hierarchy. High-level brain areas, in the fronto-parietal cortices, would send predictions to the lower-level brain areas, the sensory cortices, through feedback brain oscillations in low frequency bands (theta, alpha, low beta). In turn, when novel input arrives, the lower-level brain areas would send prediction errors, i.e., the difference between the actual input and the predictions, to the higher-level brain areas through feedforward brain oscillations in high frequency bands (high beta, gamma) (**Figure 5.8**; VanKerkoerle et al., 2014; Han & VanRullen, 2016, 2017; Alamia & VanRullen, 2019).

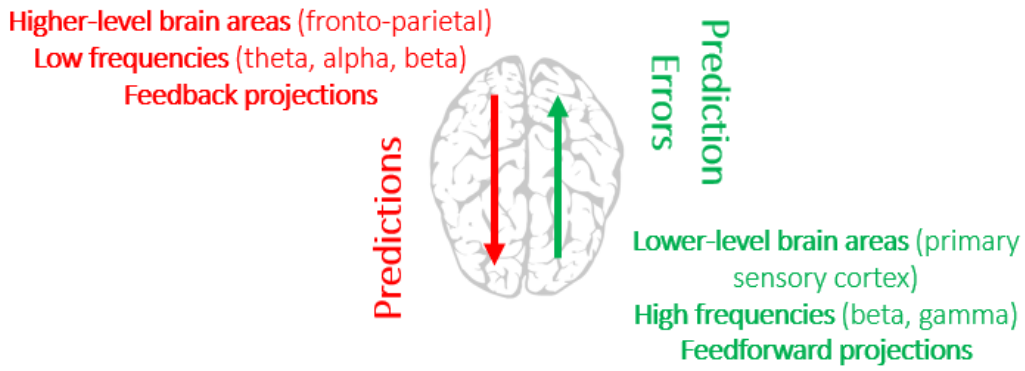

Figure 5.8: The role of brain oscillations in predictive coding. *The predictive coding theory postulates that high- and low-level brain areas exchange information through feedback and feedforward projections. High-level brain areas send predictions based on the internal model of the external world, built on recent inputs, through low-frequency brain oscillations. Low-level brain areas send in return prediction errors to update the internal model according to the novel sensory inputs through high-frequency brain oscillations.*

According to predictive coding theory, brain oscillations may be the neural support of serial dependence. By comparing the brain dynamics between trials biased by serial dependence and trials not biased towards the recent past, several hypotheses could be tested. 1) On trial n-1, the incoming visual input generates a strong update of the internal model of the external world by sending feedforward prediction errors with a high amplitude and/or an optimal phase. 2) Between trials n-1 and n, strong predictions concerning the upcoming visual inputs are sent through feedback projections, with a high amplitude and/or an optimal phase. In addition, we expect to observe an increase in the communication between high- (frontal) and low- (occipital) level brain areas, through phase-amplitude coupling, phase-phase coupling, or amplitude-amplitude coupling. 3) Finally, on trial n, the prediction error is reduced because the trial is biased toward the internal model of the brain, leading to feedforward prediction errors with a low amplitude or a non-optimal phase.

We developed a serial dependence experiment coupled with EEG recordings to test the hypothesis on brain oscillations described above. After the pilot session, we realized that performing the experiment would require a high number of experimental sessions. Indeed, serial dependence is a robust but slight effect, i.e., on average 5-10% on the total number of trials are biased due to serial dependence (Fischer and Whitney, 2014; Liberman et al., 2014; Cicchini et al., 2014; Burr and Cicchini, 2014). And to perform reliable phase analyses, at least ~250-300 trials per condition are required (VanRullen, 2016b). Unfortunately, we faced time constraints that did not allow us to do this experiment considering the high number of experimental sessions

that would be required. Nevertheless, we would like to perform this experiment in the future to assess whether brain oscillations underlie serial dependence according to the predictive coding theory.

Chapter 6. Alpha brain oscillations travel at the mesoscopic scale: their propagation influences visual perception.

We hypothesized that the spatial component of brain oscillations plays a crucial role in visual perception. First, we focused on mesoscopic oscillatory traveling waves, i.e., neural activity that propagates *within* a single brain area (e.g., V1) throughout few mm of cortex. Invasive recordings in animals showed that delta (0.5-4 Hz), theta (4-7 Hz), alpha (8-14 Hz), beta (15-30 Hz) and gamma (>30 Hz) oscillations act as traveling waves (Petsche et al., 1984; Wright and Sergejew, 1991; Prechtl et al., 1997; Arieli et al., 1995; Freeman and Barrie, 2000; Gabriel and Eckhorn, 2003; Benucci et al., 2007; Han et al., 2008; Huang et al., 2010; Ray and Maunsell, 2011; Maris et al., 2013; Stroh et al., 2013; Muller et al., 2014; Besserve et al., 2015; Zanos et al., 2015; Towsend et al., 2015; Davis et al., 2020; Freeman, 1978; Freeman and Baird, 1987; Ketchum and Haberly, 1993; Lam et al., 2000, 2003; Murthy and Fetz, 1996; Rubino et al., 2006; Takahashi et al., 2015).

In humans, only a few studies using invasive recordings (intraEEG) in drug-resistant epileptic patients showed the propagation of theta, alpha, and beta mesoscopic traveling waves (Takahashi et al., 2001; Zhang and Jacobs, 2015; Sreekumar et al., 2021).

To date, the functional role of mesoscopic oscillatory traveling waves has been poorly studied, especially in humans, and thus remains ill-defined. The aim of the studies presented below was to investigate whether the spatio-temporal organization of alpha induced brain oscillations across the retinotopic space played a role in visual perception.

1. A functional role of mesoscopic alpha traveling waves on visual perception: insights from psychophysics

The use of invasive recordings is limited in humans, for obvious ethics reasons, leading to the study of mesoscopic traveling waves being more difficult. An elegant manner to overcome this problem is to use the power of psychophysics, associated with the great knowledge we have about the anatomy, physiology, and functioning of the human visual system. The development of the experiments presented in this Chapter relies on two main points: the role of phase on visual perception, and the retinotopic organization of the early visual areas.

Visual perception is modulated periodically by the phase of low frequency brain oscillations (theta, 4-7 Hz; alpha, 8-13 Hz), with periods associated to a high probability of stimulus perception, i.e., optimal phase, and, opposite periods associated to a low probability of stimulus perception, i.e., non-optimal phase (Busch et al., 2009; Mathewson et al., 2009; Varela et al., 1981; Dugué et al., 2011, 2015; Samaha et al., 2015, 2017; Fakche et al., 2022; Merholz et al., 2021; for review VanRullen 2016; Kienitz et al., 2021). Interestingly, studies suggest that the phase of low-frequency brain oscillations accounts for less than 20% of the trial-by-trial variability in behavioral performance (Busch et al., 2009; Dugué et al., 2011a, 2015; Fakche et al., 2022). By taking into account the spatial organization of brain oscillations, we hypothesize that we should explain a larger proportion of the variance observed in the empirical data. Indeed, if brain oscillations are propagating across the early visual areas, such as V1, the optimal phase for perception would be modulated as a function of time and space. To illustrate this hypothesis, let us consider the representation in V1 of two visual stimuli, and a low-frequency brain oscillation that propagates across V1, with the optimal phase for perception color-coded in red. We observe that at a same moment in time, the representation of the visual stimulus 1 is in an optimal phase for perception while the representation of the stimulus 2 is in a non-optimal phase for perception (**Figure 6.1, Left panel**). As time passes, the brain oscillation travels, and the pattern reverses (**Figure 6.1, Right panel**). The optimal phase for perception of the two visual stimuli depends on the spatio-temporal organization of mesoscopic brain oscillation.

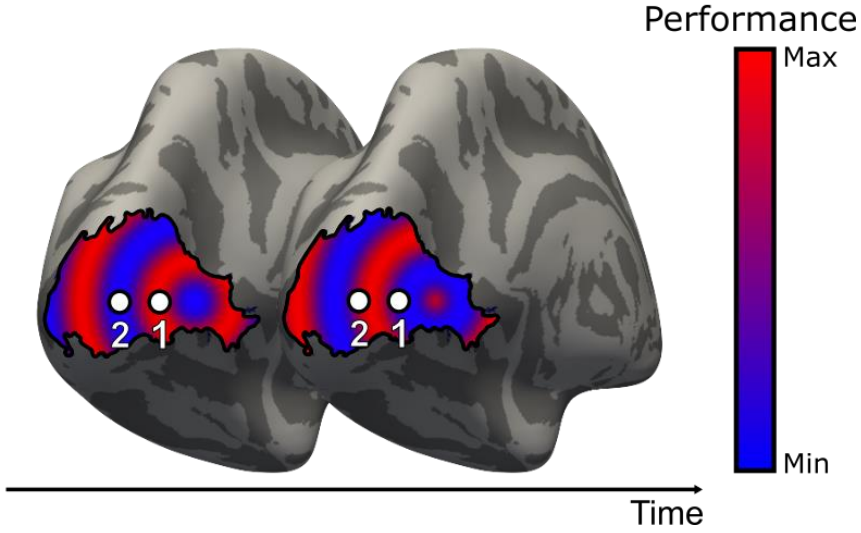

Figure 6.1: Optimal phase shift for perception indexes the presence of a mesoscopic traveling wave. *Representation of the left hemisphere of an inflated human brain. Black outline, V1 area. Dots, representation of two visual stimuli in the retinotopic space. A brain oscillation is*

propagating across V1, with its optimal phase for perception color-coded in red, and the opposite, non-optimal phase color-coded in blue.

Interestingly, this hypothesis can be tested with psychophysics (Sokoliuk and VanRullen, 2016). According to the retinotopic organization of V1, it is possible to display visual stimuli on the screen with known position in the cortex; and then, measure the optimal phase for each of these positions. It is thus possible to infer the presence of mesoscopic traveling waves in V1, and investigate their role on visual perception with psychophysics.

2. PUBLICATION: Fakche & Dugué. Perceptual cycles travel across the retinotopic space.

Perceptual cycles travel across retinotopic space

Camille Fakche[1] and Laura Dugué[1,2]

[1] Université Paris Cité, CNRS, Integrative Neuroscience and Cognition Center, F-75006 Paris, France

[2] Institut Universitaire de France (IUF), Paris, France

Corresponding Author:

Camille Fakche

camille.fakche@gmail.com

Acknowledgements

This project has received funding from the European Research Council (ERC) under the European Union's Horizon 2020 research and innovation program (grant agreement No 852139 – Laura Dugué) and the Agence Nationale de la Recherche (ANR) - Deutsche Forschungsgemeinschaft (DFG) program (grant agreement No J18P08ANR00 – Laura Dugué). We also thank Kirsten Petras, Andrea Alamia, Rufin VanRullen and Frédéric Chavane for their useful comments on the manuscript.

Summary

Visual perception waxes and wanes periodically as a function of the phase of low-frequency brain oscillations (theta, 4-7 Hz; alpha, 8-13 Hz) [1-9]. Perceptual cycles are defined as the corresponding periodic modulation of perceptual performance (review [10, 11]). Here, using psychophysics, we tested the hypothesis that brain oscillations travel across the visual cortex, leading to predictable perceptual consequences across the visual field, i.e., perceptual cycles travel across the retinotopic visual space. An oscillating disk (inducer) was presented in the periphery of the visual field to induce brain oscillations at low frequencies (4, 6, 8 or 10 Hz) at a specific retinotopic cortical location. Target stimuli at threshold (50% detection) were displayed at random times during the periodic disk stimulation, at one of three possible distances from the disk. Electroencephalography (EEG) was recorded while participants performed a detection task. EEG analyses showed that the periodic stimulation produced a complex brain oscillation composed of the induced frequency and its first harmonic likely due to the overlap of the periodic response and the neural response to individual stimuli. This complex oscillation, which originated from a precise retinotopic position, modulated detection performance periodically at each target position and at each frequency. Critically, the optimal behavioral phase, i.e., of highest performance, of the 8 Hz and 10 Hz oscillations (alpha range) consistently shifted across target distance to the inducer. Together, the results demonstrate that alpha-induced perceptual cycles traveled across the retinotopic space in human observers at a propagation speed between 0.2 and 0.4 m/s.

Results

Studies suggest that the phase of low-frequency brain oscillations accounts for <20% of the trial-by-trial variability in behavioral performance [1, 4-6, 8, 12, 13]. We hypothesize that if brain oscillations are the support of visual perception, they should explain a larger portion of the variance observed in empirical data. We propose that not only the temporal aspect of brain signals but also their spatial organization must be jointly considered when investigating their

functional role. Invasive studies in mammals reveal that low-frequency oscillatory activity propagates within individual visual areas (V1, V2, V4, MT) with a phase shift between the source of the neural activity and more distal retinotopic positions [14-24]. In humans, although a few invasive studies in patients showed that low-frequency oscillations can propagate within individual non-visual brain areas [25-27], there is no electro-physiological study to date investigating the propagation of low-frequency oscillations in individual visual areas. This may be due to several methodological constraints including, for invasive studies, the usual lack of intracranial coverage over the visual system, and for non-invasive studies, the poor spatial resolution of magnetoencephalography (MEG) and EEG. The aim of the present study is to circumvent these issues. We build on [28] and use a well-established psychophysics approach combined with EEG and eye-tracking, to assess the propagation of brain oscillations across the visual cortex, leading to predictable perceptual consequences across the visual field, i.e., perceptual cycles travel across the retinotopic space.

Participants (n=15) performed a threshold visual detection task, while a luminance oscillating disk was concurrently presented in the periphery (eccentricity: 7.5°) to induce theta/alpha brain oscillations (4, 6, 8 and 10 Hz; EEG simultaneously recorded). Near-threshold target stimuli appeared at one of three possible eccentricities between a central fixation cross and the disk (**Figure 1A**; adjusted according to cortical magnification so each target measured 0.8 mm of diameter and were placed 0.8 mm away from each other in the cortex; see **Figure 1B**). We tested whether (1) the periodic disk stimulation modulates detection performance periodically at each target position, (2) the optimal phase (of highest performance) shifts as a function of distance from the disk suggesting that perceptual cycles travel across space (**Figure 1C**), and (3) the occurrence of such traveling properties depends on the induced frequency.

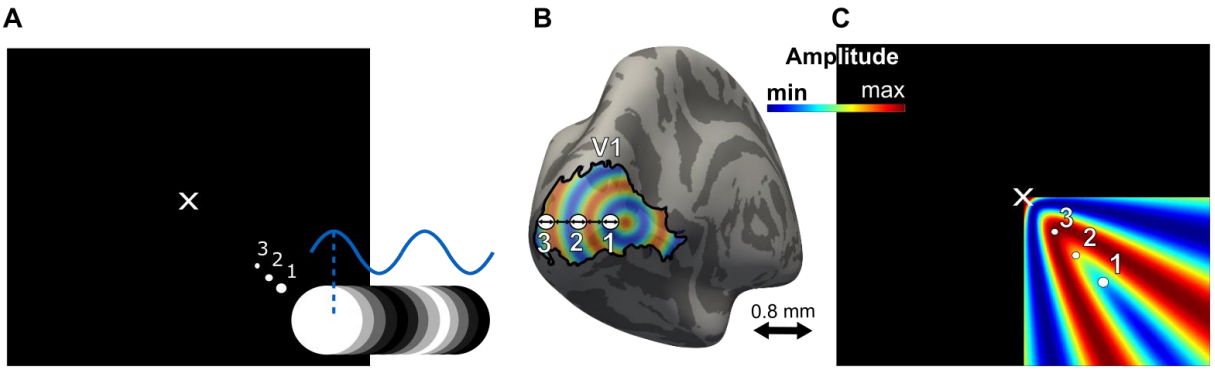

Figure 1. Experimental protocol. A. *A luminance oscillating disk (inducer) was presented in the periphery to induce brain oscillations in the visual cortex (e.g., V1). Participants were instructed to detect visual targets at threshold (50% detection) at three different positions in the retinotopic space, based on cortical magnification. Disks oscillated for a 30-seconds period during which 6 to 18 targets were presented at random times according to a decreasing probability distribution. Participants pressed the space bar when they detected the target (1-s response window after target onset)* ***B.*** *In the visual cortex, visual targets measured 0.8 mm of diameter and were placed 0.8 mm away from each other.* ***C.*** *Hypothesis: the oscillating disk, presented in the lower right corner, induced a brain oscillation that traveled across the retinotopic space (note that we concentrate our predictions to the quadrant in which the disk is presented). At an instant t, position 3 is located at the optimal phase of the oscillation (leading to the highest performance; i.e., max Amplitude), while position 1 is located at the non-optimal phase (i.e., min Amplitude).*

EEG activity was analyzed using frequency decomposition (Fast Fourier Transform, FFT, performed on the time series of each participant and electrode) and Event-Related Potentials (ERPs) measures to ensure that we successfully induced brain oscillations and to characterize the shape of the evoked response. First, peaks in the spectrum (as measured per SNR, averaged across participants and electrodes) were identified for each induced frequency (4, 6, 8 and 10 Hz; SNR > 1.43) and their first harmonics (8, 12, 16 and 20 Hz; SNR > 1.56), with topographies showing brain activity in the occipital cortex (for simplicity, frequencies were rounded to a whole number; real values are displayed in **Figure 2 left side of each panel**). Second, ERP analyses showed that the evoked signal is a complex oscillation composed of the induced frequency and its first harmonic (**Figure 2 right side of each panel**). We further

computed an FFT on the ERPs of electrode Oz. Peaks were again identified for each induced frequency (4, 6, 8 and 10 Hz; SNR > 2.52) and their first harmonics (8, 12, 16 and 20 Hz; SNR > 4.31; data not shown). These complex evoked responses were interpreted as the overlap between the periodic brain response (i.e., inducer) and the neural population response to individual stimuli (i.e., contrast change) at low frequencies, or alternatively, to the nonlinear nature of the visual system, i.e., nonlinear systems produce complex output consisting of the input frequency and multiple harmonics [29, 30]. Together, the EEG analyses confirm that we successfully induced theta/alpha oscillations in the visual cortex and show that the evoked signal is a complex oscillation composed of the induced frequency and its first harmonic [29, 30].

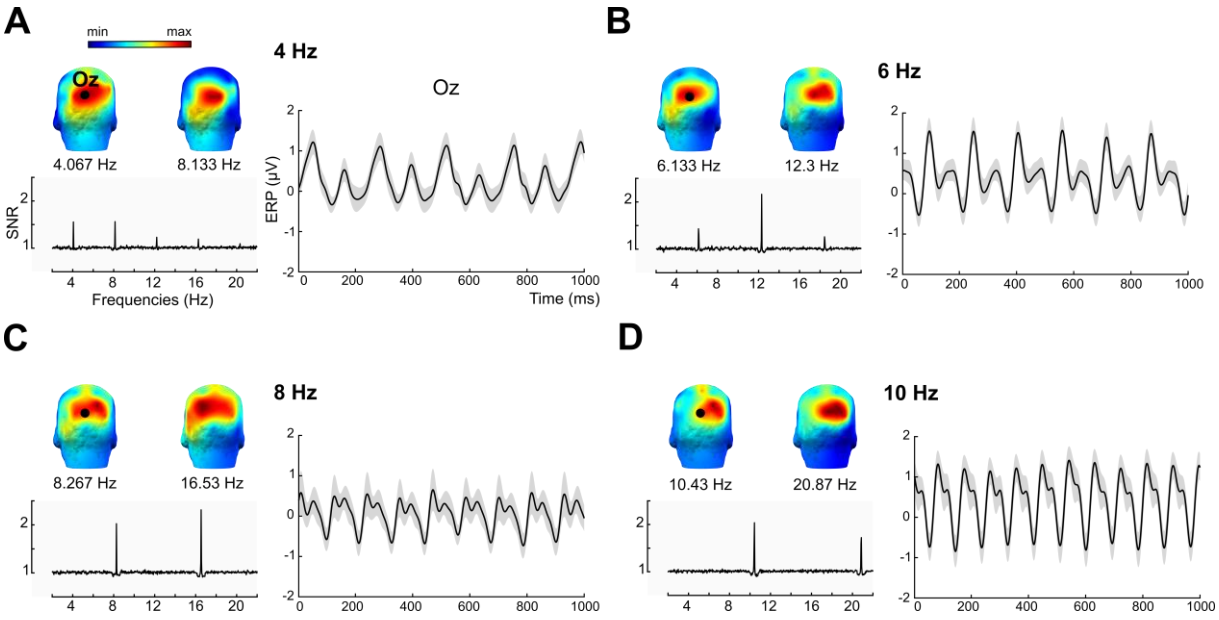

Figure 2. The oscillating disk evokes complex brain oscillations in the occipital cortex. *Left side of each panel, Fast Fourier Transform analyses performed on the EEG time series. Right side of each panel, ERP analyses, for induced frequencies of* ***A.*** *4,* ***B.*** *6,* ***C.*** *8 and* ***D.*** *10 Hz (rounded frequency values). Signal-to-noise ratio (SNR) amplitude averaged across 15 participants and all 62 electrodes, from 2 to 22 Hz. In each panel, a peak in SNR is identified for the induced frequency and its first harmonic. Topographies of the two SNR peaks revealed that we successfully induced brain oscillations in the visual cortex. Black dot, Electrode Oz. ERP of the Oz electrode computed on one-second epochs (the first-second epoch was removed to each 30-seconds blocks to avoid the EEG transient evoked response; each block*

represented 29 1-second epochs) averaged across participants (n=15). Solid black line, averaged ERP. Shaded area, standard error of the mean.

Second, we investigated whether detection performance was modulated periodically for each induced frequency and each target position. Targets (from 6 to 18 targets per 30 seconds-blocks) can appear at random delays during the periodic disk stimulation (from 1s to 29s from disk onset). Targets were binned according to the phase of the oscillating disk (7 bins/cycle; least number of bins to sample one oscillatory period while allowing a large number of trials per bin to achieve high statistical power). In each bin, detection performance was computed as per hit rate (correct target detection) for each participant, frequency, and target position. Finally, the data were averaged across participants and, given the complex shape of the ERP (**Figure 2**), fit to a complex sine function, separately for each frequency and target position (see **STAR Methods**). Detection performance showed a significant oscillatory pattern for each target position and frequency (Monte Carlo, Bonferroni corrected across frequencies and positions, p-value threshold < 0.01, corresponding to a Z-score threshold of 2.64, and a Cohen's d threshold of 1.86; **Figure 3**), and a clear optimal phase (of highest performance). The inducer modulated detection performance periodically, at each target position and at each frequency, with an average amplitude modulation (optimal to non-optimal hit rate difference) of 44.8 ± 3.4 %. A complementary analysis showed that behavioral performance was better explained when taking into account the spatial position of the targets. Specifically, we compared the amplitude modulation when detection performance was calculated disregarding target position, with the amplitude modulation calculated independently for each target position and then averaged across positions (two-tailed t-tests Bonferroni corrected for multiple comparisons: 4 Hz, p-value < 0.01, Cohen's d = -0.36, CI = [-0.05; -0.02]; 6 Hz, p-value < 0.01, Cohen's d = -0.28, CI = [-0.04; -0.01]; 8 Hz, p-value < 0.01, Cohen's d = -0.30, CI = [-0.04, -0.01]; 10 Hz, p-value < 0.01, Cohen's d = -0.58, CI = [-0.05; -0.03]). The amplitude modulation was significantly stronger when calculated position-by-position, suggesting that taking into account the spatial position of visual targets better explain perceptual performance.

Critically, we tested whether (1) perceptual cycles propagate across the retinotopic space, and (2) the occurrence of such traveling properties depends on the induced frequency. Propagation is defined as a shift in the optimal phase between two positions. To assess whether the optimal phase shifted as a function of target position, we computed the phase-locking values of the optimal phase (i.e., phase concentration of the distribution of optimal phases obtained with a bootstrap procedure; see **STAR Methods**) for each participant, target position, and frequency. A linear mixed effects model was implemented with frequency (4, 6, 8, 10 Hz), target position (1, 2, 3) and their interaction as fixed effects. Participant's intercepts and slopes for the effect of frequency and target position were considered random effects. The effects of frequency ($t(176) = 0.01$, p-value = 0.99, estimate ± standard error < 0.01 ± 0.01) and target position were not significant ($t(176) = 1.36$, p-value = 0.17, estimate = 0.02 ± 0.01). The interaction between frequency and target position was, however, significant ($t(176) = -0.01$, p-value = 0.05, estimate = -0.01 ± 0.01). Post-hoc analyses on the optimal phase difference (see **STAR Methods**; reported in degrees for easier readability of **Figure 3**) between each pair of target position (1 and 3, 1 and 2, and 2 and 3; Monte Carlo, FDR corrected across frequencies and positions, p-value threshold of 0.01, corresponding to Z-score threshold of 2.24, and a Cohen's d threshold of 1.41) revealed a significant phase shift between positions 1 and 2, and 1 and 3 for 8 Hz- and 10 Hz-induced frequencies (**Figure 3C,D**). We found no significant phase shift for 4 Hz- and 6 Hz-induced frequencies (**Figure 3A,B**). Together, the results demonstrate that the optimal phase of alpha perceptual cycles shifted across target positions, suggesting that the alpha-induced oscillations traveled across the retinotopic cortical space. This effect cannot merely be explained by low-level luminance masking as confirmed with a control experiment (see **Supplemental Information, Control experiment**) nor by a decreased phase estimation accuracy at low frequencies (see **Supplemental Information, Figure S1,** showing that the amplitude modulation is in fact higher at low compared to high induced frequency).

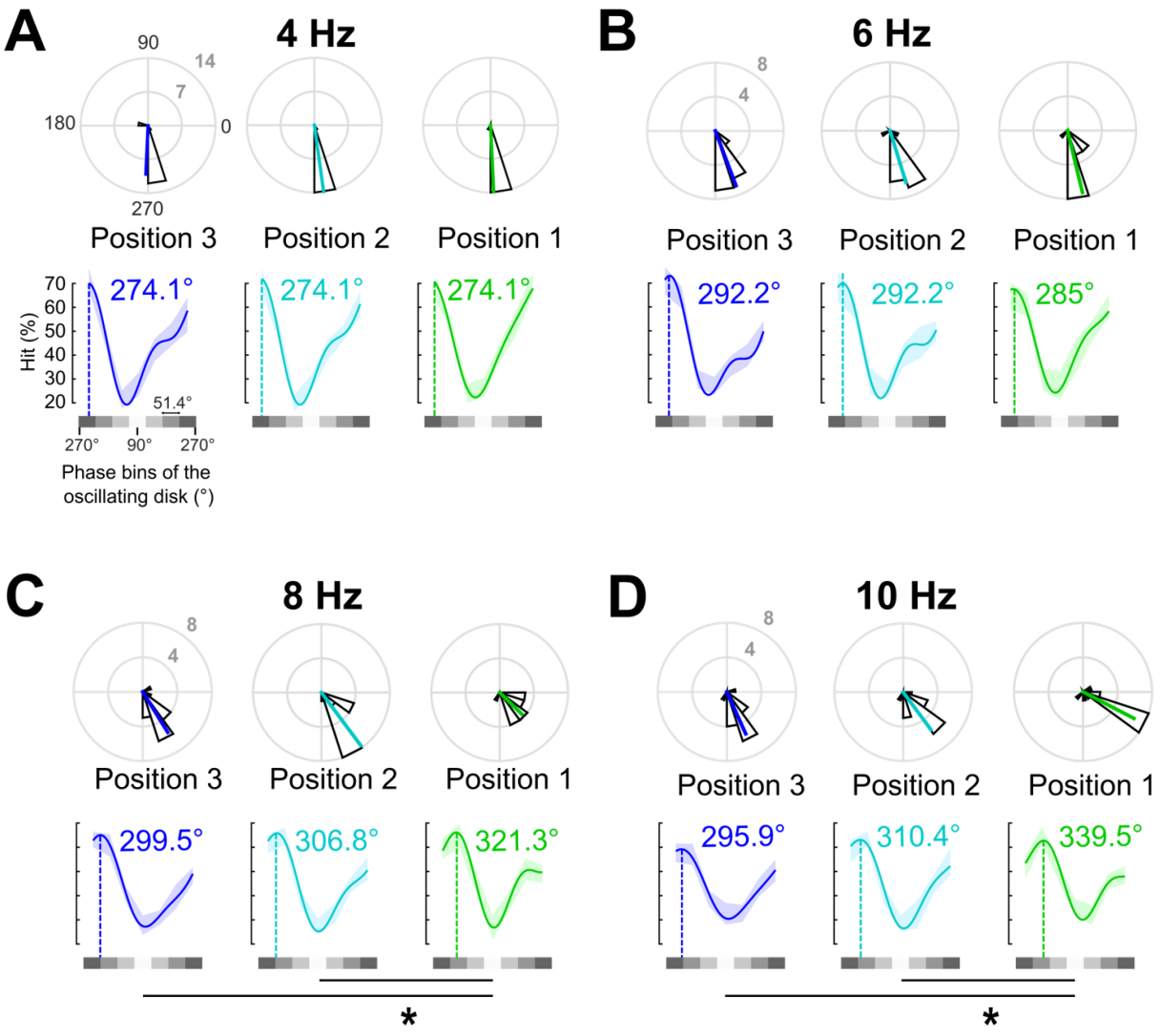

Figure 3. The optimal phase of alpha perceptual cycles shifts between target positions. *Lower graph of each panel, hit rate averaged across participants (n=15), binned as a function of the phase of the oscillating disk, and fitted to a complex sine function. Shaded colored area, 95 confidence intervals. Solid line, sine fit. Dotted line, optimal phase in degrees. Top graph of each panel, rose plot distribution of the optimal phase across participants. Colored solid line, optimal phase averaged across participants. Gray scale, phase bins of the oscillating disk. Each bin represents 51.4° of the oscillatory cycle.* ***A.*** *results for induced frequencies of* ***A.*** *4,* ***B.*** *6,* ***C.*** *8 and* ***D.*** *10 Hz. Performance was significantly modulated periodically at each target position and frequency (Monte Carlo, Bonferroni corrected across target positions and frequencies, p-value threshold < 0.01). The optimal phase shifted between positions 1 and 2, and 1 and 3 for 8 Hz- and 10 Hz-induced frequencies (Monte Carlo, FDR corrected, p-value threshold of 0.01). There was no significant phase shift for 4 Hz- and 6 Hz-induced frequencies.*

Finally, when converting the phase shift observed between target positions 1 and 2, and 1 and 3 into milliseconds (5 ms and 8 ms for 8 Hz, and 8 ms and 12 ms for 10 Hz, respectively) and

given the cortical distance between two target positions (0.8 mm distance edge-to-edge) as well as the targets' cortical size (0.8 mm diameter), one can estimate that alpha-induced brain oscillations traveled across the retinotopic space at a propagation speed ranging from 0.2 to 0.4 m/s.

Discussion

Using psychophysics and EEG, we investigated whether perceptual cycles travel across the retinotopic space in humans. The results showed that visual perception at each target position is modulated periodically at the induced frequency, replicating previous results [31-38]. Critically, the optimal phase for visual perception shifted between the target position closest to the inducer and the more distant targets. This effect was observed exclusively for alpha frequencies (8 Hz and 10 Hz; and cannot be simply explained by a mere luminance masking confound), with a propagation speed of 0.2-0.4 m/s. Together, the results support the hypothesis that alpha-induced brain oscillations travel across the visual cortex to modulate performance periodically across space and time.

Neural traveling waves, a growing, yet largely understudied field. A traveling wave is the propagation of neural activity over space with a constant shift in the peak latency between the origin of the signal and more distal positions [39, 40]. A growing literature reports that neural activity can travel *between* cortical areas, so-called macroscopic traveling waves. Monkey electrophysiology studies revealed that alpha oscillations travel between visual regions from V4 to V1, while gamma oscillations travel from V1 to V4 [41]. In humans, macroscopic oscillatory traveling waves have been reported using invasive (electrocorticography, ECoG, [42-47]) and non-invasive (EEG, e.g., [44, 48-60]; MEG, [44, 61-64]) recordings.

Critically, mesoscopic waves [39, 40] travel *within* individual brain regions (e.g., V1) spanning millimeters. Studies using invasive recordings with high spatial and temporal resolution (Local field potential, LFP; Multielectrode arrays, MEAs; Voltage-sensitive dyes, VSDs) showed non-oscillatory traveling activity in visual cortices of mammals (cats, monkeys, rats) (anesthetized:

207 [65-75]; awake: [76-82]). Mesoscopic non-oscillatory traveling waves have also been observed
208 in non-visual, sensory, and motor cortices of mammals (cats, rats, guinea pigs, monkeys)
209 (anesthetized: [83-89]; awake: [90-94]), and in reptiles (salamander) (anesthetized: [95-97]).
210 Much fewer studies have focused on mesoscopic oscillatory traveling waves. They showed
211 that delta (0.5-4 Hz), theta (4-7 Hz), alpha (8-14 Hz), beta (15-30 Hz) and gamma (>30 Hz)
212 oscillations can propagate within individual visual areas of mammals and turtles [14-24, 98,
213 99]. Low-frequency oscillations were shown to also propagate in the olfactory bulb and cortex
214 [100, 101]; and beta oscillations in the motor cortex [102, 103]. In humans, only a few studies,
215 using invasive recordings in patients, showed the propagation of theta, alpha, and beta
216 mesoscopic traveling waves [25-27], but only in non-visual cortical areas. There is no electro-
217 physiological study to date investigating the propagation of low-frequency oscillations in
218 individual human visual areas.

219 Finally, if a few studies have investigated the functional role of propagating oscillatory activity
220 at the macroscopic (memory: [47, 51, 52]; attention: [41, 53]; saccadic eye movements: [60];
221 visual perception: [48, 49, 54-59]), and mesoscopic levels (attention: [19]; memory: [17];
222 motricity: [25, 102]; saccadic eye movements: [24]; visual perception: [23, 104]), very little is
223 known about the link between oscillatory activity propagation within individual visual areas and
224 perceptual performance, especially in human.

225 The present study builds on [28] and addresses this clear gap in the literature. Using
226 psychophysics, we showed that alpha-induced oscillations travel within individual visual areas,
227 leading perceptual cycles to travel across the retinotopic space.

228 *Oscillatory Mesoscopic Traveling Waves in visual areas have clear perceptual consequences.*
229 Sokoliuk and VanRullen [28] (2016) reasoned that were an induced-oscillation propagated
230 across the visual cortex, it should have perceptual consequences across the retinotopic visual
231 space. Using a similar psychophysical paradigm, they found a shift of the behavioral optimal
232 phase as a function of distance from the inducer. Contrary to our results, however, they
233 observed this effect for both frequencies of 5 Hz (theta) and 10 Hz (alpha), but not 15 Hz, while

here we show a shift exclusively for alpha-induced frequencies (8 Hz and 10 Hz; but not 4 Hz and 6 Hz). These discrepant results can be explained by a number of critical differences between the two studies. First, our EEG results revealed that the oscillating disk produced a complex neural response composed of the induced frequency and its first harmonic, coherent with the nature of the visual system [29, 30, 36]. Thus, one must fit the behavioral response with a corresponding complex sine function to accurately capture the non-linearity of the neural response. Since the EEG was not recorded in Sokoliuk and VanRullen [28] (2016), the shape of the induced oscillation was unknown. Second, to ensure that the three targets activated the same number neurons in the visual regions, hence landing in a similar spatial extent (spatial phase) of the traveling wave, we adjusted the size of each target to cortical magnification. Third, in our study, the same participants (n=15) performed all four frequency conditions thus ensuring equal statistical power and no inter-participant variability (n=5 for 5 Hz, n=7 for 10 Hz and n=15 for a 10-Hz replication set, and n=4 for 15Hz in [28]). Finally, we used eye-tracking to ensure stable fixation, critical when investigating retinotopic propagation.

Propagation of alpha but not theta oscillations. Attention is the cognitive function that selects relevant information to facilitate its processing while still being able to flexibly redeploy resources to other information if necessary [105-107]. Studies have shown that when covert attention (in the absence of head or eye movements) is sustained at a given spatial location, information is sampled periodically at the alpha frequency (review [11, 108]). In other words, visual performance fluctuates over time along with the phase of alpha oscillations, in detection tasks in which the target stimulus appeared always at the same spatial location [1-3, 5-8, 13]. However, when multiple stimuli are presented, attention rhythmically samples information at the theta frequency [4, 9, 109-113] (review [10, 11, 108]).

Here, while we did not explicitly manipulate covert attention, participants fixated at the center of the screen and targets appeared in a constrained location suggesting that covert, voluntary spatial attention was sustained on the bottom right quadrant. This manipulation likely recruited alpha sampling, which potentially favored the propagation of alpha-induced oscillations

(although alpha-induced oscillations could also potentially travel in the absence of attention). One can speculate that the propagation of alpha oscillations away from the main attention focus could allow the observer to periodically monitor other nearby locations allowing for flexible attentional reallocation when a target appears. Further studies are necessary to investigate this hypothesis.

Speed and spatial extent of mesoscopic traveling waves. Our results show that alpha waves travel across the retinotopic space at a propagation speed of 0.2-0.4 m/s. Such observation is in line with results from the animal literature showing that transient neural signals travel within visual regions at a propagation speed of 0.06-0.4 m/s (0.2 m/s on average) from ~2 mm to ~7 mm of cortex [66-68, 70-79, 81, 82], as well as with studies showing that low-frequency oscillations propagate within visual areas at a speed of 0.01-0.6 m/s (0.25 m/s on average) [14, 16-18, 21, 23, 24, 98, 99]. Additionally, given a phase difference of ~7° to ~30° between target positions, it is unlikely that more than one (spatial) cycle (360°) of oscillatory activity propagates across such a small portion of the visual cortex (see **Figure 1**), in line with previous observations [24, 26].

Finally, given our specific manipulation (contrast change) and the observed propagation of perceptual cycles, it is likely that our paradigm has preferentially probed alpha traveling waves in area V1 (with small receptive fields). Studies, however, have shown that a single visual stimulation can propagate simultaneously within several brain areas, e.g., V1 and V2 [21], suggesting that this simultaneity may be crucial for the integration of retinotopic information in parallel, across multiple visual areas [21]. Future electrophysiological studies are necessary to validate this hypothesis.

Conclusion. Using a carefully designed psychophysical protocol, combined with EEG and eye-tracking, our study demonstrates that alpha perceptual cycles travel across the retinotopic visual space in humans, at a propagation speed of 0.2-0.4 m/s. These results suggest that alpha-induced brain oscillations travel across the visual cortex to modulate performance periodically across space and time.

References

1. Busch, N.A., Dubois, J., and VanRullen, R. (2009). The Phase of Ongoing EEG Oscillations Predicts Visual Perception. J. Neurosci. 29, 7869–7876.

2. Mathewson, K.E., Gratton, G., Fabiani, M., Beck, D.M., and Ro, T. (2009). To See or Not to See: Prestimulus α Phase Predicts Visual Awareness. J. Neurosci. 29, 2725–2732.

3. Valera, F.J., Toro, A., Roy John, E., and Schwartz, E.L. (1981). Perceptual framing and cortical alpha rhythm. Neuropsychologia 19, 675–686.

4. Dugué, L., Marque, P., and VanRullen, R. (2015). Theta Oscillations Modulate Attentional Search Performance Periodically. Journal of Cognitive Neuroscience 27, 945–958.

5. Dugué, L., Marque, P., and VanRullen, R. (2011). The Phase of Ongoing Oscillations Mediates the Causal Relation between Brain Excitation and Visual Perception. J. Neurosci. 31, 11889–11893.

6. Samaha, J., Gosseries, O., and Postle, B.R. (2017). Distinct Oscillatory Frequencies Underlie Excitability of Human Occipital and Parietal Cortex. J. Neurosci. 37, 2824–2833.

7. Samaha, J., and Postle, B.R. (2015). The Speed of Alpha-Band Oscillations Predicts the Temporal Resolution of Visual Perception. Current Biology 25, 2985–2990.

8. Fakche, C., VanRullen, R., Marque, P., and Dugué, L. (2022). α Phase-Amplitude Tradeoffs Predict Visual Perception. eNeuro. 1-16.

9. Merholz, G., Grabot, L., VanRullen, R., and Dugué, L. (2022). Periodic attention operates faster during more complex visual search. Scientific Reports. 12(1), 1-14.

10. VanRullen, R. (2016). Perceptual Cycles. Trends in Cognitive Sciences. 20, 723–735.

11. Kienitz, R., Schmid, M.C., and Dugué, L. Rhythmic sampling revisited: Experimental paradigms and neural mechanisms. European Journal of Neuroscience n/a.

12. Baumgarten, T.J., Schnitzler, A., and Lange, J. (2015). Beta oscillations define discrete perceptual cycles in the somatosensory domain. PNAS 112, 12187–12192.

13. Busch, N.A., and VanRullen, R. (2010). Spontaneous EEG oscillations reveal periodic sampling of visual attention. PNAS 107, 16048–16053.

14. Sanchez-Vives, M.V., and McCormick, D.A. (2000). Cellular and network mechanisms of rhythmic recurrent activity in neocortex. Nat Neurosci 3, 1027–1034.

15. Huang, X., Troy, W.C., Yang, Q., Ma, H., Laing, C.R., Schiff, S.J., and Wu, J.-Y. (2004). Spiral Waves in Disinhibited Mammalian Neocortex. J. Neurosci. 24, 9897–9902.

16. Benucci, A., Frazor, R.A., and Carandini, M. (2007). Standing Waves and Traveling Waves Distinguish Two Circuits in Visual Cortex. Neuron 55, 103–117.

17. Han, F., Caporale, N., and Dan, Y. (2008). Reverberation of Recent Visual Experience in Spontaneous Cortical Waves. Neuron 60, 321–327.

18. Ray, S., and Maunsell, J.H.R. (2011). Different Origins of Gamma Rhythm and High-Gamma Activity in Macaque Visual Cortex. PLOS Biology 9, e1000610, 1-9.

19. Maris, E., Womelsdorf, T., Desimone, R., and Fries, P. (2013). Rhythmic neuronal synchronization in visual cortex entails spatial phase relation diversity that is modulated by stimulation and attention. NeuroImage 74, 99–116.

20. Stroh, A., Adelsberger, H., Groh, A., Rühlmann, C., Fischer, S., Schierloh, A., Deisseroth, K., and Konnerth, A. (2013). Making Waves: Initiation and Propagation of Corticothalamic Ca2+ Waves In Vivo. Neuron 77, 1136–1150.

21. Muller, L., Reynaud, A., Chavane, F., and Destexhe, A. (2014). The stimulus-evoked population response in visual cortex of awake monkey is a propagating wave. Nat Commun 5(1), 1-14.

22. Townsend, R.G., Solomon, S.S., Chen, S.C., Pietersen, A.N.J., Martin, P.R., Solomon, S.G., and Gong, P. (2015). Emergence of Complex Wave Patterns in Primate Cerebral Cortex. J. Neurosci. 35, 4657–4662.

23. Davis, Z.W., Muller, L., Martinez-Trujillo, J., Sejnowski, T., and Reynolds, J.H. (2020). Spontaneous travelling cortical waves gate perception in behaving primates. Nature 587, 432–436.

24. Zanos, T.P., Mineault, P.J., Nasiotis, K.T., Guitton, D., and Pack, C.C. (2015). A Sensorimotor Role for Traveling Waves in Primate Visual Cortex. Neuron 85, 615–627.

25. Takahashi, K., Saleh, M., Penn, R., and Hatsopoulos, N. (2011). Propagating Waves in Human Motor Cortex. Frontiers in Human Neuroscience 5, 1-8.

26. Zhang, H., and Jacobs, J. (2015). Traveling Theta Waves in the Human Hippocampus. J. Neurosci. 35, 12477–12487.

27. Sreekumar, V., Wittig, J.H., Chapeton, J.I., Inati, S.K., and Zaghloul, K.A. (2021). Low frequency traveling waves in the human cortex coordinate neural activity across spatial scales. BioRxiv, 1-48.

28. Sokoliuk, R., and VanRullen, R. (2016). Global and local oscillatory entrainment of visual behavior across retinotopic space. Sci Rep 6(1), 1-12

29. Heinrich, S.P. (2010). Some thoughts on the interpretation of steady-state evoked potentials. Doc Ophthalmol 120, 205–214.

30. Norcia, A.M., Appelbaum, L.G., Ales, J.M., Cottereau, B.R., and Rossion, B. (2015). The steady-state visual evoked potential in vision research: A review. Journal of Vision 15(6), 4-4

31. Stefanics, G., Hangya, B., Hernádi, I., Winkler, I., Lakatos, P., and Ulbert, I. (2010). Phase Entrainment of Human Delta Oscillations Can Mediate the Effects of Expectation on Reaction Speed. J. Neurosci. 30, 13578–13585.

32. Mathewson, K.E., Prudhomme, C., Fabiani, M., Beck, D.M., Lleras, A., and Gratton, G. (2012). Making Waves in the Stream of Consciousness: Entraining Oscillations in EEG Alpha and Fluctuations in Visual Awareness with Rhythmic Visual Stimulation. Journal of Cognitive Neuroscience 24, 2321–2333.

33. Henry, M.J., and Obleser, J. (2012). Frequency modulation entrains slow neural oscillations and optimizes human listening behavior. PNAS 109, 20095–20100.

34. Henry, M.J., Herrmann, B., and Obleser, J. (2014). Entrained neural oscillations in multiple frequency bands comodulate behavior. PNAS 111, 14935–14940.

35. Graaf, T.A. de, Gross, J., Paterson, G., Rusch, T., Sack, A.T., and Thut, G. (2013). Alpha-Band Rhythms in Visual Task Performance: Phase-Locking by Rhythmic Sensory Stimulation. PLOS ONE 8, e60035, 1-12.

36. Spaak, E., Lange, F.P. de, and Jensen, O. (2014). Local Entrainment of Alpha Oscillations by Visual Stimuli Causes Cyclic Modulation of Perception. J. Neurosci. 34, 3536–3544.

373 37. Oever, S. ten, and Sack, A.T. (2015). Oscillatory phase shapes syllable perception.
374 PNAS 112, 15833–15837.

375 38. Kizuk, S.A.D., and Mathewson, K.E. (2017). Power and Phase of Alpha Oscillations
376 Reveal an Interaction between Spatial and Temporal Visual Attention. Journal of Cognitive
377 Neuroscience 29, 480–494.

378 39. Sato, T.K., Nauhaus, I., and Carandini, M. (2012). Traveling Waves in Visual Cortex.
379 Neuron 75, 218–229.

380 40. Muller, L., Chavane, F., Reynolds, J., and Sejnowski, T.J. (2018). Cortical travelling
381 waves: mechanisms and computational principles. Nat Rev Neurosci 19, 255–268.

382 41. Kerkoerle, T. van, Self, M.W., Dagnino, B., Gariel-Mathis, M.-A., Poort, J., Togt, C. van
383 der, and Roelfsema, P.R. (2014). Alpha and gamma oscillations characterize feedback and
384 feedforward processing in monkey visual cortex. PNAS 111, 14332–14341.

385 42. Nir, Y., Staba, R.J., Andrillon, T., Vyazovskiy, V.V., Cirelli, C., Fried, I., and Tononi, G.
386 (2011). Regional Slow Waves and Spindles in Human Sleep. Neuron 70, 153–169.

387 43. Meij, R. van der, Kahana, M., and Maris, E. (2012). Phase–Amplitude Coupling in
388 Human Electrocorticography Is Spatially Distributed and Phase Diverse. J. Neurosci. 32, 111–
389 123.

390 44. Alexander, D.M., Jurica, P., Trengove, C., Nikolaev, A.R., Gepshtein, S., Zvyagintsev,
391 M., Mathiak, K., Schulze-Bonhage, A., Ruescher, J., Ball, T., et al. (2013). Traveling waves
392 and trial averaging: The nature of single-trial and averaged brain responses in large-scale
393 cortical signals. NeuroImage 73, 95–112.

394 45. Bahramisharif, A., Gerven, M.A.J. van, Aarnoutse, E.J., Mercier, M.R., Schwartz, T.H.,
395 Foxe, J.J., Ramsey, N.F., and Jensen, O. (2013). Propagating Neocortical Gamma Bursts Are
396 Coordinated by Traveling Alpha Waves. J. Neurosci. 33, 18849–18854.

397 46. Muller, L., Piantoni, G., Koller, D., Cash, S.S., Halgren, E., and Sejnowski, T.J. (2016).
398 Rotating waves during human sleep spindles organize global patterns of activity that repeat
399 precisely through the night. eLife 5, e17267, 1-16.

400 47. Zhang, H., Watrous, A.J., Patel, A., and Jacobs, J. (2018). Theta and Alpha Oscillations
401 Are Traveling Waves in the Human Neocortex. Neuron 98, 1269-1281.e4.

402 48. Schack, B., Weiss, S., and Rappelsberger, P. (2003). Cerebral information transfer
403 during word processing: Where and when does it occur and how fast is it? Human Brain
404 Mapping 19, 18–36.

405 49. Shevelev, I.A., Kamenkovich, V.M., Bark, E.D., Verkhlutov, V.M., Sharaev, G.A., and
406 Mikhailova, E.S. (2000). Visual illusions and travelling alpha waves produced by flicker at alpha
407 frequency. International Journal of Psychophysiology 39, 9–20.

408 50. Burkitt, G.R., Silberstein, R.B., Cadusch, P.J., and Wood, A.W. (2000). Steady-state
409 visual evoked potentials and travelling waves. Clinical Neurophysiology 111, 246–258.

410 51. Sauseng, P., Klimesch, W., Gruber, W., Doppelmayr, M., Stadler, W., and Schabus, M.
411 (2002). The interplay between theta and alpha oscillations in the human electroencephalogram
412 reflects the transfer of information between memory systems. Neuroscience Letters 324, 121–
413 124.

414 52. Alexander, D.M., Arns, M.W., Paul, R.H., Rowe, D.L., Cooper, N., Esser, A.H.,
415 Fallahpour, K., Stephan, B.C.M., Heesen, E., Breteler, R., et al. (2006). Eeg markers for
416 cognitive decline in elderly subjects with subjective memory complaints. J. Integr. Neurosci.
417 05, 49–74.

418 53. Alexander, D.M., Hermens, D.F., Keage, H.A.D., Clark, C.R., Williams, L.M., Kohn,
419 M.R., Clarke, S.D., Lamb, C., and Gordon, E. (2008). Event-related wave activity in the EEG
420 provides new marker of ADHD. Clinical Neurophysiology 119, 163–179.

421 54. Patten, T.M., Rennie, C.J., Robinson, P.A., and Gong, P. (2012). Human Cortical
422 Traveling Waves: Dynamical Properties and Correlations with Responses. PLOS ONE 7,
423 e38392, 1-10.

424 55. Fellinger, R., Gruber, W., Zauner, A., Freunberger, R., and Klimesch, W. (2012).
425 Evoked traveling alpha waves predict visual-semantic categorization-speed. NeuroImage 59,
426 3379–3388.

427 56. Alamia, A., and VanRullen, R. (2019). Alpha oscillations and traveling waves:
428 Signatures of predictive coding? PLOS Biology 17, e3000487, 1-26.

429 57. Lozano-Soldevilla, D., and VanRullen, R. (2019). The Hidden Spatial Dimension of
430 Alpha: 10-Hz Perceptual Echoes Propagate as Periodic Traveling Waves in the Human Brain.
431 Cell Reports 26, 374-380.e4.

432 58. Pang (庞兆阳), Z., Alamia, A., and VanRullen, R. (2020). Turning the Stimulus On and
433 Off Changes the Direction of α Traveling Waves. eNeuro 7, 1-11.

434 59. King, J.-R., and Wyart, V. (2021). The Human Brain Encodes a Chronicle of Visual
435 Events at Each Instant of Time Through the Multiplexing of Traveling Waves. J. Neurosci. 41,
436 7224–7233.

437 60. Giannini, M., Alexander, D.M., Nikolaev, A.R., and van Leeuwen, C. (2018). Large-
438 Scale Traveling Waves in EEG Activity Following Eye Movement. Brain Topogr 31, 608–622.

439 61. Ribary, U., Ioannides, A.A., Singh, K.D., Hasson, R., Bolton, J.P., Lado, F., Mogilner,
440 A., and Llinás, R. (1991). Magnetic field tomography of coherent thalamocortical 40-Hz
441 oscillations in humans. PNAS 88, 11037–11041.

442 62. Thorpe, S.G., Nunez, P.L., and Srinivasan, R. (2007). Identification of wave-like spatial
443 structure in the SSVEP: Comparison of simultaneous EEG and MEG. Statistics in Medicine
444 26, 3911–3926.

445 63. Cottereau, B., Lorenceau, J., Gramfort, A., Clerc, M., Thirion, B., and Baillet, S. (2011).
446 Phase delays within visual cortex shape the response to steady-state visual stimulation.
447 NeuroImage 54, 1919–1929.

448 64. van Ede, F., van Pelt, S., Fries, P., and Maris, E. (2015). Both ongoing alpha and
449 visually induced gamma oscillations show reliable diversity in their across-site phase-relations.
450 Journal of Neurophysiology 113, 1556–1563.

451 65. Bringuier, V., Chavane, F., Glaeser, L., and Frégnac, Y. (1999). Horizontal Propagation
452 of Visual Activity in the Synaptic Integration Field of Area 17 Neurons. Science 283, 695–699.

453 66. Jancke, D., Chavane, F., Naaman, S., and Grinvald, A. (2004). Imaging cortical
454 correlates of illusion in early visual cortex. Nature 428, 423–426.

455 67. Roland, P.E., Hanazawa, A., Undeman, C., Eriksson, D., Tompa, T., Nakamura, H.,
456 Valentiniene, S., and Ahmed, B. (2006). Cortical feedback depolarization waves: A mechanism
457 of top-down influence on early visual areas. PNAS 103, 12586–12591.

458 68. Lippert, M.T., Takagaki, K., Xu, W., Huang, X., and Wu, J.-Y. (2007). Methods for
459 Voltage-Sensitive Dye Imaging of Rat Cortical Activity With High Signal-to-Noise Ratio. Journal
460 of Neurophysiology 98, 502–512.

461 69. Sharon, D., Jancke, D., Chavane, F., Na'aman, S., and Grinvald, A. (2007). Cortical
462 Response Field Dynamics in Cat Visual Cortex. Cerebral Cortex 17, 2866–2877.

463 70. Xu, W., Huang, X., Takagaki, K., and Wu, J. (2007). Compression and Reflection of
464 Visually Evoked Cortical Waves. Neuron 55, 119–129.

465 71. Takagaki, K., Zhang, C., Wu, J.-Y., and Lippert, M.T. (2008). Crossmodal propagation
466 of sensory-evoked and spontaneous activity in the rat neocortex. Neuroscience Letters 431,
467 191–196.

468 72. Nauhaus, I., Busse, L., Ringach, D.L., and Carandini, M. (2012). Robustness of
469 Traveling Waves in Ongoing Activity of Visual Cortex. J. Neurosci. 32, 3088–3094.

470 73. Nauhaus, I., Busse, L., Carandini, M., and Ringach, D.L. (2009). Stimulus contrast
471 modulates functional connectivity in visual cortex. Nat Neurosci 12, 70–76.

472 74. Gao, X., Xu, W., Wang, Z., Takagaki, K., Li, B., and Wu, J. -y. (2012). Interactions
473 between two propagating waves in rat visual cortex. Neuroscience 216, 57–69.

474 75. Rekauzke, S., Nortmann, N., Staadt, R., Hock, H.S., Schöner, G., and Jancke, D.
475 (2016). Temporal Asymmetry in Dark–Bright Processing Initiates Propagating Activity across
476 Primary Visual Cortex. J. Neurosci. 36, 1902–1913.

477 76. Slovin, H., Arieli, A., Hildesheim, R., and Grinvald, A. (2002). Long-Term Voltage-
478 Sensitive Dye Imaging Reveals Cortical Dynamics in Behaving Monkeys. Journal of
479 Neurophysiology 88, 3421–3438.

480 77. Chen, Y., Geisler, W.S., and Seidemann, E. (2006). Optimal decoding of correlated
481 neural population responses in the primate visual cortex. Nat Neurosci 9, 1412–1420.

482 78. Sit, Y.F., Chen, Y., Geisler, W.S., Miikkulainen, R., and Seidemann, E. (2009). Complex
483 Dynamics of V1 Population Responses Explained by a Simple Gain-Control Model. Neuron
484 64, 943–956.

485 79. Reynaud, A., Masson, G.S., and Chavane, F. (2012). Dynamics of Local Input
486 Normalization Result from Balanced Short- and Long-Range Intracortical Interactions in Area
487 V1. J. Neurosci. 32, 12558–12569.

488 80. Zhang, Q., Wen, Y., Zhang, D., She, L., Wu, J., Dan, Y., and Poo, M. (2012). Priming
489 with real motion biases visual cortical response to bistable apparent motion. PNAS 109,
490 20691–20696.

491 81. Yang, Z., Heeger, D.J., Blake, R., and Seidemann, E. (2015). Long-range traveling
492 waves of activity triggered by local dichoptic stimulation in V1 of behaving monkeys. Journal
493 of Neurophysiology 113, 277–294.

494 82. Chemla, S., Reynaud, A., Volo, M. di, Zerlaut, Y., Perrinet, L., Destexhe, A., and
495 Chavane, F. (2019). Suppressive Traveling Waves Shape Representations of Illusory Motion
496 in Primary Visual Cortex of Awake Primate. J. Neurosci. 39, 4282–4298.

497 83. Petersen, C.C.H., Grinvald, A., and Sakmann, B. (2003). Spatiotemporal Dynamics of
498 Sensory Responses in Layer 2/3 of Rat Barrel Cortex Measured In Vivo by Voltage-Sensitive
499 Dye Imaging Combined with Whole-Cell Voltage Recordings and Neuron Reconstructions. J.
500 Neurosci. 23, 1298–1309.

501 84. Derdikman, D., Hildesheim, R., Ahissar, E., Arieli, A., and Grinvald, A. (2003). Imaging
502 Spatiotemporal Dynamics of Surround Inhibition in the Barrels Somatosensory Cortex. J.
503 Neurosci. 23, 3100–3105.

504 85. Tsytsarev, V., Yamazaki, T., Ribot, J., and Tanaka, S. (2004). Sound frequency
505 representation in cat auditory cortex. NeuroImage 23, 1246–1255.

506 86. Civillico, E.F., and Contreras, D. (2006). Integration of Evoked Responses in
507 Supragranular Cortex Studied With Optical Recordings In Vivo. Journal of Neurophysiology
508 96, 336–351.

509 87. Song, W.-J., Kawaguchi, H., Totoki, S., Inoue, Y., Katura, T., Maeda, S., Inagaki, S.,
510 Shirasawa, H., and Nishimura, M. (2006). Cortical Intrinsic Circuits Can Support Activity
511 Propagation through an Isofrequency Strip of the Guinea Pig Primary Auditory Cortex.
512 Cerebral Cortex 16, 718–729.

513 88. Nishimura, M., Shirasawa, H., Kaizo, H., and Song, W.-J. (2007). New Field With
514 Tonotopic Organization in Guinea Pig Auditory Cortex. Journal of Neurophysiology 97, 927–
515 932.

516 89. Reimer, A., Hubka, P., Engel, A.K., and Kral, A. (2011). Fast Propagating Waves within
517 the Rodent Auditory Cortex. Cerebral Cortex 21, 166–177.

518 90. Petersen, C.C.H., Hahn, T.T.G., Mehta, M., Grinvald, A., and Sakmann, B. (2003).
519 Interaction of sensory responses with spontaneous depolarization in layer 2/3 barrel cortex.
520 PNAS 100, 13638–13643.

521 91. Ferezou, I., Haiss, F., Gentet, L.J., Aronoff, R., Weber, B., and Petersen, C.C.H. (2007).
522 Spatiotemporal Dynamics of Cortical Sensorimotor Integration in Behaving Mice. Neuron 56,
523 907–923.

524 92. Ferezou, I., Bolea, S., and Petersen, C.C.H. (2006). Visualizing the Cortical
525 Representation of Whisker Touch: Voltage-Sensitive Dye Imaging in Freely Moving Mice.
526 Neuron 50, 617–629.

527 93. Luczak, A., Barthó, P., Marguet, S.L., Buzsáki, G., and Harris, K.D. (2007). Sequential
528 structure of neocortical spontaneous activity in vivo. PNAS 104, 347–352.

529 94. Witte, R.S., Rousche, P.J., and Kipke, D.R. (2007). Fast wave propagation in auditory
530 cortex of an awake cat using a chronic microelectrode array. J. Neural Eng. 4, 68–78.

531 95. Cinelli, A.R., Hamilton, K.A., and Kauer, J.S. (1995). Salamander olfactory bulb
532 neuronal activity observed by video rate, voltage-sensitive dye imaging. III. Spatial and
533 temporal properties of responses evoked by odorant stimulation. Journal of Neurophysiology
534 73, 2053–2071.

535 96. Cinelli, A.R., and Kauer, J.S. (1995). Salamander olfactory bulb neuronal activity
536 observed by video rate, voltage-sensitive dye imaging. II. Spatial and temporal properties of
537 responses evoked by electric stimulation. Journal of Neurophysiology 73, 2033–2052.

538 97. Orbach, H.S., and Cohen, L.B. (1983). Optical monitoring of activity from many areas
539 of the in vitro and in vivo salamander olfactory bulb: a new method for studying functional
540 organization in the vertebrate central nervous system. J. Neurosci. 3, 2251–2262.

541 98. Prechtl, J.C., Bullock, T.H., and Kleinfeld, D. (2000). Direct evidence for local oscillatory
542 current sources and intracortical phase gradients in turtle visual cortex. PNAS 97, 877–882.

543 99. Prechtl, J.C., Cohen, L.B., Pesaran, B., Mitra, P.P., and Kleinfeld, D. (1997). Visual
544 stimuli induce waves of electrical activity in turtle cortex. PNAS 94, 7621–7626.

545 100. Lam, Y.-W., Cohen, L.B., and Zochowski, M.R. (2003). Odorant specificity of three
546 oscillations and the DC signal in the turtle olfactory bulb. European Journal of Neuroscience
547 17, 436–446.

548 101. Lam, Y.-W., Cohen, L.B., Wachowiak, M., and Zochowski, M.R. (2000). Odors Elicit
549 Three Different Oscillations in the Turtle Olfactory Bulb. J. Neurosci. 20, 749–762.

550 102. Rubino, D., Robbins, K.A., and Hatsopoulos, N.G. (2006). Propagating waves mediate
551 information transfer in the motor cortex. Nat Neurosci 9, 1549–1557.

552 103. Takahashi, K., Kim, S., Coleman, T.P., Brown, K.A., Suminski, A.J., Best, M.D., and
553 Hatsopoulos, N.G. (2015). Large-scale spatiotemporal spike patterning consistent with wave
554 propagation in motor cortex. Nat Commun 6, 7169, 1-11.

555 104. Besserve, M., Lowe, S.C., Logothetis, N.K., Schölkopf, B., and Panzeri, S. (2015).
556 Shifts of Gamma Phase across Primary Visual Cortical Sites Reflect Dynamic Stimulus-
557 Modulated Information Transfer. PLOS Biology 13, e1002257, 1-29.

558 105. Carrasco, M. (2011). Visual attention: The past 25 years. Vision Research 51, 1484–
559 1525.

560 106. Dugué, L., Merriam, E.P., Heeger, D.J., and Carrasco, M. (2020). Differential impact of
561 endogenous and exogenous attention on activity in human visual cortex. Sci Rep 10, 21274,
562 1-16.

563 107. Dugué, L., Merriam, E.P., Heeger, D.J., and Carrasco, M. (2018). Specific Visual
564 Subregions of TPJ Mediate Reorienting of Spatial Attention. Cerebral Cortex 28, 2375–2390.

565 108. Dugué, L., and VanRullen, R. (2017). Transcranial Magnetic Stimulation Reveals
566 Intrinsic Perceptual and Attentional Rhythms. Frontiers in Neuroscience 11, 1-7.

567 109. Landau, A.N., and Fries, P. (2012). Attention Samples Stimuli Rhythmically. Current
568 Biology 22, 1000–1004.

569 110. Fiebelkorn, I.C., Saalmann, Y.B., and Kastner, S. (2013). Rhythmic Sampling within
570 and between Objects despite Sustained Attention at a Cued Location. Current Biology 23,
571 2553–2558.

572 111. Song, K., Meng, M., Chen, L., Zhou, K., and Luo, H. (2014). Behavioral Oscillations in
573 Attention: Rhythmic α Pulses Mediated through θ Band. J. Neurosci. 34, 4837–4844.

574 112. Huang, Y., Chen, L., and Luo, H. (2015). Behavioral Oscillation in Priming: Competing
575 Perceptual Predictions Conveyed in Alternating Theta-Band Rhythms. J. Neurosci. 35, 2830–
576 2837.

577 113. Dugué, L., Beck, A.-A., Marque, P., and VanRullen, R. (2019). Contribution of FEF to
578 Attentional Periodicity during Visual Search: A TMS Study. eNeuro 6, 1-10.

579 114. Strasburger, H., Rentschler, I., and Jüttner, M. (2011). Peripheral vision and pattern
580 recognition: A review. Journal of vision, 11(5):13, 1-82.

581 115. Delorme, A., and Makeig, S. (2004). EEGLAB: an open source toolbox for analysis of
582 single-trial EEG dynamics including independent component analysis. Journal of
583 Neuroscience Methods 134, 9–21.

584 116. Rossion, B., Prieto, E.A., Boremanse, A., Kuefner, D., and Van Belle, G. (2012). A
585 steady-state visual evoked potential approach to individual face perception: Effect of inversion,
586 contrast-reversal and temporal dynamics. NeuroImage 63, 1585–1600.

587 117. Liu-Shuang, J., Norcia, A.M., and Rossion, B. (2014). An objective index of individual
588 face discrimination in the right occipito-temporal cortex by means of fast periodic oddball
589 stimulation. Neuropsychologia 52, 57–72.

590 118. Vanrullen, R., and Dubois, J. (2011). The Psychophysics of Brain Rhythms. Front.
591 Psychol. 1-10.

592 119. Carrasco, M., and McElree, B. (2001). Covert attention accelerates the rate of visual
593 information processing. Proceedings of the National Academy of Sciences 98, 5363–5367.

120. Reed, A.V. (1973). Speed-accuracy trade-off in recognition memory. Science 181, 574–576.

121. Wickelgren, W.A. (1977). Speed-accuracy tradeoff and information processing dynamics. Acta Psychologica 41, 67–85.

122. Watt, J., Borhani, R., and Katsaggelos, A.K. (2020). Machine Learning Refined: Foundations, Algorithms, and Applications (Cambridge University Press).

123. Fawcett, I.P., Barnes, G.R., Hillebrand, A., and Singh, K.D. (2004). The temporal frequency tuning of human visual cortex investigated using synthetic aperture magnetometry. NeuroImage 21, 1542–1553.

124. Srinivasan, R., Fornari, E., Knyazeva, M.G., Meuli, R., and Maeder, P. (2007). fMRI responses in medial frontal cortex that depend on the temporal frequency of visual input. Exp Brain Res 180, 677–691.

125. Meteyard, L., and Davies, R.A.I. (2020). Best practice guidance for linear mixed-effects models in psychological science. Journal of Memory and Language 112, 104092, 1-83.

126. VanRullen, R. (2016). How to Evaluate Phase Differences between Trial Groups in Ongoing Electrophysiological Signals. Frontiers in Neuroscience 10.1-22.

127. Cohen, M.X. (2014). Analyzing Neural Time Series Data: Theory and Practice (MIT Press).

128. Berens, P. (2009). CircStat: A MATLAB Toolbox for Circular Statistics. Journal of Statistical Software 31, 1–21.

STAR Methods

Participants

18 participants (9 females, 16 right-handed, mean ± sd age: 26.2 ± 4.1 years) were recruited for the experiment. Three were excluded because they did not fulfill at least one of the analysis criteria (see analysis section below). 15 participants (7 females, 13 right-handed, mean ± sd age: 25.5 ± 3 years) were recruited for an additional control experiment (see **Supplemental Information**). All participants were free from medication affecting the central nervous system, reported no history of psychiatric or neurological disorders, gave their written informed consent and were compensated for their participation. The study was approved by the local French ethics committee Ouest IV (IRB #2020-A00859-30) and followed the Declaration of Helsinki.

Stimuli

Stimuli were designed with PsychToolbox 3.0.12, running in Matlab R2014b 64-bit (The MathWorks, Natick, MA), and displayed with a ProPixx Projector (VPixx Technologies, Saint-Bruno, QC, Canada), on a 139 x 77.5 cm projection screen (1920 x 1080 pixels; 480 Hz refresh rate), at 122 cm distance. Three different stimuli were generated: a fixation cross, a peripheral disk, and three small dots (targets). The arms of the fixation cross measured 0.15 degrees of visual angle (°) of length and 0.03° of width. The size and position of the targets were computed according to cortical magnification (Human cortical magnification factor = $\frac{23.07}{eccentricity + 0.75}$ [114]) so that each target (diameter) represented a 0.8 mm portion of cortex spaced by 0.8 mm edge-to-edge (radius: 0.09°, 0.1° and 0.12°; eccentricity: 4.1°, 4.5° and 4.9°). The peripheral disk (inducer) was displayed on the lower right corner at 7.5° of eccentricity (from the center of the disk; radius: 1.75°). The background color was black, and the fixation cross at 50% of contrast relative to the background. Target contrasts were titrated for each participant, each position, and each frequency, using a staircase procedure (see below). The peripheral disk was oscillating sinusoidally in luminance, from black to white (i.e., from 0% to 100% of contrast; one period: black-to-white-to-black), at frequencies in the theta and alpha range: 4.07, 6.13, 8.27 and 10.43 Hz. For clarity, we rounded these values to 4, 6, 8, and 10 Hz.

Eye tracker

Participant's head was maintained with a headrest and chinrest. An infrared video-camera system (EyeLink 1000 plus 5.08, SR Research, Ottawa, Canada) was used to ensure that participants maintained their gaze on the fixation cross throughout the block. The block only started when participants was successfully maintaining fixation. When a gaze deviation of >2° from the center of the screen was detected during the presentation of a target (-150 ms to +100 ms around target onset) or a blink, we considered that the participant broke fixation and the trial was removed from the analysis (112.6 ± 112.5 trials on average across participants, leading to a total number of trials of 5015.5 ± 209.8 trials per participant). Supernumerary

652 blocks were added at the end of each run to compensate for rejected trials. Participants
653 received feedback at the end of each block to remind them to minimize blinking and to maintain
654 fixation.

655 **EEG**

656 EEG was recorded using a 64-channels actiChamp system (Brain Products GmbH). The
657 ground was placed at the Fpz position, and the right mastoid was used as reference (DC
658 recording; 1000 Hz sampling rate).

659 **Procedure**

660 Participants performed five sessions: four psychophysics sessions (one sessions for each
661 induced frequency; frequency order randomized across participants), and one EEG session.
662 The psychophysics sessions were composed of the staircases and two runs of 50 blocks each.
663 The EEG session contained four runs of 24 blocks each (one run for each induced frequency).

664 For both the staircases and the main task, each block lasted 30 seconds during which the
665 peripheral disk continuously oscillated in luminance. 6 to 18 targets were presented at random
666 times (excluding the first and the last seconds, and with at least one second interval between
667 targets) during three frames (6.3 ms) according to a decreasing probability distribution (~10
668 targets per block on average). The number of targets for the three positions was randomized
669 across blocks (and pseudorandomized across runs). Participants were instructed to press the
670 space bar when they detected a target (in a 1-second time window after which their response
671 was not considered; target presentation and response window composed a trial).

672 A one-up/one-down staircase with decreasing steps was performed separately for each target
673 position to titrate the contrast of the target to reach about 50% detection. Each staircase was
674 composed of 7 blocks, as described above, except that the targets appeared always at the
675 same position. During the main task, target contrasts were adjusted every 15 blocks to
676 maintain the same detection level across the entire session. Target contrasts averaged across
677 participants were 2.59 ± 0.18 %, 1.83 ± 0.11 %, 2.37 ± 0.15 %, for position 1, 2, and 3,

678 respectively, for the 4 Hz-induced frequency; 2.77 ± 0.2 %, 1.9 ± 0.13 %, 2.41 ± 0.15 %, for
679 position 1, 2, and 3, respectively, for 6 Hz; 2.09 ± 0.24 %, 1.94 ± 0.15 %, 2.43 ± 0.16 %, for
680 position 1, 2, and 3, respectively, for 8 Hz; and 2.82 ± 0.3 %, 1.88 ± 0.16 %, 2.32 ± 0.14 %, for
681 position 1, 2, and 3, respectively, for 10 Hz.

682 **EEG Analysis**

683 Analyses were performed with EEGLab 13.6.5 ([115]; Swartz Center for Computational
684 Neuroscience, UC San Diego, California) running in Matlab.

685 *Preprocessing.* EEG data and channel location were imported into EEGLab. EEG data were
686 re-referenced to the average of the right and left mastoids. A high-pass filter at 0.1 Hz and a
687 notch filter between 48 and 52 Hz were applied, to respectively remove slow drifts and 50 Hz
688 electric noise. The signal was further down sampled to 512 Hz. Visual inspection allowed to
689 identify electrodes with low signal-to-noise ratio, which were then interpolated (spherical
690 interpolation). Independent component analysis (ICA) was performed to remove blink
691 components, after a visual inspection of their time courses and topographies. Data were
692 epoched from trial onset (0s) to the end of the block (+30s).

693 *Fast Fourier Transform.* FFT were computed (Matlab function: fft) on epoched EEG data, and
694 the amplitude was extracted for each electrode, epoch, and frequency. The signal-to-noise
695 ratio (SNR) was computed on the amplitude extracted from the FFT, for each electrode, as the
696 ratio of the amplitude at each frequency to the average of the 20 surroundings frequencies (10
697 frequencies on either side, excluding the immediately adjacent frequencies; note that the SNR
698 could mathematically not be estimated at the edges of the spectra), as described in [116, 117].
699 SNR averaged across participants, epochs and electrodes were plotted to ensure that the
700 oscillating disk successfully induced brain signal at the corresponding frequency.
701 Topographies were plotted at the peak of the induced frequency and its first harmonic.

702 *Event-Related Potentials (ERPs).* Previously preprocessed EEG timeseries were further
703 bandpass filtered between 1.5 Hz and 30 Hz, and baseline corrected from -400 to 0 ms from

block onset. Epochs of one second were defined, excluding the first second of each 30 seconds-block to avoid the transient EEG response due to stimulus onset. Participants' ERPs were computed as the averaged of all resulting epochs. ERPs averaged across participants for electrode Oz were plotted with the standard error of the mean. Electrode Oz was selected because it is the electrode with the highest amplitude across the four induced frequencies. The ERP plots allowed us to identify that the brain oscillation induced by the oscillating disk was a complex oscillation composed of the induced frequency and its first harmonic. Therefore, we fitted the behavioral data to a complex sine function.

FFT on ERPs. FFT was computed (1500 points zero padding) on the Oz ERP for each participant. The amplitude was extracted, and the SNR was computed as previously described.

Behavioral analysis

Behavioral analyses were performed with Matlab R2014b (The MathWorks, Natick, MA). The following dependent variables were computed: hit rates as main dependent variable, i.e., percentage of correct responses, and median reaction times as secondary dependent variables, for each target position and frequency. Hit rates averaged across frequencies were 47.55 ± 0.74 %, 45.75 ± 0.73 %, and 44.78 ± 0.69 % for position 1, 2, and 3, respectively. Median reaction times averaged across frequencies were 511 ± 8 ms, 512 ± 8 ms, and 510 ± 9 ms for position 1, 2, and 3, respectively. A two-way repeated-measures ANOVA was performed for each dependent variable to assess the effect of frequency and target position. For hit rates, there was a main effect of target position ($F(2, 28) = 11.02$, $SS = 237.43$, p-value < 0.01, $eta^2 = 44.04$) but no effect of frequency ($F(3, 42) = 0.45$, $SS = 10.19$, p-value $= 0.71$, $eta^2 = 3.15$) nor of their interaction ($F(6, 84) = 0.29$, $SS = 10.82$, p-value $= 0.93$). For median reaction times, there was a main effect of frequency ($F(3, 42) = 4.21$, $SS = 5111.99$, p-value $= 0.01$, $eta^2 = 23.14$), but no main effect of target position ($F(2, 28) = 0.34$, $SS = 98.34$, p-value $= 0.71$, $eta^2 = 2.39$), nor of their interaction ($F(6, 84) = 0.74$, $SS = 456.48$, p-value $= 0.61$). The absence of significant interaction between frequency and target positions in any of these two tests confirm successful contrast manipulation, i.e., the detection performance does not rely

on an interaction between frequency and target positions. As argued in [11] and [118], reaction time fluctuations do not unambiguously demonstrate rhythms in cognitive processes as they can also be the by-product of the external stimulation and are sensitive to changes in decision criteria [106, 107, 119-121]. The behavioral phase analyses thus focused on hit rates as the main dependent variable.

Phase effect on detection performance. Each target was assigned to one of 7 phase bins of the periodic stimulation depending on the delay at which they appeared during the block. Hit and false alarm rates were computed for each target position, frequency, and phase bin. For each block and target position, false alarms (participants reported perceiving a target while no target had been presented; participants were instructed to respond in the 1s-window following the target, after which the response was considered a false alarm) were binned as a function of the phase of the oscillating disk. To allow for a fair comparison between hit and false alarms, only the false alarms that were in the same phase bins as the targets (but in a different 100-ms period) were considered for further analysis (e.g., if 2 targets were presented at position 1 within the given block, and binned in bins number 2 and 6, only false alarms that were binned in bins number 2 and 6 were considered for further analysis). To allocate a false alarm to one of the three target positions (a false alarm is, by definition, at none of the position), a bootstrap procedure was performed (100 repetitions). One participant was excluded from the analysis at this point because the number of false alarms exceeded the number of targets presented.

Given the ERP results (see **Figure 2**) showing a complex neural response composed of the induced frequency and its first harmonic, behavioral data were fitted to a complex sine function (Eq1) with the following free parameters: $x[1]$ and $x[2]$ the amplitude and the phase offset of the induced frequency, respectively, $x[3]$ and $x[4]$ the amplitude and the phase offset of the first harmonic, respectively, and $x[5]$ the baseline level. To find the parameters that best fit the data, we used a Least Squares cost function, i.e., the cost function computed the total squared errors, i.e., the sum of squared errors, between the fit and the data, thus giving a measure of

how well the data are fitted. The best fit is the one whose parameters minimize the total error [122].

$$(Eq1)\ \ x[1] * \left(sin(2 * \pi * T + x[2])\right) + \ x[3] * (sin\left(2 * \pi * \frac{T}{2} + x[4]\right)) + \ x[5]$$

We then performed a Monte Carlo procedure on the fitted amplitude to evaluate whether the fitted data was modulated periodically as a function of the phase. 50,000 surrogates were generated for each participant, target position and frequency, by randomly assigning correct responses, i.e., for each target, we randomly assigned an incorrect or a correct response based on the averaged performance, and false alarms, i.e., a number of false alarms at an associated random delay was randomly assigned to each block, based on the average number of false alarms throughout the experiment. Hit and false alarm rates were then computed for each phase bin, position, and frequency, and fitted to the same sine function (Eq1). The surrogate distributions of the 50,000 fitted amplitudes for the induced frequency and its first harmonic separately were compared to the empirical fitted amplitudes. P-values were obtained by computing the proportion of fitted amplitudes equal or higher than the empirical fitted amplitude (fitted amplitudes: free parameters $x[1]$ and $x[3]$ from (Eq1)). Two participants were excluded from the analysis at this point because no significant phase effect was observed in the hit rates at position 1 in the 4-Hz condition (Bonferroni correction for multiple comparisons, i.e., the three positions; p-value threshold of 0.01). The reasoning for selecting this exclusion criterium is that a slow 4-Hz stimulation should induce a large effect in behavior [28, 123, 124], and such an effect should be the strongest the closest from the inducer. Note that false alarms were low in each phase bins (< 0.5%) and not significantly modulated periodically (except for the induced frequency 8 Hz, at position 1, $p < 0.01$; the p-value for the others induced frequencies and positions were not significant: Bonferroni correction across frequencies and positions, p-value threshold < 0.01, corresponding to a Z-score threshold of 2.64, and a Cohen's d threshold of 1.86). Consequently, in the next steps of the analysis, only hit rates were considered.

A group level analysis was also performed. Empirical and surrogate data were averaged across participants, and the same Monte Carlo procedure as presented above was performed. Bonferroni (p-value threshold < 0.01) was used to correct for multiple comparisons.

Variance explained by the spatial organization of targets. We hypothesized that the spatial organization of brain oscillations should explain a larger variance in the behavioral phase effect. To test this hypothesis, the hit rate was computed for each frequency and phase bin, regardless of target position. The hit rate was then fitted to the complex sine function (Eq1) and the amplitude modulation, i.e., difference in hit rate between the optimal and the non-optimal phase, was computed for each frequency and participant. Two-tailed t-tests were used to assess whether the amplitude modulation averaged across the three target positions was significantly different than the amplitude modulation computed across targets independently of their position, for each frequency.

Optimal phase shift between target positions for each induced brain oscillation. The optimal phase, i.e., the position on the fitted curve at maximal performance, was extracted for each target position and frequency, on data averaged across participants. We asked whether the optimal phase shift as a function of target positions was different between the four induced frequency conditions, i.e., whether there is a significant interaction between frequency and target position. We used a linear mixed effect model [125] to test for such an interaction.

We first computed phase-locking values for each optimal phase. The phase-locking value is obtained by dividing complex vectors, i.e., amplitude and phase information, by their length (i.e., amplitude), thus normalizing for amplitude and keeping only the phase, and then, computing the mean across the normalized vectors [126, 127]. Thus, to convert our measure of optimal phase in phase-locking values: 1) We created a distribution of optimal phases. The distribution was obtained with a bootstrap procedure. We generated 1,000 surrogate datasets by randomly selecting trials with an equal probability sampling from the initial datasets, and computing the optimal phase from each surrogate dataset, for each participant, frequency, and target position. 2) We converted the obtained optimal phases into complex vectors. The phase-

locking values were fitted to a linear mixed effects model with frequencies and target positions as fixed effects, and participants as random effect. Post-hoc tests allowed to assess which specific frequencies displayed a shift in the optimal phase. Here, the optimal phases were converted in radians. We created a one-cycle sine wave with the phase offset of the oscillating disk and extracted the phase values in radians along the entire cycle. We were then able to do a correspondence between the optimal phase extracted from data fitting, and the phase values in radians extracted from this one-cycle sine wave fit. Note that the same procedure was applied participant-by-participant to obtain rose plots of the individual optimal phase with the function circ_plot from the Circular Statistics Toolbox ([128], P. Berens, CircStat: A Matlab Toolbox for Circular Statistics, Journal of Statistical Software, Volume 31, Issue 10, 2009, http://www.jstatsoft.org/v31/i10), for each frequency and target position. The optimal phase in radians was compared between target positions by computing the pairwise phase difference with the function circ_dist from the Circular Statistics Toolbox. Statistics were performed with a Monte Carlo procedure. 50 000 datasets were created for each target position and frequency, by randomly assigning detection performance according to the average values for each pair of positions (positions 1 and 2, 1 and 3, 2 and 3), and by considering the original distribution of the number of targets across participants and phase bins. The data were fitted to the sine function (Eq1). The optimal phase was computed and converted in radians, and the phase difference was obtained for each pair of position. Thus, we obtained a surrogate of 50 000 phase differences for each pair of positions and each frequency. By computing the proportion of surrogate phase difference equal or higher than the real phase difference, we obtained p-values, FDR corrected for multiple comparisons across target positions and frequencies (p-value threshold of 0.01).

Supplemental Information

Supplemental Figure

The amplitude modulation, i.e., difference in hit rate between the optimal and the non-optimal phase, was computed on data averaged across participants, for each frequency and target position. A two-way repeated-measures ANOVA revealed a significant main effect of the frequency ($F(3, 42) = 31.48$, SS = 0.77, p-value < 0.01, $eta^2 = 69.22$), and no main effect of the target position ($F(2, 28) = 1.10$, SS = 0.01, p-value = 0.34, $eta^2 = 7.29$), nor of the interaction ($F(6, 84) = 0.73$, SS = 0.02, p-value = 0.62). The amplitude modulation was of 53.16 ± 2.91 % for 4 Hz, 49.04 ± 3.55 % for 6 Hz, 40.24 ± 2.84 % for 8 Hz, and 36.87 ± 2.59 % for 10 Hz (**Figure S1**). Post-hoc two-tailed t-tests showed that the amplitude modulation was higher for 4 Hz compared to 6 Hz (p-value = 0.03, Cohen's d = 0.32, CI = [0.01; 0.07]), 8 Hz (p-value < 0.01, Cohen's d = 1.16, CI = [0.09; 0.16]) and 10 Hz (p-value < 0.01, Cohen's d = 1.52, CI = [0.12; 0.20]), for 6 Hz compared to 8 Hz (p-value < 0.01, Cohen's d = 0.70, CI = [0.05; 0.12]) and 10 Hz (p-value < 0.01, Cohen's d = 1.01, CI = [0.08; 0.15]), and higher for 8 Hz compared to 10 Hz (p-value = 0.05, Cohen's d = 0.32, CI = [0; 0.06]). In summary, the amplitude modulation decreases with increasing frequency but is constant across target positions.

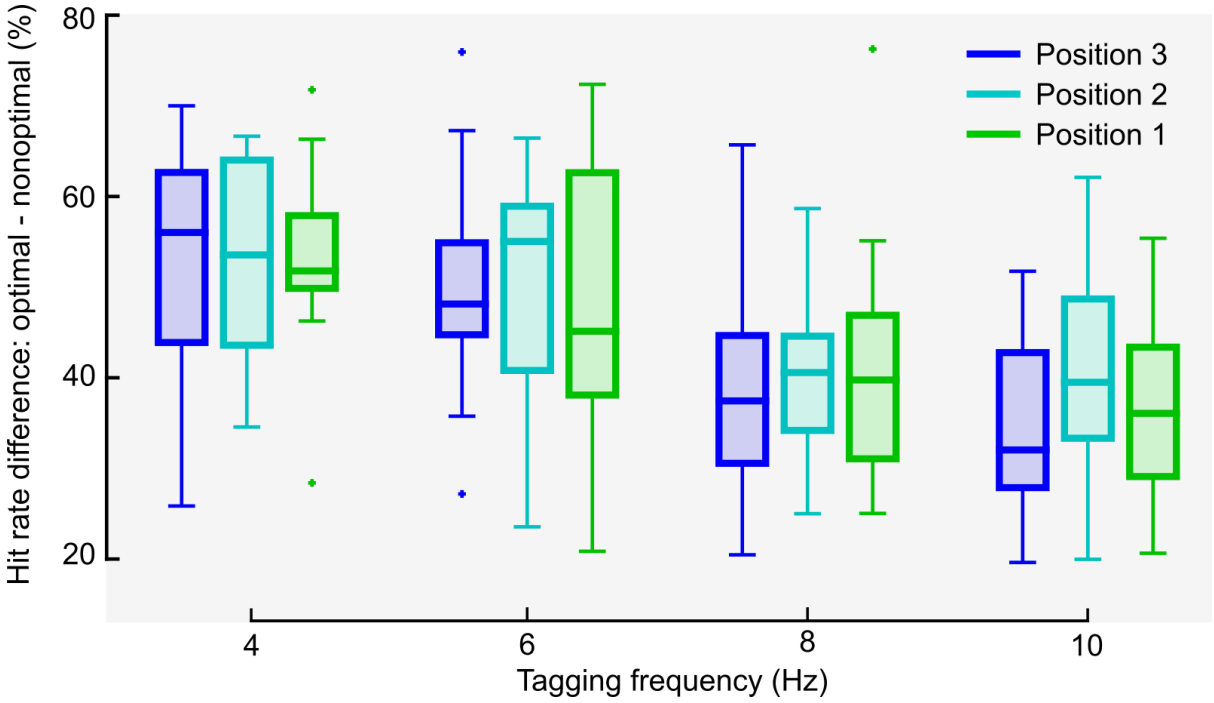

Figure S1. The amplitude modulation decreased with increasing induced frequency. *Amplitude computed as the difference between the maximum and the minimum hit rate. Dots, individual outlier data. A two-way repeated-measures ANOVA revealed a significant main effect of frequency ($F(3, 42) = 31.48$, SS = 0.77, p-value < 0.01, $eta^2 = 69.22$).*

Control experiment

Procedure

The targets were of same size and location as in the main experiment. The peripheral disk was, however, not modulated sinusoidally but was flashed (during three frames, for a total of 6.3 ms) at 7 different levels of luminance (7 contrast levels: 5%, 20.8%, 36.7%, 52.5%, 68.3%, 84.2% and 100%) at the same time as target onset to test for luminance masking. There was 20% of catch trials in which the disk was flashed but not the target.

As for the main experiment, the control experiment first included a staircase procedure to adjust the contrast of each target, for each participant, to reach 50% detection. In 7 blocks, the luminance of the disk was set at 50% contrast. For each block, 6 to 18 targets were presented (~10 targets/trials per block on average), thus the staircase procedure contained an average of 70 trials.

Then, participants performed four runs of 38 blocks each in two separate experimental sessions of approximately 1h30 each (no EEG recording for this control experiment). Each contrast level was displayed the same number of times (~217 targets per contrast level). Target contrasts were adjusted every 15 blocks to maintain the same detection level across the entire session.

Analyses

47.5 ± 56.4 targets were rejected from the analysis due to blinks or saccade eye movements. Hit rates, i.e., percentage of correct detection, median reaction times and target contrasts were computed for each target position. Hit rates were 57.18 ± 1.1 %, 51.74 ± 0.35 %, and 45.82 ± 0.76 % for position 1, 2 and 3, respectively. Median reaction times were 474 ± 2 ms, 511 ± 3 ms, and 525 ± 3 ms, for position 1, 2, and 3, respectively. Target contrasts were 0.61 ± 0.01 %, 1.16 ± 0.04 %, and 0.71 ± 0.02 %, for position 1, 2, and 3, respectively. A one-way repeated-measures ANOVA was performed for each dependent variable to assess the effect of target position. For hit rates, there was no main effect of target position ($F(1,14) = 2.52$, p-value = 0.09, $eta^2 = 15.29$). For median reaction times, there was also no main effect of target position ($F(1,14) = 1.24$, p-value = 0.30, $eta^2 = 8.16$). The absence of a significant main effect of target positions in any of these two tests confirm successful contrast manipulation. For target contrast, there was a main effect of target position ($F(1,14) = 13.68$, p-value < 0.01, $eta^2 = 49.42$), which is coherent with the staircase manipulation.

Targets were binned according to the level of luminance of the simultaneously presented disk. To emulate an oscillatory cycle (which, in the main experiment, goes from 0% contrast to 100% and back to 0%), we used a bootstrap procedure (5 000 repetitions) randomly assigning half of the targets to one half of the cycle (from contrast 0% to 100%), while the other half was assigned to the second half of the cycle (from contrast 100% to 0%), thus resulting in 13 luminance levels.

The number of false alarms (i.e., participants responded a target was present while it was absent), and the number of hits were computed for each target position and for the 13 luminance levels. Individual data and data averaged across participants were fit to a one-cycle sine function (EqS1) with the following free parameters: the amplitude, $x[1]$, the phase offset, $x[2]$, the baseline, $x[3]$. To find the parameters that best fit the data, we used a Least Squares cost function, i.e., the cost function computed the total squared errors, i.e., the sum of squared error, between the fit and the data, giving a measure of how well the data are fitted. The best fit is the one whose parameters minimize the total error [122].

$$(EqS1)\ \ (x[1] * \big(sin(2 * \pi * T + x[2])\big) + \ x[3]$$

We performed a Monte Carlo procedure on the fitted amplitudes to assess whether the fitted data was modulated periodically by the luminance disk. 50 000 surrogates were generated for each participant by randomly assigning detection performance based on the average performance at each contrast and position (as for the empirical data, an oscillatory cycle was emulated using a bootstrap procedure). The surrogate data was fit to the one-cycle sine function (EqS1). The empirical averaged data was compared

to the averaged surrogate distribution by computing the proportion of fitted amplitudes equal or higher than the empirical fitted amplitude. P-values were corrected for multiple comparisons using Bonferroni correction (p-value threshold of 0.01). There was no significant effect of luminance, at any target position, for the false alarm ratio and thus we did not consider this variable any further.

The optimal phase, i.e., phase of highest performance, was computed for each target position on data averaged across participants. To study whether the optimal phase shifted as a function of target positions, we computed the pairwise phase difference and assessed the significance using a Monte Carlo procedure. 50 000 datasets were created for each target position by randomly assigning detection performance according to the average values for each pair of positions (positions 1 and 2, 1 and 3, 2 and 3), and by considering the original distribution of the number of targets across participants and luminance values. The data were fitted to the sine function (EqS1) and the pairwise phase difference was obtained for each pair of positions. We obtained a surrogate of 50 000 phase differences for each pair of positions. P-values were obtained by computing the proportion of surrogate phase differences equal or higher than the empirical phase difference.

Results

To assess whether the periodicity observed in behavioral data was due to luminance masking from the disk, 15 participants performed the above-mentioned control experiment. Detection performance showed a significant oscillatory pattern at each target position (Monte Carlo, Bonferroni corrected across positions, p-value threshold of 0.01, corresponding to a Z-score threshold of 2.12, and a Cohen's d threshold of 1.31, **Figure S2A**).

Seven participants took part in both the main and the control experiment. For these participants, we overlapped in **Figure S2B-H** the sine fits from the control experiment and for the 10 Hz induced frequency from the main experiment. The oscillatory patterns clearly differed between the two experiments. Crucially, unlike in the main experiment, in the control experiment no phase shift between positions was found (p-value = 1, i.e., the pairwise phase differences were the same between the empirical and surrogate datasets).

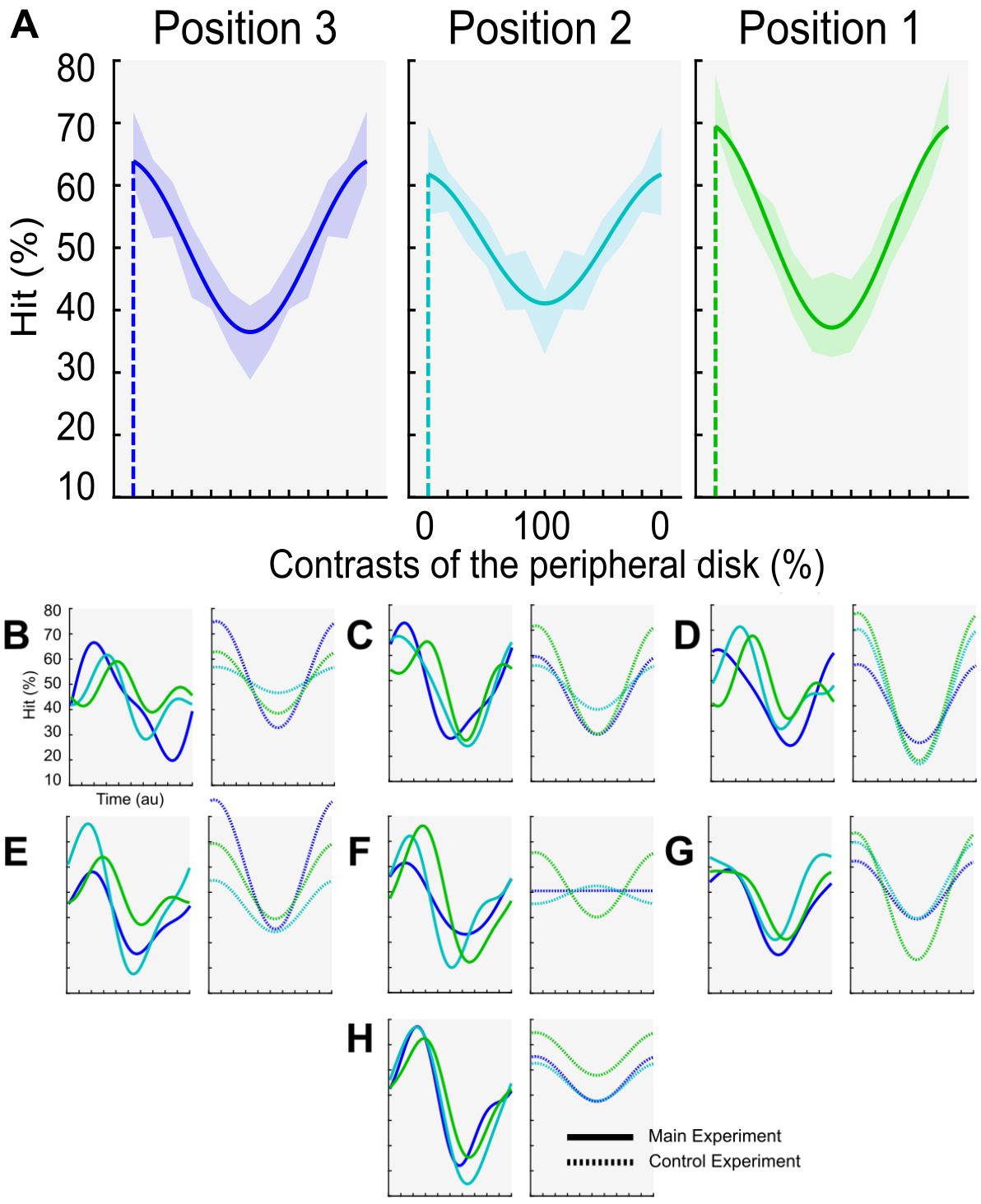

Figure S2. The propagation of perceptual cycles was not due to luminance masking. A. *Hit rate for each 13 luminance levels and the 3 target positions averaged across participants (n=15) and fitted to a one-cycle sine function. Shaded colored area, 95 confidence intervals. Solid line, fit. Dotted line, optimal phase.* ***B – H*** *Results from individual participants for the main experiment on the left and the control Experiment on the right. Green, position 1. Cyan, position 2. Blue, position 3.*

3. A novel stimulus

In our first study (Fakche and Dugué, 2022, bioRxiv), we showed with a psychophysics experiment that the optimal phase for visual perception shifted as a function of the position of visual stimuli in the retinotopic space, suggesting a functional role of alpha induced traveling waves in human early visual areas.

In a second study, we aimed to replicate this result with different parameters, selected to optimize the procedure.

3.1. Introduction

To pursue our investigations on the mesoscopic alpha traveling waves in the human visual cortex, we designed a novel stimulus to induced brain oscillations minimizing low-level luminance masking confound (thus, improving and validating the control experiment performed in the previous study). We decided to use a pattern reversing checkerboard, frequently used in SSVEP studies (Srinivasan et al., 2007; Zhu et al., 2010; Vialatte et al., 2010; Funase et al., 2015; Norcia et al., 2015). This stimulus presents two main advantages: a constant level of luminance, and a square function modulation instead of a sine function. Participants performed a similar threshold visual detection task while a pattern reversing checkerboard disk was presented in the periphery to induce alpha (10 Hz) brain oscillations. We investigated whether we were able to replicate the result of our first study, i.e., periodic stimulation modulates visual perception periodically for each visual stimulus, and that the optimal phase for perception shifts as a function of distance from the stimulating disk, suggesting that perceptual cycles travel across the retinotopic space.

3.2. Materials and Methods

The methods used in this experiment are the same as the ones used in Fakche and Dugué, 2022, bioRxiv. We are only pointing out the differences between the two experiments.

Participants. 16 participants (8 females, 15 right-handed, mean age: 24.9 ± 3.3 years) were included in the study. All participants were free from medication affecting the central nervous system, reported no history of psychiatric or neurological disorders, gave their written informed consent and were compensated for their participation. The study was approved by the local

French ethics committee Ouest IV (IRB #2020-A00859-30) and followed the Declaration of Helsinki.

Stimuli. Each target (diameter) represented 1.3 mm portion of cortex spaced by 1.3 mm edge-to-edge (radius: 0.1°, 0.12° and 0.15°; eccentricity: 3.1°, 3.5° and 4.1°). The peripheral disk was displayed on the lower right corner at 8.37° of eccentricity (from the center of the disk; radius: 4°). The background color was grey, and the fixation cross white. The peripheral disk was filled with a checkerboard composed of 12*12 white and black squares which pattern reversed every 100 ms.

Eye tracker. 16.3 ± 16.9 trials on average across participants were removed from the analysis because participants broke fixation.

Procedure. Participants performed two sessions: one psychophysics session and one EEG session. The psychophysics session was composed of the staircase and two runs of 42 blocks each. The EEG session contained one run of 42 blocks.
Target contrasts averaged across participants were 33.74 ± 2.69 %, 62.24 ± 1.59%, 48.24 ± 2.55 %, for the position 1, 2, and 3.

EEG Analysis. Electrode PO3 was selected for ERP analysis because it was the electrode with the highest amplitude on the topography of the FFT on EEG time series (**Figure 6.3)**.

Behavioral analysis. Hit rates were 50.55 ± 3.01 %, 51.58 ± 1.08 %, and 50.15 ± 1.7 % for position 1, 2, and 3, respectively. Median reaction times were 490 ± 10 ms, 499 ± 9 ms, and 500 ± 7 ms for position 1, 2, and 3, respectively. A one-way repeated-measures ANOVA was performed for each dependent variable to assess the effect of target position. For hit rates, there was no main effect of target position ($F(2, 30) = 0.148$, SS = 17.39, p-value = 0.8634, eta^2 = 0.97), suggesting that we successfully manipulated target contrast across positions. There was a main effect of target position for median reaction times ($F(2, 30) = 4.357$, SS = 996.953, p-value = 0.0218, eta^2 = 22.51) and for target contrasts ($F(2, 30) = 84.902$, SS = 10565.729, p-value < 0.0001, eta^2 = 84.99).

Because we used an inducer modulated by a square function, instead of created a one-cycle sine wave with the phase offset of the oscillating disk to extract the phase values in radians

along the entire circle, we created a one-cycle sine waves with the phase offset observed in the ERPs.

3.3. Results

Participants (n = 16) performed a threshold visual detection task, while a pattern reversing checkerboard disk was presented in the periphery to induce brain oscillations at 10 Hz in the occipital cortex. Near-threshold target stimuli appeared at one of three possible eccentricities between a central fixation cross and the disk (**Figure 6.2**; adjusted according to cortical magnification). We aimed to replicate our previous experiment (Fakche and Dugué, 2022, bioRxiv), and investigate whether the optimal phase for perception shifts as a function of target position.

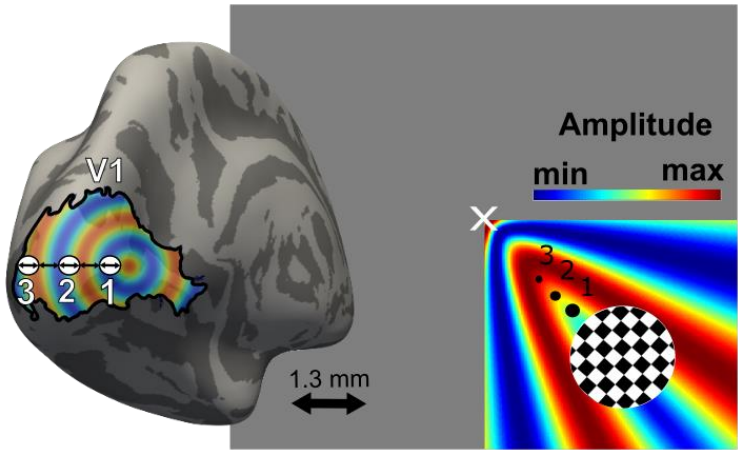

Figure 6.2: Experimental protocol. *A pattern reversing checkerboard disk was presented in the periphery to induce alpha brain oscillations in the occipital cortex (e.g., V1). Participants were instructed to detect visual targets at threshold (50% detection) at three different positions in the retinotopic space (visual targets measured 1.3 mm and were placed 1.3 mm away from each other). The disk was presented for a 30-seconds period during which 6 to 18 targets were presented at random times. We hypothesized that the disk, presented in the lower right corner, induced a brain oscillation that traveled across the retinotopic space (note that we concentrate our predictions to the quadrant in which the disk is presented). At an instant t, position 3 is located at the optimal phase of the oscillation (leading to the highest performance; i.e., max Amplitude), while position 1 is located at the non-optimal phase (i.e., min Amplitude).*

EEG activity was analyzed using a frequency decomposition (Fast Fourier Transform, FFT, performed on the time series for each participant and electrode) and Event-Related Potentials (ERPs) measures to control for successful frequency inducing at 10 Hz and characterize the shape of the evoked response. First, a peak in the spectrum (as measured per

SNR, averaged across participants and electrodes) was identified for the induced frequency, 10 Hz (SNR = 1.56) and its first harmonic, 20 Hz (SNR = 1.39), with topographies showing a brain activity in the occipital cortex, lateralized in the left occipital cortex (the checkboard disk was displayed in the right visual field; **Figure 6.3**). We further computed an FFT on the ERP of electrode PO3. A peak was again identified for the induced frequency (10 Hz, SNR = 2.68) and its first harmonic (20 Hz, SNR = 3.59). ERP analyses showed that the evoked signal was a complex oscillation composed of the induced frequency and its first harmonic (**Figure 6.3**), likely corresponding to an overlap between the periodic brain response (i.e., inducer) and the neuronal population response to individual stimuli (i.e., contrast change), or alternatively, to the nonlinear nature of the visual system (Heinrich, 2010; Norcia et al., 2015). Together, the EEG analyses confirm that we successfully induced 10 Hz oscillation in the visual cortex with a pattern reversing checkerboard, and show that the evoked signal is a complex oscillation composed of the induced frequency and its first harmonic (Heinrich, 2010; Norcia et al., 2015).

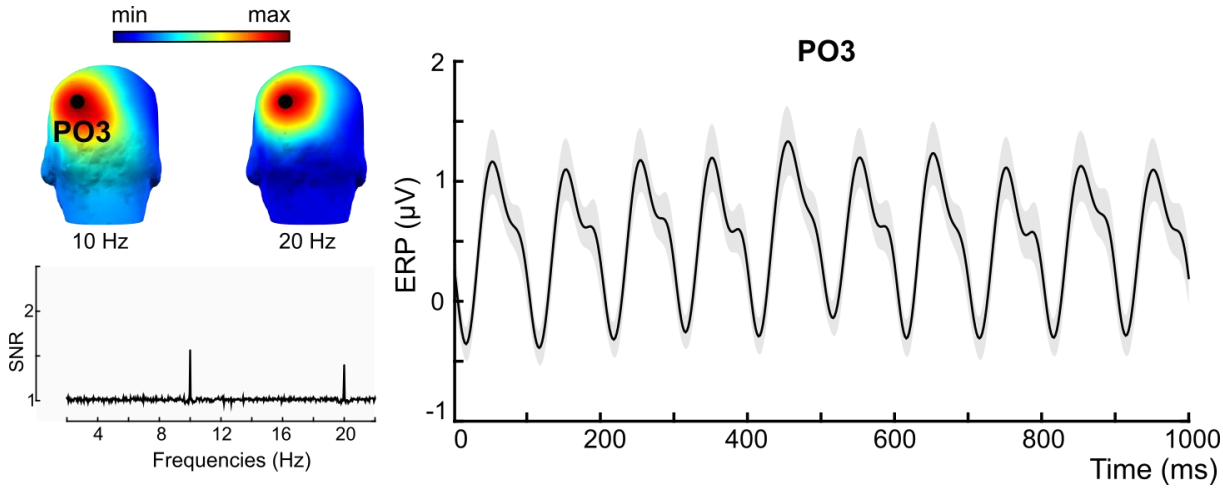

Figure 6.3: The pattern reversing checkerboard disk evoked complex brain oscillations in the visual cortex. *Left panel, Fast Fourier Transform analyses performed on the EEG time series. Signal-to-noise ratio (SNR) amplitude averaged across 16 participants and all 62 electrodes, from 2 to 22 Hz. A peak in SNR was identified for the frequency 10 Hz and its first harmonic 20 Hz. Topographies of the two SNR peaks revealed that we successfully induced brain oscillations in the left visual cortex. Black dot, Electrode PO3. Right panel, ERP analyses. ERP of the PO3 electrode computed on one-second epoch (the first-second epoch was removed to each 30-seconds block to avoid the EEG transient evoked response; each block represented 29 1-second epochs) averaged across participants (n=16). Solid black line, averaged ERP. Shaded area, standard error of the mean.*

Then, we investigated whether detection performance was modulated periodically at 10 Hz, for each target position. Targets (from 6 to 18 targets per 30-seconds-blocks) can appear at

random delays during the periodic disk stimulation (from 1s to 29s from disk onset), and were binned according to the periodic stimulation (7 bins/cycle). In each bin, detection performance was computed as per hit rate (correct target detection), for each participant and target position. Finally, the data were averaged across participants and given the complex shape of the ERP (**Figure 6.3**), fitted to a complex sine function, separately for each target position. Detection performance showed a significant oscillatory pattern for each target position (Monte Carlo, Bonferroni corrected across positions, p-value threshold of 0.01, corresponding to a Z-score threshold of 2.13, and a Cohen's d threshold of 1.26; **Figure 6.4**), and a clear optimal phase (of highest performance). The inducer modulated detection performance periodically, with an amplitude modulation (hit rate difference between the optimal and the non-optimal detection performance) of 45.73 ± 2.9 %, 27.8 ± 2.08 %, and 18.21 ± 1.9 % for position 1, 2, and 3, respectively. We further observed that all 16 participants showed a significant oscillatory pattern (Monte-Carlo, Bonferroni corrected across positions, p-value < 0.01) for the position 1, 7 participants showed a significant oscillatory pattern for the position 2, and for the position 3, only one participant showed a significant oscillatory pattern.

The checkerboard inducer modulated detection performance periodically, however, our results suggest that the amplitude of induced brain oscillation decreased drastically according to the distance of travel. Especially for the position 3, the amplitude of the oscillation appeared to be very low, and consequently, it made it more difficult to estimate the optimal phase for perception at this position. We still performed some exploratory analyses to investigate the presence of traveling perceptual cycles despite the underestimation of the optimal phase at target positions 2 and 3.

To assess whether the optimal phase shifted as a function of target position, we computed the optimal phase difference (reported in degrees for easier readability in **Figure 6.4**) between each pair of target positions (1 and 3, 1 and 2, and 2 and 3). There was a significant shift of the optimal phase between positions 2 and 3 (**Figure 6.4**; Monte Carlo, Bonferroni corrected across pairs, p-value threshold of 0.01, corresponding to a Z-score threshold of 2.13, and a Cohen's d threshold of 1.26), but not between the other pairs of positions ($p > 0.09$). We further observed a significant phase difference (Monte-Carlo, FDR corrected across pairs, p-value < 0.05) between position 2 and 3 for three participants, between position 1 and 3 for three participants, and between position 1 and 2 for five participants.

When converting the phase shift observed into milliseconds (13.1 ms) and given the cortical distance between two target positions (1.3 mm distance edge-to-edge) as well as the

targets' cortical size (1.3 mm diameter), one can estimate that alpha-induced brain oscillations traveled across the retinotopic space at a propagation speed of 0.2 m/s between the position 2 and 3.

Our results suggest that alpha-induced brain oscillations traveled between position 2 and 3. However, the amplitude of the oscillatory pattern was very low for the third position, and almost absent at the level of the participant, leading to a non-robust estimation of the optimal phase for position 3. In addition, when we computed the optimal phase participant by participant (polar plots in **Figure 6.4**), we observed a great interindividual variability.

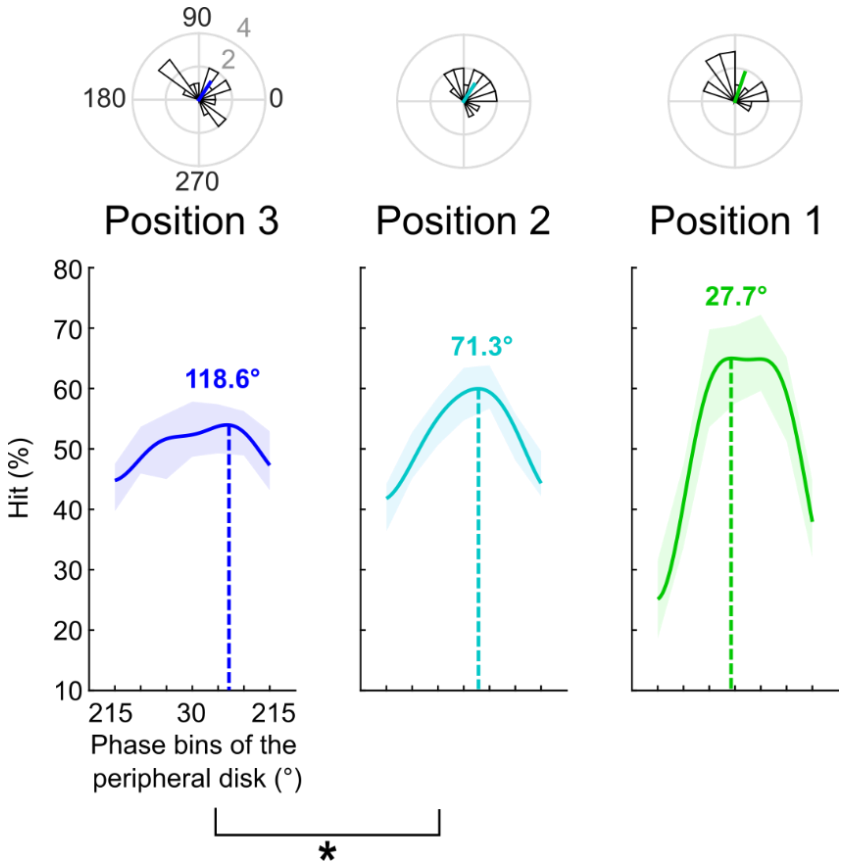

***Figure 6.4: The amplitude of the oscillatory pattern decreased with distance from the checkerboard**. Lower graphs, hit rate averaged across participants (n=16), binned as a function of the phase of the checkerboard, and fitted to a complex sine function. Shaded colored area, 95 confidence intervals. Solid line, Sine fit. Dotted line, Optimal phase in degrees. Upper graphs, rose plot of the optimal phases across participants. Colored solid line, Optimal phases averaged across participants.*

The evoked brain activity was a complex oscillation composed of the induced frequency at 10 Hz and it first harmonic at 20 Hz. We asked whether the induced frequency or the first

harmonic alone could better explain the behavioral performance. To investigate separately the role of the 10 Hz and the 20 Hz component, we repeated the previous analysis with a fit to a one-cycle sine function, on data binned every 100 ms (same binning as previously) and every 50 ms, respectively.

For the 10 Hz component, detection performance averaged across participants showed a significant oscillatory pattern for each target positions (Monte Carlo, Bonferroni corrected across positions, p-value threshold of 0.01, corresponding to a Z-score threshold of 2.13, and a Cohen's d threshold of 1.26). We further observed that 14 participants showed a significant oscillatory pattern (Monte-Carlo, Bonferroni corrected across positions, p-value < 0.01) for position 1, 7 participants showed a significant oscillatory pattern for position 2, and for the position 3, only one participant showed a significant oscillatory pattern. Concerning the phase shift, we found no significant phase difference for any pair of target positions (p-value > 0.14). We also observed a significant phase difference (Monte-Carlo, FDR corrected across positions, p-value < 0.05) between position 1 and 2 for 5 participants, between position 1 and 3 for 6 participants, and between position 1 and 2 for one participant. Our results are very similar between fitting the data binned every 100 ms to the complex sine function compared with fitting to the one-cycle sine function, suggesting a strong role of the 10 Hz component.

For the 20 Hz component, detection performance averaged across participants showed a significant oscillatory pattern only for target position 1 (Monte Carlo, Bonferroni corrected across positions, p-value threshold of 0.01, corresponding to a Z-score threshold of 2.13, and a Cohen's d threshold of 1.26). We further found that two participants showed a significant oscillatory pattern (Monte Carlo, Bonferroni corrected across positions, p-value < 0.01) for the position 1, none for the position 2, and only one for the position 3. Consequently, it seems that the variance explained by the 20 Hz component in our data was very low.

3.4. Discussion

In this study, we aimed to replicate our previous results (Fakche and Dugué, 2022, bioRxiv) with a checkerboard inducer instead of a disk oscillating in luminance to induce alpha brain oscillations in the occipital cortex. The use of this novel stimulus was two-fold: minimize the luminance masking and induce brain oscillations with a stimulus modulated by a square function.

We successfully induced brain oscillations at 10 Hz with our novel stimulus. The pattern reversing checkerboard produced a complex brain activity consisting of the induced frequency

and its first harmonic, coherent with the non-linear nature of the visual system (Heinrich, 2010; Spaak et al., 2014; Norcia et al., 2015).

Visual perception was modulated periodically by the inducer. However, the amplitude of the modulation was very low at the position the farthest to the inducer. Consequently, the estimation of the optimal phase was not relevant for the three visual stimuli tested. Indeed, we did not observe a reliable shift of the optimal phase between target positions, likely because the optimal phase estimation was not reliable across participants.

4. PUBLICATION: Galas, Fakche, Baudouin & Dugué (in preparation). Spatial dynamics of perceptual rhythms.

The use of a peripheral pattern reversing checkerboard at 10 Hz did not allow us to replicate our previous results (Fakche and Dugué, 2022, bioRxiv). Thus, we decided to develop a third experiment, in collaboration with a PhD student, Laurie Galas, leading the project.

4.1. Introduction

To maximize the amplitude of the induced oscillations, we used an annulus filled with a checkerboard, instead of a peripheral disk. Based on electrophysiology (Srinivasan et al., 2007; Zhu et al., 2010; Vialatte et al., 2010; Funase et al., 2015; Norcia et al., 2015), we reasoned that such a stimulus should induce alpha brain oscillations which should tend to travel inward. This novel stimulus should thus induce a high, reliable modulation of the detection performance and a robust estimation of the optimal phase at all target positions. Then, we investigated the same hypothesis as before: 1) Inducer modulates visual perception periodically at each target position. 2) The optimal phase for perception shifts as a function of distance from the inducer, suggesting that perceptual cycles travel across the retinotopic space.

4.2. Materials and Methods

The methods used in this experiment are the same as the ones used in Fakche and Dugué, 2022, bioRxiv. We are only pointing out the small differences between the two experiments.

Participants. 21 participants (16 females, mean ± sd age: 23.2 ± 3.7 years) performed the experiment. All participants presented no neurological or psychiatric history, and they were free from medication affecting the central nervous system. All participants gave their written informed consent and received compensation for their participation. The study was conducted according to the Declaration of Helsinki and approved by a local French ethics committee Ouest IV (IRB #2020-A00859-30). 7 participants were removed from the analysis. One because of inability to perceive targets, one because of a too high false alarm ratio, one who failed the staircase procedure, and four who failed behavioral induced oscillations (see *Behavioral Analysis* section). Finally, the data of 14 participants were analyzed.

Stimuli. Each target (diameter) represented 1.3 mm portion of cortex spaced by 1 mm edge-to-edge (radius: 0.07°, 0.09° and 0.11°; eccentricity: 2.16°, 2.45° and 2.81°). An annulus filled with a checkerboard was used to induce brain oscillations. The annulus (internal radius: 3°, external radius: 15°) was surrounding the fixation cross. Each black and white square of the checkerboard annulus measured 0.31° for a spatial frequency of 3.2 squares/degree. Every 100 ms the pattern was reversed to induced 10-Hz brain oscillations (**Figure 6.5)**. The background color was grey, and the fixation white.

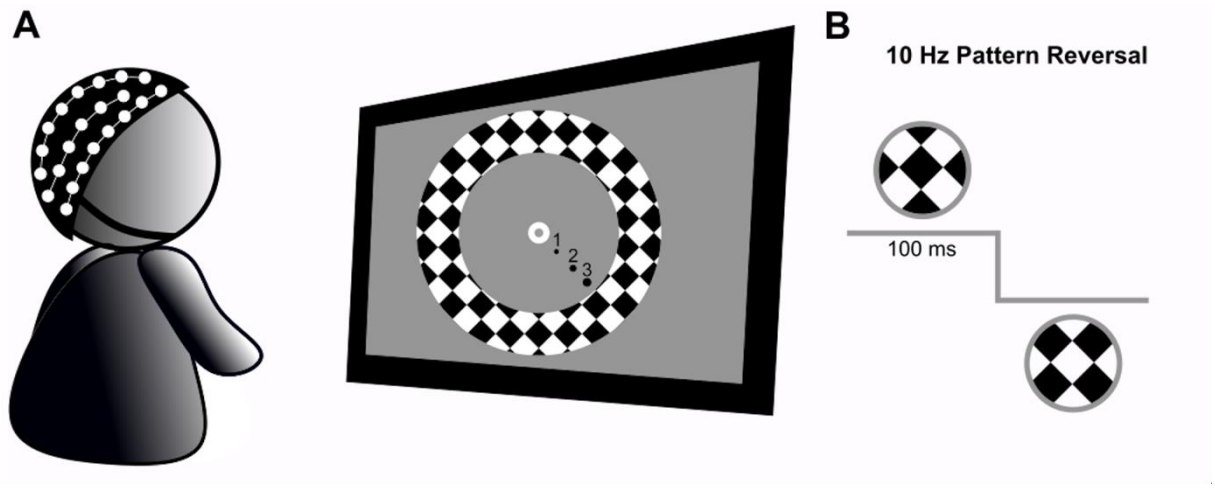

Figure 6.5: A checkerboard annulus to induce 10-Hz brain oscillations. A. *Participants performed a near-threshold detection task while a checkerboard annulus pattern reversed every 100 ms. In 1/3 of the trials, EEG was simultaneously recorded.* ***B.*** *The checkerboard pattern reversed from black to white or white to black every 100 ms.*

Eye tracker. When a gaze deviation of >1.75° from the center of the screen was detected during the presentation of a target or a blink, we considered that the participant broke fixation and the

trial was removed from the analysis (30.8 ± 19.4 trials on average across participants). Participants performed 1256.5 ± 5.3 trials on average.

Procedure. Participants performed two sessions: one psychophysics session and one EEG session. The psychophysics session was composed of the staircase procedure and two runs of 42 blocks each. The EEG session contained one run of 42 blocks.
Target contrasts averaged across participants were 61 ± 12.4 %, 51.8 ± 8.4 %, 78.2 ± 13.2 %, for the position 1, 2, and 3.

EEG analysis. One electrode with the highest amplitude on the topography of the FFT on EEG time series at 10 Hz was selected individually for each participant to plot ERPs.

Behavioral analysis. Hit rates were 53.7 ± 1.5 %, 50.5 ± 0.6 %, and 49.3 ± 1.6 % for position 1, 2, and 3, respectively. We excluded participants from further analysis when non-significant amplitude fit was observed at position 1 (FDR corrected: p-value = 0.01), the closest position from the annulus.

Because we used an inducer modulated by a square function, instead of created a one-cycle sine wave with the phase offset of the oscillating disk to extract the phase values in radians along the entire circle, we created a one-cycle sine waves with the phase offset observed in the ERPs.

4.3. Results

EEG activity was analyzed using FFT and ERP measures to control for successful 10 Hz-induced signal and characterize the shape of the evoked response. First, a peak in the spectrum (as measured per SNR, averaged across participants and electrodes) was identified for the induced frequency, 10 Hz (SNR = 2.44) and its first harmonic, 20 Hz (SNR = 1.96), with topographies showing a brain activity in the occipital cortex (**Figure 6.6**). ERP analyses showed that the evoked signal was a complex oscillation composed of the induced frequency and its first harmonic (**Figure 6.6**). Together, the EEG analyses confirm that we successfully induced 10 Hz oscillation in the visual cortex with a pattern reversing checkerboard annulus, and show that the evoked signal is a complex oscillation composed of the induced frequency and its first harmonic (Heinrich, 2010; Norcia et al., 2015).

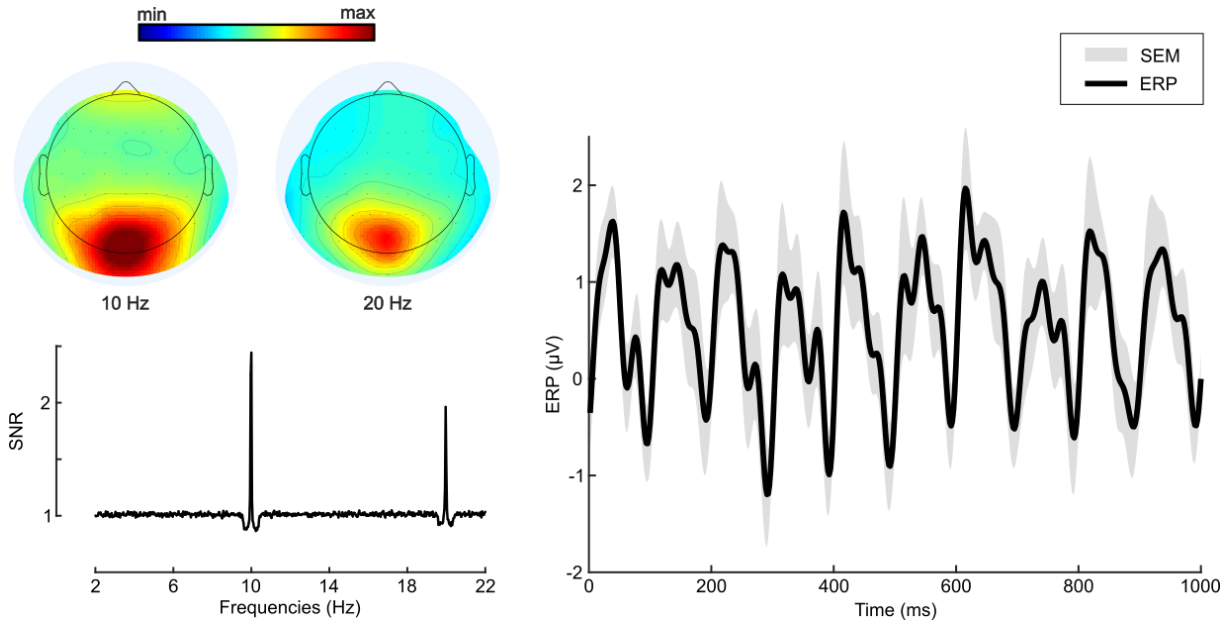

Figure 6.6: The checkerboard annulus induced 10-Hz brain oscillations with a complex shape. *Left panel, Fast Fourier Transform analyses performed on the EEG time series. Signal-to-noise ratio (SNR) amplitude averaged across 14 participants and all 62 electrodes, from 2 to 22 Hz. A peak in SNR was identified for the frequency 10 Hz and its first harmonic 20 Hz. Topographies of the two SNR peaks revealed that we successfully induced brain oscillations in the visual cortex. Right panel, ERP analyses. ERP of one electrode selected for each participant, i.e., the one with highest amplitude in the 10-Hz topography of the SNR, computed on one-second epoch, averaged across participants (n=14). Solid black line, averaged ERP. Shaded area, standard error of the mean.*

Then, we tested whether detection performance was modulated periodically at 10 Hz, for each target position. Targets (from 6 to 18 targets per 30-seconds-blocks) could appear at random delays during the periodic disk stimulation (from 1s to 29s from disk onset), and were binned according to the periodic stimulation (7 bins/cycle). In each bin, detection performance was computed as per hit rate (correct target detection), for each participant and target position. Individual data and data averaged across participants were fitted to a complex sine function, separately for each target position. Detection performance showed a significant oscillatory pattern for each target position on data averaged across participants (Monte Carlo, Bonferroni corrected across positions, p-value threshold of 0.01; **Figure 6.7.A**). One optimal phase (of highest performance) was identified for the position 1, while two optimal phases were observed for the position 2 and 3. Interestingly, the distance between the two optimal phases seemed to increase from position 2 (122°) to position 3 (163°). We also hypothesized that two optimal

phases were present at position 1, but sufficiently close to each other to merge into one optimal phase (**Figure 6.7.A**). This pattern was also found in individual data (**Figure 6.7.B-O**).

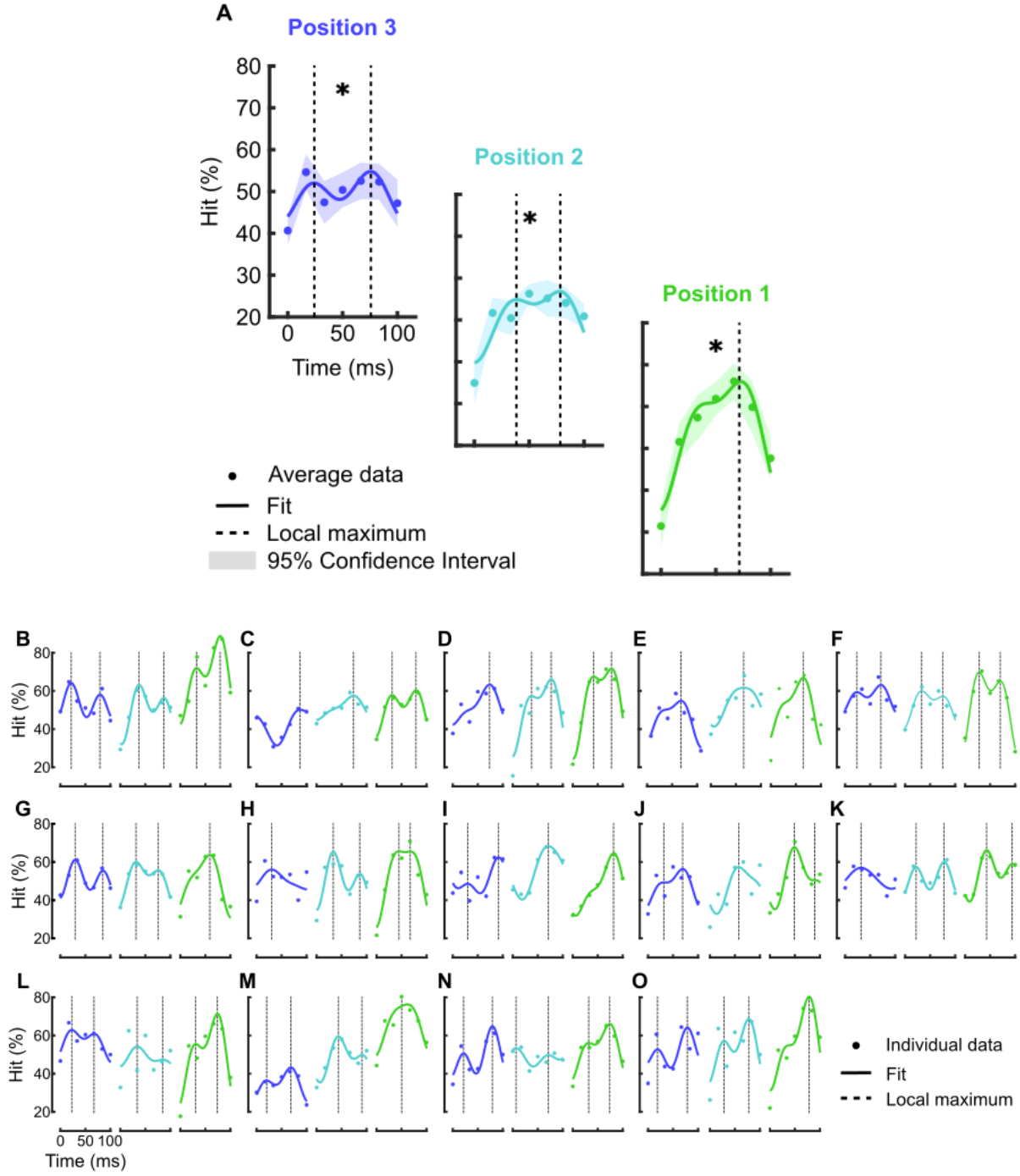

Figure 6.7: Two optimal phases for perception were observed at position 2 and 3. A. *Hit rate averaged across participants (n=14), binned as function of the phase of the checkerboard annulus, and fitted to a complex sine function. Dots, Hit rate computed for each phase bin. Solid line, Complex sine fit. Shaded area, 95 confidence intervals. Dotted line, Optimal phases.* ***B-O.*** *Results from individual participants.*

4.4. Discussion

The annulus checkerboard used in this third experiment, as the peripheral checkerboard used in the second experiment, induced 10-Hz brain oscillations with a complex shape consisting of the induced frequency and its first harmonic (Heinrich, 2010; Spaak et al., 2014; Norcia et al., 2015).

This novel inducer modulated visual performance periodically at each target position. Surprisingly, two optimal phases were observed at position 2 and position 3, i.e., the farthest from the checkerboard annulus. The distance between the two optimal phases increased from position 2 (122°) to position 3 (136°). Although two optimal phases were sometimes observed in the individual data for position 1, only one optimal phase was identified on data averaged across participants. It is possible that indeed two optimal phases were present in the data of position 1, but too close from each other to disentangle them. We hypothesized that behavioral data reflects the overlap between two mesoscopic alpha brain oscillations. One oscillation would emerge in the early visual areas, i.e., V1, and the other one in higher level areas, such as V4. According to the short cortical distance between the stimuli, we may observe a shift of the optimal phase for perception only for the oscillation in V1, because of the high spatial resolution of the receptive fields in this area. On the contrary, the lower spatial resolution of the receptive fields in V4 would not allow us to observe a phase shift between the stimuli, that would be represented in the same receptive field (**Figure 6.8**). Further analysis is ongoing to test this hypothesis. In particular, we plan to perform a source reconstruction analysis on the EEG data, in order to investigate whether brain activity is supported by one neural source in the early visual areas, and a second one in the late visual areas.

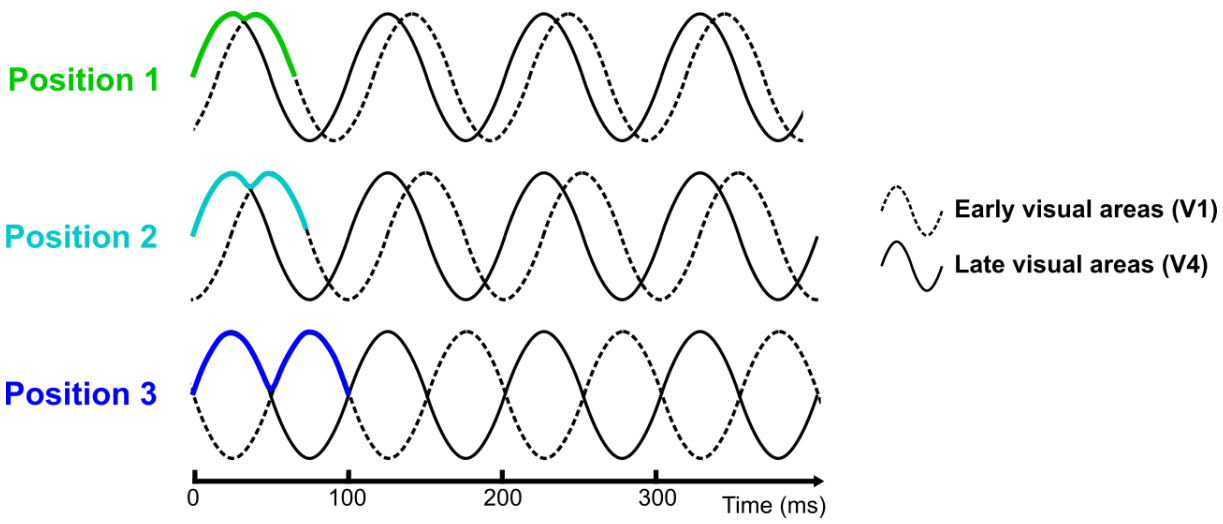

Figure 6.8: Why did we observe two optimal phases? *We hypothesized that the annulus checkerboard induced two brain oscillations, one in the early visual areas (V1) and another one in the late visual areas (V4). Considering the short cortical distance between the three target positions, the travel would be observed for the brain activity in V1 and not the one in V4 because of the reduced spatial resolution along the visual hierarchy.*

5. Summary and Discussion

In the first study (Fakche and Dugué, 2022, bioRxiv), we tested whether low-frequency brain oscillations traveled across the visual cortex, leading to predictable perceptual consequences across the visual field, i.e., perceptual cycles traveled across the retinotopic visual, with psychophysics and EEG recordings. As previously shown in the literature, we found that visual performance was modulated periodically as a function of the phase of the inducer, at the induced frequency (Stefanics et al., 2010; Mathewson et al., 2012; Henry et al., 2012, 2014; Graaf et al., 2013; Spaak et al., 2014; ten Oever and Sack, 2015; Kizuk and Mathewson, 2017). Critically, the optimal phase, i.e., of highest performance, shifted as a function of stimulus position, at alpha frequency, with a propagation speed of 0.2-0.4 m/s. These results are in favor of a functional role of mesoscopic alpha traveling waves on visual perception in humans.

In a second study, we aimed to replicate our previous results with a novel stimulus, a pattern reversing checkerboard, which presents two main advantages: a constant level of luminance, and square function modulation instead of a sine function. Unfortunately, the modulation of the perceptual performance by the checkerboard inducer was very low at the position the farthest from the inducer. The estimation of the optimal phase was not reliable at all stimulus positions, and consequently, we were not able to find a robust effect on the phase shift.

In a third study, performed in collaboration with Laurie Galas, we used a checkerboard annulus around the fixation to maximize the amplitude of the induced oscillations. Visual performance was modulated periodically by the visual inducer. Surprisingly, we observed two optimal phases for perception at target positions the farthest to the checkerboard annulus. We hypothesized that two brain oscillations are induced, one in the early visual areas and one in the late visual areas. Considering the short cortical distance between the three target positions, a phase shift would be observed for the brain activity in the early but not in the late visual areas,

because of the reduced spatial resolution along the visual hierarchy. Further analysis is ongoing to test this hypothesis.

6. Future research questions

Psychophysics is a powerful tool to investigate the role of mesoscopic traveling waves in healthy human participants. The studies presented in this Chapter demonstrated that we can use this methodology to better characterize the properties and the functional role of mesoscopic traveling waves on human cognition.

In the first study (Fakche and Dugué, 2022, bioRxiv), we showed that perceptual cycles traveled at alpha frequencies (8, 10 Hz) but not at theta frequencies (4, 6 Hz). We hypothesized that during our experiment, participants deployed their spatial endogenous attention to the lower right quadrant of the screen, i.e., to a unique position in the visual field, leading to a sampling of the visual information at the alpha frequency (Dugué and VanRullen, 2017; Kienitz et al., 2021). However, endogenous attention rhythmically samples information at the theta frequency when different spatial positions have to be processed (VanRullen, 2016a; Dugué and VanRullen, 2017; Kienitz et al., 2021). We would like to develop a new experiment to test whether theta, and not alpha, mesoscopic traveling waves modulate perceptual performance during the deployment of endogenous attention at multiple spatial positions.

We tested our hypothesis with a periodic stimulation to induce brain oscillations in the visual regions. Invasive studies in animals have shown that spontaneous activity acts as a traveling wave (Volgushev et al., 2006; Lippert, Takagaki et al., 2007; Luczak et al., 2007; Takagaki et al., 2008; Nauhaus et al., 2009, 2012). In the future, it would be of great interest to test whether 1) Spontaneous alpha oscillations in the human visual cortex are mesoscopic traveling waves, and 2) The optimal phase for perception shifts as a function of spontaneous alpha waves.

The periodic stimulations we used in the three experiments consisted of a contrast change, ideally suited for V1. We could use other stimulations, e.g., color change, to induce brain oscillations in other retinotopic visual areas, e.g., V4, and investigate their traveling properties.

Finally, in the first study (Fakche and Dugué, 2022, bioRxiv), we tested whether the shift of the optimal phase for performance depends on the frequency of induced brain oscillations. Numerous questions remain concerning the spatial extent of this phase effect.

For the moment, we do not know whether the propagation of mesoscopic traveling waves is isotropic across the retinotopic space, or anisotropic, and consequently biased toward the fovea, or the periphery, or to functionally relevant neuronal populations.

We tested the propagation of traveling waves only in the left visual hemisphere, we would like to investigate whether the propagation in the two hemispheres is similar or whether it depends on anatomical, functional, physiological differences, e.g., ocular dominance.

In sum, psychophysics experiments could be used in the future to investigate the spatial properties of mesoscopic traveling waves in human, and their functional role on visual perception.

Chapter 7. The role of the direction of propagation of alpha macroscopic traveling waves.

The results of the previous Chapter suggest that alpha brain oscillations travel at the mesoscopic scale in humans, *within* the retinotopic space early visual areas, e.g., V1. Their propagation influences visual perception periodically across space and time. These results highlight the importance of taking into account the spatio-temporal organization of brain oscillations in our research. In this Chapter, we are interested in the propagation of alpha brain oscillations at the macroscopic scale, i.e., *between* cortical areas.

In healthy humans, macroscopic oscillatory traveling waves have been reported in a broad range of frequency bands and during various cognitive tasks, with non-invasive recordings (EEG/MEG). Delta (0.5-4 Hz), theta (4-7 Hz), alpha (8-14 Hz), beta (15-30 Hz) and gamma (>30 Hz) oscillatory traveling waves have been recorded during **resting state** (Adrian and Yamagiwa, 1935; Cohn, 1948; Goldman et al., 1949; Liske et al., 1967; Giannitrapani et al., 1966, 1970; Hori et al., 1969; Barlow and Estrim, 1971; Hoovey et al., 1972; Hord et al., 1972, 1974; Inouye et al., 1983, 1995; Manjarrez et al., 2007; Nolte et al., 2008; Bahramisharif et al., 2013; Alamia and VanRullen, 2019; Pang et al., 2020), **sleep** (Giannitrapani et al., 1966; Massimini et al., 2004, 2007; Murphy et al., 2009), **visual perception** (Barlow and Estrim, 1971; Brenner et al., 1981; Maclin et al., 1983; Rodriguez et al., 1999; Shevelev et al., 2000; Burkitt et al., 2000; Schack et al., 2003; Srinivasan et al., 2006; Thorpe et al., 2007; Cottereau et al., 2011; Fellinger et al., 2012; Patten et al., 2012; Alexander et al., 2013; van Ede et al., 2015; Alamia and VanRullen, 2019; Lozano-Soldevilla and VanRullen, 2019; Pang et al., 2020; Tsoneva et al., 2021), **auditory perception** (Giannitrapani, 1970; Ribary et al., 1991; Alexander et al., 2006b, 2008, 2009), **memory processing** (Schack et al., 1999; Sauseng et al., 2002; Alexander et al., 2006a, 2008, 2009; Zhang et al., 2018), and **motor and oculomotor tasks** (Cooper and Mundy-Castle, 1960; Alexander et al., 2013; Giannini et al., 2018).

Macroscopic oscillatory traveling waves are characterized by various features: their frequency, their speed, their number, and their direction. In this Chapter, we are interested in the functional role on the propagation direction of oscillatory traveling waves during visual perception and the deployment of endogenous spatial attention.

1. A functional role of traveling waves propagation's direction?

Macroscopic oscillatory traveling waves are propagating across the whole brain. Because the cortex is organized in a hierarchal manner, with high- and low-level areas, e.g., multisensorial integrative areas vs. primary sensory areas, the direction of propagation is crucial. We hypothesized that traveling waves direction has a functional role on cognitive functions.

A few studies showed the presence of rotating traveling waves (Goldman, 1949; Muller et al., 2016), of traveling waves propagating between the left and the right hemispheres (Liske et al., 1967; Giannitrapani, 1970; Hoovey et al., 1972; Schack et al., 2003; Ito et al., 2007), and from the midline to the periphery or toward the midline (Hughes et al., 1995; Alexander et al., 2006b). But macroscopic traveling waves mostly propagate along the antero-posterior axis (e.g., Zhang et al., 2018; Giannini et al., 2018; Alamia and VanRullen, 2019; Halgren et al., 2019; Lozano-Soldevilla and VanRullen, 2019; Pang et al., 2020; King and Wyart, 2021; Tsoneva et al., 2021).

Interestingly, the propagation direction of traveling waves seems to play a functional role on cognition. One ECoG study demonstrated that the performance during a working memory task depended on traveling waves maintaining their optimal propagation direction, and not on a change in the propagation speed or in the oscillatory frequency (Zhang et al., 2018). In a task involving working and long-term memory systems, it has been shown that the memory performance was associated with the timing of the change of traveling waves' direction, from the anterior-posterior trajectory, supposed to reflect working memory processes, to a posterior-to-anterior trajectory, expected to account for long-term memory processes (Sauseng et al., 2002). In the visual modality, the direction of traveling waves appears to predict visual illusion (Shevelev et al., 2000), and word processing (Schack et al., 2003). During visual perception, alpha traveling waves shift from a feedback propagation, during the pre-stimulus period, to a feedforward propagation from the occipital to the frontal cortices at the onset of the visual stimulation, presumably to communicate visual information from the sensory cortex to higher-order level brain areas (Schack et al., 1999; Patten et al., 2012; Alamia and VanRullen, 2019; Pang et al., 2020).

In a first experiment, we studied the direction of macroscopic oscillatory traveling waves according to the cognitive function engaged in the task.

In addition, to date, a *causal* link between the direction of traveling waves propagation and cognition has not been studied. The second experiment described in this Chapter aims to fill this gap. We hypothesized that visual perception causally triggers a traveling wave in the anterior-to-posterior direction.

2. Fakche & Dugué. Manipulating cognition to manipulate traveling waves direction.

In this study, we designed an experiment allowing the engagement of two cognitive functions: the deployment of covert, endogenous spatial attention, and visual perception. We were interested in how the manipulation of different cognitive functions influences the direction of alpha macroscopic traveling waves.

2.1. Introduction

The propagation of brain oscillations across the cortex has been observed the first time by the EEG pioneers Adrian and Yamagiwa, in 1935, in humans. They found that the resting state alpha rhythm "moves" across the cortex, i.e., the peaks and throughs of the alpha cycle did not coincide between the recording oscillographs placed over the scalp (Adrian and Yamagiwa, 1935). They discovered macroscopic oscillatory traveling waves, with a constant phase shift between the origin of the signal and more distal positions (Muller et al., 2018). Since, several studies have recorded macroscopic oscillatory traveling waves in humans, with non-invasive recordings (EEG/MEG). Macroscopic oscillatory traveling waves are characterized by a propagation at a speed ranging from 0.3 to 20 m/s, over a cortical distance from 5 to 25 cm. They mostly propagate along the anteroposterior axis and the phase shift between anterior and posterior brain regions is ranging from 30 to 240° (Walter et al., 1966; Cohn, 1948; Hord et al., 1972, 1974; Suzuki, 1974; Burkitt et al., 2000; Ito et al., 2005; Zhang et al., 2018).

Interestingly, the propagation direction of traveling waves seems to play a functional role on cognition (Shevelev et al., 2000; Sauseng et al., 2002; Schack et al., 1999, 2003; Patten et al., 2012; Zhang et al., 2018; Alamia and VanRullen, 2019; Pang et al., 2020). The aim of this study is to investigate how the manipulation of cognitive functions, more specifically, visual perception and the deployment of spatial endogenous attention, influences the propagation of oscillatory traveling waves.

To date, only one study has investigated the relation between oscillatory traveling waves and attention, but without explicitly manipulating attention. They compared the brain activity recorded with EEG of healthy children and children with Attention Deficit Hyperactivity Disorder (ADHD), and they found that the amount of traveling waves activity was reduced in AHDH children, and negatively correlated with a hyperactivity score (Alexander et al., 2008). Attention is the cognitive function that selects relevant information to facilitate its processing, while being flexible to be redeployed to other sources of information if necessary (Carrasco, 2011). Numerous studies found that covert spatial endogenous attention, i.e., when attention is voluntarily deployed to a specific location in space, without any eye or head movements, was associated with alpha brain oscillations. The deployment of visuo-spatial attention leads to a decrease in the amplitude of alpha oscillations in the occipital cortex contralateral to the attended stimuli, and simultaneously to an increase in alpha oscillations in the ipsilateral cortex, presumably to inhibit the processing of incoming stimuli in the non-attended visual field. This is known as alpha lateralization (Worden et al., 2000; Sauseng et al., 2005b; Thut et al., 2006; Händel et al., 2011). We hypothesized that during the deployment of spatial endogenous attention, a top-down process, alpha oscillations would emerge in the frontal regions and travel anterior to posterior toward the occipital regions where we observe alpha lateralization.

Additionally, the propagation of macroscopic brain oscillations has been widely studied during visual perception. Several studies showed that a visual stimulation was associated to alpha traveling waves propagating from posterior to anterior brain areas (Barlow and Estrim, 1970; Burkitt et al., 2000; Srinivasan et al., 2006; Cottereau et al., 2011; Giannini et al., 2018; Alamia and VanRullen, 2019; Lozano-Soldevilla and VanRullen, 2019; Tsoneva et al., 2021). This propagation direction presumably reflects the communication of visual information from the primary sensory cortices to higher level regions.

In this study, we manipulated cognition to manipulate alpha traveling waves direction. We designed a cueing task aimed to manipulate spatial endogenous attention and in which a 10 Hz visual stimulation additionally induced alpha brain oscillations. EEG was simultaneously recorded. We expected to observe a reversal in the directionality of alpha traveling waves, from an anterior-to-posterior propagation during endogenous attention orienting (post-cue to pre-target period), to a posterior-to-anterior propagation during the visual stimulation.

2.2. Materials and Methods

Participants. 7 participants (4 females, mean ± sd age: 27.7 ± 5 years) were included in the study. All participants were free from medication affecting the central nervous system, reported no history of psychiatric or neurological disorders, gave their written informed consent and were compensated for their participation. The study was approved by the local French ethics committee Ouest IV (IRB #2020-A00859-30) and followed the Declaration of Helsinki. More participants will be recruited soon to reach a total number of 15-20 participants.

Stimuli. Stimuli were designed with PsychToolbox 3.0.12, running in Matlab R2014b 64-bit (The MathWorks, Natick, MA), and displayed with a ProPixx Projector (VPixx Technologies, Saint-Bruno, QC, Canada), on a 185x104.5 cm projection screen (1920*1080 pixels; 480 Hz refresh rate), at 122 cm distance. The stimuli consisted in a fixation cross, visual cues, small dots, and part of an annulus, i.e., named annulus for ease of reading. The arms of the fixation cross measured 0.15 degrees of visual angles (°) of length and 0.03° of width. The visual cues were a lengthening and a widening of the lower arms of the fixation cross, i.e., the left or the right lower arm to instruct the participant to orient their attention either to the left or to the right side of the screen, respectively, or both of them for the neutral cue. Left and right cues had an arm of 0.65° of length and 0.1° of width. The neutral cue had two lower arms of 0.4° of length and 0.05° of width. The annulus had an inner arc at 3.35° of eccentricity, and an outer arc at 14.88° of eccentricity, with the largest diameter of 22°. The annulus was filled with a radial checkerboard of black and white squares. The small dots were used as targets. They were displayed at 3° of eccentricity (center of dots) with a radius of 0.2°, and at a 55° angle from the horizontal line, either on the lower left or right side of the screen. The background color was grey, the fixation cross and the visual cues white. Target contrasts varied between black and grey, and were titrated for each participant according to a one-up/two-down staircase procedure to reach 70-75% detection performance. Target contrasts averaged across participants were 13.43 ± 4.21%.

Eye tracker. Participant's head was maintained with a chinrest. An infrared video-camera system (EyeLink 1000 plus 5.08, SR Research, Ottawa, Canada) was used to ensure that participants maintained their gaze on the fixation cross throughout the trial. The trial only started when participants were successfully maintaining fixation. When a gaze deviation of >2° from the center of the screen was detected or a blink, we considered that participants broke fixation, and the trial was removed from the analysis (108 ± 47 trials on average across participants). Supernumerary trials were added at the end of each block to compensate for rejected trials.

EEG. EEG was recorded using a 128-channels actiChamp system (Brain Products GmbH). The ground was placed at the Fpz position, and the right mastoid was used as reference (DC recording; 1000 Hz sampling rate).

MRI. Anatomical MRI images were obtained using a 3-T Siemens Prisma MRI scanner with a T1-weighted gradient-recalled echo (GRE) MRI sequence. The field of view (FOV) was 256 mm and voxels were 0.8*0.8*0.8 mm. MR images were acquired using echo sequences with a TE of 2.22 ms, a TR of 2400 ms and a flip angle at 9°. A multi-echo fast low angle shot (FLASH) sequence with flip angles at 5° and 30° was also used to facilitate the source reconstruction analysis (not presented). Voxels were 1*1*1 mm. The TR was 12 ms and the TE were 1.52, 2.77, 4.02, 5.27, 6.52, 7.77, 9.02, and 10.27 ms. Functional MRI consisted in four sequences where clockwise, counterclockwise wedges, expanding or contracting rings were displayed on the screen (Dougherty et al., 2003; Larsson and Heeger, 2006; Dugué et al., 2020). Stimuli were generated using Matlab R2021b 64-bit (The MathWorks, Natick, MA) and the MGL toolbox (Gardner et al., 2018) on a Macintosh computer. Voxels were 2*2*2 mm and sequences had a flip angle at 62°. The TR was 1000 ms and the TE was 35 and 32.5 ms. Each cycle took 24 s, with a pattern-reversal occurring every 250 ms.

Procedure. Participants performed two EEG sessions. The first session was composed of a training block, the staircase, and 10 blocks of 44 trials of the main task. The second session was composed of 10 blocks of 44 trials, for a total of 880 trials across the two sessions.

Each trial began with a fixation cross for 300 ms. Then, a left or a right cue was displayed for 150 ms to instruct the participant to orient their attention to the left or to right side of the screen, respectively. The number of trials with a left and a right cue was pseudo-randomized across the two sessions. After a fixed delay of 1500 ms, the 10Hz pattern reversing checkerboard annulus was displayed below the fixation cross, in the center, for 4500 ms. The target appeared randomly between 2500 and 3500 ms. Trials could be valid (75%) if the target was presented at the attended location, or invalid (25%) if the target was presented at the unattended location, requiring participants to reorient their attention. Between 3500 and 4500 ms, the fixation cross became black to indicate participants to give their answer, i.e., press the space key if they perceived the target (detection task). Each trial was separated by a random delay varying from 1500 to 2500 ms, with a 100-ms step (**Figure 7.1**). Participants were allowed to blink and close their eyes during this delay.

The staircase procedure was composed of 80 trials, as described above, except that we used a neutral cue.

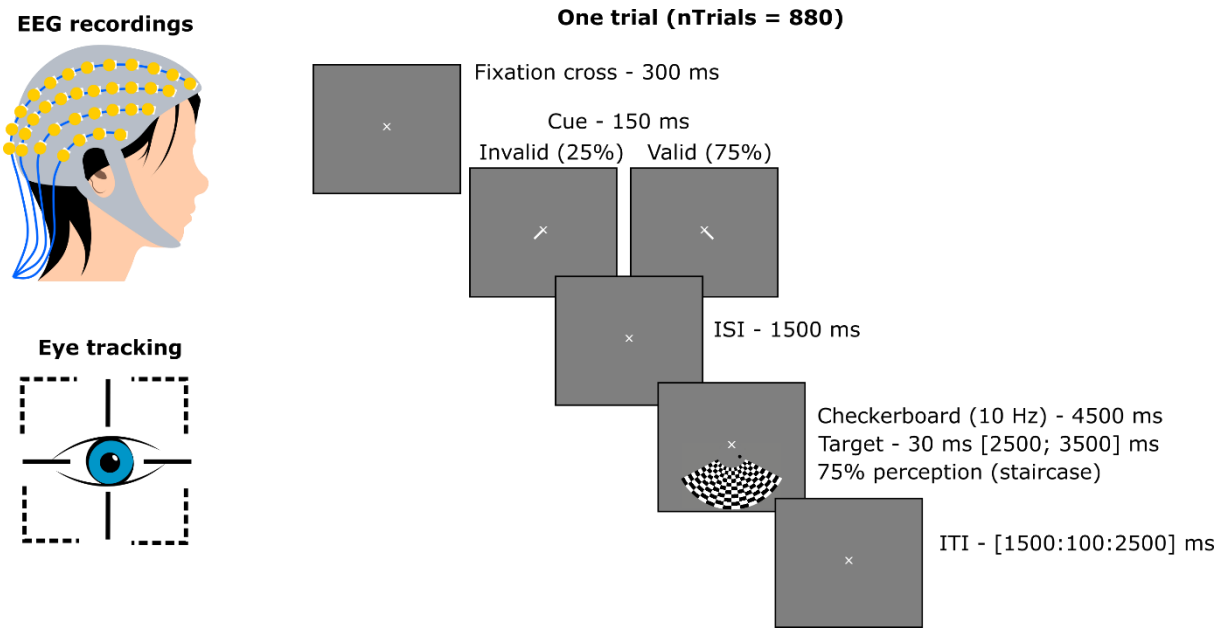

Figure 7.1: Experimental procedure. *A white fixation cross was displayed for 300 ms, followed by a left or right endogenous cue for 150 ms, used to orient participant's endogenous spatial attention. After a delay of 1500 ms, a 10Hz pattern reversing checkerboard annulus was displayed below the fixation cross, in the center, for 4500 ms. The target appeared randomly between 2500 and 3500 ms. Trials could be valid (75%) if the target was presented at the attended location, or invalid (25%) if the target was presented at the unattended location, requiring the participants to reorient their attention. Between 3500 and 4500 ms, the fixation cross become black to indicate participants to give their answer, i.e., press the space key if they perceived the target (detection task). Each trial was separated by a random delay varying from 1500 to 2500 ms, with a 100-ms step.*

Behavioral analyses. Behavioral analyses were performed with Matlab R2014b (The MathWorks, Natick, MA). The hit rate, i.e., percentage of detection, and median reaction times were computed for each participant, for valid and invalid trials separately. T-tests were performed on hit rates and median reaction times to assess whether spatial endogenous attention was successfully manipulated. Indeed, we expected a higher hit rate for valid compared to invalid trials, and no difference or a higher median reaction time for invalid trials, suggesting that the allocation of endogenous attention facilitated visual processing, and that there were no speed-accuracy tradeoffs.

EEG analyses. EEG analyses were performed with EEGLAB 13.6.5 (Swartz Center for Computational Neuroscience, UC San Diego, California; Delorme & Makeig, 2004) and custom software written in Matlab R2014b (The MathWorks, Natick, MA).

Preprocessing. EEG data and channel location were imported into EEGLab. EEG data were re-referenced to average reference. A high-pass filter at 0.1 Hz and a notch filter between 48 and 52 Hz were applied, to respectively remove slow drifts and 50 Hz electric noise. The signal was further downsampled to 512 Hz. Visual inspection allowed to identify electrodes with low signal-to-noise ratio, which were then interpolated (spherical interpolation). Time series were epoched from trial onset (0 s) to the end of the trial (8 s), and epochs corresponding to a trial removed in the behavioral analyses because of a fixation break, were removed from the EEG analyses. Epoched were merged into continuous data, and further epoched from -300 ms to +1650 ms according to the onset of the cue, separately for left and right cue, i.e., left-cue-epoch and right-cue-epoch, and from 0 ms to +3500 ms according to the onset of the 10Hz pattern reversing checkerboard annulus, i.e., annulus-epoch. The cue-epoch allows us to analyze the EEG signal during the deployment of endogenous spatial attention, and the annulus-epoch to study the EEG signal during the repetitive visual stimulation, before the response of the participant. The data were also epoched from -1500 ms to +300 ms according to the fixation cross onset, i.e., precue-epoch, in order to identify the individual alpha frequency during the precue period.

Visual inspection allowed to reject the epochs with artifacts, e.g., muscle activity, for each participant and epoch-condition (cue-epoch, annulus-epoch, and precue-epoch).

Time-frequency decomposition. A time-frequency transform (morelet wavelet) was computed on single epochs, separately for cue-epoch and annulus-epoch, with the *timefreq* function from EEGLAB. The “cycles” parameter was set from 1 to 15. The “freqs” parameter was set to [2, 20], producing 50 frequencies that increased logarithmically from 2 to 20 Hz.

Alpha Lateralization. This analysis was performed on cue and annulus-epochs. The amplitude was extracted with the *abs* function (from Matlab) from the time-frequency decomposition of each trial, electrode, cue, and participant. Time-frequency maps were plotted for left- and right-cue-epochs on data averaged across trials, electrodes, and participants. A time-frequency window of brain activity was extracted, and used to plot the topography of the difference between left- and right-cue-epochs.

Fast Fourier Transform (FFT) on the visual inducer. FFT were computed (Matlab function: *fft*) on annulus-epoch data. The amplitude was extracted for each electrode, trial and frequency. Data were averaged across trials and participants. A frequency spectrum was plotted to ensure that we induced brain oscillations at 10 Hz. The topography was plotted to identify the scalp location of the alpha-induced brain oscillations.

Resting State (RS). In order to identify the individual alpha frequency (IAF) during RS, we recorded two minutes of resting state eyes closed and eyes open, for each participant. The EEG resting state data were re-referenced to average reference, high-pass filtered at 0.1 Hz, notch filtered between 48 and 52 Hz, and downsampled to 512 Hz. Electrodes with a low signal-to-noise ratio were interpolated. The continuous data were epoched into 1-second epochs, and epochs with artifacts were rejected. The cleaned epoched data was merged into continuous data, and an FFT was applied. The amplitude was extracted for each electrode and frequency. The frequency spectrum was plotted for each participant, for both eyes closed and open, to identify the IAF during RS in both conditions.

Alpha peak modulation. We aimed to test whether the peak of alpha oscillations was modulated between the RS conditions, the precue and the postcue period. The IAF during RS was identified as explained above (*Resting State (RS)* section) for both eyes closed and open conditions. To identify the alpha frequency in the precue period, we computed an FFT on precue-epoch, extracted the amplitude for each electrode, trial and frequency. The amplitude was averaged across trials and occipital electrodes. A frequency spectrum was plotted to find the individual alpha frequency during the precue period. Concerning the alpha peaks during the postcue period, the amplitudes extracted from the time-frequency decomposition on cue-epoch were averaged across trials, occipital electrodes, and times from 800 ms to 1200 ms, i.e., during the alpha lateralization pattern. A frequency spectrum was plotted to identify the alpha frequency evoked by the sum of amplitude during left and the right cues for each participant. A one-way repeated-measures ANOVA was performed to test whether the alpha frequency was significantly modulated between the four conditions: RS eyes open, RS eyes closed, Precue and Postcue.

Traveling waves analysis at the sensor level.

Event Related Potentials (ERPs). Previously preprocessed EEG data were further filtered between 1.5 Hz and 30 Hz, and baseline corrected from -300 to 0 ms from the onset of the cue

or from the onset of the inducer, for cue- and annulus-epoch, respectively. We applied a second bandpass filter between 8 and 12 Hz on cue-epochs to reveal the alpha frequency component previously observed in the time-frequency analysis, in the ERPs data. Participant's ERPs were computed as epoch averaging for left-cue-, right-cue-, and annulus-epochs. We plotted the ERPs at different scalp locations, on Oz, POz, Pz, CPz, Cz, Fz, electrodes for annulus-ERPs, and on O2, PO4, P4, CP4, C4, F4, and O1, PO3, P3, CP3, C3, F3, electrodes for cue-ERPs, for each participant and for data averaged across participants. A constant phase shift of the ERP peak between the scalp locations is a signature of a macroscopic traveling wave (Lozano-Soldevilla and VanRullen, 2019).

Pairwise phase difference. The presence of oscillatory traveling waves was investigated by computing pairwise phase differences between non-contiguous electrodes with the function circ_dist from the Circular Statistics Toolbox (P. Berens, CircStat: A Matlab Toolbox for Circular Statistics, Journal of Statistical Software, Volume 31, Issue 10, 2009, http://www.jstatsoft.org/v31/i10), for each trial. The selected electrodes were the same as the ones chosen for the ERPs computation. We plotted the time course of the phase difference averaged across trials, participants, and pairs of electrodes, with the circ_mean function, for the alpha frequency. The standard deviation across participants was computed with the circ_std function. To test whether the phase differences were significantly different from 0, we computed Watson Williams test against 0 with the circ_wwtest function. In addition, rose plots visualized the individual phase differences averaged across trials and pairs of electrodes, with the circ_plot function.

2DFFT. To assess the presence of traveling waves and their propagation direction, we first stacked the EEG trials from previously selected electrodes to form a 2D electrode*time map, these maps were averaged across trials and participants, and then we applied a 2DFFT on the 2D map (Alamia and VanRullen, 2019; Pang et al., 2020). The results were maps with temporal frequencies on the x-axis and spatial frequencies on the y-axis. The upper and bottom quadrants represent forward and feedback traveling waves, respectively.

2.3. Results

Behavior. Participants performed a visual detection task associated with the deployment of covert, spatial endogenous attention. To ensure that endogenous attention was successfully

manipulated, hit rates, i.e., the percentage of detection, and median reaction times were computed separately for valid and invalid trials. The detection performance was significantly higher for valid compared to invalid trials (**Figure 7.2**; one-tailed t-test: p-value = 0.0015; Cohen's d = 2.2218; CI = [0.0583; Infinity]). Indeed, the allocation of endogenous attention to a specific location of the visual field facilitates the processing of the incoming visual information in the valid condition. There was also a significant difference in the median reaction times with higher reaction times for the valid condition (**Figure 7.2**; two-tailed t-test: p-value = 0.0011; Cohen's d = 0.7166; CI = [0.0244; 0.0592]). Thus, we could not conclude that higher performance in the valid condition did not depend on speed-accuracy tradeoff.

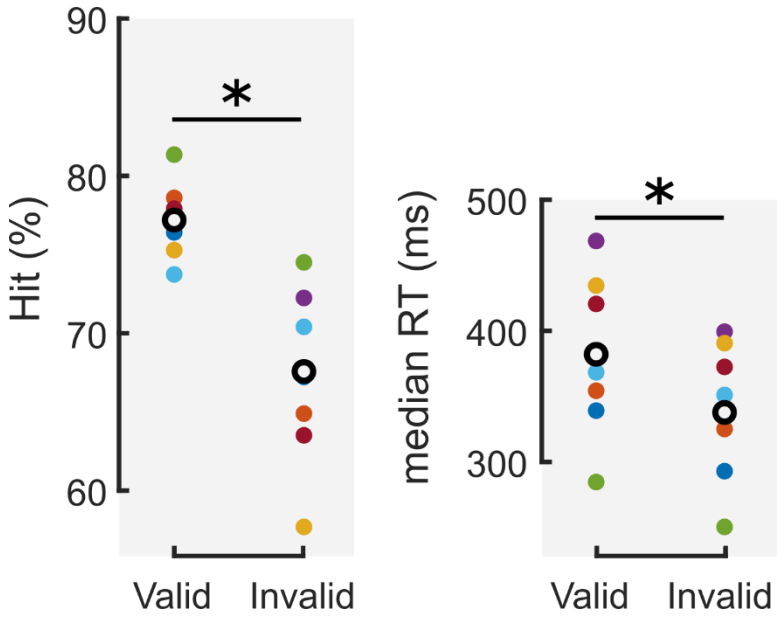

Figure 7.2: Hit rates were higher in the valid condition. *Left panel, Hit rates, Right panel, Median reaction times, computed separately for valid and invalid conditions. Color dots, Individual data. Black circles, Data averaged across participants (n=7). Both hit rates (one-tailed t-test: p-value = 0.0015; Cohen's d = 2.2218; CI = [0.0583; Infinity]) and median reaction times (two-tailed t-test: p-value = 0.0011; Cohen's d = 0.7166; CI = [0.0244; 0.0592]) were higher for the valid condition.*

Alpha Lateralization. The deployment of endogenous visuo-spatial attention leads to the emergence of a specific brain pattern, i.e., a decrease in the amplitude of alpha oscillations in the occipital cortex contralateral to the visual field of the attended stimulus, and simultaneously to an increase in alpha oscillations in the ipsilateral cortex. This is known as alpha lateralization (Worden et al., 2000; Sauseng et al., 2005b; Thut et al., 2006; Händel et al., 2011). To ensure that the attentional manipulation was associated with the alpha lateralization pattern, EEG data were epoched from -300 ms to +1650 ms according to the onset of the cue, separately for left

and right cue, i.e., left-cue-epochs and right-cue-epochs, and a time-frequency decomposition was applied on both cue-epochs. A time-frequency map of the amplitude was plotted on data averaged across participants, trials, and electrodes (**Figure 7.3**). The deployment of endogenous visuo-spatial attention was associated with the presence of brain oscillations in the alpha range, from 8 to 11 Hz, from 800 to 1200 ms after the cues' onset. The topography of the amplitude difference between left- and right-cue-epochs averaged across the previous time-frequency window showed an increase in the amplitude of alpha brain oscillations in the occipital cortex ipsilateral to the attended visual field, and a decrease in the amplitude in the contralateral occipital cortex (**Figure 7.4**). The deployment of endogenous visuo-spatial attention induced the expected alpha lateralization pattern in the occipital cortex.

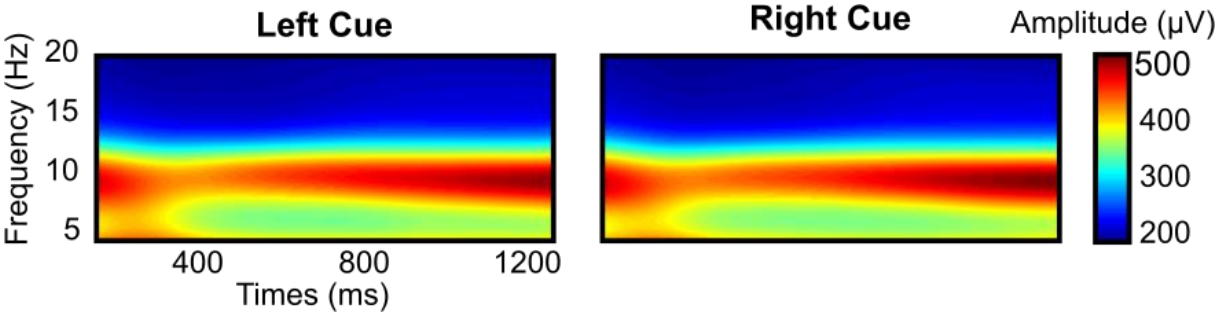

Figure 7.3: Alpha oscillations emerged after cues' onset. *Left panel, Time-frequency maps averaged across participants (n=7), trials, and electrodes, of the amplitude after the left cue onset, Right panel, After the right cue onset. Brain oscillations showed a high amplitude between 8 Hz and 11 Hz, from 800 to 1200 ms after both cues' onsets.*

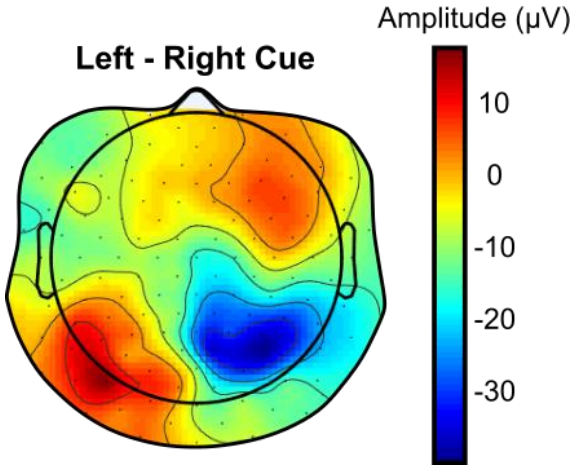

Figure 7.4: Alpha lateralization. *Topography of the amplitude difference between left and right cues conditions, averaged across the time-frequency window from 8 Hz to 11 Hz, and from 800 to 1200 ms, and across participants (n=7). There was a high amplitude of alpha oscillations in the cortex ipsilateral to the attended visual field (i.e., left one), and a low amplitude in the contralateral cortex.*

10-Hz induced brain oscillations. EEG activity during the 10Hz pattern reversing checkerboard, i.e., annulus-epochs, was analyzed using an FFT. We observed in the frequency spectrum averaged across trials, participants, and occipital electrodes, a peak at the induced frequency, i.e., 10 Hz, but also a peak at 9.14 Hz (**Figure 7.5**). This frequency could correspond to alpha brain oscillations associated with the deployment of endogenous attention, or to the endogenous alpha, naturally present in the occipital cortex. The time course of the trials consisted of a cue presentation during 150 ms, followed by a 1500-ms delay, in order to observe the deployment of spatial endogenous attention. After this delay, the checkboard was displayed for 4500 ms. Endogenous attention is a long process; thus, attention should still be under deployment during the presentation of the 10Hz pattern reversing checkerboard. For this reason, we performed the alpha lateralization analysis on the annulus-epochs. The topography of the amplitude difference between left- and right-trials of annulus-epochs averaged from 8 to 11 Hz, and from 500 to 3000 ms, showed that the alpha lateralization pattern observed during the post-cue period (**Figure 7.4**) was maintained during the checkerboard presentation, with a more central location (**Figure 7.6**).

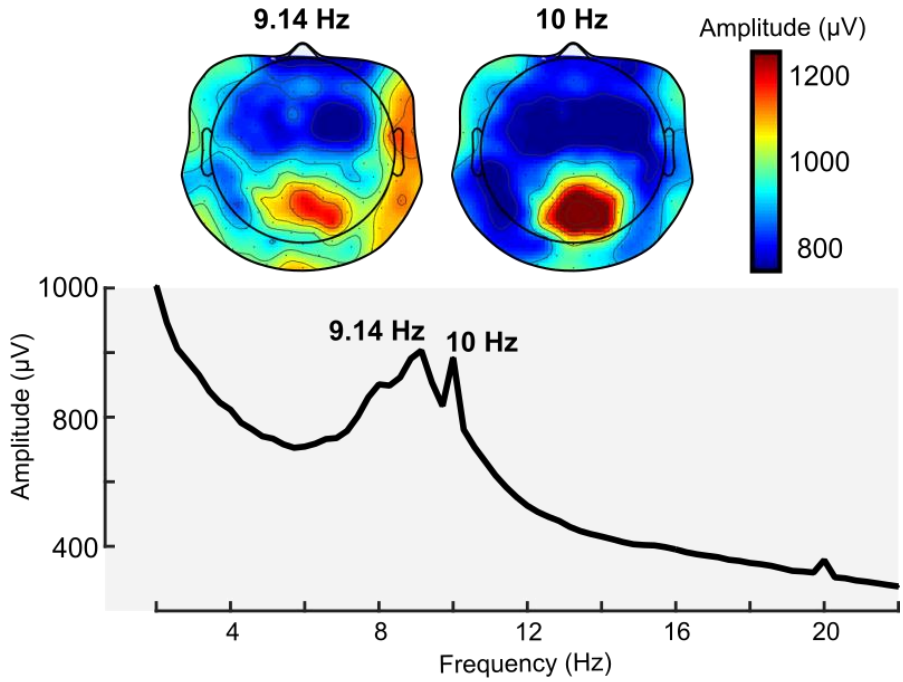

Figure 7.5: Brain oscillations during the 10Hz pattern reversing checkerboard*. Frequency spectrum of annulus-epoch data averaged across participants (n=7), trials, and occipital electrodes. Two frequency peaks were observed during the 10 Hz pattern reversing checkerboard, one at 9.14 Hz, and the other one at 10 Hz. The topographies showed that both frequency activities emerged in the occipital cortex.*

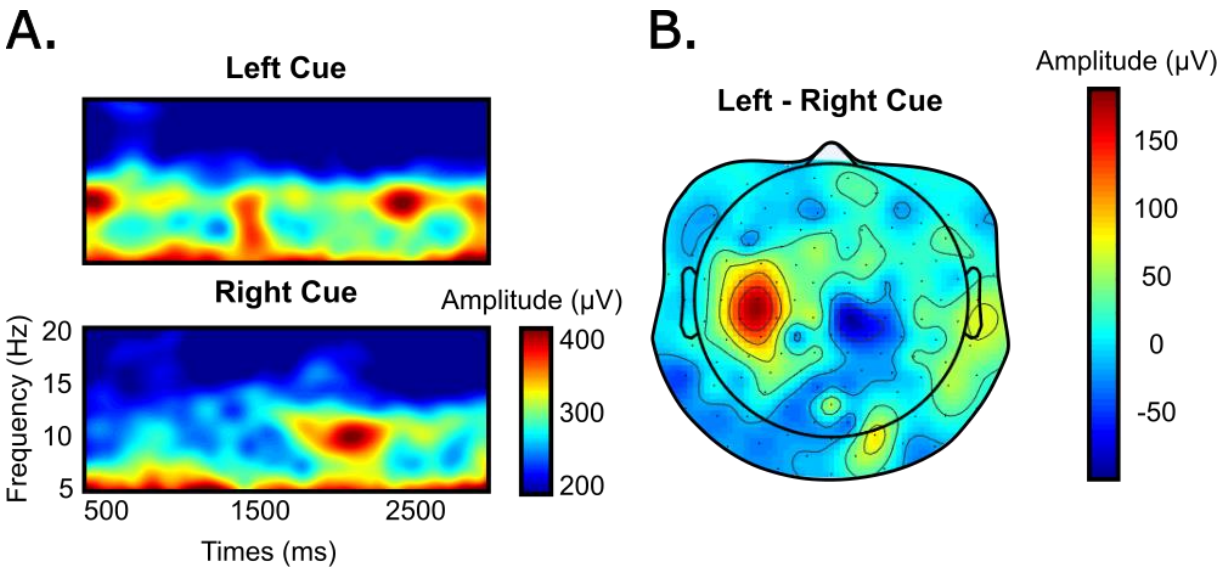

Figure 7.6: Alpha lateralization pattern subsisted during the 10Hz pattern reversing checkerboard. A. *Time-frequency maps averaged across participants (n=7), trials, and electrodes, of the amplitude after the checkerboard onset, separately for left and right cue trials. Brain oscillations showed a high amplitude between 8 Hz and 11 Hz, from 500 to 3000 ms after the checkerboard onset.* ***B.*** *Topography of the brain activity difference between left and right cues trials, averaged across the time-frequency window from 8 Hz to 11 Hz, and from 500 to 3000 ms after the checkerboard onset, and across trials and participants (n=7). The pattern of alpha lateralization observed in* ***Figure 7.4*** *after the cue onset was still present during the 10 Hz pattern reversing checkerboard, but with a more central topography.*

Alpha peak modulation. We investigated whether the individual alpha frequency was modulated between resting state (RS) eyes closed, RS eyes open, Precue, and Postcue conditions. The frequency peaks were, on averaged across participants, 10.6 Hz, 9.8 Hz, 10.6 Hz, and 10 Hz, for RS eyes closed, RS eyes open, Precue, and Postcue conditions, respectively. A one-way repeated-measures ANOVA showed a significant main effect of the factor condition (**Figure 7.7**; $F(4,7) = 3.787$; p-value = 0.0288; $eta^2 = 38.69$; SS = 3.645). Post-hoc analysis revealed that the alpha frequency was significantly higher for both the precue, and the RS eyes closed compared to RS eyes open (one-tailed t-test: p-value = 0.0168; Cohen's d = 0.8619; CI = [0.2368; Infinity]; p-value = 0.022; Cohen's d = -0.8715; CI = [0.1935; Infinity]). The other post-hoc tests were not significant (p-value > 0.0874).

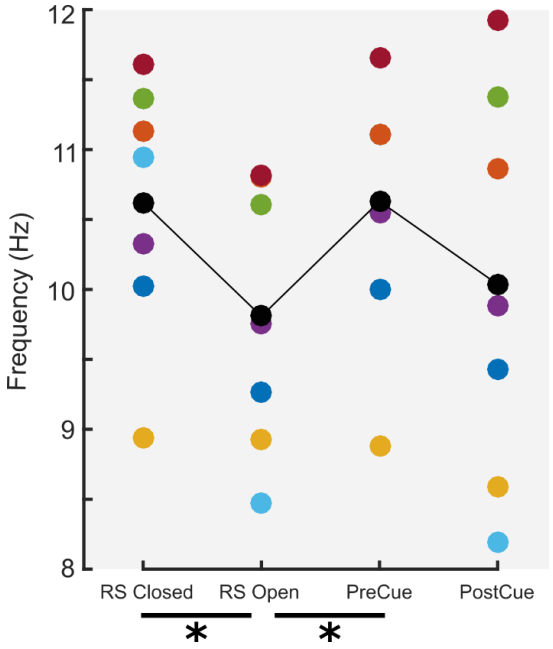

Figure 7.7: Modulation of individual alpha frequency. *Alpha frequency peaks extracted for RS eyes closed, RS eyes open, Precue and Postcue conditions. Color dots, Individual data. Black dots, Data averaged across participants (n=7). Post-hoc analysis showed that the frequencies of RS eyes closed and Precue periods were significantly higher than the frequency of RS eyes open.*

Traveling waves analysis at the sensor level. In this study, we hypothesized that brain oscillations during the deployment of endogenous attention were alpha traveling waves propagating from the frontal to the occipital electrodes. Inversely, visual stimulation would be associated with alpha traveling waves propagating in the opposite direction. We first tested whether we could identify signature of traveling waves at the sensor level.

ERPs. During the deployment of endogenous attention, we plotted the ERPs averaged across participants for spatial locations along the antero-posterior axis, lateralized in the left (O1, PO3, P3, CP3, C3, F3) or in the right (O2, PO4, P4, CP4, C4, F4) cortical hemisphere. We observed a constant shift of the ERP peaks from the frontal to the occipital electrodes between the scalp locations, suggesting that endogenous attention was associated with macroscopic traveling waves propagating in the antero-posterior direction (**Figure 7.8**).

During the 10 Hz pattern reversing checkerboard, we plotted the ERPs averaged across participants for spatial locations along the antero-posterior axis in the midline (Oz, POz, Pz, CPz, Cz, Fz – note that the checkerboard was presented in the center of the screen). There was a constant shift of the ERP peaks from the occipital to the frontal electrodes, suggesting that the

visual stimulation induced alpha traveling waves with a posterior-to-anterior direction (**Figure 7.9**).

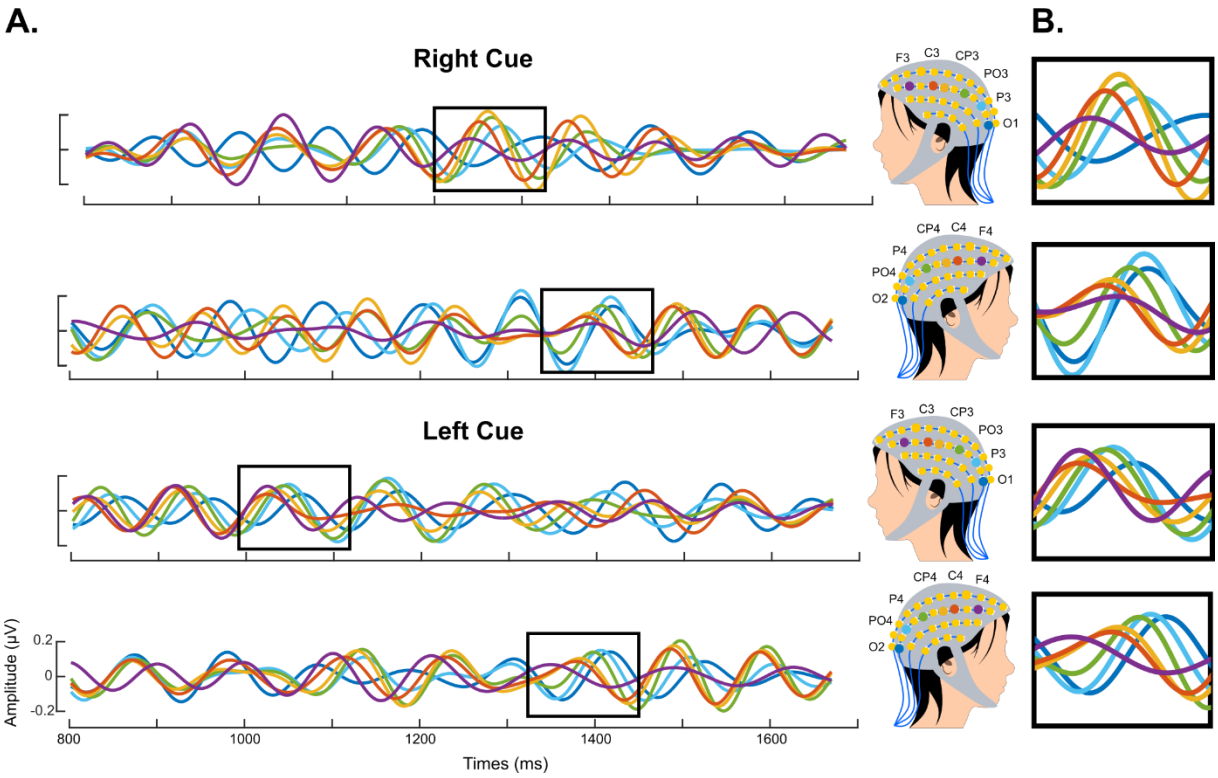

Figure 7.8: The ERP peaks shifted from frontal to occipital electrodes during the deployment of endogenous attention. A. *ERPs averaged across participants (n=7) and plotted for electrodes along the antero-posterior axis on the left (O1, PO3, P3, CP3, C3, F3) and on the right (O2, PO4, P4, CP4, C4, F4) hemisphere, from 800 to 1700 ms after the cue onset.* ***B.*** *Zoom for selected time-windows. The ERP peaks shifted along the antero-posterior axis, suggesting the presence of a traveling wave with an anterior-to-posterior direction.*

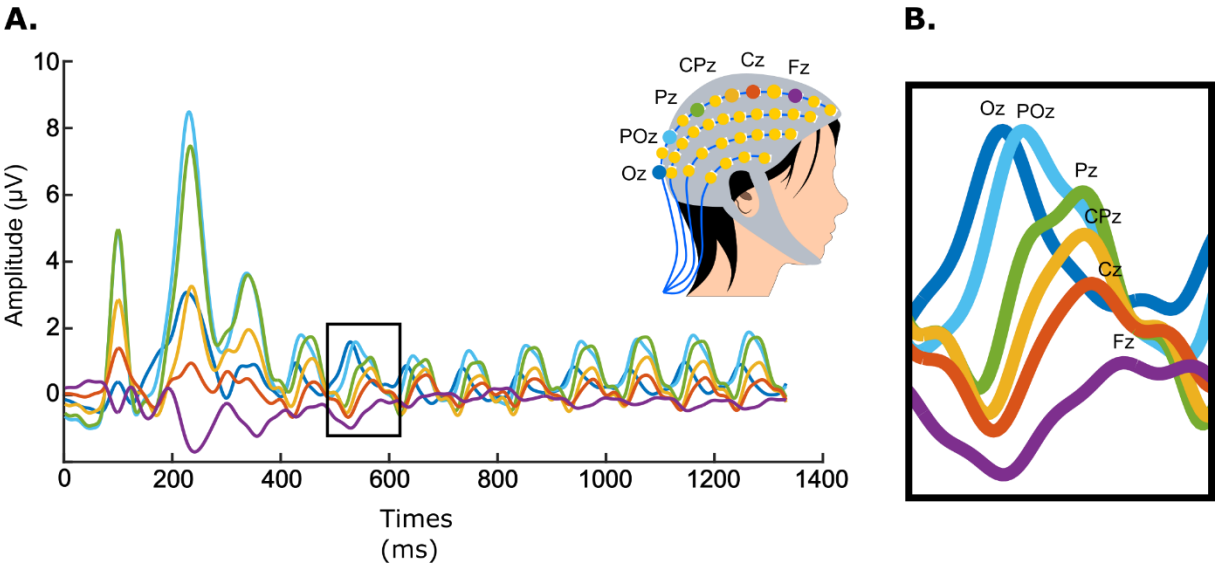

Figure 7.9: The ERP peaks shifted from occipital to frontal electrodes during the 10 Hz pattern reversing checkerboard. A. *ERPs averaged across participants (n=7) and plotted for*

midline electrodes along the antero-posterior axis (Oz, POz, Pz, CPz, Cz, Fz), from 0 to 1300 ms after the onset of the checkerboard. ***B.*** *Zoom on the period around 500 ms after the onset of the checkerboard. The ERP peaks shifted along the antero-posterior axis, suggesting the presence of a traveling wave with a posterior-to-anterior direction.*

Pairwise phase difference. We computed the pairwise phase differences between non-contiguous electrodes for spatial locations along the antero-posterior axis, lateralized in the left (O1, PO3, P3, CP3, C3, F3) or in the right (O2, PO4, P4, CP4, C4, F4) cortical hemisphere, during the deployment of endogenous attention. The phase differences were averaged across trials and pairs of electrodes, and extracted at the alpha frequency (10.8 Hz, the closest frequency to the one of 10.6 Hz identified in the *Alpha peak modulation* section, due to time-frequency decomposition). Both the time courses and the rose plots showed a phase difference of approximatively 10°, suggesting the presence of an alpha traveling wave (**Figure 7.10**). The post-hoc analysis (Watson Williams test against 0, $p < 0.05$, uncorrected) suggested that the phase difference was significant from 400 to 1500 ms after the cue onset, except for the phase difference computed on the left electrodes for the right cue, where the time window of significance was less important.

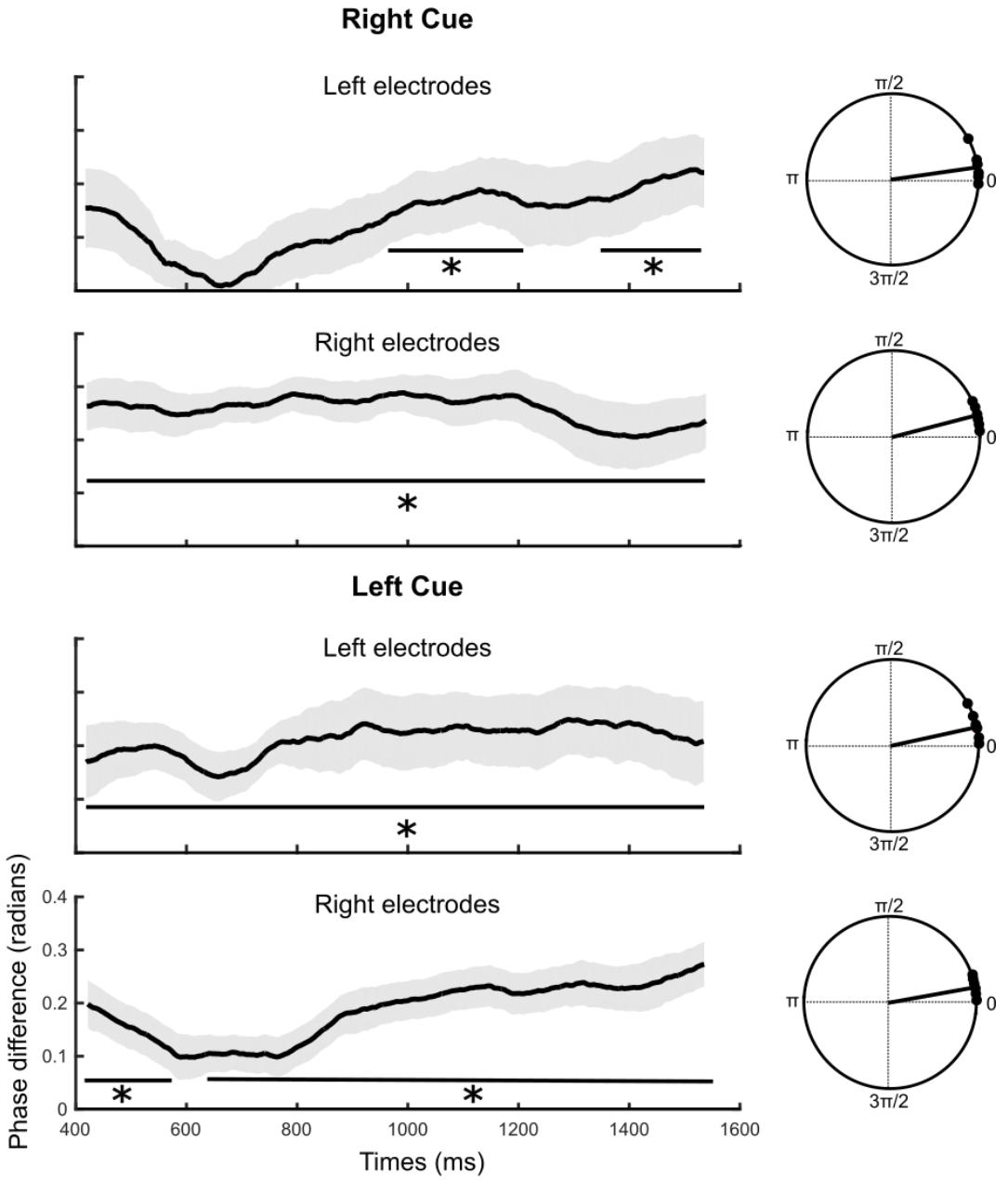

Figure 7.10: Phase differences between non-contiguous pairs of electrodes during the deployment of endogenous attention. *Black line, Phase differences between non-contiguous pairs of electrodes along the antero-posterior axis on the left (O1, PO3, P3, CP3, C3, F3) and on the right (O2, PO4, P4, CP4, C4, F4) hemisphere, averaged across pairs of electrodes, trials, and participants, extracted at 10.8 Hz and plotted from 400 to 1500 ms after the cue onset. Shaded area, Standard Error of the Mean (SEM) across participants. Insert, Rose plots with black dots, individual data, and black line, mean across participants. We observed a phase difference of approximately 10° on average.*

We performed the same analysis for spatial locations along the antero-posterior axis in the midline (Oz, POz, Pz, CPz, Cz, Fz), for the 10 Hz pattern reversing checkerboard, at 10.3 Hz (the closest frequency to the one of 10 Hz identified in the *10-Hz induced brain oscillations*

section, due to time-frequency decomposition). Both the time courses and the rose plots showed a phase difference of approximatively 30°, suggesting the presence of an alpha traveling wave (**Figure 7.11**). The post-hoc analysis (Watson Williams test against 0, $p < 0.05$, uncorrected) suggested that the phase difference was significant from 500 to 750 ms, and from 2100 to 3000 ms.

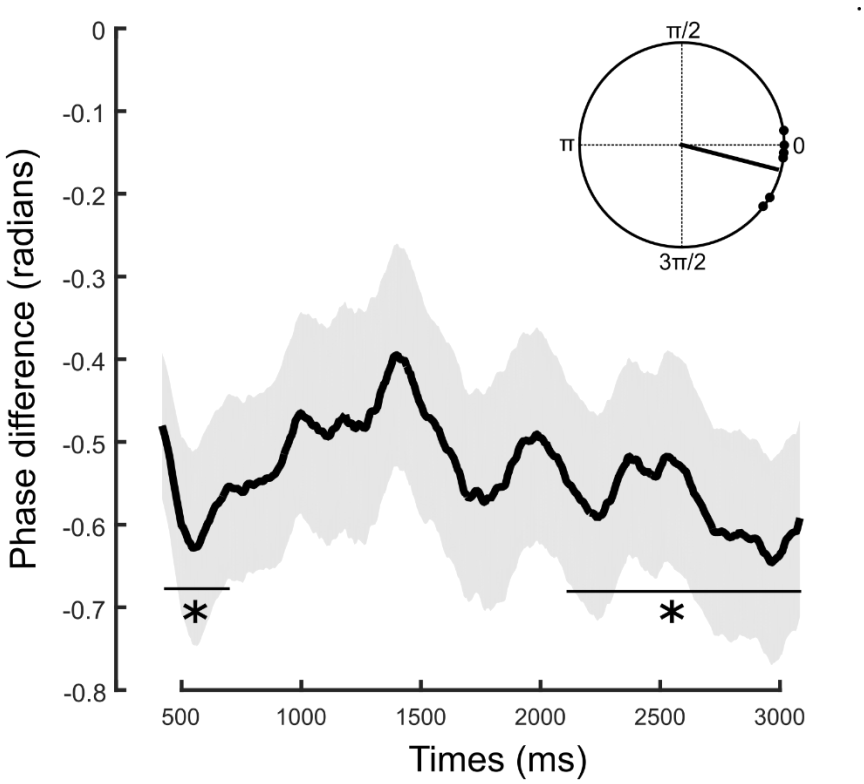

Figure 7.11: Phase differences between non-contiguous pairs of electrodes during the 10Hz pattern reversing checkerboard. *Black line, Phase differences between non-contiguous pairs of electrodes along the antero-posterior axis in the midline (Oz, POz, Pz, CPz, Cz, Fz) averaged across pairs of electrodes, trials, and participants, extracted at 10.3 Hz and plotted from 500 to 3000 ms after the checkerboard onset. Shaded area, Sem across participants. Insert, Rose plot with black dots, individual data, and black line, mean across participants. We observed a phase difference of approximately 30° on average.*

2DFFT. Finally, to further investigate the direction of traveling waves, EEG trials were stacked according to the previously selected electrodes along the posterior-to-anterior axis. Theses 2D maps were then transformed with a 2DFFT, allowing to identify forward traveling waves in the upper left quadrant, and feedback traveling waves in the bottom left quadrant. During the deployment of endogenous attention, we observed both forward and feedback traveling waves at 9.48 Hz (**Figure 7.12**). The checkerboard was associated with a strong forward traveling wave, and a lower feedback traveling wave, at 10 Hz (**Figure 7.13**).

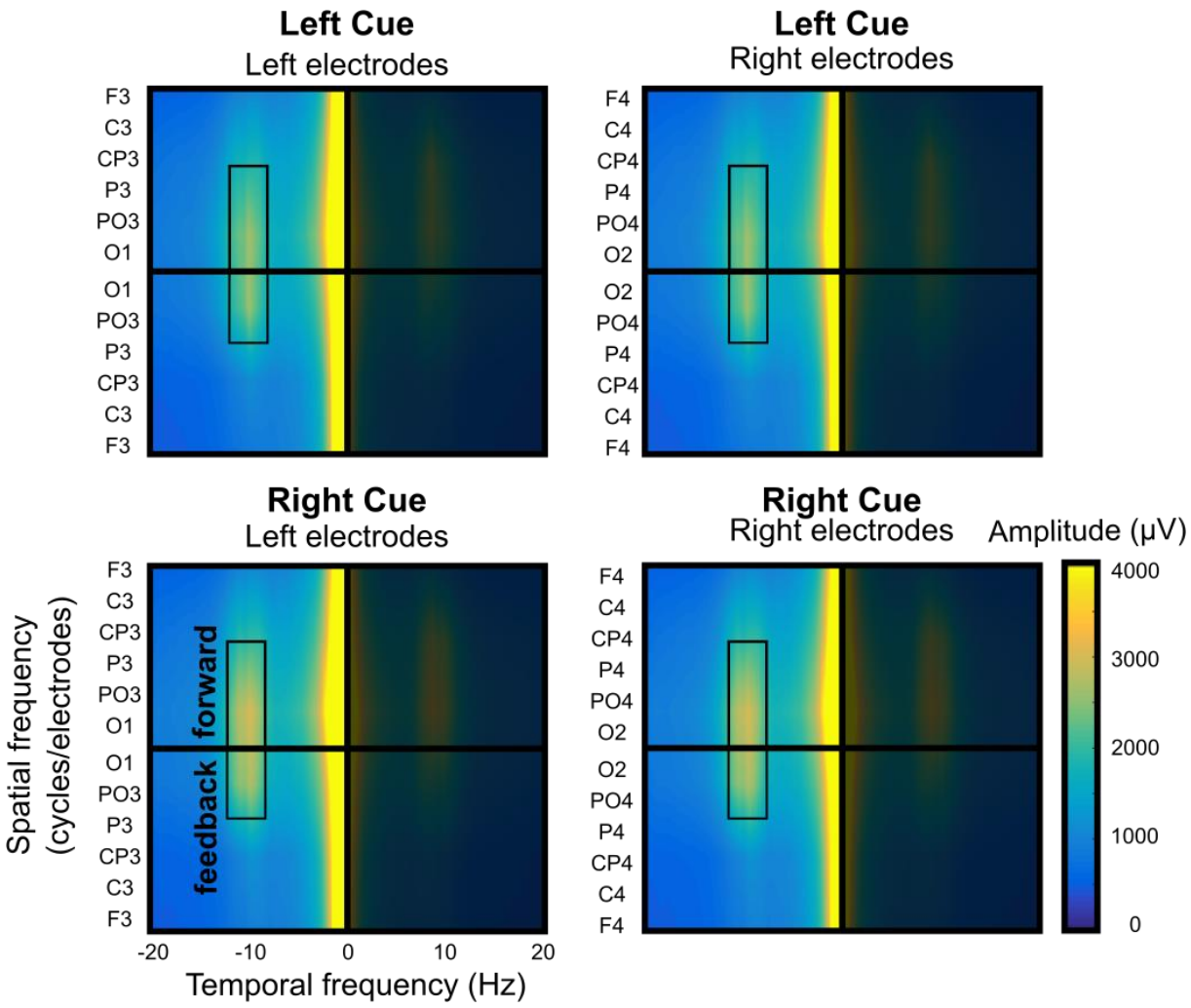

Figure 7.12: 2DFFT during the deployment of endogenous spatial attention revealed both forward and feedback traveling waves at 9.48 Hz*. Cue-epochs were stacked according to left (O1, PO3, P3, CP3, C3, F3) and right (O2, PO4, P4, CP4, C4, F4) electrodes to form 2D maps, that were then transformed with a 2DFFT. We observed an activity in the upper and lower left quadrants for each condition, suggesting the presence of feedforward and feedback traveling waves after the cue onset.*

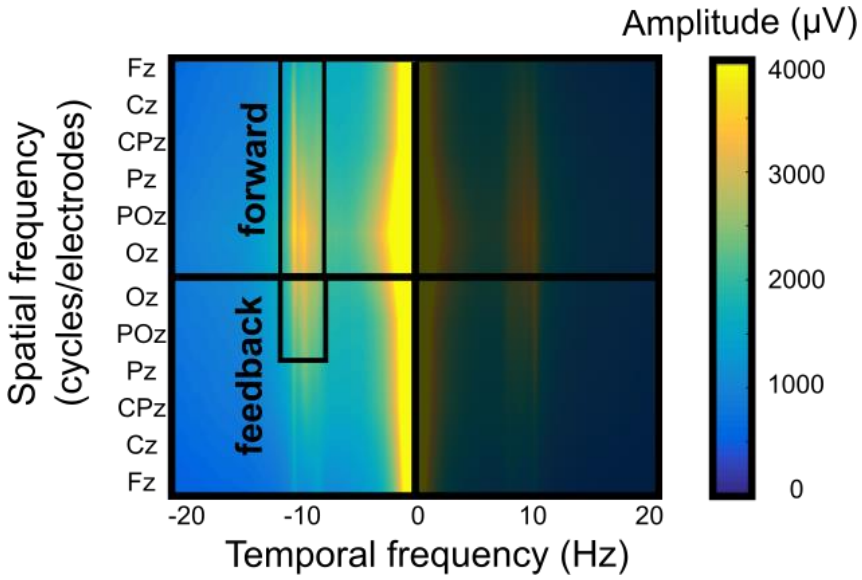

Figure 7.13: 2DFFT during the 10Hz pattern reversing checkerboard showed the presence of feedforward traveling waves at 10 Hz. *Annulus-epochs were stacked according to electrodes Oz, POz, Pz, CPz, Cz, Fz to form a 2D map, that was then transformed with a 2DFFT. We observed a strong amplitude in the upper left quadrant suggesting that the checkerboard was mainly associated with a feedforward traveling wave.*

2.4. Discussion

In this study, we investigated whether manipulating the cognitive function engaged in a task allowed to change the direction of propagation of alpha traveling waves. We hypothesized that the deployment of spatial endogenous attention was associated with traveling waves propagating from the frontal to the occipital brain areas, and that the perception of a visual stimulation would be associated with a shift of the propagation from the occipital to the frontal areas.

First, we observed that endogenous attention was manipulated. At the behavioral level, the performance was higher for the valid condition compared to invalid, suggesting that the deployment of endogenous attention allowed to facilitate the processing of visual inputs in valid trials. There were also longer reaction times for the valid trials, thus, we could not exclude a speed-accuracy tradeoff at the moment. At the electrophysiological level, the pattern of alpha lateralization, associated to the deployment of spatial endogenous attention in numerous studies (Worden et al., 2000; Sauseng et al., 2005b; Thut et al., 2006; Händel et al., 2011), was observed in every participant (data not shown) and on data averaged across participants.

The 10 Hz pattern reversing checkerboard induced alpha brain oscillations in the occipital cortex, as expected. Spatial endogenous attention was still deployed during the 10 Hz pattern reversing checkerboard, as shown by the presence of the alpha lateralization pattern after the onset of the checkerboard.

These results confirmed that we successfully manipulated endogenous attention and visual perception, both associated with the emergence of brain oscillations in the alpha frequency band.

Then, we investigated whether brain oscillations were propagating at the macroscopic scale, from frontal-to-occipital electrodes during the deployment of endogenous attention, and in the reverse direction during visual perception. Our preliminary results validated both hypotheses. After the cue onset, 9-Hz traveling waves were propagating from the frontal to occipital regions,

with an approximate phase shift of 10°. Inversely, we observed 10-Hz traveling waves propagating from the occipital to the frontal electrodes during the 10 Hz pattern reversing checkerboard, with a phase shift of approximately 30°.

These preliminary results are in line with our hypothesis. At the moment, we recorded and analyzed the data of 7 participants. We plan to recruit a larger number of participants soon to reach 15 to 20 participants in total. Statistical analysis, especially on the traveling waves analysis at the sensor level, will also be performed when we will have recruited all participants.

3. Fakche, Galas, VanRullen, Marque & Dugué. Visual perception causally triggers occipital-to-frontal alpha traveling waves.

In this second project, we tested whether there is a *causal* link between visual perception and the propagation of alpha traveling waves in the posterior-to-anterior direction. We used single pulses of TMS applied over V1 to induce phosphene perception, with the aim to investigate a causal relation between oscillatory traveling waves, cortical excitability, and the associated visual perception.

This study was performed in collaboration with Rufin VanRullen, in Toulouse. The covid pandemic has strongly impacted us and delayed the moment at which we were able to begin the data collection in human participants.

3.1. Introduction

The perception of a visual stimulus has been associated with the propagation of alpha traveling waves from occipital to frontal regions (Barlow and Estrim, 1970; Schack et al., 1999, 2003; Burkitt et al., 2000; Srinivasan et al., 2006; Cottereau et al., 2011; Giannini et al., 2018; Alamia and VanRullen, 2019; Lozano-Soldevilla and VanRullen, 2019; Tsoneva et al., 2021). Interestingly, the traveling direction seems to have functional relevance. During resting state, alpha oscillations seem to travel from the frontal to the occipital cortices, in a feedback manner (Inouye et al., 1983, 1995; Ito et al., 2007; Nolte et al., 2008; Alamia and VanRullen, 2019; Pang et al., 2020). When a visual stimulus is presented, the direction of alpha traveling waves shifts to a feedforward propagation, from the occipital to the frontal cortices, presumably to allow communication with higher-order brain areas (Schack et al., 1999; Patten et al., 2012; Alamia and VanRullen, 2019; Pang et al., 2020). In addition, the direction of traveling waves appears to predict visual illusion (Shevelev et al., 2000), and visual word processing (Schack et

al., 2003). To date, however, a causal relation between visual perception and the propagation of alpha traveling waves from occipital to frontal brain areas has not been established.

Single pulses of TMS applied over V1/V2 can elicit phosphenes (illusory percepts) depending on cortical state, i.e., phosphene perception occurs when cortical excitability is sufficiently high. Indeed, phosphene perception leads to a higher event-related potential (ERP) (Dugué et al., 2011a; Taylor et al., 2010; Samaha et al., 2017). TMS-induced phosphene perception allowed to establish a causal link between alpha oscillations, cortical excitability, and the associated perceptual performance (Romei et al., 2008; Dugué et al., 2011; Samaha et al., 2017; Fakche et al., 2022). The probability to perceive a phosphene is higher when the amplitude of alpha oscillations is low (Romei et al., 2008; Samaha et al., 2017), and fluctuates along with the alpha phase (Dugué et al., 2011a; Samaha et al., 2017), predominantly when alpha amplitude is high (Fakche et al., 2022).

Single pulses of TMS applied over the occipital cortex were also used to identify the natural frequency of the visual regions. Indeed, a way to find the intrinsic rhythm of a system is to directly perturbs it, and to measure the ensuing oscillations, i.e., the natural frequencies. Single pulses of TMS can be used as a tool to disturb the brain to investigate the features of the natural frequencies (Rosanova et al., 2009). This paradigm showed that the occipital, parietal, and frontal regions, respectively present natural frequencies in the alpha (8-12 Hz), beta (13-20 Hz) and gamma (21-50 Hz) range (Rosanova et al., 2009).

We hypothesized that the natural frequencies elicited by single pulses of TMS in the occipital regions are alpha traveling waves. In addition, we aimed to test whether there is a causal link between the feedforward propagation of traveling waves of natural frequencies and phosphene perception. We applied single pulses of TMS over V1 at perceptual threshold (~50 %) in human participants, simultaneously of an EEG recording.

3.2. Materials and Methods

Participants. Given the delays to obtain the contract to perform our experiment in Toulouse and to obtain the ethics approval, as well as the constraints of the Covid-19 pandemic, to date, the experiment is completely set up in Toulouse and the data of one participant was collected. (Note that five other participants have been also included in the study, and screened on their ability to perceived TMS-induced phosphene; their data will be collected soon.) The participant was free from medication affecting the central nervous system, reported no history of

psychiatric or neurological disorders, and fulfilled the standard inclusion criteria for TMS application (Rossi et al., 2009) as evaluated during a visit with a medical doctor. The participant gave its written informed consent and was compensated for their participation. The study was approved by the local French ethics committee Nord-Ouest I (IRB # 2020-A01026-33) and followed the Declaration of Helsinki.

Stimuli. Stimuli were designed with PsychToolbox 3.0.11, running in Matlab R2014b 32-bit (The MathWorks, Natick, MA), and displayed on a 1920 * 1080 pixels screen, with a 120 Hz refresh rate, at 57 cm distance, in a dark experiment room. The stimulus used was a fixation cross with the arms measuring 0.2 degrees of visual angle (°) of length and 0.05° of width.

Eye tracker. Participant's head was maintained with a chinrest. An infrared video-camera system (EyeLink 1000, SR Research, Ottawa, Canada) was used to ensure that the participant maintained their gaze on the fixation cross throughout the trial. The trial only started when the participant was successfully maintaining fixation. When a gaze deviation of >2° from the center of the screen was detected or a blink, we considered that the participant broke fixation and the trial was removed from the analysis (30 trials for the participant). Supernumerary trials were added at the end of each block to compensate for rejected trials.

MRI. Anatomical and functional MRI scans were collected with a 3T Philips (Amsterdam, The Netherlands) ACHIEVA scanner with a 32-channel head coil. Anatomical images were recorded with 212 sagittal slices, 0.8 mm^3 voxel size, a repetition time (TR) of 10 ms, a time echo (TE) of 4.6 ms, and a field of view (FOV) of 256 mm. A multi-echo fast low angle shot (FLASH) sequence with flip angles at 5° and 30° was also recorded to improve the source reconstruction analysis (not presented here). Functional MRI images were acquired in the transverse plan with 28 slices, 2 mm^3 voxel size, a TR of 1000 ms, a TE of 35 ms, a FOV of 192 mm, and a flip angle of 62°. We recorded four sequences with clockwise and counterclockwise wedges, expanding and contracting rings (Dougherty et al., 2003; Larsson and Heeger, 2006; Dugué et al., 2018, 2020), in order to perform individual retinotopic mapping. Each cycle lasted 24 s, with a pattern-reversal occurring every 250 ms. Stimuli were generated using Matlab R2021b 64-bit (The MathWorks, Natick, MA) and the MGL toolbox (Gardner et al., 2018) on a Macintosh computer.

Brain-navigated TMS and EEG. EEG was recorded using a 64-channels actiChamp system (Brain Products GmbH). The ground was placed at the FCz position, and the reference at the

AFz position (DC recording; 5000 Hz sampling rate). The participant's head was maintained using a chinrest and a headrest. A 70-mm figure-of-eight coil was placed over the right or left occipital pole (V1/V2; ~1 cm above the inion and ~2 cm away from the midline). Biphasic TMS pulses were applied with a Magstim Rapid2 stimulator of 3.5 Tesla (Magstim, Spring Garden Whitland, Great 137 Britain). A neuronavigation system (Brainsight, Rogue Research Inc., Montreal, Canada) was used to record the positions of the TMS coil, the EEG channels, digitized with a tracking system, and the participant's head defined by the position of the three fiducials (the nasion, the left and right periauricular points) on their anatomical MRI.

Procedure.

Phosphene screening and titration. The participant was selected based on their ability to perceive TMS-induced phosphenes. A train of 5 pulses at 20 Hz and 70% of the TMS machine output intensity, i.e., suprathreshold, was applied over the right or left occipital pole (i.e., V1/V2; Dugué et al., 2011, 2016, 2019; Lin et al., 2021) while participant kept fixating at a central fixation. The participant was asked to draw their phosphenes as precisely as possible by pressing the mouse-button to delimit the outlines of the phosphenes (see **Figure 7.14** for phosphene's drawing examples). Then, an individual phosphene perception threshold was determined. Single pulses of TMS with a fixed output intensity at 90% were applied. The participant was asked to report whether they perceived a phosphene or not (left or right arrow on the computer keyboard, respectively). At each trial, the background color of the screen was varying according to one-up/one-down staircase procedure to reach a threshold of 50% of phosphene perception.

Figure 7.14: Overlap of three phosphene drawings from the participant.

Experimental session. The participant performed 10 blocks of 50 trials each, composed of 8 blocks of test trials, and 2 blocks of catch trials (randomly interleaved). In the test trials, single pulses of TMS with an output intensity at 90% were applied, while in catch trials, the output intensity was at 50%. Throughout the experiment, the participant kept fixating a central cross. After a delay varying between 500 and 1500 ms, with a 100-ms step, the TMS pulse was applied. 1000 ms after the pulse, the fixation cross turned green, the participant had to indicate whether they perceived a phosphene or not (left or right arrow on the computer keyboard, respectively), followed by a 500-ms delay (**Figure 7.15**). The percentage of perceived-phosphene was monitored at the end of each block of test trials, and a new staircase was performed when above 75% or below 25%.

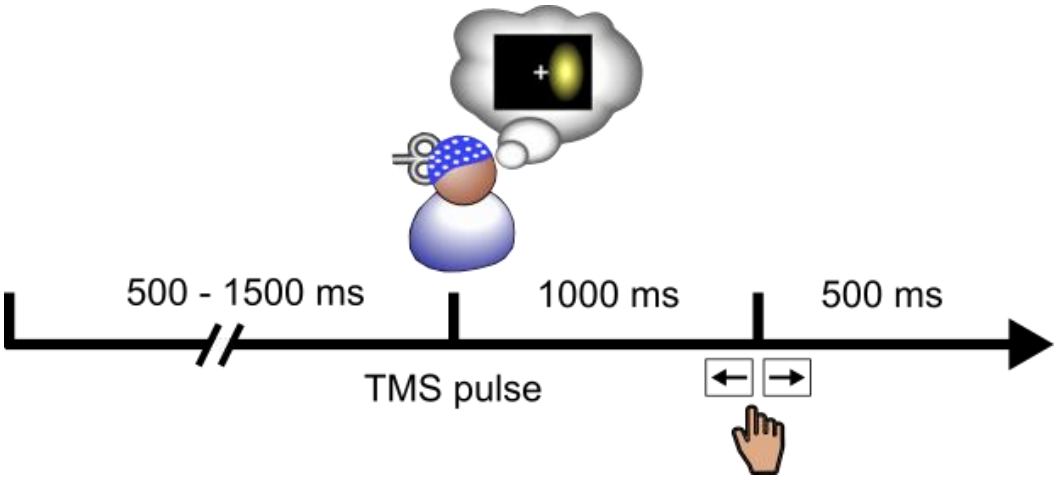

Figure 7.15: Experimental design. *After a random delay between 500 and 1500 ms, a single pulse of TMS was applied over V1/V2. After a 1000-ms delay, the participant indicated whether they perceived the phosphene or not with the right and left arrow, respectively.*

Behavioral analyses. Behavioral analyses were performed with Matlab R2014b (The MathWorks, Natick, MA). Phosphene perception and median reaction times were computed for each participant, for test and catch trials separately, to ensure that the performance was significantly lower in the catch condition, i.e., with a low TMS pulse intensity.

EEG analysis. EEG analyses were performed with Fieldtrip (Oostenveld et al., 2011; Donders Institute for Brain, Cognition and Behavior, Radboud University, Nijmegen, the Netherlands) and custom software written in Matlab R2014b (The MathWorks, Natick, MA).

Preprocessing. EEG data and channels positions were imported into Fieldtrip. Visual inspection allowed to identify electrodes with a low signal-to-noise ratio, which were then interpolated. EEG data were re-reference to the average reference, and epoched from -800 ms to +1000 ms according to the TMS pulse onset, separately for test and catch conditions. Data were

downsampled to 512 Hz. Epochs with a loss of fixation, an absence of response, and with artifacts were rejected from the analysis. Finally, the EEG signal around the TMS pulse, 15 ms before and 60 ms after, was erased and replaced by a linear interpolation, to clean the artifact induced by the TMS pulse. An Independent Component Analysis (ICA) was also performed to identify and remove the decay.

Time-frequency decomposition. A time-frequency transform (morelet wavelet) was computed on single epochs, separately for test and catch conditions, and for perceived- and unperceived-phosphene trials, with the *ft_freqanalysis* function from Fieldtrip. We used cycles that linearly increased from 1 to 20, and 93 frequencies that increased linearly from 2 to 48 Hz.

Natural frequency analysis. Rosanova et al. (2009) showed that a single pulse of TMS applied over the visual cortex induced brain oscillations in the alpha frequency band, i.e., the visual cortex responded at its natural frequency. To investigate whether we were able to replicate the results from Rosanova et al. (2009), we extracted the amplitude with *abs* function in Matlab from the time-frequency decomposition, and applied a baseline correction from -400 to -100 ms according to the onset of the TMS pulse, for each trials, channels, and frequencies. We computed the difference between normal and catch conditions, i.e., in the catch condition, we applied a pulse of TMS with a very low intensity, less susceptible to induce the brain to respond at its natural frequency, separately for perceived- and unperceived-phosphene conditions. Time-frequency maps of the difference were then plotted on data averaged across electrodes, as well as the topography.

3.3. Results

Behavior. The percentage of perceived-phosphene and median reaction times were computed separately for test and catch conditions. The percentage of perceived phosphene was 55.4% and 1%, respectively for test and catch conditions (**Figure 7.16**, left panel). The median reaction times were 294 ms and 378 ms, respectively for test and catch conditions (**Figure 7.16**, right panel). These results validate our procedure to obtain catch trials, i.e., a TMS pulse with an intensity low enough to not induce phosphene perception, and test trials with a 50%-threshold perception. We also observed that the participant was longer to respond in catch trials, presumably because phosphene perception was very low.

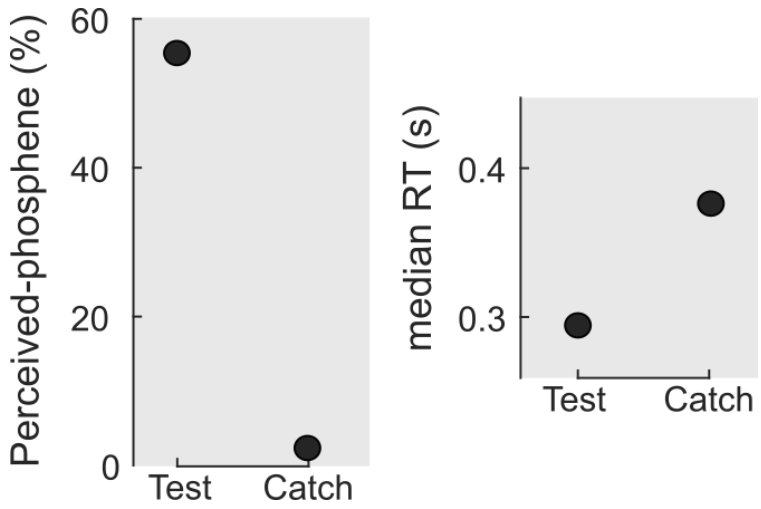

Figure 7.16: Phosphene perception was successfully manipulated*. Left panel, Percentage of perceived-phosphene, Right panel, Median reaction times, for the test and the catch conditions. Phosphene perception in the catch condition was almost null and around 50% in the test condition, as expected according to our experimental manipulation.*

Natural frequency. We hypothesized that single pulses of TMS applied over the occipital cortex in the test condition, i.e., with high TMS intensity, induced the brain to respond at its natural frequency, which is in the alpha frequency band for the occipital cortex (Rosanova et al., 2009). Time-frequency maps of the difference between normal and catch conditions of the amplitude baseline-corrected were plotted separately for perceived- and unperceived-phosphene trials, on data averaged across all electrodes. After the TMS pulse, we observed a strong brain activity in the alpha frequency band, from 10 Hz to 14 Hz, and from 0 to 700 ms, in the perceived-phosphene condition (**Figure 7.17.A**). The TMS-induced activity was localized over the left occipital cortex, i.e., where the TMS pulse was applied (**Figure 7.17.C**). Interestingly, this brain activity was not observed in the unperceived-phosphene conditions (**Figure 7.17.B**).

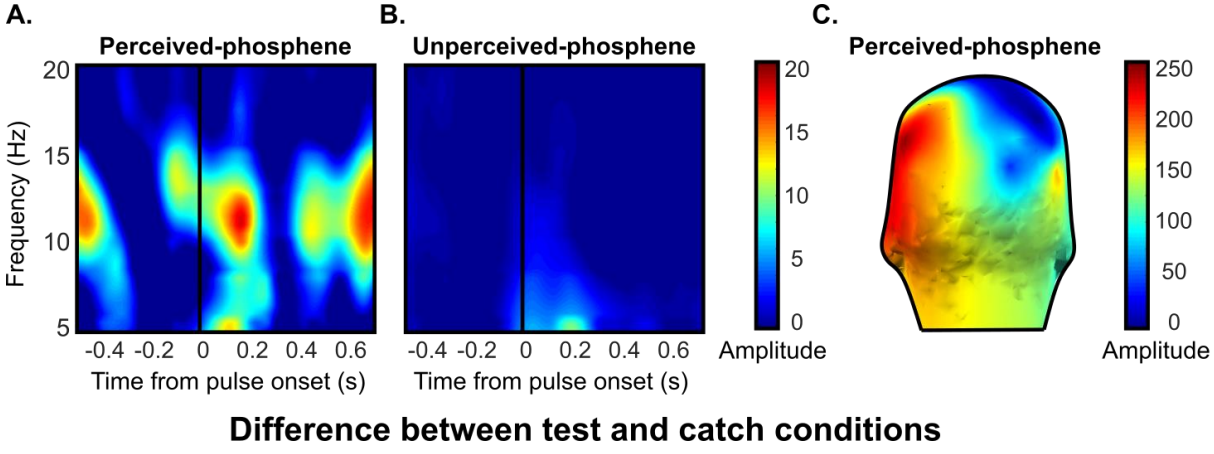

Figure 7.17: Single pulses of TMS applied over the left occipital cortex evoked brain oscillations at their natural frequency. *Amplitude difference between test and catch conditions averaged across all 61 electrodes for the participant,* ***A.*** *for the perceived-phosphene condition,* ***B.*** *for the unperceived-phosphene condition. The TMS pulse evoked brain oscillations between 0 and 700 ms, in the frequencies from 10 Hz to 14 Hz, for the perceived-phosphene condition only.* ***C.*** *Topography of the amplitude difference for the perceived-phosphene condition, averaged across 0 to 700 ms according to the pulse onset, for frequencies between 10 Hz and 14 Hz. Natural frequencies were mainly evoked in the left occipital cortex, at the location of the TMS pulse.*

3.4. Discussion

In this second study, we hypothesized that natural frequencies evoked by a single pulse of TMS applied over the occipital cortex was feedforward traveling waves. We also aimed to investigate whether there was a *causal* link between traveling waves of natural frequencies and phosphene perception. To date, we have recorded and analyzed the data of one participant.

First, we observed that single pulses of TMS applied over the visual cortex induced brain oscillations in the alpha frequency band, i.e., natural frequency of the occipital cortex (Rosanova et al., 2009). Interestingly, natural frequencies were found only in the perceived-phosphene condition, and not in the unperceived-phosphene one. The link between behavioral performance and natural frequency has not been studied yet. Our preliminary results suggest that natural frequencies in the occipital cortex are evoked only when perception occurs.

We planned to investigate whether brain oscillations at their natural frequencies are traveling waves. The data on one participant did not allow us to perform reliable analyses. Our preliminary results allowed us to validate our experimental paradigm. We will record approximately 20 participants in the following months in order to complete this study, and provide responses to our hypothesis.

4. Summary and Discussion

In the first study (Fakche and Dugué), we were interested in how the manipulation of different cognitive functions, i.e., the deployment of endogenous covert spatial attention and visual perception, influences the direction of alpha macroscopic traveling waves. At the moment, we have recorded and analyzed the data of 7 participants. Our first results showed that we efficiently manipulated endogenous attention, with the presence of the alpha lateralization

pattern in the EEG. Similarly, the 10 Hz pattern reversing checkerboard induced alpha brain oscillations in the occipital cortex. Our experimental design allowed us to manipulate two cognitive functions associated with alpha brain oscillations. We hypothesized that during the deployment of endogenous attention, brain oscillations act as traveling waves propagating from frontal to occipital areas, and that visual perception is associated with feedforward traveling waves. Our preliminary results validated both hypothesis. We observed 9-Hz traveling waves propagating from the frontal to occipital regions, with an approximate phase shift of 10°, during endogenous attention. Inversely, we observed 10-Hz traveling waves propagating from the occipital to the frontal electrodes during the 10 Hz pattern reversing checkerboard, with a phase shift of approximately 30°.

In the second study (Fakche et al.), we tested whether there was a causal link between feedforward macroscopic traveling waves at their natural frequencies and phosphene perception. Unfortunately, the data collection has been strongly delayed due to the covid pandemic and other important administrative delays. We recorded and analyzed the data of one participant. Our preliminary results suggest that single pulses of TMS applied over the visual cortex induced brain oscillations at their natural frequencies, replicating previous observation (Rosanova et al., 2009), but only when perception occurred. This is a first encouraging step to investigate our hypothesis on the causal link between feedforward traveling waves induced by TMS and visual perception.

5. Future research questions

Macroscopic oscillatory traveling waves have been mainly recorded in humans with electrophysiological techniques (MEG/EEG). Their direction of propagation at the sensor level has been linked to cognitive functions (Schack et al., 1999, 2003; Shevelev et al., 2000; Sauseng et al., 2002; Patten et al., 2012; Alamia and VanRullen, 2019; Pang et al., 2020). In the future, we would like to investigate the functional role of the direction of propagation of macroscopic oscillatory traveling waves at the *source level*. To this aim, a model considering the link between the neural sources of macroscopic traveling waves and their projection at the sensors level is currently being developed in the lab (Grabot et al., in prep). The anatomical and functional MRI recorded in both experiments will be used to model individual macroscopic traveling waves at the source level.

Part 3. General Discussion.

Chapter 8. Discussion.

In this PhD, we studied the **functional role of the spatio-temporal organization of brain oscillations on visual perception and cortical excitability**, with a multimodal approach including **psychophysics**, **neuroimaging** (EEG, MRI, oculometry), and **non-invasive stimulation** (TMS), applied to healthy human participants. Four projects for a total of 8 experiments have been developed to address this topic. In the following part, I will summarize our results and highlight the critical findings, in light with the current literature. I will also discuss outstanding questions that remains to be investigated in the future regarding the functional role of brain oscillations.

1. Synthesis of the results and general discussion

1.1. Thesis summary

For almost a century, scientists have tried to characterize the functional role of brain oscillations on cognition. Cognition encompasses many brain functions; in this PhD, we focused on visual perception (and attention to some extent). The temporal features of brain oscillations, i.e., the phase and the amplitude, have been associated to visual perception, mainly *independently* from each other. A low amplitude of alpha oscillations localized in the parieto-occipital cortices has been associated to a higher probability to perceive a subsequent visual stimulus (Ergenoglu et al., 2004; Hanslmayr et al., 2007; Van Dijk et al., 2008; Wyart and Tallon-Baudry, 2009). In visual detection tasks, the same stimulus led to differential perceptual outcomes (e.g., perceived vs unperceived) as a function of the instantaneous phase of low frequency (delta, theta, alpha) spontaneous brain oscillations over the fronto-occipital areas (Nunn and Osselton, 1974; Varela et al., 1981; Busch et al., 2009; Mathewson et al., 2009; Busch and VanRullen, 2010; Dugué et al., 2011; Fiebelkorn et al., 2013b; Hanslmayr et al., 2013; Manasseh et al., 2013). In addition, the phase and the amplitude of alpha oscillations both modulate cortical excitability, assessed with single pulses of TMS (Romei et al., 2008; Dugué et al., 2011a; Samaha et al., 2017) or with MRI (Goldman et al., 2002; Moosman et al., 2003; Scheeringa et al., 2011).

In this PhD, we hypothesized that the phase and the amplitude of alpha oscillations jointly and causally modulate cortical excitability and the subsequent visual performance.

In the first project (**Chapter 4**), we studied the causal role of the interaction between the amplitude and the phase of brain oscillations in perceptual performance, according to the predictions made by the Pulsed Inhibition theory (Jensen and Mazaheri, 2010; Klimesch et al., 2007; Mathewson et al., 2011). This theory makes two clear predictions: (1) High alpha amplitude induces an alternation between cortical states of inhibition and excitation along with phase, leading to periodic perceptual performance. (2) Low alpha amplitude is less susceptible to this phase effect. **We provided strong evidence in favor of the Pulsed Inhibition theory by establishing a *causal* link between the phase and the amplitude of alpha oscillations, cortical excitability, and visual perception (Fakche et al., 2022, eNeuro; Figure 8.1).** The phase of spontaneous alpha oscillations modulates TMS-induced phosphene perception periodically, and this phasic effect was significantly lower when the amplitude of alpha oscillations was low. The use of single pulses of TMS over the occipital cortices to induce phosphene perception allows to have a direct access to the instantaneous state of the cortex, and to the instantaneous phase of brain oscillations. In comparison to previous non-invasive, correlational, human studies (Alexander et al., 2020; Bonnefond and Jensen, 2015; Busch and VanRullen, 2010; Harris et al., 2018; Kizuk and Mathewson, 2017; Mathewson et al., 2009; Milton and Pleydell-Pearce, 2016; Ai and Ro, 2014; Hermann et al., 2016; Ng et al., 2012; Spitzer et al., 2016; Zoefel and Heil, 2013), we showed that the phase of spontaneous alpha oscillations between -π/2 and -π/4 was associated to a lower state of cortical excitability, associated with a periodic decrease in perceptual performance, mainly when the amplitude of alpha brain oscillations were high (Fakche et al., 2022).

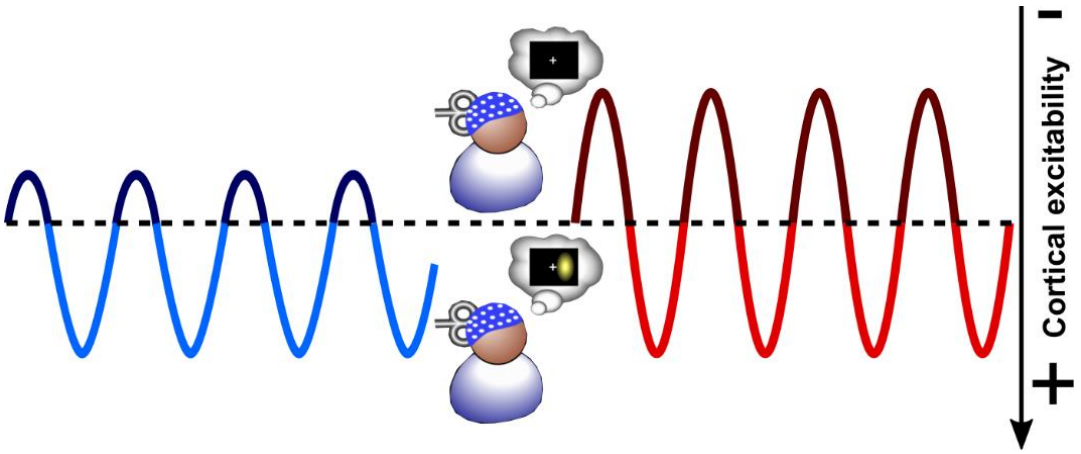

Figure 8.1: Phase-amplitude tradeoffs of alpha brain oscillations predicts cortical excitability and the subsequent visual perception, Visual Abstract from Fakche et al., 2022. *Phosphene perception is modulated periodically by the phase of alpha oscillations. This phase effect is stronger for high alpha amplitude, in red, compared to low alpha amplitude, in blue.*

The functional role of brain oscillations on visual perception has been widely studied with simple tasks. **We proposed that brain oscillations could underlie a more complex visual process: serial dependance**. Serial dependance describes that the perception of a visual stimulus is biased toward the previous similar visual inputs (Fischer and Whitney, 2014; Liberman et al., 2014; Cicchini et al., 2014; Burr and Cicchini, 2014), i.e., visual perception is built on an integrative spatiotemporal window that considers both the present visual input and the recent past. Serial dependance has been widely studied at the behavioral level, however, its neural dynamics remains ill-defined. A previous study has shown that a classification algorithm on the spatial pattern of brain activity allowed to distinguish face vs. house perception (Haxby et al., 2001). We hypothesized that the pattern of brain activity associated with face perception (and identified with a classification algorithm) would be found in stimuli biased towards face perception due to serial dependence. In addition, we hypothesized that this brain activity is oscillatory (**Chapter 5**). Two assumptions should be validated to test these hypotheses. First, serial dependence has been demonstrated to occur in face perception. Second, face perception has been associated with specific patterns of brain activity both in time and in time-frequency domains. However, neither assumption was validated by our first behavioral and electrophysiological results. **Consequently, we cannot conclude that brain oscillations play a functional role in serial dependence at the moment**.

The neuroscientific community has focused their research on the functional role of the temporal dynamics of brain oscillations for decades.

In our lab, we hypothesized that the spatio-temporal organization of brain oscillations have a functional role on cognition.

In the third project (**Chapter 6**), **we investigated whether brain oscillations propagate across the retinotopic cortex in humans, as a mesoscopic traveling wave, leading to specific perceptual consequences.** The propagation of brain oscillations within individual visual areas (V1, V2, V4, MT) have been widely recorded with invasive methods in animals (Sanchez-Vives and McCormick, 2000; Huang et al., 2004; Benucci et al., 2007; Han et al., 2008; Ray and Maunsell, 2011; Maris et al., 2013; Stroh et al., 2013; Muller et al., 2014; Zanos et al., 2015; Townsend et al., 2015; Davis et al., 2020). In humans, for ethics reasons, the use of invasive recordings is limited to patients, leading to a more complicated investigation of mesoscopic traveling waves. To overcome this issue, we developed, based on Sokoliuk and VanRullen (2016), a psychophysics experiment capitalizing on the role of phase on visual

perception (Busch et al., 2009; Mathewson et al., 2009; Varela et al., 1981; Dugué et al., 2011, 2015; Samaha et al., 2015, 2017; Fakche et al., 2022; Merholz et al., 2021; for review VanRullen 2016; Kienitz et al., 2021), and the retinotopic organization of early visual areas. **We showed that visual perception was modulated periodically across space and time by the phase of an oscillatory inducer, suggesting that alpha-induced brain oscillations travel across the retinotopic space, at a propagation speed of 0.2-0.4 m/s, to influence visual perception (Fakche and Dugué, 2022, bioRxiv; Galas, Fakche, Baudouin and Dugué, in preparation; Figure 8.2).** Our studies demonstrated that psychophysics is a powerful tool to investigate the functional role of mesoscopic traveling waves in humans.

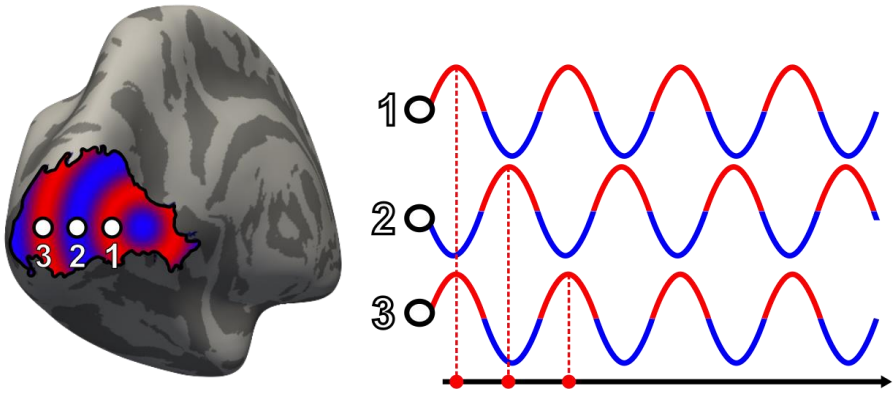

Figure 8.2: Alpha perceptual cycles travel across the visual retinotopic space. *An alpha oscillation is propagating across the retinotopic space of V1. The optimal phase for perception, in red, shifts between stimuli position.*

Finally, we were interested in the functional role of macroscopic oscillatory traveling waves (**Chapter 7**). Some studies suggest that the direction of traveling waves is modulated by cognition, during memory tasks (Sauseng et al., 2002; Zhang et al., 2018) and visual tasks (Shevelev et al., 2000; Schack et al., 1999, 2003; Patten et al., 2012; Alamia and VanRullen, 2019; Pang et al., 2020). In a first study, **we tested whether the direction of alpha macroscopic traveling waves changed as a function of the cognitive function engaged in the task**. We hypothesized that during the deployment of endogenous attention, traveling waves have an anterior-to-posterior propagation, that is reversed during visual perception. Our preliminary results showed that alpha traveling waves were propagating from the frontal to occipital regions, with an approximate phase shift of 10°, during endogenous attention. Inversely, we observed 10-Hz traveling waves propagating from the occipital to the frontal electrodes during visual perception, with a phase shift of approximately 30°. **Our first results**

suggest that manipulating cognition induces a change in the direction of macroscopic alpha traveling waves (**Figure 8.3**).

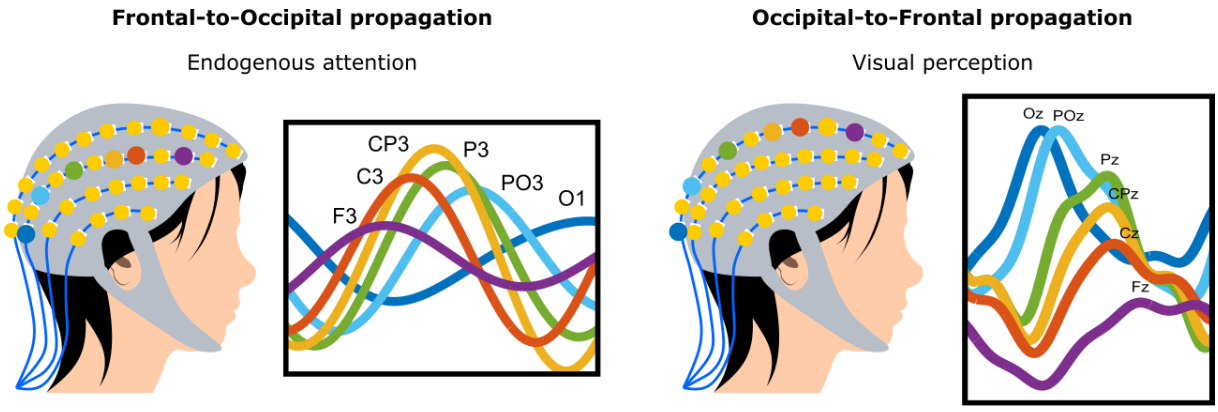

Figure 8.3: The deployment of endogenous attention and visual perception are associated with frontal-to-occipital and occipital-to-frontal alpha traveling waves, respectively. *ERPs averaged across participants (n=7) and plotted for electrodes aligned along the antero-posterior axis.*

In a second study, **we hypothesized that a single pulse of TMS applied over the occipital cortex causally triggered a feedforward traveling wave at its natural frequency, i.e., alpha**. This study, performed in collaboration with Rufin VanRullen in Toulouse, has been strongly delayed by the covid pandemic and other administrative considerations. Our preliminary results on one participant suggest that a single pulse of TMS applied over the visual cortex induced brain oscillations at their natural frequencies, replicating previous findings (Rosanova et al., 2009), but only when perception occurred. Our experimental paradigm allowed us to observe a modulation of natural frequencies by phosphene perception. This is a first encouraging step to investigate our hypothesis on the causal link between feedforward traveling waves induced by TMS and visual perception.

1.2. Considering the role of phase-amplitude tradeoffs of alpha *traveling waves* on cortical excitability and visual perception?

We established a causal link between the phase and the amplitude of spontaneous alpha oscillations, cortical excitability, and visual perception (**Chapter 4**; Fakche et al., 2022). Interestingly, we found that the phase effect had a frontal and an occipital topographic organization. In addition, the time at which the phase predicted the perceptual outcome differed by nearly half an alpha cycle between the occipital (-77 ms) and the frontal (-40 ms) regions.

This result may suggest that the neural information underlying phosphene perception is delayed with a phase shift between the frontal and the occipital regions as a macroscopic traveling wave (**Figure 8.4**). By considering the observed time difference (37 ms) and the alpha frequency recorded in our experiment (~10 Hz), the delay between the frontal and the occipital regions reflects a phase shift of 133°, which is coherent with the previous studies that observed a phase shift between occipital and frontal electrodes ranging from 145° to 180° (Cohn, 1948; Hord et al., 1972, 1974; Suzuki, 1974; Burkitt et al., 2000; Ito et al., 2005).

Several studies have already shown that visual perception was associated with alpha traveling waves propagating from the occipital to the frontal regions (Schack et al., 1999; Patten et al., 2012; Alamia and VanRullen, 2019; Pang et al., 2020). This propagation presumably reflects the communication of visual information from the sensory cortices to higher-order level brain areas.

On the other hand, it has been proposed that alpha oscillations in the occipital regions could be controlled by top-down processes from fronto-parietal areas (Klimesch et al., 2007a; Mathewson et al., 2011). Indeed, impairment of alpha oscillations in the frontal regions is associated with altered perceptual performance (Capotosto et al., 2009; Marshall et al., 2015), and alpha oscillations have been shown to carry neural information from frontal to sensory areas through feedback connections (Michalareas et al., 2016; van Kerkoerle et al., 2014). Through their top-down influence, frontal alpha could modulate the amplitude and the associated phase effect in the occipital regions (Klimesch et al., 2007).

The phase difference observed in our study (Fakche et al., 2022) is likely due to a macroscopic alpha traveling wave. According to the propagation of this traveling wave, from the frontal to the occipital electrodes or the opposite, we could disentangle the two functional roles proposed above. A member of the lab, David M. Alexander, is currently investigating this question by performing traveling waves analyses on our dataset (Alexander et al., 2019).

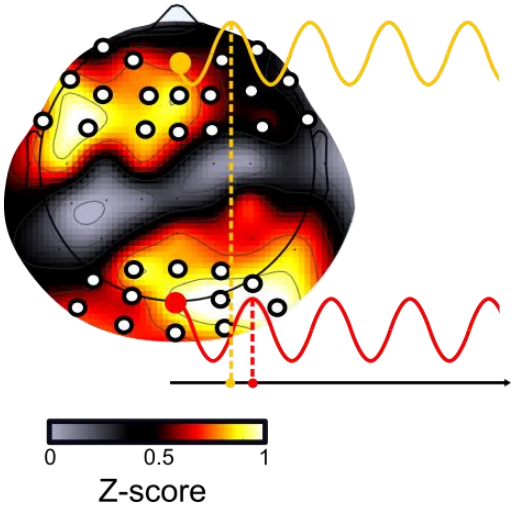

Figure 8.4: Macroscopic alpha traveling waves hypothesis. *The topography of the phase effect from Fakche et al., 2022 showed a frontal and an occipital component. A macroscopic alpha traveling waves propagating between the occipital and the frontal regions could explain the delays observed in the respective phase effects, i.e., -77 ms in the occipital region and -40 ms in the frontal region.*

1.3. Oscillatory traveling waves and predictive coding

We hypothesized that brain oscillations were the neural dynamics underlying serial dependance. The study that we developed did not allow us to respond to this question (**Chapter 5**). We would like to investigate whether brain oscillations underlie serial dependance according to the predictive coding theory. This theory describes that high-level brain areas send predictions on the following sensory inputs to the low-level brain areas, through feedback projections, and low-level brain areas compute the difference between the predictions and the actual input, i.e., prediction errors, and send it back to the high-level brain areas through feedforward projections, so that the brain can update its internal model and generate novel, adjusted predictions (Rao & Ballard, 1999, Friston et al., 2005, Bastos et al., 2012, Fontolan et al., 2014, VanKerkoerle et al., 2014, Lecaignard, 2016, Han & VanRullen, 2016, 2017, Alamia & VanRullen, 2019). In the context of serial dependance, the predictive coding explains well that visual perception is biased toward previous past visual inputs. Interestingly, the feedback and feedforward projections described in the predictive coding theory could be macroscopic oscillatory traveling waves. The predictions could be sent by traveling waves that propagate with an anterior-to-posterior direction, from the frontal to the occipital brain areas, while the prediction errors would be transmitted by traveling waves of opposite direction, i.e., posterior-to-anterior. One study showed that a predictive coding model with feedforward and feedback

brain oscillations was able to explain the emergence of traveling waves (Alamia and VanRullen, 2019). Applied to real EEG data, the model found feedforward and feedback traveling waves, in response to a visual stimulus and at rest, respectively (Alamia and VanRullen, 2019). The predictive coding theory also describes a modulation of brain activity as a function of behavior. Applied to visual perception, we can make two predictions. 1) A modulation of feedback traveling waves depends on the predictions sent to low-level brain areas, based on the strength of the brain internal representation of the external world. For example, if the same visual stimulus is presented many times, the predictions on the incoming stimulus will be very strong. We could observe a modulation of the temporal features of oscillatory traveling waves, such as a higher amplitude or an optimal phase, or of their spatiotemporal properties, e.g., a change in the propagation speed (Schack et al., 2003; Fellinger et al., 2012; Patten et al., 2012), the number of traveling waves (Alexander et al., 2006, 2008, 2009) or the timing of the change of the traveling waves direction, from postero-anterior to antero-posterior (Sauseng et al., 2002). 2) The feedforward traveling waves depend on the prediction errors, i.e., the difference between the predictions and the actual stimulus. Similarly, if the prediction error is strong, we expect to observe the same modulation of the spatio-temporal organization of traveling waves as the ones described above.

The predictive theory allows the investigation of the emergence of macroscopic traveling waves with a theoretical model, and to test the functional role of the traveling waves' properties on visual perception. A well-suited experimental protocol to study those questions would be an oddball paradigm (Lecaignard, 2016). Two visual stimuli are presented in a temporal sequence. One of them is displayed frequently, i.e., standard stimulus, while the other one presents a low probability of happening, i.e., deviant stimulus (**Figure 8.5**). The standard stimulus allows to generate a strong internal model of the external world, and consequently, strong predictions. The deviant stimulus will initiate a prediction error, that will be modulated according to the difference between the standard and the deviant. With this paradigm, we can study the functional role of feedforward and feedback traveling waves in response to standard stimulus inducing a strong vs. a low prediction, and deviant stimulus inducing a strong vs. a low prediction error.

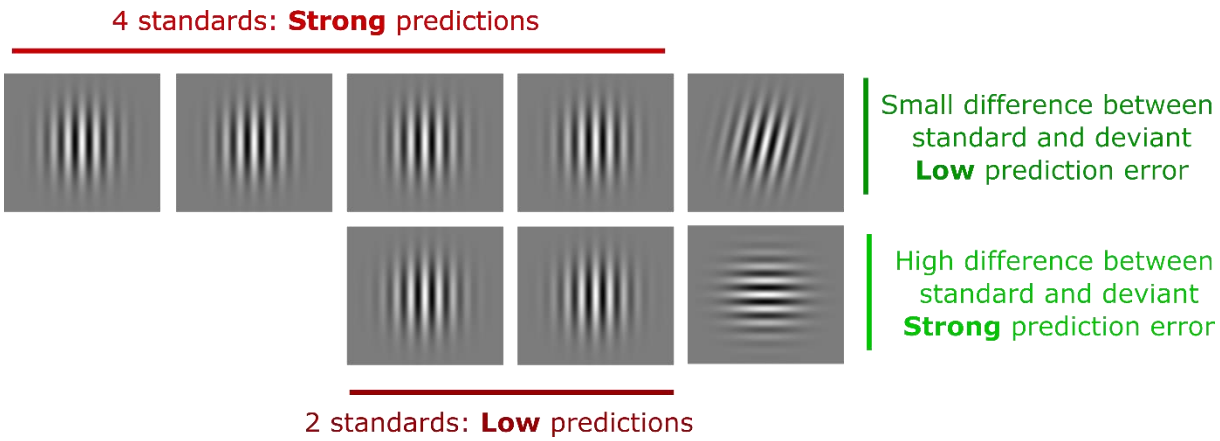

Figure 8.5: Predictive coding consequences in an oddball paradigm. *The oddball paradigm is designed with temporal sequences of a frequent stimulus, i.e., standard, and a rare stimulus, i.e., deviant. In this example, standard stimuli are vertical Gabor patches. The number of consecutives standard stimuli displayed allows to modulate the brain predictions. In addition, two rare stimuli are proposed, one Gabor patch slightly tilted to the right, i.e., small difference with the standard, and the other is a horizontal Gabor patch, i.e., strong difference. The two deviant stimuli allow to change the prediction error.*

1.4. Investigating the functional role of mesoscopic traveling waves in humans with psychophysics

With psychophysics coupled with EEG recordings, we found that alpha perceptual cycles traveled across the retinotopic visual space in humans, suggesting a functional role of mesoscopic alpha traveling waves on visual perception (**Chapter 6**; Fakche and Dugué, 2022, bioRxiv; Galas, Fakche, Baudouin and Dugué, in preparation). This study brings a novel methodology to study the role of mesoscopic traveling waves on human cognition (see also Sokoliuk & VanRullen, 2016).

The inducer that we used in the first experiment was a disk oscillating in luminance, that suffers from a masking effect. In the two following experiments, we used a pattern reversing checkerboard to induce brain oscillations, aimed to reduce luminance masking. However, the modulation of the visual performance according to the checkerboard inducer was very low for the stimuli the farthest from the inducer. Other stimulation to induce brain oscillations should be considered to improve this experimental protocol. One possibility would be to change the visual inducer, e.g., instead of modulating the luminance or using a pattern reversal, we could modulate another visual feature such as the color. This is not the best option because modulating the visual feature of the inducer will always have some confounding effect on visual perception.

Another elegant way to induce brain oscillations is to use rhythmic TMS (Thut and Pascual-Leone, 2010; Thut et al., 2011; Romei et al., 2011; Valero-Cabre et al., 2017). Rhythmic TMS, i.e., any combination of more than two pulses separated by a delay inferior to 2 seconds, allows to induced brain oscillations with a precise frequency and cortical location (Thut et al., 2011; Valero-Cabre et al., 2017), by directly modulating cortical excitability. Rhythmic TMS is thus a powerful tool to study the functional role of the spatio-temporal organization of mesoscopic traveling waves on perception.

Finally, the use of visual inducer or TMS allows to study the functional role of **induced** brain oscillations, and one cannot directly conclude on the effect of spontaneous oscillations. Invasive studies in animals have suggested that spontaneous activity acted as a traveling wave (Volgushev et al., 2006; Lippert, Takagaki et al., 2007; Luczak et al., 2007; Takagaki et al., 2008; Nauhaus et al., 2009, 2012). We could use the psychophysics experiment developed in this PhD without any inducer, and investigate whether 1) Perceptual performance is modulated periodically by the individual alpha frequency of each participant (identified with EEG recordings), and 2) The optimal phase for perception shifts between the position of the stimuli on the visual field. However, in comparison to alpha induced brain oscillations, the spontaneous ones have a lower amplitude, and it would be more difficult to estimate the phase at each position of the visual field.

1.5. What is the spatial extent of the phase effect of mesoscopic traveling waves?

In Fakche and Dugué (2022, bioRxiv) and the two follow-up studies (Galas, Fakche, Baudouin and Dugué, in preparation), we tested whether perceptual cycles traveled between three positions in the same quadrant of the retinotopic space (**Figure 8.6.1**). In Sokoliuk and VanRullen (2016), they tested five (**Figure 8.6.2**) and nine positions (**Figure 8.6.3**), in the same and in different quadrants, respectively. Each time, the stimuli were all aligned diagonally with the central fixation. Those studies always found a significant shift of the optimal phase between the stimulus the closest to the inducer, and the other positions.

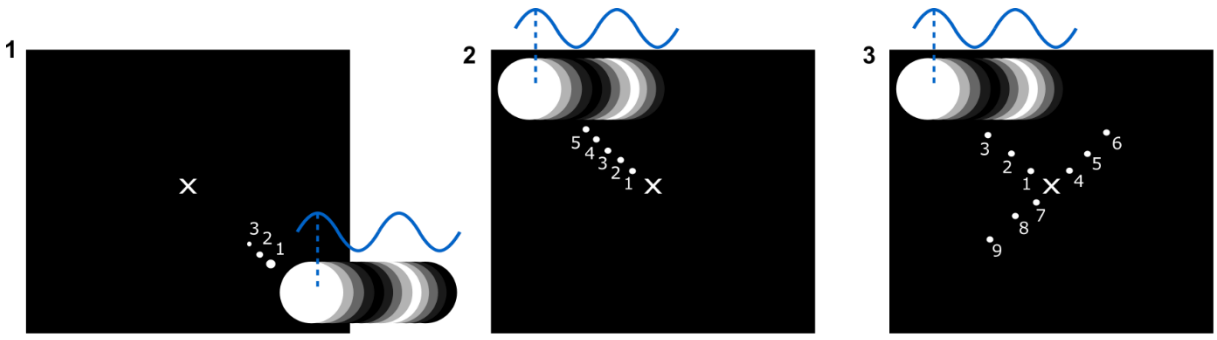

Figure 8.6: Positions of the stimuli tested to investigate whether perceptual cycles across the visual retinotopic space, in this PhD and in Sokoliuk and VanRullen (2016). 1. *Fakche and Dugué, 2022, bioRxiv.* ***2. and 3.*** *Sokoliuk and VanRullen, 2016.*

Further studies could be done to investigate the spatial extent of this phase shift.

An important question is the one of anisotropy, i.e., non-uniform propagation across space. Numerous studies provided strong evidence in favor of a propagation of mesoscopic traveling waves through the unmyelinated long-horizontal fibers present in the superficial layers (II-III) of the cortex (Tanifuji et al., 1994; Nelson and Katz, 1995; Bringuier et al., 1999; Wu et al., 2001; Contreras and Llinas, 2001; Peterson et al., 2003a; Tucker and Katz, 2003; Ferezou et al., 2006; Song et al., 2006; Knapen et al., 2007; Nauhaus et al., 2009; Reynaud et al., 2012; Muller et al., 2014; Besserve et al., 2015; Davis et al., 2020). In addition, a recent review proposed that the horizontal fibers in V1 were connected preferentially to neurons with a similar preferred orientation across short distance, and to larger neuronal populations at long distance (Chavane et al., 2022). Consequently, the question of whether neuronal activity propagates in an anisotropic or an isotropic way still needs to be answered.

One possibility would be to display numerous visual stimuli, not only aligned on the diagonal between the central fixation and the inducer, to study the propagation of mesoscopic traveling waves in multiple directions within the early visual areas (**Figure 8.7.1**). Indeed, we do not know whether mesoscopic traveling waves are propagating preferentially toward the fovea, i.e., on the diagonal between the repetitive stimulation and the central fixation in the experimental design displayed in **Figure 8.6** and **Figure 8.7.1**, or towards every direction in the retinotopic space.

We could also test whether the propagation is biased toward the fovea or toward the periphery, by presenting stimuli between the inducer and the central fixation, and between the inducer and the periphery (**Figure 8.7.2**).

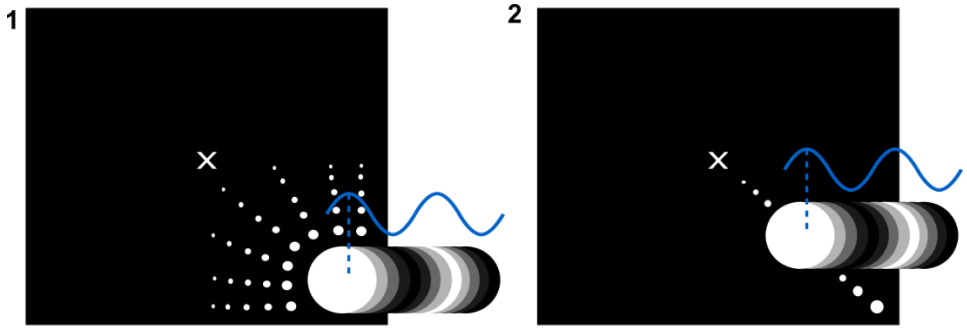

Figure 8.7: Testing the spatial extent of the role of phase across space. 1. *Testing multiple positions.* ***2.*** *Testing for propagation towards the fovea vs. towards the periphery.*

1.6. A model to study mesoscopic and macroscopic traveling waves with MEG/EEG

To overcome the issue of invasive recordings, we can also use modeling techniques to study the functional role of mesoscopic traveling waves with MEG/EEG recordings in humans.

MEG/EEG are non-invasive electrophysiological techniques widely used in healthy humans, patients, and children. Both EEG and MEG record excitatory and inhibitory postsynaptic potentials from the dendrites and soma of thousands of cortical pyramidal cells that are activated synchronously, i.e., they allow to measure the neural activity at the level of population of neurons. The main difference between the two techniques is their sensitivity to the dipole orientation. MEG is more sensitive to tangential dipoles (localized in the sulci), while EEG is sensitive to both tangential and radial dipoles (localized in the gyri). Although those methods have a very high temporal resolution, they suffer from a low spatial resolution, impacted by a strong space averaging due to volume conduction effect. For this reason, the development of models is required.

In the lab (work headed by Laetitia Grabot), a two part model (Kupers et al., 2021, 2022) is currently under development to measure mesoscopic traveling waves non-invasively. The first part aims to model the neural sources of an oscillatory mesoscopic traveling wave in V1, using individual retinotopic mapping from fMRI recordings, i.e., encoding model (**Figure 8.8.1**). The second part corresponds to the projection of the neural sources onto the MEG/EEG sensors, i.e., forward model (**Figure 8.8.2**). By comparing the predicted and the real MEG/EEG signal, Laetitia Grabot found that the model was able to distinguish MEG/EEG recordings while participants viewed a traveling compared to a standing stimulus. This first result allows to validate the model, that will be applied in the future to identify the presence and the features of mesoscopic traveling waves with MEG/EEG in humans.

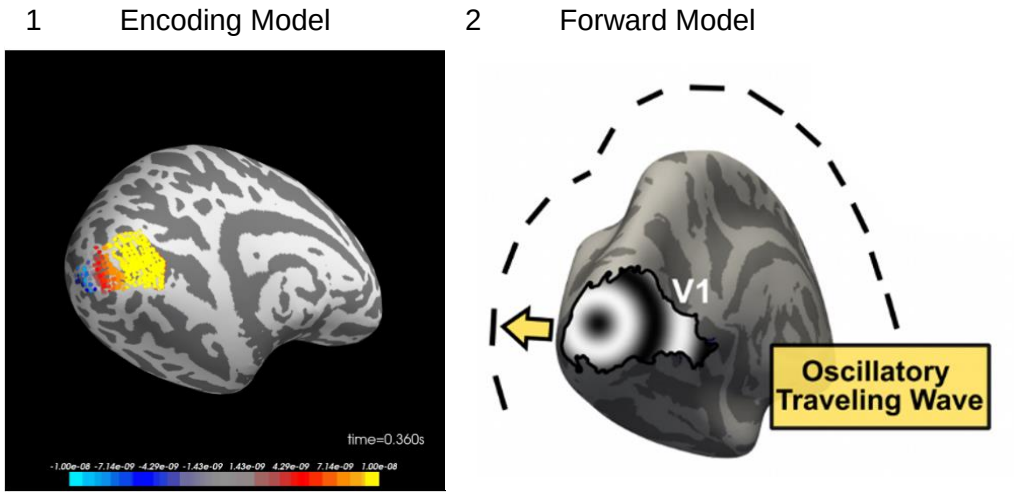

Figure 8.8: Mesoscopic traveling waves two-part modeling, by Laetitia Grabot, Garance Merholz, Jonathan Winawer, David J. Heeger and Laura Dugué. 1. *Encoding model, based on the individual retinotopy, the neural sources of a mesoscopic traveling wave in V1 are modeled across space and time.* ***2.*** *Forward model, the encoding model is projected to the MEG/EEG sensors level.*

Importantly, the same approach can be used to study macroscopic traveling waves in humans with MEG/EEG. Neural sources of a macroscopic traveling wave that propagates between brain regions can be modeled and then projected to the sensors space. It is thus possible to investigate which brain regions are involved in the emergence of macroscopic traveling waves. Once again, a model to measure macroscopic traveling waves at the source level will be developed soon in the lab, and applied to the two projects presented in **Chapter 7**.

1.7. Studying the functional role of brain oscillations: inputs from TMS

TMS is a non-invasive interventional method allowing to alter the state of cortical excitability by generating a magnetic field at the cortical surface that creates, in turn, an electrical current in the brain tissues. In this PhD, we used TMS to establish *causal* links between brain oscillations, the state of cortical excitability, and the subsequent visual performance, i.e., TMS was used as a probe of cortical excitability, and gave us access to the instantaneous phase of spontaneous brain oscillations (**Chapter 4 and 7**).

In addition, TMS can be used to identify the natural frequency of the cortex. The natural frequencies of brain oscillations have been described the first time by Rosanova et al., (2009). In their paper, they write: “In principle, a straightforward way of probing the frequency tuning of a system is to directly perturb it to detect the main rate of the ensuing oscillations, the so-called natural frequency. This approach is commonly used in physics and geology but also when

one tunes a musical instrument or, instinctively, knocks on the surface of an object to appreciate its internal structure." To better understand the intrinsic features of the cortex, we could thus disturb the brain, considered here as a system, and measure the responding brain oscillations. Rosanova et al. (2009) used single pulses of TMS to disturb the brain, applied over three distinct cortical areas: the middle/superior occipital gyrus, the superior parietal gyrus, and the middle/superior frontal gyrus. The occipital region showed brain oscillations in the alpha range (8-12 Hz), brain oscillations over the parietal region was in the beta range (13-20 Hz), and high-beta/gamma oscillations (21-50 Hz) were identified in the frontal region (**Figure 8.9**). Thus, each brain region showed an intrinsic rhythm, in a specific frequency range. Interestingly, the stimulation of the occipital region led to a response in the occipital, the parietal, and the frontal region, at respectively 10.8 Hz, 20 Hz, and 31.3 Hz; the stimulation of the parietal region led to a response in the occipital, the parietal, and the frontal region, at respectively 13.5 Hz, 18.6 Hz, and 27.3 Hz; the stimulation of the frontal region led to a response in the occipital, the parietal, and the frontal region, at respectively 10.6 Hz, 19 Hz, and 29 Hz. Whether the brain is activated directly by the single pulses of TMS or through long-range connections, each cortical region expressed oscillations at their own natural frequencies (Rosanova et al., 2009). In our last study, we hypothesized that these natural frequencies were traveling waves (**Chapter 7**). If this hypothesis is validated in the future, it will demonstrate that traveling waves are an endogenous brain process, naturally present in the cortex.

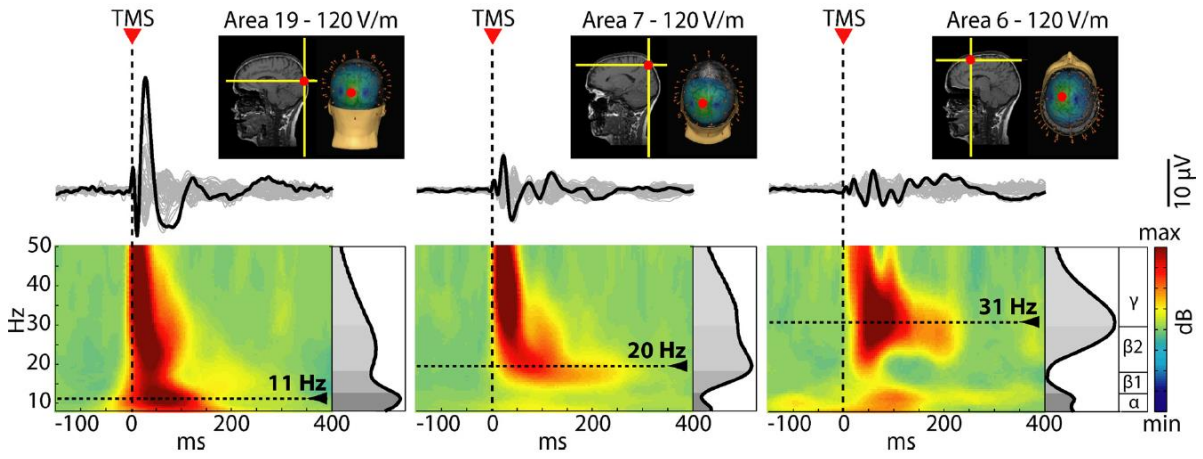

Figure 8.9: Single pulses of TMS makes the cortex resonate at its natural frequency, from Rosanova et al., 2009. *The three cortical regions of stimulation were selected for each participants based on their anatomical MRI. The time-frequency map of the amplitude spectrum of the entrained oscillations presents a distinct frequency peak, for each brain regions.*

In this PhD, we used single pulses of TMS, either to establish causal links or to makes the brain resonate at its natural frequency. Two other ways of using TMS present a great interest to study the functional role of brain oscillations: rhythmic and online TMS.

Rhythmic TMS consists at sending several pulses at a defined stimulation frequency (Thut and Pascual-Leone, 2010; Valero-Cabre et al., 2017), to induce brain oscillations at a precise frequency and location. One study identified the specific frequency and location of alpha oscillations evoked during the deployment of endogenous, covert, spatial, attention, i.e., alpha lateralization, for each participant. They demonstrated that rhythmic TMS bursts applied at this specific location, at the individual alpha frequency, allowed to drive natural brain oscillations by entrainment. This effect relied mainly on an increase in phase synchrony between endogenous alpha brain oscillations (before the rTMS) and TMS-induced oscillations (Thut et al., 2011). rTMS can be used to entrain brain oscillations naturally present during a cognitive task. It is then possible to investigate the causal, functional role of brain oscillations on cognitive performance. One study showed that alpha rTMS (10 Hz) applied over the parieto-occipital influenced perceptual performance, i.e., visual detection of targets contralateral to the rTMS was facilitated, while the visual performance ipsilateral to the rTMS was impaired. This effect was not observed for rTMS at 5 Hz and 20 Hz (Romei et al., 2010).

Online TMS consists in sending TMS pulses as a function of spontaneous brain oscillations (Valero-Cabre et al., 2017). By sending single pulses of TMS over the motor cortex according to the phase of spontaneous mu oscillations, some studies found a causal role of the phase on cortico-spinal excitability and the subsequent motor performance (**Figure 8.10**; Schaworonkow et al., 2018, 2019; Zrenner et al., 2018; Bergmann et al., 2019).

Rhythmic and online TMS can thus be used to investigate the causal role of oscillatory traveling waves on cognition.

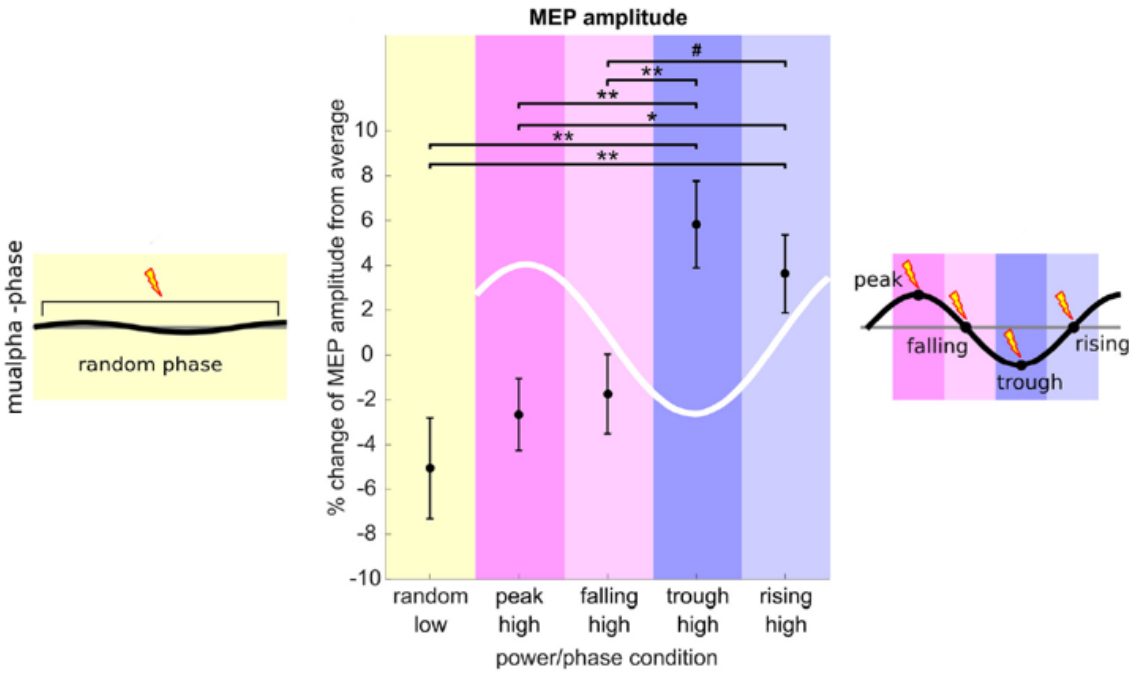

Figure 8.10: Motor Evoked Potentials (MEP) amplitude is modulated by real-time EEG triggered pulses of TMS over the motor cortex, from Bergmann et al., 2019*. Single pulses of TMS were applied over the human motor cortex, as a function of the phase of spontaneous mu oscillations, recorded with online EEG. The MEP amplitude was significantly higher when the TMS pulses were sent at the trough and at the rising phase of mu oscillations, compared to TMS pulses sending at the peak or at the falling phase.*

1.7. What about perception under overt condition?

Every experiment performed in this PhD was done under covert condition, i.e., participants were not allowed to make eyes or head movements during the task. This constraint allows stable retinal image in the brain visual areas. Covert perception is a powerful constraint to investigate the functional role of brain oscillations on visual perception. However, this does not reflect daily life behavior.

During visual exploration (or natural reading), we are under overt condition, i.e., head and eyes movements occur. Foveal and parafoveal visual information are present in the visual field at the same time (Murray et al., 2013). In a recent review, Jensen et al. (2021) proposed a pipelining processing of the visual information, i.e., several visual information is processed simultaneously at different levels of the cortical hierarchy. Alpha brain oscillations would be the key mechanism to coordinate the pipelining processing across space and time. In the **Figure 8.11**, at moment t0, the viewer is fixating the woman. The foveal image of the woman is processed sequentially through the cortical hierarchy, from the retina to the inferior temporal

cortex, involved in object recognition. Simultaneously, the parafoveal image of the dog is also processed, at different levels of the cortical hierarchy. Visual exploration thus depends on a serial processing within specific brain regions, and on parallel processing across different brain regions. Jensen et al. (2021) proposed that the phase of alpha brain oscillations would time the processing of the foveal and the parafoveal information, as well as the timing of the saccades towards a new visual input. Interestingly, the transfer of visual representations between the different levels of the cortical hierarchy would be coordinated by the propagation of alpha traveling waves (Jensen et al., 2021). According to this theory, alpha traveling waves would have a functional role on visual perception under overt condition.

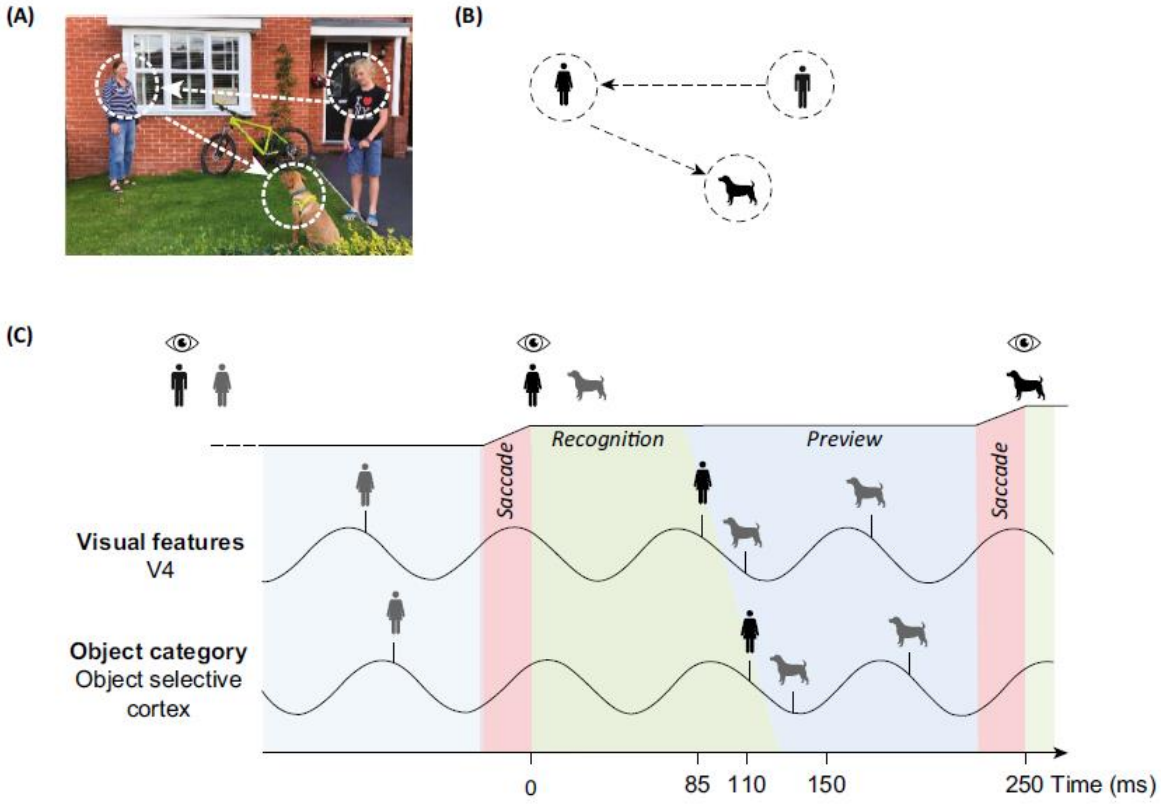

Figure 8.11: Pipelining processing gated by alpha oscillations during visual exploration, from Jensen et al., 2021. (A, B) *Participants fixate the boy, and then saccade to the woman, to finally saccade to the dog.* ***(C)*** *The temporal organization of the pipelining mechanism is supported by alpha brain oscillations, here, a 12 Hz oscillation. At the peak of the alpha cycle, the brain is in a state of cortical inhibition, while as we go to the trough of the alpha cycle, inhibition decreases. At time t0, participants are making a saccade toward the woman, phase-locked to the peak of the alpha cycle. The visual features of the woman and the dog are processed sequentially in V4. Interestingly, when the woman representation reaches the stage of the object selective cortex, the representation of the dog is simultaneously processed in V4. This parallel processing is well explained by an alpha traveling wave propagating across the visual cortical hierarchy.*

2. Perspectives

2.1. Multiple traveling waves: how their interaction can modulate cognitive functions?

In this PhD, we investigated the functional role of *one* oscillatory mesoscopic and *one* oscillatory macroscopic traveling wave on visual perception. But the brain receives continuously numerous perceptual inputs at the same time on top of its endogenous activity. Multiple oscillatory activities occur simultaneously in the cortex. We hypothesize that multiple traveling waves are present at the same time within a single brain area (mesoscopic traveling waves), and in distinct cortical regions (macroscopic traveling waves), and that their interaction should modulate cognitive functions.

Indeed, some studies have already demonstrated that multiple mesoscopic traveling waves take place simultaneously in V1 (Grinvald et al., 1994; Wu et al., 1999; Contreras and Llinas, 2001; Civillico and Contreras, 2006; Gao et al., 2012; Reynaud et al., 2012; Chemla et al., 2019). Interestingly, according to their spatio-temporal characteristics, e.g., their frequency, the delay between their onset of activity, etc., they could: 1) Exert a suppressive mechanism on each other, 2) Merge with each other, 3) Remain segregated. We hypothesize that the different interactions between mesoscopic traveling waves should affect differently visual perception. Let us consider two traveling waves in V1 evoked by two distinct visual stimuli. If the traveling waves exert a suppressive mechanism on each other, we could imagine that the perception of one visual stimulus is improved and facilitated at the expense of the other one, or maybe that the visual perception of both stimuli is impaired. Similarly, we could imagine that the fusion of traveling waves influences the perception of the visual stimuli, maybe by favoring the perception of a unique percept although two visual stimuli are presented. In fact, it is possible to propose lots of different predictions on the functional role of the interaction of multiple traveling waves. Interestingly, Gao et al. (2012) proposed an efficient paradigm, in anesthetized animals, to elicit the three possible interactions between traveling waves by simply modulating the inter-stimulus interval between the two presented visual stimuli. We would like to use this paradigm in human participants, either with invasive recordings in drug-resistant epileptic patients with intraEEG, or in healthy participants with the development of a new psychophysics experiment.

The triggering of two macroscopic traveling waves at the same time has been poorly studied for the moment. One study found that two alpha traveling waves, evoked respectively in the left and right visual cortices, appeared simultaneously, and were superimposed on the scalp (Lozano-Soldevilla and VanRullen, 2019). However, their functional role on visual perception has not yet been investigated. At a macroscopic scale, it has already been shown that brain oscillations localized in distinct cortical regions could interact with each other, with the coupling of their properties, i.e., phase-phase coupling, phase-amplitude coupling, amplitude-amplitude coupling, and that this coupling mechanism has a functional role on cognition (Canolty and Knight, 2010; Hyafil et al., 2015). It has been suggested that such interactions would underlie the communication of information between different brain regions, e.g., between visual and motor regions during motor imagery (deLange et al., 2008), or between visual and frontal regions during a visual attention task (Mazaheri et al., 2009, 2010). By taking into account the interaction between multiple traveling waves, we should better explain their functional role on cognition.

2.2. What is the link between mesoscopic and macroscopic traveling waves?

Macroscopic and mesoscopic traveling waves present several differences, notably their speed and their spatial extent, i.e., macroscopic traveling waves are ten times faster than the mesoscopic ones, and they are propagating over several cm of cortex compared to a few mm for the mesoscopic traveling waves. They also share common features. Both mesoscopic and macroscopic oscillatory traveling waves present a positive correlation between their frequency and their propagation speed (Petsche and Stumpf, 1960; Freeman and Barrie, 2000; Zhang and Jacobs, 2015; Patten et al., 2012; Zhang et al., 2018; Tsoneva et al., 2021). In addition, only one cycle of the oscillation appears to travel within a single brain area (Bao and Wu, 2003; Zanos et al., 2015; Zhang and Jacobs, 2015), and between brain regions (Walter et al., 1966; Cohn, 1948; Hord et al., 1972, 1974; Suzuki, 1974; Burkitt et al., 2000; Ito et al., 2005; Zhang et al., 2018). Numerous studies suggest that their spatio-temporal characteristics influence cognitive functions. Consequently, we wonder what is the link between the brain activity recorded at the mesoscopic and at the macroscopic level? One theory has been proposed by Hendriks et al. (2014). They showed with a model that macroscopic traveling waves recorded with EEG could be explained by the slow propagation of mesoscopic traveling waves over small cortical distance, mediated by intra-cortical axons, at a propagation speed of 0.3 m/s (Hendriks et al., 2014). We would like to investigate this hypothesis by analyzing data from

local, invasive iEEG recordings in epileptic patients, simultaneously of an EEG recording. Thus, we will be able to investigate the presence and the interaction of mesoscopic and macroscopic traveling waves at the same time.

3. Final word

Brain oscillations are ubiquitous in the brain. They emerge at different scales, i.e., in cells, local neuronal networks, and at the whole brain scale; and they have been recorded in a wide range of species. Since their discovery in 1929, brain oscillations have been proposed to be a crucial neural mechanism of cognition. In this PhD, we provide strong evidence in favor of a functional role of the spatiotemporal organization of brain oscillations in human visual perception, with a multimodal approach including psychophysics, neuroimaging and non-invasive stimulation. We have made a conscious effort to continuously share our research with the scientific community, leading to interesting feedback on our works, possibilities of collaborations, and discussions on numerous outstanding questions. I strongly believe that a better understanding of brain oscillations will lead to important discoveries in neuroscience. With this PhD, I am happy to have contributed to this important research on brain oscillations, and I wish to pursue this line of research in the future.

Bibliography

Adrian, E. D., & Yamagiwa, K. (1935). The origin of the Berger rhythm. Brain: A Journal of Neurology.

Adrian, E. D., & Matthews, B. H. (1934a). The Berger rhythm: potential changes from the occipital lobes in man. Brain, 57(4), 355-385.

Adrian, E. D., & Matthews, B. H. (1934b). The interpretation of potential waves in the cortex. The Journal of physiology, 81(4), 440-471.

Agarwal, G., Stevenson, I. H., Berényi, A., Mizuseki, K., Buzsáki, G., & Sommer, F. T. (2014). Spatially distributed local fields in the hippocampus encode rat position. Science, 344(6184), 626-630.

Ai, L., & Ro, T. (2014). The phase of prestimulus alpha oscillations affects tactile perception. Journal of neurophysiology, 111(6), 1300-1307.

Alais, D., Leung, J., & Van der Burg, E. (2017). Linear summation of repulsive and attractive serial dependencies: Orientation and motion dependencies sum in motion perception. Journal of Neuroscience, 37(16), 4381-4390.

Alamia, A., & VanRullen, R. (2019). Alpha oscillations and traveling waves: Signatures of predictive coding? PLoS Biology, 17(10), e3000487, 1-26.

Albowitz, B., & Kuhnt, U. (1993). Evoked changes of membrane potential in guinea pig sensory neocortical slices: an analysis with voltage-sensitive dyes and a fast optical recording method. Experimental brain research, 93(2), 213-225.

Albowitz, B., & Kuhnt, U. (1991). Spatio-temporal distribution of epileptiform potentials in the hippocampal slice: recordings with voltage-sensitive dyes. European Journal of Neuroscience, 3(6), 570-586.

Albowitz, B., Kuhnt, U., & Ehrenreich, L. (1990). Optical recording of epileptiform voltage changes in the neocortical slice. Experimental brain research, 81(2), 241-256.

Alexander, K. E., Estepp, J. R., & Elbasiouny, S. M. (2020). Effects of neuronic shutter observed in the EEG alpha rhythm. Eneuro, 7(5).

Alexander, D. M., Ball, T., Schulze-Bonhage, A., & van Leeuwen, C. (2019). Large-scale cortical travelling waves predict localized future cortical signals. PLoS computational biology, 15(11), e1007316.

Alexander, D. M., Jurica, P., Trengove, C., Nikolaev, A. R., Gepshtein, S., Zvyagintsev, Mathiak, M. K., Schulze-Bonhage, A., Ruescher, J., Ball, T., & van Leeuwen, C. (2013). Traveling waves and trial averaging: the nature of single-trial and averaged brain responses in large-scale cortical signals. Neuroimage, 73, 95-112.

Alexander, D. M., Flynn, G. J., Wong, W., Whitford, T. J., Harris, A. W., Galletly, C. A., & Silverstein, S. M. (2009). Spatio-temporal EEG waves in first episode schizophrenia. Clinical Neurophysiology, 120(9), 1667-1682.

Alexander, D. M., Hermens, D. F., Keage, H. A., Clark, C. R., Williams, L. M., Kohn, M. R., Clarke, S. D., Lamb, C., & Gordon, E. (2008). Event-related wave activity in the EEG provides new marker of ADHD. Clinical Neurophysiology, 119(1), 163-179.

Alexander, D. M., Arns, M. W., Paul, R. H., Rowe, D. L., Cooper, N., Esser, A. H., Fallahpour, K., Stephan, B. C. M., Heesen, E., Breteler, R., Williams, L. M., & Gordon, E. (2006). EEG markers for cognitive decline in elderly subjects with subjective memory complaints. Journal of Integrative Neuroscience, 5(01), 49-74.

Andersen, P., Andersson, S. A., & Lømo, T. (1966). Patterns of spontaneous rhythmic activity within various thalamic nuclei. Nature, 211(5051), 888-889.

Arieli, A., Sterkin, A., Grinvald, A., & Aertsen, A. D. (1996). Dynamics of ongoing activity: explanation of the large variability in evoked cortical responses. Science, 273(5283), 1868-1871.

Arieli, A., Shoham, D. O. R. O. N., Hildesheim, R. I. N. A., & Grinvald, A. M. I. R. A. M. (1995). Coherent spatiotemporal patterns of ongoing activity revealed by real-time optical imaging coupled with single-unit recording in the cat visual cortex. Journal of neurophysiology, 73(5), 2072-2093.

Babiloni, C., Babiloni, F., Carducci, F., Cincotti, F., Cocozza, G., Del Percio, C., Moretti, V. D., & Rossini, P. M. (2002). Human cortical electroencephalography (EEG) rhythms during the observation of simple aimless movements: a high-resolution EEG study. Neuroimage, 17(2), 559-572.

Bahramisharif, A., van Gerven, M. A., Aarnoutse, E. J., Mercier, M. R., Schwartz, T. H., Foxe, J. J., ... & Jensen, O. (2013). Propagating neocortical gamma bursts are coordinated by traveling alpha waves. Journal of Neuroscience, 33(48), 18849-18854.

Baker, S. N., Olivier, E., & Lemon, R. N. (1997). Coherent oscillations in monkey motor cortex and hand muscle EMG show task-dependent modulation. The Journal of physiology, 501(1), 225-241.

Bakin, J. S., Kwon, M. C., Masino, S. A., Weinberger, N. M., & Frostig, R. D. (1996). Suprathreshold auditory cortex activation visualized by intrinsic signal optical imaging. Cerebral Cortex, 6(2), 120-130.

Barker, A. T., Jalinous, R., & Freeston, I. L. (1985). Non-invasive magnetic stimulation of human motor cortex. The Lancet, 325(8437), 1106-1107.

Barlow, J. S., & Estrin, T. (1971). Comparative phase characteristics of induced and intrinsic alpha activity. Electroencephalography and clinical neurophysiology, 30(1), 1-9.

Bastos, A. M., Usrey, W. M., Adams, R. A., Mangun, G. R., Fries, P., & Friston, K. J. (2012). Canonical microcircuits for predictive coding. Neuron, 76(4), 695-711.

Baumgarten, T. J., Schnitzler, A., & Lange, J. (2015). Beta oscillations define discrete perceptual cycles in the somatosensory domain. Proceedings of the National Academy of Sciences, 112(39), 12187-12192.

Belitski, A., Gretton, A., Magri, C., Murayama, Y., Montemurro, M. A., Logothetis, N. K., & Panzeri, S. (2008). Low-frequency local field potentials and spikes in primary visual cortex convey independent visual information. Journal of Neuroscience, 28(22), 5696-5709.

Belluscio, M. A., Mizuseki, K., Schmidt, R., Kempter, R., & Buzsáki, G. (2012). Cross-frequency phase–phase coupling between theta and gamma oscillations in the hippocampus. Journal of Neuroscience, 32(2), 423-435.

Benucci, A., Frazor, R. A., & Carandini, M. (2007). Standing waves and traveling waves distinguish two circuits in visual cortex. Neuron, 55(1), 103-117.

Berens P (2009) CircStat: a MATLAB toolbox for circular statistics. J Stat Softw 31:1–21.

Berger, H. (1929). Über das elektroenkephalogramm des menschen. Archiv für psychiatrie und nervenkrankheiten, 87(1), 527-570.

Bergmann, T. O., Lieb, A., Zrenner, C., & Ziemann, U. (2019). Pulsed facilitation of corticospinal excitability by the sensorimotor μ-alpha rhythm. Journal of Neuroscience, 39(50), 10034-10043.

Besserve, M., Lowe, S. C., Logothetis, N. K., Schölkopf, B., & Panzeri, S. (2015). Shifts of gamma phase across primary visual cortical sites reflect dynamic stimulus-modulated information transfer. PLoS biology, 13(9), e1002257, 1-29.

Boiten, F., Sergeant, J., & Geuze, R. (1992). Event-related desynchronization: the effects of energetic and computational demands. Electroencephalography and clinical neurophysiology, 82(4), 302-309.

Bollimunta A, Chen Y, Schroeder CE, Ding M (2008) Neuronal mechanisms of cortical alpha oscillations in awake-behaving macaques. J Neurosci 28:9976–9988.

Bonnefond, M., & Jensen, O. (2015). Gamma activity coupled to alpha phase as a mechanism for top-down controlled gating. PloS one, 10(6), e0128667.

Brenner, D., Okada, Y., Maclin, E., Williamson, S. J., & Kaufman, L. (1981). Evoked magnetic fields reveal different visual areas in human cortex. In Biomagnetism, 431-444.

Bringuier, V., Chavane, F., Glaeser, L., & Frégnac, Y. (1999). Horizontal propagation of visual activity in the synaptic integration field of area 17 neurons. Science, 283(5402), 695-699.

Brookes, M. J., Gibson, A. M., Hall, S. D., Furlong, P. L., Barnes, G. R., Hillebrand, A., Singh, K. D., Holliday, I. E., Francis, T. S., & Morris, P. G. (2005). GLM-beamformer method demonstrates stationary field, alpha ERD and gamma ERS co-localisation with fMRI BOLD response in visual cortex. Neuroimage, 26(1), 302-308.

Brown, D. A., Gähwiler, B. H., Griffith, W. H., & Halliwell, J. V. (1990). Chapter Membrane currents in hippocampal neurons. Progress in brain research, 83, 141-160.

Burgess, N., O'Keefe, J., & Recce, M. (1992). Using hippocampal ‘place cells' for navigation, exploiting phase coding. Advances in neural information processing systems, 5, 929-936.

Burkitt, G. R., Silberstein, R. B., Cadusch, P. J., & Wood, A. W. (2000). Steady-state visual evoked potentials and travelling waves. Clinical Neurophysiology, 111(2), 246-258.

Burns, B. D. (1950). Some properties of the cat's isolated cerebral cortex. The Journal of physiology, 111(1-2), 50-68.

Burr, D., & Cicchini, G. M. (2014). Vision: efficient adaptive coding. Current Biology, 24(22), R1096-R1098.

Busch, N. A., & VanRullen, R. (2010). Spontaneous EEG oscillations reveal periodic sampling of visual attention. Proceedings of the National Academy of Sciences, 107(37), 16048-16053.

Busch, N. A., Dubois, J., & VanRullen, R. (2009). The phase of ongoing EEG oscillations predicts visual perception. Journal of Neuroscience, 29(24), 7869-7876.

Buzsáki, G., & Tingley, D. (2018). Space and time: The hippocampus as a sequence generator. Trends in cognitive sciences, 22(10), 853-869.

Buzsáki, G. (2002). Theta oscillations in the hippocampus. Neuron, 33(3), 325-340.

Canolty, R. T., & Knight, R. T. (2010). The functional role of cross-frequency coupling. Trends in cognitive sciences, 14(11), 506-515.

Canolty, R. T., Edwards, E., Dalal, S. S., Soltani, M., Nagarajan, S. S., Kirsch, H. E., Berger, M.S., Barbaro M.N., & Knight, R. T. (2006). High gamma power is phase-locked to theta oscillations in human neocortex. science, 313(5793), 1626-1628.

Capotosto, P., Babiloni, C., Romani, G. L., & Corbetta, M. (2009). Frontoparietal cortex controls spatial attention through modulation of anticipatory alpha rhythms. Journal of Neuroscience, 29(18), 5863-5872.

Carrasco, M. (2011). Visual attention: The past 25 years. Vision Research 51, 1484–1525.

Carrasco, M., and McElree, B. (2001). Covert attention accelerates the rate of visual information processing. Proceedings of the National Academy of Sciences 98, 5363–5367.

Cassim, F., Szurhaj, W., Sediri, H., Devos, D., Bourriez, J. L., Poirot, I., Derambure, P., Defebvre, L., & Guieu, J. D. (2000). Brief and sustained movements: differences in event-related (de) synchronization (ERD/ERS) patterns. Clinical neurophysiology, 111(11), 2032-2039.

Chagnac-Amitai, Y., & Connors, B. W. (1989). Horizontal spread of synchronized activity in neocortex and its control by GABA-mediated inhibition. Journal of neurophysiology, 61(4), 747-758.

Chakarov, V., Naranjo, J. R., Schulte-Mönting, J., Omlor, W., Huethe, F., & Kristeva, R. (2009). Beta-range EEG-EMG coherence with isometric compensation for increasing modulated low-level forces. Journal of neurophysiology, 102(2), 1115-1120.

Chakravarthi, R., & VanRullen, R. (2012). Conscious updating is a rhythmic process. Proceedings of the National Academy of Sciences, 109(26), 10599-10604.

Chang, H. T. (1951). Dendritic potential of cortical neurons produced by direct electrical stimulation of the cerebral cortex. Journal of neurophysiology, 14(1), 1-21.

Chavane, F., Perrinet, L. U., & Rankin, J. (2022). Revisiting horizontal connectivity rules in V1: from like-to-like towards like-to-all. Brain Structure and Function, 1-17.

Chemla, S., Reynaud, A., Di Volo, M., Zerlaut, Y., Perrinet, L., Destexhe, A., & Chavane, F. (2019). Suppressive traveling waves shape representations of illusory motion in primary visual cortex of awake primate. Journal of Neuroscience, 39(22), 4282-4298.

Chen, Y., & Huang, X. (2016). Modulation of alpha and beta oscillations during an n-back task with varying temporal memory load. Frontiers in psychology, 6, 2031, 1-10.

Chen, Y., Geisler, W. S., & Seidemann, E. (2006). Optimal decoding of correlated neural population responses in the primate visual cortex. Nature neuroscience, 9(11), 1412-1420.

Chervin, R. D., Pierce, P. A., & Connors, B. W. (1988). Periodicity and directionality in the propagation of epileptiform discharges across neocortex. Journal of Neurophysiology, 60(5), 1695-1713.

Cheyne, D., Gaetz, W., Garnero, L., Lachaux, J. P., Ducorps, A., Schwartz, D., & Varela, F. J. (2003). Neuromagnetic imaging of cortical oscillations accompanying tactile stimulation. Cognitive brain research, 17(3), 599-611.

Childers, D. G. (1977). Evoked responses: Electrogenesis, models, methodology, and wavefront reconstruction and tracking analysis. Proceedings of the IEEE, 65(5), 611-626.

Cicchini, G. M., Mikellidou, K., & Burr, D. (2017). Serial dependencies act directly on perception. Journal of vision, 17(14), 6-6.

Cicchini, G. M., Anobile, G., & Burr, D. C. (2014). Compressive mapping of number to space reflects dynamic encoding mechanisms, not static logarithmic transform. Proceedings of the National Academy of Sciences, 111(21), 7867-7872.

Cinelli, A. R., & Kauer, J. S. (1995). Salamander olfactory bulb neuronal activity observed by video rate, voltage-sensitive dye imaging. II. Spatial and temporal properties of responses evoked by electric stimulation. Journal of neurophysiology, 73(5), 2033-2052.

Cinelli, A. R., Hamilton, K. A., & Kauer, J. S. (1995). Salamander olfactory bulb neuronal activity observed by video rate, voltage-sensitive dye imaging. III. Spatial and temporal properties of responses evoked by odorant stimulation. Journal of neurophysiology, 73(5), 2053-2071.

Civillico, E. F., & Contreras, D. (2006). Integration of evoked responses in supragranular cortex studied with optical recordings in vivo. Journal of neurophysiology, 96(1), 336-351.

Clayton, M. S., Yeung, N., & Cohen Kadosh, R. (2018). The many characters of visual alpha oscillations. European Journal of Neuroscience, 48(7), 2498-2508.

Cohen, M. X. (2014). Analyzing neural time series data: theory and practice. MIT press.

Cohn, R. (1948). The occipital alpha rhythm: a study of phase variations. Journal of neurophysiology, 11(1), 31-37.

Collins, T. (2021). Serial dependence occurs at the level of both features and integrated object representations. Journal of Experimental Psychology: General. Advance online publication. 1-13.

Collins, T. (2020). Serial dependence alters perceived object appearance. Journal of Vision, 20(13), 9-9.

Collins, T. (2019). The perceptual continuity field is retinotopic. Scientific reports, 9(1), 1-6.

Conner, C. R., Ellmore, T. M., Pieters, T. A., DiSano, M. A., & Tandon, N. (2011). Variability of the relationship between electrophysiology and BOLD-fMRI across cortical regions in humans. Journal of Neuroscience, 31(36), 12855-12865.

Contreras, D., & Llinás, R. (2001). Voltage-sensitive dye imaging of neocortical spatiotemporal dynamics to afferent activation frequency. Journal of Neuroscience, 21(23), 9403-9413.

Contreras, D., Destexhe, A., Sejnowski, T. J., & Steriade, M. (1997). Spatiotemporal patterns of spindle oscillations in cortex and thalamus. Journal of Neuroscience, 17(3), 1179-1196.

Contreras, D., Destexhe, A., Sejnowski, T. J., & Steriade, M. (1996). Control of spatiotemporal coherence of a thalamic oscillation by corticothalamic feedback. Science, 274(5288), 771-774.

Cooper, N. R., Croft, R. J., Dominey, S. J., Burgess, A. P., & Gruzelier, J. H. (2003). Paradox lost? Exploring the role of alpha oscillations during externally vs. internally directed attention and the implications for idling and inhibition hypotheses. International journal of psychophysiology, 47(1), 65-74.

Cooper, R., & Mundy-Castle, A. C. (1960). Spatial and temporal characteristics of the alpha rhythm: a toposcopic analysis. Electroencephalography and clinical neurophysiology, 12(1), 153-165.

Corbett, J. E., Fischer, J., & Whitney, D. (2011). Facilitating stable representations: Serial dependence in vision. PLoS One, 6(1), e16701.

Cottereau, B., Lorenceau, J., Gramfort, A., Clerc, M., Thirion, B., & Baillet, S. (2011). Phase delays within visual cortex shape the response to steady-state visual stimulation. Neuroimage, 54(3), 1919-1929.

Cracco, R. Q. (1972). Traveling waves of the human scalp-recorded somatosensory evoked response: effects of differences in recording technique and sleep on somatosensory and somatomotor responses. Electroencephalography and clinical neurophysiology, 33(6), 557-566.

Crone, N. E., Miglioretti, D. L., Gordon, B., Sieracki, J. M., Wilson, M. T., Uematsu, S., & Lesser, R. P. (1998). Functional mapping of human sensorimotor cortex with electrocorticographic spectral analysis. I. Alpha and beta event-related desynchronization. Brain: a journal of neurology, 121(12), 2271-2299.

Csicsvari, J., Jamieson, B., Wise, K. D., & Buzsáki, G. (2003). Mechanisms of gamma oscillations in the hippocampus of the behaving rat. Neuron, 37(2), 311-322.

Csicsvari, J., Hirase, H., Mamiya, A., & Buzsáki, G. (2000). Ensemble patterns of hippocampal CA3-CA1 neurons during sharp wave–associated population events. Neuron, 28(2), 585-594.

Darrow, C. W., & Hicks, R. G. (1965). Interarea electroencephalographic phase relationships following sensory and ideational stimuli. Psychophysiology, 1(4), 337-346.

Davis, Z. W., Muller, L., Martinez-Trujillo, J., Sejnowski, T., & Reynolds, J. H. (2020). Spontaneous travelling cortical waves gate perception in behaving primates. Nature, 587(7834):432-436.

De Lange, F. P., Jensen, O., Bauer, M., & Toni, I. (2008). Interactions between posterior gamma and frontal alpha/beta oscillations during imagined actions. Frontiers in human neuroscience, 2, 7, 1-12.

Deiber, M. P., Missonnier, P., Bertrand, O., Gold, G., Fazio-Costa, L., Ibanez, V., & Giannakopoulos, P. (2007). Distinction between perceptual and attentional processing in working memory tasks: a study of phase-locked and induced oscillatory brain dynamics. Journal of cognitive neuroscience, 19(1), 158-172.

Delaney, K. R., Gelperin, A., Fee, M. S., Flores, J. A., Gervais, R., Tank, D. W., & Kleinfeld, D. (1994). Waves and stimulus-modulated dynamics in an oscillating olfactory network. Proceedings of the National Academy of Sciences, 91(2), 669-673.

Delorme A, Makeig S (2004) EEGLAB: an open source toolbox for analysis of single-trial EEG dynamics including independent component analysis. J Neurosci Methods 134:9–21.

Demir, R., Haberly, L. B., & Jackson, M. B. (1999). Sustained and accelerating activity at two discrete sites generate epileptiform discharges in slices of piriform cortex. Journal of Neuroscience, 19(4), 1294-1306.

Demiralp, T., Bayraktaroglu, Z., Lenz, D., Junge, S., Busch, N. A., Maess, B., Ergen, M., & Herrmann, C. S. (2007). Gamma amplitudes are coupled to theta phase in human EEG during visual perception. International journal of psychophysiology, 64(1), 24-30.

Derdikman, D., Hildesheim, R., Ahissar, E., Arieli, A., & Grinvald, A. (2003). Imaging spatiotemporal dynamics of surround inhibition in the barrels somatosensory cortex. Journal of Neuroscience, 23(8), 3100-3105.

Dougherty, R. F., Koch, V. M., Brewer, A. A., Fischer, B., Modersitzki, J., & Wandell, B. A. (2003). Visual field representations and locations of visual areas V1/2/3 in human visual cortex. Journal of vision, 3(10), 1-1.

Dugué, L., Merriam, E. P., Heeger, D. J., & Carrasco, M. (2020). Differential impact of endogenous and exogenous attention on activity in human visual cortex. Scientific reports, 10(1), 1-16.

Dugué, L., Beck, A. A., Marque, P., & VanRullen, R. (2019). Contribution of FEF to attentional periodicity during visual search: a TMS study. eNeuro, 6(3), 1-10.

Dugué, L., Merriam, E.P., Heeger, D.J., and Carrasco, M. (2018). Specific Visual Subregions of TPJ Mediate Reorienting of Spatial Attention. Cerebral Cortex 28, 2375–2390.

Dugué, L., & VanRullen, R. (2017). Transcranial magnetic stimulation reveals intrinsic perceptual and attentional rhythms. Frontiers in Neuroscience, 11, 154, 1-7.

Dugué, L., Roberts, M., & Carrasco, M. (2016). Attention reorients periodically. Current Biology, 26(12), 1595-1601.

Dugué, L., Marque, P., & VanRullen, R. (2015a). Theta oscillations modulate attentional search performance periodically. Journal of cognitive neuroscience, 27(5), 945-958.

Dugué, L., McLelland, D., Lajous, M., & VanRullen, R. (2015a). Attention searches nonuniformly in space and in time. Proceedings of the National Academy of Sciences, 112(49), 15214-15219.

Dugué, L., Marque, P., & VanRullen, R. (2011a). The phase of ongoing oscillations mediates the causal relation between brain excitation and visual perception. Journal of neuroscience, 31(33), 11889-11893.

Dugué, L., Marque, P., & VanRullen, R. (2011b). Transcranial magnetic stimulation reveals attentional feedback to area V1 during serial visual search. PLoS One, 6(5), e19712.

Dujardin, K., Derambure, P., Defebvre, L., Bourriez, J. L., Jacquesson, J. M., & Guieu, J. D. (1993). Evaluation of event-related desynchronization (ERD) during a recognition task: effect of attention. Electroencephalography and clinical neurophysiology, 86(5), 353-356.

Eckhorn, R., Bauer, R., Jordan, W., Brosch, M., Kruse, W., Munk, M., & Reitboeck, H. J. (1988). Coherent oscillations: A mechanism of feature linking in the visual cortex? Biological cybernetics, 60(2), 121-130.

Ekstrom, A. D., Caplan, J. B., Ho, E., Shattuck, K., Fried, I., & Kahana, M. J. (2005). Human hippocampal theta activity during virtual navigation. Hippocampus, 15(7), 881-889.

Ekstrom, A. D., Kahana, M. J., Caplan, J. B., Fields, T. A., Isham, E. A., Newman, E. L., & Fried, I. (2003). Cellular networks underlying human spatial navigation. Nature, 425(6954), 184-188.

Engel, A. K., & Fries, P. (2010). Beta-band oscillations—signaling the status quo? Current opinion in neurobiology, 20(2), 156-165.

Epstein, C. M. (2008). TMS stimulation coils. In Oxford handbook of transcranial stimulation.

Ergenoglu, T., Demiralp, T., Bayraktaroglu, Z., Ergen, M., Beydagi, H., & Uresin, Y. (2004). Alpha rhythm of the EEG modulates visual detection performance in humans. Cognitive brain research, 20(3), 376-383.

Ermentrout, G. B., & Kleinfeld, D. (2001). Traveling electrical waves in cortex: insights from phase dynamics and speculation on a computational role. Neuron, 29(1), 33-44.

Ermentrout, G. B., & Kopell, N. (1998). Fine structure of neural spiking and synchronization in the presence of conduction delays. Proceedings of the National Academy of Sciences, 95(3), 1259-1264.

Fakche, C., VanRullen, R., Marque, P., & Dugué, L. (2022) Alpha phase-amplitude tradeoffs predicts visual perception. eNeuro, 0244, 1-19.

Faraday, M. (1832). V. Experimental researches in electricity. Philosophical transactions of the Royal Society of London, (122), 125-162.

Fawcett, I.P., Barnes, G.R., Hillebrand, A., and Singh, K.D. (2004). The temporal frequency tuning of human visual cortex investigated using synthetic aperture magnetometry. NeuroImage 21, 1542–1553.

Fellinger, R., Gruber, W., Zauner, A., Freunberger, R., & Klimesch, W. (2012). Evoked traveling alpha waves predict visual-semantic categorization-speed. NeuroImage, 59(4), 3379-3388.

Ferezou, I., Haiss, F., Gentet, L. J., Aronoff, R., Weber, B., & Petersen, C. C. (2007). Spatiotemporal dynamics of cortical sensorimotor integration in behaving mice. Neuron, 56(5), 907-923.

Ferezou, I., Bolea, S., & Petersen, C. C. (2006). Visualizing the cortical representation of whisker touch: voltage-sensitive dye imaging in freely moving mice. Neuron, 50(4), 617-629.

Fiebelkorn, I. C., Pinsk, M. A., & Kastner, S. (2018). A dynamic interplay within the frontoparietal network underlies rhythmic spatial attention. Neuron, 99(4), 842-853.

Fiebelkorn, I. C., Saalmann, Y. B., & Kastner, S. (2013a). Rhythmic sampling within and between objects despite sustained attention at a cued location. Current Biology, 23(24), 2553-2558.

Fiebelkorn, I. C., Snyder, A. C., Mercier, M. R., Butler, J. S., Molholm, S., & Foxe, J. J. (2013b). Cortical cross-frequency coupling predicts perceptual outcomes. Neuroimage, 69, 126-137.

Fischer, J., & Whitney, D. (2014). Serial dependence in visual perception. Nature neuroscience, 17(5), 738-743.

Fleidervish, I. A., Binshtok, A. M., & Gutnick, M. J. (1998). Functionally distinct NMDA receptors mediate horizontal connectivity within layer 4 of mouse barrel cortex. Neuron, 21(5), 1055-1065.

Fontolan, L., Morillon, B., Liegeois-Chauvel, C., & Giraud, A. L. (2014). The contribution of frequency-specific activity to hierarchical information processing in the human auditory cortex. Nature communications, 5(1), 1-10.

Fornaciai, M., & Park, J. (2020). Neural dynamics of serial dependence in numerosity perception. Journal of Cognitive Neuroscience, 32(1), 141-154.

Fornaciai, M., & Park, J. (2018a). Early numerosity encoding in visual cortex is not sufficient for the representation of numerical magnitude. Journal of Cognitive Neuroscience, 30(12), 1788-1802.

Fornaciai, M., & Park, J. (2018b). Attractive serial dependence in the absence of an explicit task. Psychological Science, 29(3), 437-446.

Freeman, W. J., & Barrie, J. M. (2000). Analysis of spatial patterns of phase in neocortical gamma EEGs in rabbit. Journal of neurophysiology, 84(3), 1266-1278.

Freeman, W. J., & Baird, B. (1987). Relation of olfactory EEG to behavior: spatial analysis. Behavioral neuroscience, 101(3), 393.

Freeman, W. J. (1978). Spatial properties of an EEG event in the olfactory bulb and cortex. Electroencephalography and clinical neurophysiology, 44(5), 586-605.

Friedman-Hill, S., Maldonado, P. E., & Gray, C. M. (2000). Dynamics of striate cortical activity in the alert macaque: I. Incidence and stimulus-dependence of gamma-band neuronal oscillations. Cerebral cortex, 10(11), 1105-1116.

Friedrich, R. W., Habermann, C. J., & Laurent, G. (2004). Multiplexing using synchrony in the zebrafish olfactory bulb. Nature neuroscience, 7(8), 862-871.

Friedrich, R. W., & Korsching, S. I. (1998). Chemotopic, combinatorial, and noncombinatorial odorant representations in the olfactory bulb revealed using a voltage-sensitive axon tracer. Journal of Neuroscience, 18(23), 9977-9988.

Fries, P. (2009). Neuronal gamma-band synchronization as a fundamental process in cortical computation. Annual review of neuroscience, 32, 209-224.

Friston, K. (2012). The history of the future of the Bayesian brain. NeuroImage, 62(2), 1230-1233.

Friston, K. (2005). A theory of cortical responses. Philosophical transactions of the Royal Society B: Biological sciences, 360(1456), 815-836.

Fritsche, M., Mostert, P., & de Lange, F. P. (2017). Opposite effects of recent history on perception and decision. Current Biology, 27(4), 590-595.

Fukunishi, K., Murai, N., & Uno, H. (1992). Dynamic characteristics of the auditory cortex of guinea pigs observed with multichannel optical recording. Biological cybernetics, 67(6), 501-509.

Funase, A., Wakita, K., Itai, A., & Takumi, I. (2015, December). SSVEP by checkerboard related to grid size and board size. In 2015 Asia-Pacific Signal and Information Processing Association Annual Summit and Conference (APSIPA) (pp. 1141-1144). IEEE.

Gabriel, A., & Eckhorn, R. (2003). A multi-channel correlation method detects traveling γ-waves in monkey visual cortex. Journal of neuroscience methods, 131(1-2), 171-184.

Gao, X., Xu, W., Wang, Z., Takagaki, K., Li, B., & Wu, J. Y. (2012). Interactions between two propagating waves in rat visual cortex. Neuroscience, 216, 57-69.

Gaztelu, M., García-Austt, E., & Bullock, T. H. (1991). Electrocorticograms of hippocampal and dorsal cortex of two reptiles: comparison with possible mammalian homologs. Brain, Behavior and Evolution, 37(3), 144-160.

Genç, E., Bergmann, J., Singer, W., & Kohler, A. (2015). Surface area of early visual cortex predicts individual speed of traveling waves during binocular rivalry. Cerebral cortex, 25(6), 1499-1508.

Gervais, R., Kleinfeld, D., Delaney, K. R., & Gelperin, A. (1996). Central and reflex neuronal responses elicited by odor in a terrestrial mollusk. Journal of neurophysiology, 76(2), 1327-1339.

Gerwig M, Niehaus L, Kastrup O, Stude P, Diener HC (2005) Visual cortex excitability in migraine evaluated by single and paired magnetic stimuli. Headache 45:1394–1399.

Gevins, A. S., Cutillo, B. A., Bressler, S. L., Morgan, N. H., White, R. M., Illes, J., & Greer, D. S. (1989). Event-related covariances during a bimanual visuomotor task. II. Preparation and feedback. Electroencephalography and Clinical Neurophysiology/Evoked Potentials Section, 74(2), 147-160.

Giannini, M., Alexander, D. M., Nikolaev, A. R., & van Leeuwen, C. (2018). Large-scale traveling waves in EEG activity following eye movement. Brain topography, 31(4), 608-622.

Giannitrapani, D. (1970). EEG changes under differing auditory stimulations. Archives of general psychiatry, 23(5), 445-453.

Giannitrapani, D., Sorkin, A. I., & Enenstein, J. (1966). Laterality preference of children and adults as related to interhemispheric EEG phase activity. Journal of the neurological sciences, 3(2), 139-150.

Goense, J. B., & Logothetis, N. K. (2008). Neurophysiology of the BOLD fMRI signal in awake monkeys. Current Biology, 18(9), 631-640.

Goldman, R. I., Stern, J. M., Engel Jr, J., & Cohen, M. S. (2002). Simultaneous EEG and fMRI of the alpha rhythm. Neuroreport, 13(18), 2487, 1-11.

Goldman, S., Santelmann Jr, W. F., Vivian, W. E., & Goldman, D. (1949). Traveling waves in the brain. Science, 109(2838), 524-524.

González, J., Gamundi, A., Rial, R., Nicolau, M. C., de Vera, L., & Pereda, E. (1999). Nonlinear, fractal, and spectral analysis of the EEG of lizard, Gallotia galloti. American Journal of Physiology-Regulatory, Integrative and Comparative Physiology, 277(1), R86-R93.

Graaf, T.A. de, Gross, J., Paterson, G., Rusch, T., Sack, A.T., and Thut, G. (2013). Alpha-Band Rhythms in Visual Task Performance: Phase-Locking by Rhythmic Sensory Stimulation. PLOS ONE 8, e60035, 1-12.

Gray, C. M., & Singer, W. (1989). Stimulus-specific neuronal oscillations in orientation columns of cat visual cortex. Proceedings of the National Academy of Sciences, 86(5), 1698-1702.

Grinvald, A., Lieke, E. E., Frostig, R. D., & Hildesheim, R. (1994). Cortical point-spread function and long-range lateral interactions revealed by real-time optical imaging of macaque monkey primary visual cortex. Journal of Neuroscience, 14(5), 2545-2568.

Grinvald, A., Manker, A., & Segal, M. (1982). Visualization of the spread of electrical activity in rat hippocampal slices by voltage-sensitive optical probes. The Journal of physiology, 333(1), 269-291.

Guderian, S., Schott, B. H., Richardson-Klavehn, A., & Düzel, E. (2009). Medial temporal theta state before an event predicts episodic encoding success in humans. Proceedings of the National Academy of Sciences, 106(13), 5365-5370.

Gutierrez, B. C., Pita Almenar, M. R., Cantero, M. D. R., & Cantiello, H. F. (2021). Honeybee Brain Oscillations Are Generated by Microtubules. The Concept of a Brain Central Oscillator. Frontiers in Molecular Neuroscience, 217, 1-12.

Haegens, S., Nácher, V., Hernández, A., Luna, R., Jensen, O., & Romo, R. (2011a). Beta oscillations in the monkey sensorimotor network reflect somatosensory decision making. Proceedings of the National Academy of Sciences, 108(26), 10708-10713.

Haegens, S., Nácher, V., Luna, R., Romo, R., & Jensen, O. (2011b). α-Oscillations in the monkey sensorimotor network influence discrimination performance by rhythmical inhibition of neuronal spiking. Proceedings of the National Academy of Sciences, 108(48), 19377-19382.

Haegens S, Barczak A, Musacchia G, Lipton ML, Mehta AD, Lakatos P, Schroeder CE (2015) Laminar profile and physiology of the alpha rhythm in primary visual, auditory, and somatosensory regions of neocortex. J Neurosci 35:14341–14352.

Halgren, M., Ulbert, I., Bastuji, H., Fabó, D., Erőss, L., Rey, M., Devinskyk, O., Doylek, W. K., Mak-McCullyl, R., Halgrenm, E., Wittnerb, L., Chauvelh, P., Heitn, G., Eskandara, E., Mandello, A., & Cash, S. S. (2019). The generation and propagation of the human alpha rhythm. Proceedings of the National Academy of Sciences, 116(47), 23772-23782.

Han, B., & VanRullen, R. (2017). The rhythms of predictive coding? Pre-stimulus phase modulates the influence of shape perception on luminance judgments. Scientific reports, 7(1), 1-10.

Han, B., & VanRullen, R. (2016). Shape perception enhances perceived contrast: evidence for excitatory predictive feedback?. Scientific reports, 6(1), 1-10.

Han, F., Caporale, N., & Dan, Y. (2008). Reverberation of recent visual experience in spontaneous cortical waves. Neuron, 60(2), 321-327.

Händel, B. F., Haarmeier, T., & Jensen, O. (2011). Alpha oscillations correlate with the successful inhibition of unattended stimuli. Journal of cognitive neuroscience, 23(9), 2494-2502.

Hangya, B., Tihanyi, B. T., Entz, L., Fabó, D., Eróss, L., Wittner, L., Jakus, R., Varga, V., Freund, T. F., & Ulbert, I. (2011). Complex propagation patterns characterize human cortical activity during slow-wave sleep. Journal of Neuroscience, 31(24), 8770-8779.

Hanslmayr, S., Volberg, G., Wimber, M., Dalal, S. S., & Greenlee, M. W. (2013). Prestimulus oscillatory phase at 7 Hz gates cortical information flow and visual perception. Current Biology, 23(22), 2273-2278.

Hanslmayr, S., Volberg, G., Wimber, M., Raabe, M., Greenlee, M. W., & Bäuml, K. H. T. (2011). The relationship between brain oscillations and BOLD signal during memory formation: a combined EEG–fMRI study. Journal of Neuroscience, 31(44), 15674-15680.Sciences, 106(13), 5365-5370.

Hanslmayr, S., Aslan, A., Staudigl, T., Klimesch, W., Herrmann, C. S., & Bäuml, K. H. (2007). Prestimulus oscillations predict visual perception performance between and within subjects. Neuroimage, 37(4), 1465-1473.

Harmony, T. (2013). The functional significance of delta oscillations in cognitive processing. Frontiers in integrative neuroscience, 7, 83, 1-10.

Harris, A. M., Dux, P. E., & Mattingley, J. B. (2018). Detecting unattended stimuli depends on the phase of prestimulus neural oscillations. Journal of Neuroscience, 38(12), 3092-3101.

Haxby, J. V., Gobbini, M. I., Furey, M. L., Ishai, A., Schouten, J. L., & Pietrini, P. (2001). Distributed and overlapping representations of faces and objects in ventral temporal cortex. Science, 293(5539), 2425-2430.

Heinrich, S.P. (2010). Some thoughts on the interpretation of steady-state evoked potentials. Doc Ophthalmol 120, 205–214.

Helfrich, R. F., Fiebelkorn, I. C., Szczepanski, S. M., Lin, J. J., Parvizi, J., Knight, R. T., & Kastner, S. (2018). Neural mechanisms of sustained attention are rhythmic. Neuron, 99(4), 854-865.

Henry, M.J., and Obleser, J. (2012). Frequency modulation entrains slow neural oscillations and optimizes human listening behavior. PNAS 109, 20095–20100.

Henry, M.J., Herrmann, B., and Obleser, J. (2014). Entrained neural oscillations in multiple frequency bands comodulate behavior. PNAS 111, 14935–14940.

Herding, J., Spitzer, B., & Blankenburg, F. (2016). Upper beta band oscillations in human premotor cortex encode subjective choices in a vibrotactile comparison task. Journal of cognitive neuroscience, 28(5), 668-679.

Hernández-Pérez, J. J., Cooper, K. W., & Newman, E. L. (2020). Medial entorhinal cortex activates in a traveling wave in the rat. Elife, 9, e52289, 1-20.

Herrmann, B., Henry, M. J., Haegens, S., & Obleser, J. (2016). Temporal expectations and neural amplitude fluctuations in auditory cortex interactively influence perception. Neuroimage, 124, 487-497.

Herweg, N. A., Solomon, E. A., & Kahana, M. J. (2020). Theta oscillations in human memory. Trends in cognitive sciences, 24(3), 208-227.

Hindriks, R., van Putten, M. J., & Deco, G. (2014). Intra-cortical propagation of EEG alpha oscillations. Neuroimage, 103, 444-453.

Holsheimer, J., & da Silva Lopes, F. H. (1989). Propagation velocity of epileptiform activity in the hippocampus. Experimental brain research, 77(1), 69-78.

Holz, E. M., Glennon, M., Prendergast, K., & Sauseng, P. (2010). Theta–gamma phase synchronization during memory matching in visual working memory. Neuroimage, 52(1), 326-335.

Honkanen, R., Rouhinen, S., Wang, S. H., Palva, J. M., & Palva, S. (2015). Gamma oscillations underlie the maintenance of feature-specific information and the contents of visual working memory. Cerebral cortex, 25(10), 3788-3801.

Hoovey, Z. B., Heinemann, U., & Creutzfeldt, O. D. (1972). Inter-hemispheric" synchrony" of alpha waves. Electroencephalography & Clinical Neurophysiology.

Hord, D., Tracy, M., & Naitoh, P. (1974). Intra-hemispheric phase relationships during self-regulated alpha activity. Electroencephalography and clinical neurophysiology, 37(2), 133-136.

Hord, D., Naitoh, P., & Johnson, L. (1972). Intensity and coherence contours during self-regulated high alpha activity. Electroencephalography and clinical neurophysiology, 32(4), 429-433.

Hori, H., Hayasaka, K., Sato, K., Harada, O., & Iwata, H. (1969). A study on phase relationship in human alpha activity. Correlation of different regions. Electroencephalography and clinical neurophysiology, 26(1), 19-24.

Hsiao, F. J., Lin, Y. Y., Hsieh, J. C., Wu, Z. A., Ho, L. T., & Chang, Y. (2006). Oscillatory characteristics of face-evoked neuromagnetic responses. International journal of psychophysiology, 61(2), 113-120.

Hu, H., Vervaeke, K., & Storm, J. F. (2002). Two forms of electrical resonance at theta frequencies, generated by M-current, h-current and persistent Na+ current in rat hippocampal pyramidal cells. The Journal of physiology, 545(3), 783-805.

Huang, Y., Chen, L., & Luo, H. (2015). Behavioral oscillation in priming: competing perceptual predictions conveyed in alternating theta-band rhythms. Journal of Neuroscience, 35(6), 2830-2837.

Huang, X., Xu, W., Liang, J., Takagaki, K., Gao, X., & Wu, J. Y. (2010). Spiral wave dynamics in neocortex. Neuron, 68(5), 978-990.

Huang, X., Troy, W. C., Yang, Q., Ma, H., Laing, C. R., Schiff, S. J., & Wu, J. Y. (2004). Spiral waves in disinhibited mammalian neocortex. Journal of Neuroscience, 24(44), 9897-9902.

Hughes, S. W., & Crunelli, V. (2005). Thalamic mechanisms of EEG alpha rhythms and their pathological implications. The Neuroscientist, 11(4), 357-372.

Hughes, J. R., Ikram, A., & Fino, J. J. (1995). Characteristics of travelling waves under various conditions. Clinical Electroencephalography, 26(1), 7-22.

Hughes, J. R., Kuruvilla, A., & Fino, J. J. (1992). Topographic analysis of visual evoked potentials from flash and pattern reversal stimuli: evidence for “travelling waves”. Brain topography, 4(3), 215-228.

Hussain SJ, Claudino L, Bönstrup M, Norato G, Cruciani G, Thompson R, Zrenner C, Ziemann U, Buch E, Cohen LG (2019) Sensorimotor oscillatory phase-power interaction gates resting human corticospinal output. Cereb Cortex 29:3766–3777.

Hyafil, A., Giraud, A. L., Fontolan, L., & Gutkin, B. (2015). Neural cross-frequency coupling: connecting architectures, mechanisms, and functions. Trends in neurosciences, 38(11), 725-740.

Inouye, T., Shinosaki, K., Toi, S., Matsumoto, Y., & Hosaka, N. (1995). Potential flow of a activity in the human electroencephalogram. Neuroscience letters, 187(1), 29-32.

Inouye, T., Shinosaki, K., Iyama, A., Matsumoto, Y., Toi, S., & Ishihara, T. (1994). Potential flow of frontal midline theta activity during a mental task in the human electroencephalogram. Neuroscience Letters, 169(1-2), 145-148.

Inouye, T., Shinosaki, K., & Yagasaki, A. (1983). The direction of spread of alpha activity over the scalp. Electroencephalography and clinical neurophysiology, 55(3), 290-300.

Ito, J., Nikolaev, A. R., & Leeuwen, C. V. (2007). Dynamics of spontaneous transitions between global brain states. Human brain mapping, 28(9), 904-913.

Ito, J., Nikolaev, A. R., & Van Leeuwen, C. (2005). Spatial and temporal structure of phase synchronization of spontaneous alpha EEG activity. Biological cybernetics, 92(1), 54-60.

Jaggard, J. B., Wang, G. X., & Mourrain, P. (2021). Non-REM and REM/paradoxical sleep dynamics across phylogeny. Current opinion in neurobiology, 71, 44-51.

Jancke, D., Chavane, F., Naaman, S., & Grinvald, A. (2004). Imaging cortical correlates of illusion in early visual cortex. Nature, 428(6981), 423-426.

Jensen, O., Pan, Y., Frisson, S., & Wang, L. (2021). An oscillatory pipelining mechanism supporting previewing during visual exploration and reading. Trends in cognitive sciences, 25(12), 1033-1044.

Jensen, O., Spaak, E., & Zumer, J. M. (2014). Human brain oscillations: From physiological mechanisms to analysis and cognition. Magnetoencephalography: From signals to dynamic cortical networks, 471-517.

Jensen, O., & Mazaheri, A. (2010). Shaping functional architecture by oscillatory alpha activity: gating by inhibition. Frontiers in human neuroscience, 4, 186, 1-8.

Jensen, O., & Colgin, L. L. (2007). Cross-frequency coupling between neuronal oscillations. Trends in cognitive sciences, 11(7), 267-269.

Jensen, O., Gelfand, J., Kounios, J., & Lisman, J. E. (2002). Oscillations in the alpha band (9–12 Hz) increase with memory load during retention in a short-term memory task. Cerebral cortex, 12(8), 877-882.

John-Saaltink, E. S., Kok, P., Lau, H. C., & De Lange, F. P. (2016). Serial dependence in perceptual decisions is reflected in activity patterns in primary visual cortex. Journal of Neuroscience, 36(23), 6186-6192.

Jones, S. R., Kerr, C. E., Wan, Q., Pritchett, D. L., Hämäläinen, M., & Moore, C. I. (2010). Cued spatial attention drives functionally relevant modulation of the mu rhythm in primary somatosensory cortex. Journal of Neuroscience, 30(41), 13760-13765.

Kahana, M. J., Sekuler, R., Caplan, J. B., Kirschen, M., & Madsen, J. R. (1999). Human theta oscillations exhibit task dependence during virtual maze navigation. Nature, 399(6738), 781-784.

Kammer T, Baumann LW (2010) Phosphene thresholds evoked with single and double TMS pulses. Clin Neurophysiol 121:376–379.

Ketchum, K. L., & Haberly, L. B. (1993). Synaptic events that generate fast oscillations in piriform cortex. Journal of Neuroscience, 13(9), 3980-3985.

Kienitz, R., Schmid, M. C., & Dugué, L. (2021). Rhythmic sampling revisited: experimental paradigms and neural mechanisms. European Journal of Neuroscience, 1-15.

Kilavik, B. E., Zaepffel, M., Brovelli, A., MacKay, W. A., & Riehle, A. (2013). The ups and downs of beta oscillations in sensorimotor cortex. Experimental neurology, 245, 15-26.

Kim, U., Bal, T., & McCormick, D. A. (1995). Spindle waves are propagating synchronized oscillations in the ferret LGNd in vitro. Journal of Neurophysiology, 74(3), 1301-1323.

King, J. R., & Wyart, V. (2021). The human brain encodes a chronicle of visual events at each instant of time through the multiplexing of traveling waves. Journal of Neuroscience, 41(34), 7224-7233.

Kitano, M., Kasamatsu, T., Norcia, A. M., & Sutter, E. E. (1995). Spatially distributed responses induced by contrast reversal in cat visual cortex. Experimental brain research, 104(2), 297-309.

Kizuk, S. A., & Mathewson, K. E. (2017). Power and phase of alpha oscillations reveal an interaction between spatial and temporal visual attention. Journal of Cognitive Neuroscience, 29(3), 480-494.

Kleinfeld, D., Delaney, K. R., Fee, M. S., Flores, J. A., Tank, D. W., & Gelperin, A. (1994). Dynamics of propagating waves in the olfactory network of a terrestrial mollusk: an electrical and optical study. Journal of Neurophysiology, 72(3), 1402-1419.

Klimesch, W., Sauseng, P., & Hanslmayr, S. (2007a). EEG alpha oscillations: the inhibition–timing hypothesis. Brain research reviews, 53(1), 63-88.

Klimesch, W., Hanslmayr, S., Sauseng, P., Gruber, W. R., & Doppelmayr, M. (2007b). P1 and traveling alpha waves: evidence for evoked oscillations. Journal of neurophysiology, 97(2), 1311-1318.

Klimesch, W., Doppelmayr, M., Schwaiger, J., Auinger, P., & Winkler, T. H. (1999). Paradoxical'alpha synchronization in a memory task. Cognitive Brain Research, 7(4), 493-501.

Klimesch, W., Doppelmayr, M., Pachinger, T., & Ripper, B. (1997). Brain oscillations and human memory: EEG correlates in the upper alpha and theta band. Neuroscience letters, 238(1-2), 9-12.

Klimesch, W., Schimke, H., Doppelmayr, M., Ripper, B., Schwaiger, J., & Pfurtscheller, G. (1996). Event-related desynchronization (ERD) and the Dm effect: does alpha desynchronization during encoding predict later recall performance? International journal of psychophysiology, 24(1-2), 47-60.

Klopp, J., Halgren, E., Marinkovic, K., & Nenov, V. (1999). Face-selective spectral changes in the human fusiform gyrus. Clinical Neurophysiology, 110(4), 676-682.

Knapen, T., van Ee, R., & Blake, R. (2007). Stimulus motion propels traveling waves in binocular rivalry. PLoS One, 2(8), e739, 1-7.

Knowles, W. D., Traub, R. D., & Strowbridge, B. W. (1987). The initiation and spread of epileptiform bursts in the in vitro hippocampal slice. Neuroscience, 21(2), 441-455.

Koch, S. P., Werner, P., Steinbrink, J., Fries, P., & Obrig, H. (2009). Stimulus-induced and state-dependent sustained gamma activity is tightly coupled to the hemodynamic response in humans. Journal of Neuroscience, 29(44), 13962-13970.

Korotkova, T., Ponomarenko, A., Monaghan, C. K., Poulter, S. L., Cacucci, F., Wills, T., Hasselmo, M. E., & Lever, C. (2018). Reconciling the different faces of hippocampal theta: The role of theta oscillations in cognitive, emotional and innate behaviors. Neuroscience & Biobehavioral Reviews, 85, 65-80.

Kösem, A., Gramfort, A., & Van Wassenhove, V. (2014). Encoding of event timing in the phase of neural oscillations. Neuroimage, 92, 274-284.

Kraus, B. J., Robinson II, R. J., White, J. A., Eichenbaum, H., & Hasselmo, M. E. (2013). Hippocampal "time cells": time versus path integration. Neuron, 78(6), 1090-1101.

Kupers, E. R., Benson, N. C., Carrasco, M., & Winawer, J. (2022). Asymmetries around the visual field: From retina to cortex to behavior. PLOS Computational Biology, 18(1), e1009771.

Kupers, E. R., Benson, N. C., & Winawer, J. (2021). A visual encoding model links magnetoencephalography signals to neural synchrony in human cortex. NeuroImage, 245, 118655.

Laaris, N., Carlson, G. C., & Keller, A. (2000). Thalamic-evoked synaptic interactions in barrel cortex revealed by optical imaging. Journal of Neuroscience, 20(4), 1529-1537.

Lachaux, J. P., Fonlupt, P., Kahane, P., Minotti, L., Hoffmann, D., Bertrand, O., & Baciu, M. (2007). Relationship between task-related gamma oscillations and BOLD signal: New insights from combined fMRI and intracranial EEG. Human brain mapping, 28(12), 1368-1375.

Lakatos, P., Shah, A. S., Knuth, K. H., Ulbert, I., Karmos, G., & Schroeder, C. E. (2005) An oscillatory hierarchy controlling cortical excitability and stimulus processing. J Neurophysiol 94: 1904–1911.

Lam, Y. W., Cohen, L. B., & Zochowski, M. R. (2003). Odorant specificity of three oscillations and the DC signal in the turtle olfactory bulb. European Journal of Neuroscience, 17(3), 436-446.

Lam, Y. W., Cohen, L. B., Wachowiak, M., & Zochowski, M. R. (2000). Odors elicit three different oscillations in the turtle olfactory bulb. Journal of Neuroscience, 20(2), 749-762.

Landau, A. N., & Fries, P. (2012). Attention samples stimuli rhythmically. Current biology, 22(11), 1000-1004.

Lange, J., Oostenveld, R., & Fries, P. (2013). Reduced occipital alpha power indexes enhanced excitability rather than improved visual perception. Journal of Neuroscience, 33(7), 3212-3220.

Larsson, J., & Heeger, D. J. (2006). Two retinotopic visual areas in human lateral occipital cortex. Journal of neuroscience, 26(51), 13128-13142.

Laufs, H., Kleinschmidt, A., Beyerle, A., Eger, E., Salek-Haddadi, A., Preibisch, C., & Krakow, K. (2003). EEG-correlated fMRI of human alpha activity. Neuroimage, 19(4), 1463-1476.

Lecaignard, F. (2016). Predictive coding in auditory processing: insights from advanced modeling of EEG and MEG mismatch responses (Doctoral dissertation, Université de Lyon).

Lee, S. H., Blake, R., & Heeger, D. J. (2007). Hierarchy of cortical responses underlying binocular rivalry. Nature neuroscience, 10(8), 1048-1054.

Lee, S. H., Blake, R., & Heeger, D. J. (2005). Traveling waves of activity in primary visual cortex during binocular rivalry. Nature neuroscience, 8(1), 22-23.

Leske, S., Tse, A., Oosterhof, N. N., Hartmann, T., Müller, N., Keil, J., & Weisz, N. (2014). The strength of alpha and beta oscillations parametrically scale with the strength of an illusory auditory percept. Neuroimage, 88, 69-78.

Liberman, A., Manassi, M., & Whitney, D. (2018). Serial dependence promotes the stability of perceived emotional expression depending on face similarity. Attention, Perception, & Psychophysics, 80(6), 1461-1473.

Liberman, A., Fischer, J., & Whitney, D. (2014). Serial dependence in the perception of faces. Current biology, 24(21), 2569-2574.

Lilly, J. C., & Cherry, R. B. (1954). Surface movements of click responses from acoustic cerebral cortex of cat: leading and trailing edges of a response figure. Journal of Neurophysiology, 17(6), 521-532.

Lin YJ, Shukla L, Dugué L, Valero-Cabré A, Carrasco M (2021) Transcranial magnetic stimulation entrains alpha oscillatory activity in occipital cortex. Sci Rep 11:18562.

Linkenkaer-Hansen, K., Nikulin, V. V., Palva, S., Ilmoniemi, R. J., & Palva, J. M. (2004). Prestimulus oscillations enhance psychophysical performance in humans. Journal of Neuroscience, 24(45), 10186-10190.

Liou, J. Y., Smith, E. H., Bateman, L. M., McKhann, G. M., Goodman, R. R., Greger, B., Davis, T. S., Kellis, S. S., House, P. A., & Schevon, C. A. (2017). Multivariate regression methods for estimating velocity of ictal discharges from human microelectrode recordings. Journal of neural engineering, 14(4), 044001.

Lippert, M. T., Takagaki, K., Xu, W., Huang, X., & Wu, J. Y. (2007). Methods for voltage-sensitive dye imaging of rat cortical activity with high signal-to-noise ratio. Journal of neurophysiology, 98(1), 502-512.

Liske, E., Hughes, H. M., & Stowe, D. E. (1967). Cross-correlation of human alpha activity: normative data. Electroencephalogr Clin Neurophysiol, 22(5):429-36.

Liu-Shuang, J., Norcia, A.M., and Rossion, B. (2014). An objective index of individual face discrimination in the right occipito-temporal cortex by means of fast periodic oddball stimulation. Neuropsychologia 52, 57–72.

Logothetis, N. K., Pauls, J., Augath, M., Trinath, T., & Oeltermann, A. (2001). Neurophysiological investigation of the basis of the fMRI signal. nature, 412(6843), 150-157.

London, J. A., Cohen, L. B., & Wu, J. Y. (1989). Optical recordings of the cortical response to whisker stimulation before and after the addition of an epileptogenic agent. Journal of Neuroscience, 9(6), 2182-2190.

Loomis, A. L., Harvey, E. N., & Hobart, G. (1935). Further observations on the potential rhythms of the cerebral cortex during sleep. Science, 82(2122), 198-200.

Lőrincz, M. L., Kékesi, K. A., Juhász, G., Crunelli, V., & Hughes, S. W. (2009). Temporal framing of thalamic relay-mode firing by phasic inhibition during the alpha rhythm. Neuron, 63(5), 683-696.

Lozano-Soldevilla, D., & VanRullen, R. (2019). The hidden spatial dimension of alpha: 10-Hz perceptual echoes propagate as periodic traveling waves in the human brain. Cell reports, 26(2), 374-380.

Lubenov, E. V., & Siapas, A. G. (2009). Hippocampal theta oscillations are travelling waves. Nature, 459(7246), 534-539.

Luczak, A., Barthó, P., Marguet, S. L., Buzsáki, G., & Harris, K. D. (2007). Sequential structure of neocortical spontaneous activity in vivo. Proceedings of the National Academy of Sciences, 104(1), 347-352.

Luo, H., & Poeppel, D. (2007). Phase patterns of neuronal responses reliably discriminate speech in human auditory cortex. Neuron, 54(6), 1001-1010.

Maccaferri, G., & McBain, C. J. (1996). The hyperpolarization-activated current (Ih) and its contribution to pacemaker activity in rat CA1 hippocampal stratum oriens-alveus interneurones. The Journal of physiology, 497(1), 119-130.

MacCormick, D. A., & Pape, H. C. (1990). Properties of a hyperpolarization-activated cation current and its role in rhythmic oscillation in thalamic relay neurones. The Journal of physiology, 431(1), 291-318.

MacDonald, C. J., Lepage, K. Q., Eden, U. T., & Eichenbaum, H. (2011). Hippocampal "time cells" bridge the gap in memory for discontiguous events. Neuron, 71(4), 737-749.

Maclin, E., Okada, Y. C., Kaufman, L., & Williamson, S. J. (1983). Retinotopic map on the visual cortex for eccentrically placed patterns: first noninvasive measurement. Il Nuovo Cimento D, 2(2), 410-419.

Madsen KH, Karabanov AN, Krohne LG, Safeldt MG, Tomasevic L, Siebner HR (2019) No trace of phase: corticomotor excitability is not tuned by phase of pericentral mu-rhythm. Brain Stimul 12:1261–1270.

Maldonado, P. E., Friedman-Hill, S., & Gray, C. M. (2000). Dynamics of striate cortical activity in the alert macaque: II. Fast time scale synchronization. Cerebral Cortex, 10(11), 1117-1131.

Manasseh, G., De Balthasar, C., Sanguinetti, B., Pomarico, E., Gisin, N., Grave De Peralta, R., & Gonzalez Andino, S. L. (2013). Retinal and post-retinal contributions to the quantum efficiency of the human eye revealed by electrical neuroimaging. Frontiers in psychology, 4, 845, 1-13.

Manassi, M., Liberman, A., Kosovicheva, A., Zhang, K., & Whitney, D. (2018). Serial dependence in position occurs at the time of perception. Psychonomic Bulletin & Review, 25(6), 2245-2253.

Manassi, M., Liberman, A., Chaney, W., & Whitney, D. (2017). The perceived stability of scenes: serial dependence in ensemble representations. Scientific reports, 7(1), 1-9.

Manjarrez, E., Vázquez, M., & Flores, A. (2007). Computing the center of mass for traveling alpha waves in the human brain. Brain research, 1145, 239-247.

Manning, J. R., Jacobs, J., Fried, I., & Kahana, M. J. (2009). Broadband shifts in local field potential power spectra are correlated with single-neuron spiking in humans. Journal of Neuroscience, 29(43), 13613-13620.

Maris, E., Womelsdorf, T., Desimone, R., & Fries, P. (2013). Rhythmic neuronal synchronization in visual cortex entails spatial phase relation diversity that is modulated by stimulation and attention. Neuroimage, 74, 99-116.

Marshall, T. R., O'Shea, J., Jensen, O., & Bergmann, T. O. (2015). Frontal eye fields control attentional modulation of alpha and gamma oscillations in contralateral occipitoparietal cortex. Journal of Neuroscience, 35(4), 1638-1647.

Massimini, M., Ferrarelli, F., Esser, S. K., Riedner, B. A., Huber, R., Murphy, M., Peterson, M. J., & Tononi, G. (2007). Triggering sleep slow waves by transcranial magnetic stimulation. Proceedings of the National Academy of Sciences, 104(20), 8496-8501.

Massimini, M., Huber, R., Ferrarelli, F., Hill, S., & Tononi, G. (2004). The sleep slow oscillation as a traveling wave. Journal of Neuroscience, 24(31), 6862-6870.

Mathewson, K.E., Prudhomme, C., Fabiani, M., Beck, D.M., Lleras, A., and Gratton, G. (2012). Making Waves in the Stream of Consciousness: Entraining Oscillations in EEG Alpha and Fluctuations in Visual Awareness with Rhythmic Visual Stimulation. Journal of Cognitive Neuroscience 24, 2321–2333.

Mathewson, K. E., Lleras, A., Beck, D. M., Fabiani, M., Ro, T., & Gratton, G. (2011). Pulsed out of awareness: EEG alpha oscillations represent a pulsed-inhibition of ongoing cortical processing. Frontiers in psychology, 2, 99, 1-15.

Mathewson, K. E., Gratton, G., Fabiani, M., Beck, D. M., & Ro, T. (2009). To see or not to see: prestimulus α phase predicts visual awareness. Journal of Neuroscience, 29(9), 2725-2732.

Matsui, T., Murakami, T., & Ohki, K. (2016). Transient neuronal coactivations embedded in globally propagating waves underlie resting-state functional connectivity. Proceedings of the National Academy of Sciences, 113(23), 6556-6561.

Mazaheri, A., & Jensen, O. (2010). Rhythmic pulsing: linking ongoing brain activity with evoked responses. Frontiers in human neuroscience, 4, 177.

Mazaheri, A., Coffey-Corina, S., Mangun, G. R., Bekker, E. M., Berry, A. S., & Corbett, B. A. (2010). Functional disconnection of frontal cortex and visual cortex in attention-deficit/hyperactivity disorder. Biological psychiatry, 67(7), 617-623.

Mazaheri, A., Nieuwenhuis, I. L., Van Dijk, H., & Jensen, O. (2009). Prestimulus alpha and mu activity predicts failure to inhibit motor responses. Human brain mapping, 30(6), 1791-1800.

McFarland, D. J., Miner, L. A., Vaughan, T. M., & Wolpaw, J. R. (2000). Mu and beta rhythm topographies during motor imagery and actual movements. Brain topography, 12(3), 177-186.

Merholz, G., Grabot, L., VanRullen, R., and Dugué, L. (2022). Periodic attention operates faster during more complex visual search. Scientific Reports. 12(1), 1-14.

Merker, B. (2013). Cortical gamma oscillations: the functional key is activation, not cognition. Neuroscience & Biobehavioral Reviews, 37(3), 401-417.

Meteyard, L., and Davies, R.A.I. (2020). Best practice guidance for linear mixed-effects models in psychological science. Journal of Memory and Language 112, 104092, 1-83.

Michalareas, G., Vezoli, J., Van Pelt, S., Schoffelen, J. M., Kennedy, H., & Fries, P. (2016). Alpha-beta and gamma rhythms subserve feedback and feedforward influences among human visual cortical areas. Neuron, 89(2), 384-397.

Michel, R., Dugué, L., & Busch, N. A. (2021). Distinct contributions of alpha and theta rhythms to perceptual and attentional sampling. European Journal of Neuroscience.

Miles, R., Traub, R. D., & Wong, R. K. (1988). Spread of synchronous firing in longitudinal slices from the CA3 region of the hippocampus. Journal of Neurophysiology, 60(4), 1481-1496.

Milton, A., & Pleydell-Pearce, C. W. (2016). The phase of pre-stimulus alpha oscillations influences the visual perception of stimulus timing. Neuroimage, 133, 53-61.

Mitra, A., Snyder, A. Z., Tagliazucchi, E., Laufs, H., & Raichle, M. E. (2015). Propagated infra-slow intrinsic brain activity reorganizes across wake and slow wave sleep. Elife, 4, e10781, 1-19.

Montemurro, M. A., Rasch, M. J., Murayama, Y., Logothetis, N. K., & Panzeri, S. (2008). Phase-of-firing coding of natural visual stimuli in primary visual cortex. Current biology, 18(5), 375-380.

Monto, S., Palva, S., Voipio, J., & Palva, J. M. (2008). Very slow EEG fluctuations predict the dynamics of stimulus detection and oscillation amplitudes in humans. Journal of Neuroscience, 28(33), 8268-8272.

Moosmann, M., Ritter, P., Krastel, I., Brink, A., Thees, S., Blankenburg, F., Taskin, B., Hellmuth, O., & Villringer, A. (2003). Correlates of alpha rhythm in functional magnetic resonance imaging and near infrared spectroscopy. Neuroimage, 20(1), 145-158.

Mukamel, R., Gelbard, H., Arieli, A., Hasson, U., Fried, I., & Malach, R. (2005). Coupling between neuronal firing, field potentials, and FMRI in human auditory cortex. Science, 309(5736), 951-954.

Muller, L., Chavane, F., Reynolds, J., & Sejnowski, T. J. (2018). Cortical travelling waves: mechanisms and computational principles. Nature Reviews Neuroscience, 19(5), 255-268.

Muller, L., Piantoni, G., Koller, D., Cash, S. S., Halgren, E., & Sejnowski, T. J. (2016). Rotating waves during human sleep spindles organize global patterns of activity that repeat precisely through the night. Elife, 5, e17267, 1-16.

Muller, L., Reynaud, A., Chavane, F., & Destexhe, A. (2014). The stimulus-evoked population response in visual cortex of awake monkey is a propagating wave. Nature communications, 5(1), 1-14.

Müller, N., Lorenz, I., Langguth, B., & Weisz, N. (2013a). rTMS induced tinnitus relief is related to an increase in auditory cortical alpha activity. PloS one, 8(2), e55557, 1-16.

Müller, N., Keil, J., Obleser, J., Schulz, H., Grunwald, T., Bernays, R. L., Hans-Jürgen, H., & Weisz, N. (2013b). You can't stop the music: Reduced auditory alpha power and coupling between auditory and memory regions facilitate the illusory perception of music during noise. Neuroimage, 79, 383-393.

Murphy, M., Riedner, B. A., Huber, R., Massimini, M., Ferrarelli, F., & Tononi, G. (2009). Source modeling sleep slow waves. Proceedings of the National Academy of Sciences, 106(5), 1608-1613.

Murray, W. S., Fischer, M. H., & Tatler, B. W. (2013). Serial and parallel processes in eye movement control: Current controversies and future directions. Quarterly Journal of Experimental Psychology, 66(3), 417-428.

Murthy, V. N., & Fetz, E. E. (1996). Oscillatory activity in sensorimotor cortex of awake monkeys: synchronization of local field potentials and relation to behavior. Journal of neurophysiology, 76(6), 3949-3967.

Nauhaus, I., Busse, L., Ringach, D. L., & Carandini, M. (2012). Robustness of traveling waves in ongoing activity of visual cortex. Journal of Neuroscience, 32(9), 3088-3094.

Nauhaus, I., Busse, L., Carandini, M., & Ringach, D. L. (2009). Stimulus contrast modulates functional connectivity in visual cortex. Nature neuroscience, 12(1), 70-76.

Nelson, D. A., & Katz, L. C. (1995). Emergence of functional circuits in ferret visual cortex visualized by optical imaging. Neuron, 15(1), 23-34.

Neuenschwander, S., & Singer, W. (1996). Long-range synchronization of oscillatory light responses in the cat retina and lateral geniculate nucleus. Nature, 379(6567), 728-733.

Neuper, C., Wörtz, M., & Pfurtscheller, G. (2006). ERD/ERS patterns reflecting sensorimotor activation and deactivation. Progress in brain research, 159, 211-222.

Ng, B. S. W., Schroeder, T., & Kayser, C. (2012). A precluding but not ensuring role of entrained low-frequency oscillations for auditory perception. Journal of Neuroscience, 32(35), 12268-12276.

Niessing, J., Ebisch, B., Schmidt, K. E., Niessing, M., Singer, W., & Galuske, R. A. (2005). Hemodynamic signals correlate tightly with synchronized gamma oscillations. science, 309(5736), 948-951.

Nikitin, E. S., & Balaban, P. M. (2000). Optical Recording of Odor-Evoked Responses in the Olfactory Brain of the Naıve and Aversively Trained Terrestrial Snails. Learning & Memory, 7(6), 422-432.

Nir, Y., Staba, R. J., Andrillon, T., Vyazovskiy, V. V., Cirelli, C., Fried, I., & Tononi, G. (2011). Regional slow waves and spindles in human sleep. Neuron, 70(1), 153-169.

Nishimura, M., Shirasawa, H., Kaizo, H., & Song, W. J. (2007). New field with tonotopic organization in guinea pig auditory cortex. Journal of neurophysiology, 97(1), 927-932.

Nolte, G., Ziehe, A., Nikulin, V. V., Schlögl, A., Krämer, N., Brismar, T., & Müller, K. R. (2008). Robustly estimating the flow direction of information in complex physical systems. Physical review letters, 100(23), 234101.

Norcia, A. M., Appelbaum, L. G., Ales, J. M., Cottereau, B. R., & Rossion, B. (2015). The steady-state visual evoked potential in vision research: A review. Journal of vision, 15(6), 4-4.

Novak, J. L., & Wheeler, B. C. (1989). Two-dimensional current source density analysis of propagation delays for components of epileptiform bursts in rat hippocampal slices. Brain research, 497(2), 223-230.

Nunez, P. L., & Srinivasan, R. (2006). A theoretical basis for standing and traveling brain waves measured with human EEG with implications for an integrated consciousness. Clinical neurophysiology, 117(11), 2424-2435.

Nunez, P. L. (1989). Generation of human EEG by a combination of long and short range neocortical interactions. Brain topography, 1(3), 199-215.

Nunez, P. L. (1981). A study of origins of the time dependencies of scalp EEG: II-experimental support of theory. IEEE Transactions on Biomedical Engineering, (3), 281-288.

Nunez, P. L. (1974). The brain wave equation: a model for the EEG. Mathematical Biosciences, 21(3-4), 279-297.

Nunn, C. M. H., & Osselton, J. W. (1974). The influence of the EEG alpha rhythm on the perception of visual stimuli. Psychophysiology, 11(3), 294-303.

Oever, S. ten, and Sack, A.T. (2015). Oscillatory phase shapes syllable perception. PNAS 112, 15833–15837.

Oostenveld, R., Fries, P., Maris, E., & Schoffelen, J. M. (2011). FieldTrip: open source software for advanced analysis of MEG, EEG, and invasive electrophysiological data. Computational intelligence and neuroscience, 2011.

Orbach, H. S., & Cohen, L. B. (1983). Optical monitoring of activity from many areas of the in vitro and in vivo salamander olfactory bulb: a new method for studying functional organization in the vertebrate central nervous system. Journal of Neuroscience, 3(11), 2251-2262.

Osipova, D., Hermes, D., & Jensen, O. (2008). Gamma power is phase-locked to posterior alpha activity. PloS one, 3(12), e3990.

Osipova, D., Takashima, A., Oostenveld, R., Fernández, G., Maris, E., & Jensen, O. (2006). Theta and gamma oscillations predict encoding and retrieval of declarative memory. Journal of neuroscience, 26(28), 7523-7531.

Ossandón, T., Jerbi, K., Vidal, J. R., Bayle, D. J., Henaff, M. A., Jung, J., Minotti, L., Bertrand, O., Kahane, P., & Lachaux, J. P. (2011). Transient suppression of broadband gamma power in the default-mode network is correlated with task complexity and subject performance. Journal of Neuroscience, 31(41), 14521-14530.

Palmer, S. E. (1999). Vision science: Photons to phenomenology. MIT press.

Pang, Z., Alamia, A., & VanRullen, R. (2020). Turning the Stimulus On and Off Changes the Direction of α Traveling Waves. eNeuro, 7(6), 1-11.

Pastalkova, E., Itskov, V., Amarasingham, A., & Buzsáki, G. (2008). Internally generated cell assembly sequences in the rat hippocampus. Science, 321(5894), 1322-1327.

Patel, J., Schomburg, E. W., Berényi, A., Fujisawa, S., & Buzsáki, G. (2013). Local generation and propagation of ripples along the septotemporal axis of the hippocampus. Journal of Neuroscience, 33(43), 17029-17041.

Patel, J., Fujisawa, S., Berényi, A., Royer, S., & Buzsáki, G. (2012). Traveling theta waves along the entire septotemporal axis of the hippocampus. Neuron, 75(3), 410-417.

Patten, T. M., Rennie, C. J., Robinson, P. A., & Gong, P. (2012). Human cortical traveling waves: dynamical properties and correlations with responses. PLoS One, 7(6), e38392, 1-10.

Petersen, C. C., Grinvald, A., & Sakmann, B. (2003a). Spatiotemporal dynamics of sensory responses in layer 2/3 of rat barrel cortex measured in vivo by voltage-sensitive dye imaging combined with whole-cell voltage recordings and neuron reconstructions. Journal of neuroscience, 23(4), 1298-1309.

Petersen, C. C., Hahn, T. T., Mehta, M., Grinvald, A., & Sakmann, B. (2003b). Interaction of sensory responses with spontaneous depolarization in layer 2/3 barrel cortex. Proceedings of the National Academy of Sciences, 100(23), 13638-13643.

Petsche, H., & Stumpf, C. (1960). Topographic and toposcopic study of origin and spread of the regular synchronized arousal pattern in the rabbit. Electroencephalography and clinical neurophysiology, 12(3), 589-600.

Pfurtscheller, G., & Da Silva, F. L. (1999). Event-related EEG/MEG synchronization and desynchronization: basic principles. Clinical neurophysiology, 110(11), 1842-1857.

Pfurtscheller, G., Stancak Jr, A., & Neuper, C. (1996). Post-movement beta synchronization. A correlate of an idling motor area? Electroencephalography and clinical neurophysiology, 98(4), 281-293.

Prechtl, J. C., Bullock, T. H., & Kleinfeld, D. (2000). Direct evidence for local oscillatory current sources and intracortical phase gradients in turtle visual cortex. Proceedings of the National Academy of Sciences, 97(2), 877-882.

Prechtl, J. C., Cohen, L. B., Pesaran, B., Mitra, P. P., & Kleinfeld, D. (1997). Visual stimuli induce waves of electrical activity in turtle cortex. Proceedings of the National Academy of Sciences, 94(14), 7621-7626.

Prechtl, J. C. (1994). Visual motion induces synchronous oscillations in turtle visual cortex. Proceedings of the National Academy of Sciences, 91(26), 12467-12471.

Purves, D., Paydarfar, J. A., & Andrews, T. J. (1996). The wagon wheel illusion in movies and reality. Proceedings of the National Academy of Sciences, 93(8), 3693-3697.

Quigley, C. (2021). Forgotten rhythms? Revisiting the first evidence for rhythms in cognition. European Journal of Neuroscience, 1-11.

Ramirez, J. M., Tryba, A. K., & Peña, F. (2004). Pacemaker neurons and neuronal networks: an integrative view. Current opinion in neurobiology, 14(6), 665-674.

Rao, R. P., & Ballard, D. H. (1999). Predictive coding in the visual cortex: a functional interpretation of some extra-classical receptive-field effects. Nature neuroscience, 2(1), 79-87.

Rasch, M. J., Gretton, A., Murayama, Y., Maass, W., & Logothetis, N. K. (2008). Inferring spike trains from local field potentials. Journal of neurophysiology, 99(3), 1461-1476.

Ray, S., & Maunsell, J. H. (2011). Different origins of gamma rhythm and high-gamma activity in macaque visual cortex. PLoS biology, 9(4), e1000610.

Ray, S., Crone, N. E., Niebur, E., Franaszczuk, P. J., & Hsiao, S. S. (2008a). Neural correlates of high-gamma oscillations (60–200 Hz) in macaque local field potentials and their potential implications in electrocorticography. Journal of Neuroscience, 28(45), 11526-11536.

Ray, S., Hsiao, S. S., Crone, N. E., Franaszczuk, P. J., & Niebur, E. (2008b). Effect of stimulus intensity on the spike–local field potential relationship in the secondary somatosensory cortex. Journal of Neuroscience, 28(29), 7334-7343.

Reddy, L., Remy, F., Vayssiere, N., & VanRullen, R. (2011). Neural correlates of the continuous wagon wheel illusion: a functional MRI study. Human brain mapping, 32(2), 163-170.

Reed, A.V. (1973). Speed-accuracy trade-off in recognition memory. Science 181, 574–576.

Reimer, A., Hubka, P., Engel, A. K., & Kral, A. (2011). Fast propagating waves within the rodent auditory cortex. Cerebral Cortex, 21(1), 166-177.

Rekauzke, S., Nortmann, N., Staadt, R., Hock, H. S., Schöner, G., & Jancke, D. (2016). Temporal asymmetry in dark–bright processing initiates propagating activity across primary visual cortex. Journal of Neuroscience, 36(6), 1902-1913.

Reynaud, A., Masson, G. S., & Chavane, F. (2012). Dynamics of local input normalization result from balanced short-and long-range intracortical interactions in area V1. Journal of neuroscience, 32(36), 12558-12569.

Ribak CE, Yan XX (2000) GABA neurons in the neocortex. In: GABA in the nervous system: the view at fifty years (Martin DL, Olsen RW, eds), pp 357–368. Philadelphia: Lippincott Williams and Wilkins.

Ribary, U., Ioannides, A. A., Singh, K. D., Hasson, R., Bolton, J. P., Lado, F., Mogilner, A., & Llinas, R. (1991). Magnetic field tomography of coherent thalamocortical 40-Hz oscillations in humans. Proceedings of the National Academy of Sciences, 88(24), 11037-11041.

Rice, D. M., & Hagstrom, E. C. (1989). Some evidence in support of a relationship between human auditory signal-detection performance and the phase of the alpha cycle. Perceptual and motor skills, 69(2), 451-457.

Rodriguez, E., George, N., Lachaux, J. P., Martinerie, J., Renault, B., & Varela, F. J. (1999). Perception's shadow: long-distance synchronization of human brain activity. Nature, 397(6718), 430-433.

Roelfsema, P. R., Engel, A. K., König, P., & Singer, W. (1997). Visuomotor integration is associated with zero time-lag synchronization among cortical areas. Nature, 385(6612), 157-161.

Roland, P. E., Hanazawa, A., Undeman, C., Eriksson, D., Tompa, T., Nakamura, H., Valentiniene, S., & Ahmed, B. (2006). Cortical feedback depolarization waves: a mechanism

of top-down influence on early visual areas. Proceedings of the National Academy of Sciences, 103(33), 12586-12591.

Romei, V., Driver, J., Schyns, P. G., & Thut, G. (2011). Rhythmic TMS over parietal cortex links distinct brain frequencies to global versus local visual processing. Current biology, 21(4), 334-337.

Romei, V., Gross, J., & Thut, G. (2010). On the role of prestimulus alpha rhythms over occipito-parietal areas in visual input regulation: correlation or causation?. Journal of Neuroscience, 30(25), 8692-8697.

Romei, V., Brodbeck, V., Michel, C., Amedi, A., Pascual-Leone, A., & Thut, G. (2008). Spontaneous fluctuations in posterior α-band EEG activity reflect variability in excitability of human visual areas. Cerebral cortex, 18(9), 2010-2018.

Rossi, S., Hallett, M., Rossini, P. M., Pascual-Leone, A., & Safety of TMS Consensus Group. (2009). Safety, ethical considerations, and application guidelines for the use of transcranial magnetic stimulation in clinical practice and research. Clinical neurophysiology, 120(12), 2008-2039.

Rossion, B., Prieto, E.A., Boremanse, A., Kuefner, D., and Van Belle, G. (2012). A steady-state visual evoked potential approach to individual face perception: Effect of inversion, contrast-reversal and temporal dynamics. NeuroImage 63, 1585–1600.

Rousselet, G. A., Husk, J. S., Bennett, P. J., & Sekuler, A. B. (2007). Single-trial EEG dynamics of object and face visual processing. Neuroimage, 36(3), 843-862.

Rubino, D., Robbins, K. A., & Hatsopoulos, N. G. (2006). Propagating waves mediate information transfer in the motor cortex. Nature neuroscience, 9(12), 1549-1557.

Sakihara, K., Gunji, A., Furushima, W., & Inagaki, M. (2012). Event-related oscillations in structural and semantic encoding of faces. Clinical Neurophysiology, 123(2), 270-277.

Samaha, J., Iemi, L., Haegens, S., & Busch, N. A. (2020). Spontaneous brain oscillations and perceptual decision-making. Trends in cognitive sciences, 24(8), 639-653.

Samaha, J., Gosseries, O., & Postle, B. R. (2017). Distinct oscillatory frequencies underlie excitability of human occipital and parietal cortex. Journal of Neuroscience, 37(11), 2824-2833.

Samaha, J., & Postle, B. R. (2015). The speed of alpha-band oscillations predicts the temporal resolution of visual perception. Current Biology, 25(22), 2985-2990.

Sanchez-Vives, M. V., & McCormick, D. A. (2000). Cellular and network mechanisms of rhythmic recurrent activity in neocortex. Nature neuroscience, 3(10), 1027-1034.

Sato, T. K., Nauhaus, I., & Carandini, M. (2012). Traveling waves in visual cortex. Neuron, 75(2), 218-229.

Sauseng, P., Klimesch, W., Gruber, W. R., & Birbaumer, N. (2008). Cross-frequency phase synchronization: a brain mechanism of memory matching and attention. Neuroimage, 40(1), 308-317.

Sauseng, P., Klimesch, W., Doppelmayr, M., Pecherstorfer, T., Freunberger, R., & Hanslmayr, S. (2005a). EEG alpha synchronization and functional coupling during top-down processing in a working memory task. Human brain mapping, 26(2), 148-155.

Sauseng, P., Klimesch, W., Stadler, W., Schabus, M., Doppelmayr, M., Hanslmayr, S., Gruber, W. R., & Birbaumer, N. (2005b). A shift of visual spatial attention is selectively associated with human EEG alpha activity. European Journal of Neuroscience, 22(11), 2917-2926.

Sauseng, P., Klimesch, W., Gruber, W., Doppelmayr, M., Stadler, W., & Schabus, M. (2002). The interplay between theta and alpha oscillations in the human electroencephalogram reflects the transfer of information between memory systems. Neuroscience letters, 324(2), 121-124.

Schack, B., Weiss, S., & Rappelsberger, P. (2003). Cerebral information transfer during word processing: where and when does it occur and how fast is it? Human brain mapping, 19(1), 18-36.

Schack, B., Rappelsberger, P., Weiss, S., & Möller, E. (1999). Adaptive phase estimation and its application in EEG analysis of word processing. Journal of neuroscience methods, 93(1), 49-59.

Schaworonkow NC, Gordon P, Belardinelli P, Ziemann U, Bergmann TO, Zrenner C (2018) m-Rhythm extracted with personalized EEG filters correlates with corticospinal excitability in real-time phase triggered EEG-TMS. Front Neurosci 12:1–6.

Schaworonkow N, Triesch J, Ziemann U, Zrenner C (2019) EEG-triggered TMS reveals stronger brain state-dependent modulation of motor evoked potentials at weaker stimulation intensities. Brain Stimul 12:110–118.

Scheeringa, R., Fries, P., Petersson, K. M., Oostenveld, R., Grothe, I., Norris, D. G., Hagoort, P., & Bastiaansen, M. C. (2011a). Neuronal dynamics underlying high-and low-frequency EEG oscillations contribute independently to the human BOLD signal. Neuron, 69(3), 572-583.

Scheeringa, R., Mazaheri, A., Bojak, I., Norris, D. G., & Kleinschmidt, A. (2011b). Modulation of visually evoked cortical FMRI responses by phase of ongoing occipital alpha oscillations. Journal of Neuroscience, 31(10), 3813-3820.

Scheeringa, R., Petersson, K. M., Oostenveld, R., Norris, D. G., Hagoort, P., & Bastiaansen, M. C. (2009). Trial-by-trial coupling between EEG and BOLD identifies networks related to alpha and theta EEG power increases during working memory maintenance. Neuroimage, 44(3), 1224-1238.

Scheeringa, R., Bastiaansen, M. C., Petersson, K. M., Oostenveld, R., Norris, D. G., & Hagoort, P. (2008). Frontal theta EEG activity correlates negatively with the default mode network in resting state. International journal of psychophysiology, 67(3), 242-251.

Schubert, R., Haufe, S., Blankenburg, F., Villringer, A., & Curio, G. (2009). Now you'll feel it, now you won't: EEG rhythms predict the effectiveness of perceptual masking. Journal of cognitive neuroscience, 21(12), 2407-2419.

Schütt, H. H., Harmeling, S., Macke, J. H., & Wichmann, F. A. (2016). Painfree and accurate Bayesian estimation of psychometric functions for (potentially) overdispersed data. Vision research, 122, 105-123.

Schwartzkroin, P. A., & Prince, D. A. (1978). Cellular and field potential properties of epileptogenic hippocampal slices. Brain research, 147(1), 117-130.

Schweitzer, P., Madamba, S. G., & Siggins, G. R. (2003). The sleep-modulating peptide cortistatin augments the h-current in hippocampal neurons. Journal of Neuroscience, 23(34), 10884-10891.

Senoussi, M., Moreland, J. C., Busch, N. A., & Dugué, L. (2019). Attention explores space periodically at the theta frequency. Journal of Vision, 19(5), 22-22.

Sharon, D., Jancke, D., Chavane, F., Na'aman, S., & Grinvald, A. (2007). Cortical response field dynamics in cat visual cortex. Cerebral Cortex, 17(12), 2866-2877.

Shaw, J. C., & McLachlan, K. R. (1968). The association between alpha rhythm propagation time and level of arousal. Psychophysiology, 4(3), 307-310.

Shevelev, I. A., Kamenkovich, V. M., Bark, E. D., Verkhlutov, V. M., Sharaev, G. A., & Mikhailova, E. S. (2000). Visual illusions and travelling alpha waves produced by flicker at alpha frequency. International Journal of Psychophysiology, 39(1), 9-20.

Singh, K. D., Barnes, G. R., Hillebrand, A., Forde, E. M., & Williams, A. L. (2002). Task-related changes in cortical synchronization are spatially coincident with the hemodynamic response. Neuroimage, 16(1), 103-114.

Sit, Y. F., Chen, Y., Geisler, W. S., Miikkulainen, R., & Seidemann, E. (2009). Complex dynamics of V1 population responses explained by a simple gain-control model. Neuron, 64(6), 943-956.

Skaggs, W. E., McNaughton, B. L., Wilson, M. A., & Barnes, C. A. (1996). Theta phase precession in hippocampal neuronal populations and the compression of temporal sequences. Hippocampus, 6(2), 149-172.

Slovin, H., Arieli, A., Hildesheim, R., & Grinvald, A. (2002). Long-term voltage-sensitive dye imaging reveals cortical dynamics in behaving monkeys. Journal of neurophysiology, 88(6), 3421-3438.

Smith, E. H., Liou, J. Y., Davis, T. S., Merricks, E. M., Kellis, S. S., Weiss, S. A., Greger, B., House, P. A., McKhann II, G. M., Goodman, R. R., Emerson, R. G., Bateman, L. M., Trevelyan, A. J., & Schevon, C. A. (2016). The ictal wavefront is the spatiotemporal source of discharges during spontaneous human seizures. Nature communications, 7(1), 1-12.

Sokoliuk, R., & VanRullen, R. (2016). Global and local oscillatory entrainment of visual behavior across retinotopic space. Scientific Reports, 6(1), 1-12.

Song, K., Meng, M., Chen, L., Zhou, K., & Luo, H. (2014). Behavioral oscillations in attention: rhythmic α pulses mediated through θ band. Journal of Neuroscience, 34(14), 4837-4844.

Song, W. J., Kawaguchi, H., Totoki, S., Inoue, Y., Katura, T., Maeda, S., Inagaki, S., Shirasawa, H., & Nishimura, M. (2006). Cortical intrinsic circuits can support activity propagation through an isofrequency strip of the guinea pig primary auditory cortex. Cerebral cortex, 16(5), 718-729.

Spaak, E., Lange, F.P. de, and Jensen, O. (2014). Local Entrainment of Alpha Oscillations by Visual Stimuli Causes Cyclic Modulation of Perception. J. Neurosci. 34, 3536–3544.

Spitzer, B., & Haegens, S. (2017). Beyond the status quo: a role for beta oscillations in endogenous content (re) activation. eNeuro, 4(4), 1-15.

Spitzer, B., Blankenburg, F., & Summerfield, C. (2016). Rhythmic gain control during supramodal integration of approximate number. NeuroImage, 129, 470-479.

Spitzer, B., Gloel, M., Schmidt, T. T., & Blankenburg, F. (2014). Working memory coding of analog stimulus properties in the human prefrontal cortex. Cerebral Cortex, 24(8), 2229-2236.

Spitzer, B., & Blankenburg, F. (2011). Stimulus-dependent EEG activity reflects internal updating of tactile working memory in humans. Proceedings of the National Academy of Sciences, 108(20), 8444-8449.

Sreekumar, V., Wittig, J. H., Chapeton, J. I., Inati, S. K., & Zaghloul, K. A. (2021). Low frequency traveling waves in the human cortex coordinate neural activity across spatial scales. BioRxiv, 2020-03, 1-48.

Srinivasan, R., Fornari, E., Knyazeva, M. G., Meuli, R., & Maeder, P. (2007). fMRI responses in medial frontal cortex that depend on the temporal frequency of visual input. Experimental brain research, 180(4), 677-691.

Srinivasan, R., Bibi, F. A., & Nunez, P. L. (2006). Steady-state visual evoked potentials: distributed local sources and wave-like dynamics are sensitive to flicker frequency. Brain topography, 18(3), 167-187.

Stanley, D. A., Roy, J. E., Aoi, M. C., Kopell, N. J., & Miller, E. K. (2018). Low-beta oscillations turn up the gain during category judgments. Cerebral Cortex, 28(1), 116-130.

Staudigl, T., & Hanslmayr, S. (2013). Theta oscillations at encoding mediate the context-dependent nature of human episodic memory. Current biology, 23(12), 1101-1106.

Stefanics, G., Hangya, B., Hernádi, I., Winkler, I., Lakatos, P., and Ulbert, I. (2010). Phase Entrainment of Human Delta Oscillations Can Mediate the Effects of Expectation on Reaction Speed. J. Neurosci. 30, 13578–13585.

Stefanou MI, Desideri D, Belardinelli P, Zrenner C, Ziemann U (2018) Phase synchronicity of m-rhythm determines efficacy of interhemispheric communication between human motor cortices. J Neurosci 38:10525–10534.

Steriade, M., & Deschenes, M. (1984). The thalamus as a neuronal oscillator. Brain Research Reviews, 8(1), 1-63.

Sterman, M. B., Kaiser, D. A., & Veigel, B. (1996). Spectral analysis of event-related EEG responses during short-term memory performance. Brain topography, 9(1), 21-30.

Strasburger, H., Rentschler, I., and Jüttner, M. (2011). Peripheral vision and pattern recognition: A review. Journal of vision, 11(5):13, 1-82.

Strauß, A., Henry, M. J., Scharinger, M., & Obleser, J. (2015). Alpha phase determines successful lexical decision in noise. Journal of Neuroscience, 35(7), 3256-3262.

Stroh, A., Adelsberger, H., Groh, A., Rühlmann, C., Fischer, S., Schierloh, A., Deisseroth, K., & Konnerth, A. (2013). Making waves: initiation and propagation of corticothalamic Ca2+ waves in vivo. Neuron, 77(6), 1136-1150.

Sugitani, M., Sugai, T., Tanifuji, M., Murase, K., & Onoda, N. (1994). Optical imaging of the in vitro guinea pig piriform cortex activity using a voltage-sensitive dye. Neuroscience letters, 165(1-2), 215-218.

Sutor, B., Hablitz, J. J., Rucker, F., & Ten Bruggencate, G. (1994). Spread of epileptiform activity in the immature rat neocortex studied with voltage-sensitive dyes and laser scanning microscopy. Journal of neurophysiology, 72(4), 1756-1768.

Suzuki, H. (1974). Phase relationships of alpha rhythm in man. The Japanese journal of physiology, 24(6), 569-586.

Takagaki, K., Zhang, C., Wu, J. Y., & Lippert, M. T. (2008). Crossmodal propagation of sensory-evoked and spontaneous activity in the rat neocortex. Neuroscience letters, 431(3), 191-196.

Takahashi, K., Kim, S., Coleman, T. P., Brown, K. A., Suminski, A. J., Best, M. D., & Hatsopoulos, N. G. (2015). Large-scale spatiotemporal spike patterning consistent with wave propagation in motor cortex. Nature communications, 6(1), 1-11.

Takahashi, K., Saleh, M., Penn, R. D., & Hatsopoulos, N. (2011). Propagating waves in human motor cortex. Frontiers in human neuroscience, 5, 40.

Tallon-Baudry, C. (2009). The roles of gamma-band oscillatory synchrony in human visual cognition. Front Biosci, 14(321-332), 26, 1-12.

Tallon-Baudry, C., Bertrand, O., Peronnet, F., & Pernier, J. (1998). Induced γ-band activity during the delay of a visual short-term memory task in humans. Journal of Neuroscience, 18(11), 4244-4254.

Tang, Y., Liu, D., Li, Y., Qiu, Y., & Zhu, Y. (2008, August). The time-frequency representation of the ERPs of face processing. In 2008 30th Annual International Conference of the IEEE Engineering in Medicine and Biology Society (pp. 4114-4117). IEEE.

Tanifuji, M., Sugiyama, T., & Murase, K. (1994). Horizontal propagation of excitation in rat visual cortical slices revealed by optical imaging. Science, 266(5187), 1057-1059.

Taniguchi, I., Horikawa, J., Moriyama, T., & Nasu, M. (1992). Spatio-temporal pattern of frequency representation in the auditory cortex of guinea pigs. Neuroscience letters, 146(1), 37-40.

Taubert, J., Alais, D., & Burr, D. (2016). Different coding strategies for the perception of stable and changeable facial attributes. Scientific reports, 6(1), 1-7.

Taylor, P. C., Walsh, V., & Eimer, M. (2010). The neural signature of phosphene perception. Human brain mapping, 31(9), 1408-1417.

Ten Oever, S., & Sack, A. T. (2015). Oscillatory phase shapes syllable perception. Proceedings of the National Academy of Sciences, 112(52), 15833-15837.

Terman, D., Bose, A., & Kopell, N. (1996). Functional reorganization in thalamocortical networks: Transition between spindling and delta sleep rhythms. Proceedings of the National Academy of Sciences, 93(26), 15417-15422.

Thatcher, R. W., Krause, P. J., & Hrybyk, M. (1986). Cortico-cortical associations and EEG coherence: a two-compartmental model. Electroencephalography and clinical neurophysiology, 64(2), 123-143.

Thielscher, A., Antunes, A., & Saturnino, G. B. (2015, August). Field modeling for transcranial magnetic stimulation: a useful tool to understand the physiological effects of TMS? In 2015 37th annual international conference of the IEEE engineering in medicine and biology society (EMBC) (pp. 222-225). IEEE.

Thorpe, S. G., Nunez, P. L., & Srinivasan, R. (2007). Identification of wave-like spatial structure in the SSVEP: Comparison of simultaneous EEG and MEG. Statistics in medicine, 26(21), 3911-3926.

Thut, G., Veniero, D., Romei, V., Miniussi, C., Schyns, P., & Gross, J. (2011). Rhythmic TMS causes local entrainment of natural oscillatory signatures. Current biology, 21(14), 1176-1185.

Thut, G., & Pascual-Leone, A. (2010). A review of combined TMS-EEG studies to characterize lasting effects of repetitive TMS and assess their usefulness in cognitive and clinical neuroscience. Brain topography, 22(4), 219-232.

Thut, G., Nietzel, A., Brandt, S. A., & Pascual-Leone, A. (2006). α-Band electroencephalographic activity over occipital cortex indexes visuospatial attention bias and predicts visual target detection. Journal of Neuroscience, 26(37), 9494-9502.

Torrence, R. D., Troup, L. J., Rojas, D. C., & Carlson, J. M. (2021). Enhanced contralateral theta oscillations and N170 amplitudes in occipitotemporal scalp regions underlie attentional bias to fearful faces. International Journal of Psychophysiology, 165, 84-91.

Townsend, R. G., Solomon, S. S., Chen, S. C., Pietersen, A. N., Martin, P. R., Solomon, S. G., & Gong, P. (2015). Emergence of complex wave patterns in primate cerebral cortex. Journal of Neuroscience, 35(11), 4657-4662.

Traub, R. D., Whittington, M. A., Buhl, E. H., Jefferys, J. G., & Faulkner, H. J. (1999). On the mechanism of the γ→ β frequency shift in neuronal oscillations induced in rat hippocampal slices by tetanic stimulation. Journal of Neuroscience, 19(3), 1088-1105.

Traub, R. D., Whittington, M. A., Colling, S. B., Buzsaki, G. X. J. J. G., & Jefferys, J. G. (1996). Analysis of gamma rhythms in the rat hippocampus in vitro and in vivo. The Journal of physiology, 493(2), 471-484.

Treder, M. S. (2020). MVPA-light: a classification and regression toolbox for multi-dimensional data. Frontiers in Neuroscience, 14, 289.

Tsau, Y., Guan, L. I., & Wu, J. Y. (1998). Initiation of spontaneous epileptiform activity in the neocortical slice. Journal of neurophysiology, 80(2), 978-982.

Tsoneva, T., Garcia-Molina, G., & Desain, P. (2021). SSVEP phase synchronies and propagation during repetitive visual stimulation at high frequencies. Scientific reports, 11(1), 1-13.

Tsytsarev, V., Yamazaki, T., Ribot, J., & Tanaka, S. (2004). Sound frequency representation in cat auditory cortex. Neuroimage, 23(4), 1246-1255.

Tucker, T. R., & Katz, L. C. (2003). Spatiotemporal patterns of excitation and inhibition evoked by the horizontal network in layer 2/3 of ferret visual cortex. Journal of Neurophysiology, 89(1), 488-500.

Uhlhaas, P. J., Pipa, G., Neuenschwander, S., Wibral, M., & Singer, W. (2011). A new look at gamma? High-(> 60 Hz) γ-band activity in cortical networks: function, mechanisms and impairment. Progress in biophysics and molecular biology, 105(1-2), 14-28.

Uno, H., Murai, N., & Fukunishi, K. (1993). The tonotopic representation in the auditory cortex of the guinea pig with optical recording. Neuroscience letters, 150(2), 179-182.

Van der Meij, R., Kahana, M., & Maris, E. (2012). Phase–amplitude coupling in human electrocorticography is spatially distributed and phase diverse. Journal of Neuroscience, 32(1), 111-123.

Van Dijk, H., Schoffelen, J. M., Oostenveld, R., & Jensen, O. (2008). Prestimulus oscillatory activity in the alpha band predicts visual discrimination ability. Journal of Neuroscience, 28(8), 1816-1823.

Van Ede, F., Van Pelt, S., Fries, P., & Maris, E. (2015). Both ongoing alpha and visually induced gamma oscillations show reliable diversity in their across-site phase-relations. Journal of neurophysiology, 113(5), 1556-1563.

Van Ede, F., Köster, M., & Maris, E. (2012). Beyond establishing involvement: quantifying the contribution of anticipatory α-and β-band suppression to perceptual improvement with attention. Journal of neurophysiology, 108(9), 2352-2362.

Van Kerkoerle, T., Self, M. W., Dagnino, B., Gariel-Mathis, M. A., Poort, J., Van Der Togt, C., & Roelfsema, P. R. (2014). Alpha and gamma oscillations characterize feedback and feedforward processing in monkey visual cortex. Proceedings of the National Academy of Sciences, 111(40), 14332-14341.

Van Vreeswijk, C., Abbott, L. F., & Ermentrout, G. B. (1994). When inhibition not excitation synchronizes neural firing. Journal of computational neuroscience, 1(4), 313-321.

VanRullen, R. (2016a). Perceptual cycles. Trends in cognitive sciences, 20(10), 723-735.

VanRullen, R. (2016b). How to evaluate phase differences between trial groups in ongoing electrophysiological signals. Frontiers in neuroscience, 10, 426.

VanRullen, R., and Dubois, J. (2011). The Psychophysics of Brain Rhythms. Front. Psychol. 1-10.

VanRullen, R. (2007). The continuous Wagon Wheel Illusion depends on, but is not identical to neuronal adaptation. Vision Research, 47(16), 2143-2149.

VanRullen, R., Reddy, L., & Koch, C. (2006). The continuous wagon wheel illusion is associated with changes in electroencephalogram power at~ 13 Hz. Journal of Neuroscience, 26(2), 502-507.

VanRullen, R., Reddy, L., & Koch, C. (2005). Attention-driven discrete sampling of motion perception. Proceedings of the National Academy of Sciences, 102(14), 5291-5296.

VanRullen, R., & Koch, C. (2003). Is perception discrete or continuous? Trends in cognitive sciences, 7(5), 207-213.

Valera, F. J., Toro, A., John, E. R., & Schwartz, E. L. (1981). Perceptual framing and cortical alpha rhythm. Neuropsychologia, 19(5), 675-686.

Valero-Cabré, A., Amengual, J. L., Stengel, C., Pascual-Leone, A., & Coubard, O. A. (2017). Transcranial magnetic stimulation in basic and clinical neuroscience: A comprehensive review of fundamental principles and novel insights. Neuroscience & Biobehavioral Reviews, 83, 381-404.

Verzeano, M., & Negishi, K. (1960). Neuronal Activity in Cortical and Thalamic Networks: A study with multiple microelectrodes. The Journal of general physiology, 43(6), 177-195.

Vialatte, F. B., Maurice, M., Dauwels, J., & Cichocki, A. (2010). Steady-state visually evoked potentials: focus on essential paradigms and future perspectives. Progress in neurobiology, 90(4), 418-438.

Vijayan, S., & Kopell, N. J. (2012). Thalamic model of awake alpha oscillations and implications for stimulus processing. Proceedings of the National Academy of Sciences, 109(45), 18553-18558.

Vinck, M., Lima, B., Womelsdorf, T., Oostenveld, R., Singer, W., Neuenschwander, S., & Fries, P. (2010). Gamma-phase shifting in awake monkey visual cortex. Journal of neuroscience, 30(4), 1250-1257.

Volgushev, M., Chauvette, S., Mukovski, M., & Timofeev, I. (2006). Precise long-range synchronization of activity and silence in neocortical neurons during slow-wave sleep. Journal of Neuroscience, 26(21), 5665-5672.

Von Leeuwen, W. S. (1964). Complementarity of different analysis methods. Electroencephalography and Clinical Neurophysiology, 16(1-2), 136-139.

Voskuyl, R. A., & Albus, H. (1985). Spontaneous epileptiform discharges in hippocampal slices induced by 4-aminopyridine. Brain research, 342(1), 54-66.

Vyazovskiy, V. V., Faraguna, U., Cirelli, C., & Tononi, G. (2009). Triggering slow waves during NREM sleep in the rat by intracortical electrical stimulation: effects of sleep/wake history and background activity. Journal of neurophysiology, 101(4), 1921-1931.

Wadman, W. J., & Gutnick, M. J. (1993). Non-uniform propagation of epileptiform discharge in brain slices of rat neocortex. Neuroscience, 52(2), 255-262.

Wagner, T., Rushmore, J., Eden, U., & Valero-Cabre, A. (2009). Biophysical foundations underlying TMS: setting the stage for an effective use of neurostimulation in the cognitive neurosciences. cortex, 45(9), 1025-1034.

Wagner, T., Valero-Cabre, A., & Pascual-Leone, A. (2007). Noninvasive human brain stimulation. Annu. Rev. Biomed. Eng., 9, 527-565.

Walter, D. O., Rhodes, J. M., Brown, D., & Adey, W. R. (1966). Comprehensive spectral analysis of human EEG generators in posterior cerebral regions. Electroencephalography and clinical neurophysiology, 20(3), 224-237.

Wang, X. J. (2010). Neurophysiological and computational principles of cortical rhythms in cognition. Physiological reviews, 90(3), 1195-1268.

Watt, J., Borhani, R., and Katsaggelos, A.K. (2020). Machine Learning Refined: Foundations, Algorithms, and Applications (Cambridge University Press).

Weisz, N., Wühle, A., Monittola, G., Demarchi, G., Frey, J., Popov, T., & Braun, C. (2014). Prestimulus oscillatory power and connectivity patterns predispose conscious somatosensory perception. Proceedings of the National Academy of Sciences, 111(4), E417-E425.

Weisz, N., Moratti, S., Meinzer, M., Dohrmann, K., & Elbert, T. (2005). Tinnitus perception and distress is related to abnormal spontaneous brain activity as measured by magnetoencephalography. PLoS medicine, 2(6), e153, 1-8.

Whittingstall, K., & Logothetis, N. K. (2009). Frequency-band coupling in surface EEG reflects spiking activity in monkey visual cortex. Neuron, 64(2), 281-289.

Whittington, M. A., Traub, R. D., Kopell, N., Ermentrout, B., & Buhl, E. H. (2000). Inhibition-based rhythms: experimental and mathematical observations on network dynamics. International journal of psychophysiology, 38(3), 315-336.

Whittington, M. A., Traub, R. D., & Jefferys, J. G. (1995). Synchronized oscillations in interneuron networks driven by metabotropic glutamate receptor activation. Nature, 373(6515), 612-615.

Wickelgren, W.A. (1977). Speed-accuracy tradeoff and information processing dynamics. Acta Psychologica 41, 67–85.

Wilson, H. R., Blake, R., & Lee, S. H. (2001). Dynamics of travelling waves in visual perception. Nature, 412(6850), 907-910.

Wimmer, K., Ramon, M., Pasternak, T., & Compte, A. (2016). Transitions between multiband oscillatory patterns characterize memory-guided perceptual decisions in prefrontal circuits. Journal of Neuroscience, 36(2), 489-505.

Witte, R. S., Rousche, P. J., & Kipke, D. R. (2007). Fast wave propagation in auditory cortex of an awake cat using a chronic microelectrode array. Journal of neural engineering, 4(2), 68, 1-11.

Worden, M. S., Foxe, J. J., Wang, N., & Simpson, G. V. (2000). Anticipatory biasing of visuospatial attention indexed by retinotopically specific α-bank electroencephalography increases over occipital cortex. Journal of Neuroscience, 20(6), 1-6.

Wright, J. J., & Sergejew, A. A. (1991). Radial coherence, wave velocity and damping of electrocortical waves. Electroencephalography and clinical Neurophysiology, 79(5), 403-412.

Wu, J. Y., Guan, L., Bai, L., & Yang, Q. (2001). Spatiotemporal properties of an evoked population activity in rat sensory cortical slices. Journal of neurophysiology, 86(5), 2461-2474.

Wu, J. Y., Guan, L., & Tsau, Y. (1999). Propagating activation during oscillations and evoked responses in neocortical slices. Journal of Neuroscience, 19(12), 5005-5015.

Wyart, V., & Tallon-Baudry, C. (2009). How ongoing fluctuations in human visual cortex predict perceptual awareness: baseline shift versus decision bias. Journal of Neuroscience, 29(27), 8715-8725.

Xia, Y., Leib, A. Y., & Whitney, D. (2016). Serial dependence in the perception of attractiveness. Journal of vision, 16(15), 28-28.

Xu, W., Huang, X., Takagaki, K., & Wu, J. Y. (2007). Compression and reflection of visually evoked cortical waves. Neuron, 55(1), 119-129.

Yang, Z., Heeger, D. J., Blake, R., & Seidemann, E. (2015). Long-range traveling waves of activity triggered by local dichoptic stimulation in V1 of behaving monkeys. Journal of neurophysiology, 113(1), 277-294.

Ylinen, A., Bragin, A., Nádasdy, Z., Jandó, G., Szabo, I., Sik, A., & Buzsáki, G. (1995). Sharp wave-associated high-frequency oscillation (200 Hz) in the intact hippocampus: network and intracellular mechanisms. Journal of Neuroscience, 15(1), 30-46.

Yuan, H., Liu, T., Szarkowski, R., Rios, C., Ashe, J., & He, B. (2010). Negative covariation between task-related responses in alpha/beta-band activity and BOLD in human sensorimotor cortex: an EEG and fMRI study of motor imagery and movements. Neuroimage, 49(3), 2596-2606.

Yuste, R., Tank, D. W., & Kleinfeld, D. (1997). Functional study of the rat cortical microcircuitry with voltage-sensitive dye imaging of neocortical slices. Cerebral cortex (New York, NY: 1991), 7(6), 546-558.

Zaehle, T., Fründ, I., Schadow, J., Thärig, S., Schoenfeld, M. A., & Herrmann, C. S. (2009). Inter-and intra-individual covariations of hemodynamic and oscillatory gamma responses in the human cortex. Frontiers in human neuroscience, 3, 8, 1-12.

Zanos, T. P., Mineault, P. J., Nasiotis, K. T., Guitton, D., & Pack, C. C. (2015). A sensorimotor role for traveling waves in primate visual cortex. Neuron, 85(3), 615-627.

Zanos, S., Zanos, T. P., Marmarelis, V. Z., Ojemann, G. A., & Fetz, E. E. (2012). Relationships between spike-free local field potentials and spike timing in human temporal cortex. Journal of neurophysiology, 107(7), 1808-1821.

Zauner, A., Gruber, W., Himmelstoß, N. A., Lechinger, J., & Klimesch, W. (2014). Lexical access and evoked traveling alpha waves. NeuroImage, 91, 252-261.

Zhang, H., Watrous, A. J., Patel, A., & Jacobs, J. (2018). Theta and alpha oscillations are traveling waves in the human neocortex. Neuron, 98(6), 1269-1281.

Zhang, H., & Jacobs, J. (2015). Traveling theta waves in the human hippocampus. Journal of Neuroscience, 35(36), 12477-12487.

Zhang, Q. F., Wen, Y., Zhang, D., She, L., Wu, J. Y., Dan, Y., & Poo, M. M. (2012). Priming with real motion biases visual cortical response to bistable apparent motion. Proceedings of the National Academy of Sciences, 109(50), 20691-20696.

Zhang, Y., & Ding, M. (2010). Detection of a weak somatosensory stimulus: Role of the prestimulus mu rhythm and its top–down modulation. Journal of cognitive neuroscience, 22(2), 307-322.

Zheng, C., Bieri, K. W., Hsiao, Y. T., & Colgin, L. L. (2016). Spatial sequence coding differs during slow and fast gamma rhythms in the hippocampus. Neuron, 89(2), 398-408.

Zhu, D., Bieger, J., Garcia Molina, G., & Aarts, R. M. (2010). A survey of stimulation methods used in SSVEP-based BCIs. Computational intelligence and neuroscience, 2010.

Zoefel, B., & Heil, P. (2013). Detection of near-threshold sounds is independent of EEG phase in common frequency bands. Frontiers in psychology, 4, 262.

Zrenner C, Desideri D, Belardinelli P, Ziemann U (2018) Real-time EEG-defined excitability states determine efficacy of TMS-induced plasticity in human motor cortex. Brain Stimul 11:374–389.

Zumer, J. M., Brookes, M. J., Stevenson, C. M., Francis, S. T., & Morris, P. G. (2010). Relating BOLD fMRI and neural oscillations through convolution and optimal linear weighting. Neuroimage, 49(2), 1479-1489.

Tables of figures.

Part 1. General Introduction.

Chapter 1. Brain oscillations, ubiquitous in the brain.

Chapter 2. Cortical traveling waves.

Chapter 3. Aim of this PhD.

Part 2. Experimental Work.

Chapter 4. Causal link between the phase and amplitude of spontaneous alpha oscillations, cortical excitability and visual perception.

Chapter 5. Brain oscillations, the neural dynamics underlying serial dependance.

Chapter 6. Alpha brain oscillations travel at the mesoscopic scale: their propagation influences visual perception.

Chapter 7. The role of the direction of propagation of alpha macroscopic traveling waves.

Part 3. General Discussion.

Chapter 8. Discussion.